AFRL-AFOSR-UK-TR-2014-0046

GLOBAL LINEAR STABILITY ANALYSIS OF THE SPOKE OSCILLATION IN HALL EFFECT THRUSTERS

D. Escobar
E. Ahedo

UNIVERSIDAD POLITECNICA DE MADRID
CALLE RAMIRO DE MAEZTU 7
MADRID, 28040 SPAIN

EOARD Grant 13-3033

Report Date: July 2014

Final Report from 15 May 2013 to 14 May 2014

Air Force Research Laboratory
Air Force Office of Scientific Research
European Office of Aerospace Research and Development
Unit 4515, APO AE 09421-4515

REPORT DOCUMENTATION PAGE

Form Approved OMB No. 0704-0188

1. REPORT DATE *(DD-MM-YYYY)* 15 July 2014	**2. REPORT TYPE** Final Report	**3. DATES COVERED *(From – To)*** 15 May 2013 – 14 May 2014

4. TITLE AND SUBTITLE

GLOBAL LINEAR STABILITY ANALYSIS OF THE SPOKE OSCILLATION IN HALL EFFECT THRUSTERS

5a. CONTRACT NUMBER

FA8655-13-1-3033

5b. GRANT NUMBER

Grant 13-3033

5c. PROGRAM ELEMENT NUMBER

61102F

6. AUTHOR(S)

D. Escobar
E. Ahedo

5d. PROJECT NUMBER

5d. TASK NUMBER

5e. WORK UNIT NUMBER

7. PERFORMING ORGANIZATION NAME(S) AND ADDRESS(ES)

UNIVERSIDAD POLITECNICA DE MADRID
CALLE RAMIRO DE MAEZTU 7
MADRID, 28040 SPAIN

8. PERFORMING ORGANIZATION REPORT NUMBER

N/A

9. SPONSORING/MONITORING AGENCY NAME(S) AND ADDRESS(ES)

EOARD
Unit 4515
APO AE 09421-4515

10. SPONSOR/MONITOR'S ACRONYM(S)

AFRL/AFOSR/IOE (EOARD)

11. SPONSOR/MONITOR'S REPORT NUMBER(S)

AFRL-AFOSR-UK-TR-2014-0046

12. DISTRIBUTION/AVAILABILITY STATEMENT

Distribution A: Approved for public release; distribution is unlimited.

13. SUPPLEMENTARY NOTES

14. ABSTRACT

While the Hall Effect Thruster is a relatively mature technology that has been flown in several missions, the physics of the processes governing the thruster dynamics are not yet completely understood. In particular, the so-called anomalous diffusion, a short term for the excessive electron conductivity both inside and outside of the thruster, remains an unclear phenomenon. It is commonly agreed that a central cause for the higher-than-expected electron mobility are correlated azimuthal oscillations that create an effective azimuthal force. Recent experimental results, obtained independently in Michigan and Princeton with modern thrusters, confirm the existence of a low-frequency azimuthal oscillation, called rotating spoke, of similar nature as those originally detected in the 1960's by Janes and Lowder. This project aims at studying theoretically these oscillations by means of a global stability analysis of the Hall discharge against azimuthal disturbances. A central goal of the study will be to determine and quantify in terms of scaling laws their role in anomalous diffusion.

15. SUBJECT TERMS

EOARD, Hall thruster, space plasma propulsion, electric propulsion, rotating-spoke oscillation

16. SECURITY CLASSIFICATION OF:			**17. LIMITATION OF ABSTRACT**	**18, NUMBER OF PAGES**	**19a. NAME OF RESPONSIBLE PERSON** Kevin P. Bollino
a. REPORT UNCLAS	**b. ABSTRACT** UNCLAS	**c. THIS PAGE** UNCLAS	SAR	152	**19b. TELEPHONE NUMBER** *(Include area code)* 011-44-1895616163

Standard Form 298 (Rev. 8/98)
Prescribed by ANSI Std. Z39-18

GLOBAL LINEAR STABILITY ANALYSIS OF THE SPOKE OSCILLATION IN HALL EFFECT THRUSTERS: FINAL REPORT

Authors:
D. Escobar
E. Ahedo

E.T.S.I. AERONÁUTICOS
UNIVERSIDAD POLITÉCNICA DE MADRID, SPAIN

Final Report, July 15th, 2014

Contracting Entity: EOARD
Award: FA8655-13-1-3033

Abstract

While the Hall Effect Thruster is a relatively mature technology that has been flown in several missions, the physics of the processes governing the thruster dynamics are not yet completely understood. In particular, the so-called anomalous diffusion, a short term for the excessive electron conductivity both inside and outside of the thruster, remains an unclear phenomenon. It is commonly agreed that a central cause for the higher-than-expected electron mobility are correlated azimuthal oscillations that create an effective azimuthal force. Recent experimental results, obtained independently in Michigan and Princeton with modern thrusters, confirm the existence of a low-frequency azimuthal oscillation, called rotating spoke, of similar nature as those originally detected in the 1960's by Janes and Lowder. This project aims at studying theoretically these oscillations by means of a global stability analysis of the Hall discharge against azimuthal disturbances. A central goal of the study will be to determine and quantify in terms of scaling laws their role in anomalous diffusion.

Contents

List of Figures

List of Tables

Chapter 1

Introduction

1.1 Motivation

Over the last decade great efforts have been dedicated into the understanding of the physics of Hall Effect Thrusters. However, there are still central phenomena that are poorly understood. The main one is the so-called anomalous diffusion, associated to an excessive electron axial current that cannot be explained with classical collisional theories. Forty years ago, Morozov [2] suggested near-wall conductivity and turbulent diffusion as the two plausible causes for the anomalous diffusion. Near-wall conductivity, also called electron-wall collisionality, is related to the interaction of electrons with the lateral walls of the thruster and would be enhanced by secondary electron emission. Recent advances on modelling this process by our team EP2 [3] and others [4] have concluded that electron-wall collisionality is insufficient to explain the experimentally observed anomalous diffusion, which leaves turbulent diffusion as the main candidate.

Many oscillation modes have been identified experimentally or theoretically in Hall effect thrusters, propagating longitudinally, azimuthally or obliquely, the main modes ranging from a few kHz to tens of MHz [5]. Low frequency modes are of hydrodynamic character, whereas high frequency modes are mainly electromagnetic. In general, azimuthal modes, which involve a higher spatial dimensionality as they combine axial inhomogeneities with an azimuthal propagation, are less amenable to analysis and therefore are less understood.

Turbulent diffusion would be due to correlated azimuthal oscillations of plasma density and electric field both in the ionization and acceleration regions of the thruster, but the debate is still open on whether the relevant ones are low-frequency or high-frequency (or even both). The study here proposed is centred on low-frequency azimuthal oscillations, more precisely, in what is conventionally called the rotating-spoke oscillation [5], which is a firm candidate to contribute to anomalous diffusion.

The rotating-spoke was first detected in 1966 by Janes and Lowder [6] who already suggested it as a diffusion mechanism. It was later measured at Stanford by Chesta et al. [7] on modern Hall thrusters both at low and high voltages. The rotating spoke has regained much attention in the last years, through experiments at Princeton PPL [8, 9] and Michigan

PEPL [10], which have obtained vivid videos and other detailed data of the oscillations in Hall thrusters of different design and size, and under different operating conditions. In order to understand the effect of this spoke on the time-averaged response of the discharge, these experiments need to be supported by theoretical models. Due to the strong interconnection of physical processes in a Hall discharge and large inhomogeneities, the formulation of these models is likely to be not simple and to involve much mathematical apparel. We still hope that the picture of the diffusion mechanism can be simplified to its essentials once it is understood.

The rotating-spoke, being a low-frequency oscillation, is basically a hydrodynamic mode, which can be studied using fluid models of the discharge in the electrostatic and quasineutral approximation. Since 2000 our team EP2 has been at the forefront of developing physically well-based models of the Hall discharge [11, 12, 3, 13] and later applying them to linear oscillation studies [14, 15, 16, 17]. The project aims to add the rotating-spoke to that discussion, by comparing theoretical and experimental findings.

1.2 Activities of the project

The activities of the project can be summarized as:

- Bibliographical review: Taking the work of Choueiri [5] as starting point, a detailed review and classification of the experimental data and theoretical studies of oscillations in Hall thrusters will be carried out. Special attention here will be devoted to theoretical studies, and the classification will be based on the different physical-mathematical models that are proposed, the simplifications and assumptions that are made to develop and solve them, and the connections among the different studies. Many of these analyses focus on the acceleration region, where the ionization can be safely neglected, and on the high frequency regime. However, experimental results show the presence of azimuthal oscillations in the low frequency range located mostly in the ionization region and appearing normally in the ionization part of the current-voltage curve.

- Local linear stability. This is the type of analysis more common in the literature. It consists in freezing the plasma magnitudes at a fixed axial location of the steady-state solution and carry out a normal stability analysis on the constant-coefficient equations, which reduces to an algebraic problem. The resulting local dispersion relation is solved either analytically or numerically. Here we will complete the work presented in Ref. [18], where we showed results on local linear stability of the ionization region against small perturbations. These indicated the existence of an instability that gives rise to an azimuthal oscillation with a mode number m=1.

- Fluid model with azimuthal gradients: The axial three-fluid model we developed in 2000-2005 for both steady-state and axial stability studies will be here extended to include azimuthal terms. Then, temporal and azimuthal effects will be linearised yielding the final model for our analysis.

- Global linear stability. This is the central task of this project. The above local linear stability analysis is not consistent when the discharge is strongly inhomogeneous, as it is the case here. The lack of consistency manifests itself in the different ways that inhomogeneities can be frozen in the local stability analysis. This explains, for instance, that different stability criteria are found in the literature for the same instability [19].

The global linear stability analysis deals with the variable-coefficient differential equations. The spatial integration plus homogeneous boundary conditions yield the global dispersion relation for the mode frequency. The solution of the dispersion relation will determine the dominant azimuthal mode (i.e. the one with the maximum growth rate) in terms of the parameters governing the steady-state solution (discharge voltage, mass flow, magnetic strength). Instability thresholds can be determined too. We already followed successfully this global procedure in Ref. [14] for longitudinal oscillations, although at that time we did not recognize in the results the breathing mode mechanism [20]. In principle, the same procedure can be followed for azimuthally non-symmetric modes.

- Discussion of azimuthal modes. The first goal here is a comparison of our azimuthal modes with the rotating spokes observed at Princeton and Michigan. Additionally, the possible similarities with the breathing mode will be searched. The second goal is the study of correlations of plasma variables that can lead to a time-averaged azimuthal force explaining anomalous diffusion. An investigation of the influence of different control parameters on the instability and the azimuthal force will be carried out. The derivation of main locations, trends, and scaling laws for that azimuthal force would be a much-desired result. Nonetheless, it must be noted that the azimuthally-correlated force is a non-linear effect, so a fully consistent assessment is beyond the present linear analysis.

- Further actions. If the conclusions from the global linear stability study support a relevant role of the rotating-spoke in anomalous diffusion, a proposal will be sketched, which will set the route for affording a non-linear stability analysis of the azimuthal modes and a consistent determination of the resulting anomalous diffusion force. Other aspects of interest arising as the research progresses are included in this task too.

1.3 Organization of the report

This report is organized as follows:

- Chapter 1 is this introduction.

- Chapter 2 is devoted to a complete and thorough bibliography review on spoke oscillations.

- Chapter 3 focuses on local linear stability analyses both of the acceleration and ionization regions of the HET discharge.

- Chapter 4 presents the low frequency global linear stability analysis of the Hall discharge, starting with the development of the model, continuing with the use of the model to obtain results and finalizing with a discussion.

- Conclusions and a list of publications derived from this study are given in Chapter 5.

Chapter 2

Bibliography review

This chapter presents a summary of the state-of-the-art on the topic of anomalous diffusion in Hall Effect Thrusters (HET) and its possible relation with azimuthal oscillations.

2.1 Hall thrusters

Hall thrusters are a type of electric plasma propulsion device initially developed in the 1960's by both the USA [21] and the former USSR [22, 23] independently. The development continued in the shadow in the USSR to reach a mature status in the 1970's and 1980's. In the 1990's the advanced state of this Russian technology reached western countries, which rapidly restarted the analysis and development of modern Hall thrusters. Nowadays, there are several companies manufacturing Hall thrusters for operational use in USA, Russia and Europe. The main applications of these thrusters are low-thrust propulsion of interplanetary probes, orbital raising of satellites, and north-south station-keeping of geostationary satellites [24]. There are two basic variants of Hall Thrusters, the Stationary Plasma Thruster (SPTs) and the Thruster with Anode Layer (TAL). The main difference between them is the material of the walls of the devices, ceramic for the SPT model and metallic for the TAL.

The operation principle of a typical Hall thruster is as follows [25, 26]. A strong radial magnetic field is imposed together with an axial electric field inside a coaxial channel where a neutral gas, typically Xenon, is used as propellant. There are three species of particles involved: neutrals, that are injected from the rear part of the channel and flow axially towards the thruster exit; electrons, that are introduced by the cathode located just outside the channel and flow towards the anode, next to the neutral injector, describing a **E**x**B** closed drift in the azimuthal direction due to the orthogonal electric and magnetic fields; and ions, that are created by volume ionization of neutrals from collisions with the counter-streaming electrons and are accelerated axially by the electric field in the channel and the near plume. The magnetic field is such that electrons are strongly magnetized (i.e., the electron Larmor radius is much smaller than the typical length scale of the thruster) while ions are unmagnetized (i.e, ion motion is mostly driven by the electric field).

The main control parameters of a typical HET are the mass flow of neutral gas through the injector, the electric voltage between anode and cathode and the externally imposed magnetic field. The current is an output of the dynamical system and depends on the ionization, defining the ion current, and the magnetic field, controlling the electron current. It is quite common to represent the performance of a thruster in the current-voltage map (I-V). For given magnetic field and mass flow rate, the variation of the current with the voltage is characterized by two separate regimes of operation: a regime of incomplete ionization where the current rapidly increases with the voltage and a regime of current saturation where the current is fairly insensitive to changes in the discharge voltage. The lower the ionization potential of the neutral gas is, the clearer the separation between the two regimes is [27]. The electron current emitted by the cathode towards the anode is needed for the ionization process. Thus, the smaller it is the better the efficiency of the thruster is. And in fact, the optimal point of operation of typical Hall thrusters is located in between the two regimes of the I-V curve where the electron current is the smallest. In order to ensure that the device does not get charged, a second electron current is emitted by the cathode to compensate the ion current emitted by the thruster.

A list of typical operating conditions is presented below based on the SPT-100 model, a well analysed HET model:

1. outer radius: $r_{out} = 5cm$
2. inner radius: $r_{in} = 3.5cm$
3. channel length: $L_{ch} = 2.5cm$
4. mass flow: $\dot{m}_{inj} = 4.8mg/s$
5. discharge voltage: $V_d = 300V$
6. magnetic field: $B_{max} = 230G$
7. discharge current: $I_d = 4.5A$
8. power: $P_d = 1.35kW$
9. efficiency: $\eta = 0.48$
10. specific impulse: $I_{sp} = 1600s$
11. thrust: $T = 83mN$
12. electric field: $E_{max} = 100V/cm$
13. neutral density: $n_n = 10^{19}m^{-3}$
14. plasma density: $n = 10^{17}m^{-3}$

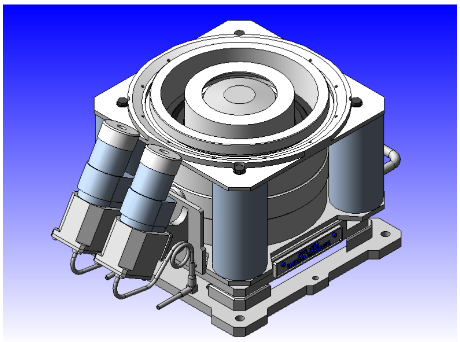

Figure 2.1: PPS-1350 Hall effect thruster

2.2 Anomalous diffusion

Since the early stages of the Hall thruster technology development, it has been clear that the electron conductivity inside the channel and in the plume is too high to be explained by the classical collisional theory [27]. That is why the term anomalous diffusion is used to refer to the higher-than-expected electron current. The radial magnetic field and the axial electric field trap the electrons in an azimuthal closed-drift and, according to classical theory, the only mechanism that allows the electrons to move axially are collisions with other species. However, the electron conductivity measured experimentally is between one and two orders of magnitude higher than the expected one from collisions. Thus, another mechanism is suspected to modify electron dynamics and reduce the electron resistivity. Currently there is no agreement within the Hall thruster community, but the most accepted explanations for the anomalous diffusion are two [28]:

- plasma oscillations and turbulence (referred to as Bohm-type diffusion as well): correlated azimuthal oscillations of density and electric field can induce a net axial electron current [29, 6].
- near wall conductivity: secondary electrons emitted by the walls introduce a net axial current [30].

Some authors propose other explanations such as very-high frequency oscillations inside the plasma sheaths attached to the walls [31, 32], electron cyclotron orbit distortion to steep gradients of the electric field [33, 34] or some other different mechanisms [35, 36, 37]. But unfortunately, even though many HETs have already been flown, the underlying physics of the electron excessive diffusion are not properly understood.

Although experimental evidence is not unanimous, most common general properties of the anomalous diffusion are:

a) It is present in the whole channel as well as in the plume of the thruster [38]. Experiments show that the electron conductivity is higher than expected both inside and outside the thruster, even if the processes taking place in the channel and in the plume are completely different.

b) It is higher outside than inside the channel [39]. It has been shown experimentally that the electron conductivity seems to be higher in the near field plume than in the channel. Furthermore, several numerical models that make use of empirical parameters to describe the anomalous diffusion need to use different fitting parameters inside and outside the thruster to properly match experimental results [40].

c) There is a dip of electron conductivity in the region of high magnetic and electric fields [38, 39] or, as some authors suggest, in the region of high electron drift shear [41, 42]. Based on this and the previous property, it has been proposed in the past that both azimuthal oscillations and near wall conductivity enhance the electron cross field diffusion: the former in the near plume and the latter inside the thruster.

d) The electron mobility scales as $1/B$ rather than as $1/B^2$ as verified experimentally with laser interferometry (LIF) in [43, 44]. This fact seems to indicate that the cause of the anomalous diffusion cannot be the near wall conductivity since in that case it would scale as $1/B^2$.

e) The magnetic field topology greatly affects the electron conductivity [2] and thus the anomalous diffusion. A negative axial gradient of the magnetic field inside the channel increases importantly the electron current needed to sustain the discharge. This property justifies why the magnetic field is normally designed to peak roughly at the thruster exit in modern HETs.

From a mathematical point of view, the anomalous diffusion due to azimuthal oscillations can be expressed as [6]:

$$j_{ez} = \frac{e}{AB}\int nE_\theta dA$$

where A is the cross section of the HET and the rest of symbols are as usual. The corresponding Bohm diffusion coefficient can then be expressed as

$$\alpha = \frac{j_{ez}}{j_{e\theta}} = \frac{1}{\langle nE_z\rangle}\frac{1}{2\pi}\int_0^{2\pi} nE_\theta d\theta = \frac{\langle nE_\theta\rangle}{\langle nE_z\rangle}$$

where $\langle\rangle$ represents an average over the azimuthal direction.

Yoshikawa and Rose [29] developed a statistical theory in the 1960's based on Fourier expansions of electron conservation equations. This theory shows the connection between the azimuthal oscillations and the enhanced plasma conductivity detected in experiments. The theory states that the Bohm-type diffusion coefficient, empirically estimated by Bohm as 1/16, can be expressed mathematically as:

$$\alpha = \frac{\pi}{4}\langle(n-n_0)^2\rangle/n_0^2$$

where n is the time-varying plasma density, n_0 is its steady state value and $\langle\rangle$ represents an average over time.

In the same direction, a simple model describing how azimuthal heterogeneities can enhance electron conductivity was presented more recently by Baranov *et al.* [45]. And numerical simulations with artificial azimuthal electric fields superimposed to simulated $r-z$ fields [46, 47, 48, 49] show how electron particles drift axially due to the presence of the azimuthal electric field.

Nevertheless, the anomalous diffusion is not believed to be a unique feature of Hall Thrusters. That is why several experiments have been recently designed and carried out to do basic research and analyse the anomalous diffusion mechanism in devices much simpler than typical HETs [50, 51, 36, 52].

Near wall conductivity does not seem to explain the anomalous diffusion since many $r-z$ simulation codes [3, 4, 53] include a near wall conductivity model and still need a Bohm-type diffusion contribution to reproduce the anomalous diffusion measured experimentally. Thus, it seems that azimuthal oscillations could play a major role in explaining the anomalously high electron mobility.

To sum up, the topic of anomalous diffusion is one of the remaining uncertainties that need to be clarified in order to fully understand the physics of HETs. And this is the key to improve their efficiency, increase their flexibility and enlarge their range of operation as required for many future missions [54]. As an additional outcome, truly predictive numerical codes could be developed that would in turn reduce the development costs of new HETs by allowing accurate numerical simulations of processes such as wall erosion, currently the main limiting factor of the lifetime of these devices.

2.3 Time scales

Ions and neutrals exhibit an axial motion driven by electric acceleration and gas expansion respectively. Based on the mass flow and typical neutral density, it is possible to estimate the axial velocity of the neutrals as $u_{nz} = \dot{m}/n_n A \sim 0.2km/s$. The corresponding residence time inside the thruster is $t_n = L_{ch}/u_n z \sim 0.12ms$, which is equivalent to a frequency of $\omega_n = 1/t_n \sim 8kHz$. In the case of the ions, their axial velocity can be estimated as $u_{iz} = \sqrt{\eta_a e V_d/m_i} \sim 14km/s$ where an efficiency of 80% ($\eta_a \sim 0.8$) for the electric acceleration process and the mass of the Xenon ion ($m_i = 2.18 \cdot 10^{-25}kg$) have been used. The resulting residence time is $t_i \sim 1.8\mu s$ which is equivalent to a frequency of $\omega_i \sim 500kHz$.

The motion of electron particles can be regarded as the sum of different oscillations and drifts, each one of them characterized by a different time scale:

- *gyro-motion*: the usual circular motion of electrons around magnetic lines is defined by the electron cyclotron frequency $\omega_{ce} = eB_{max}/m_e \sim 4GHz$

- *wall-to-wall bounce*: only high energy electrons overcome the potential fall of the sheaths and hit the wall. The rest of them are trapped in a periodic motion along the magnetic field line from one wall the other. The characteristic radial velocity is $u_{er} = 1.5 \cdot 10^3 km/s$, this is, a period of $t_w = \Delta r/u_{er} \sim 0.01\mu s$ and a frequency of $\omega_w \sim 100MHz$.

- ***ExB** drift*: the azimuthal drift velocity can be estimated as $u_{e\theta} = E_{max}/B_{max} \sim 400km/s$. Based on the median radius, the estimated period is $t_{e\theta} = \pi(r_{out} + r_{in})/u_{e\theta} \sim 0.66\mu s$ and the corresponding frequency is $\omega_e \sim 1.5MHz$

- *axial drift*: in HET experiments the electron current is typically measured as one-third of the ion current. Thus, making use of the quasi-neutrality condition, the electron axial velocity can be estimated as $u_{ez} \sim -5km/s$, resulting in a residence time of $t_e \sim 5.4\mu s$.

Besides, the electron temperature within the channel is normally around $T_e = 30eV$ which is equivalent to an electron thermal velocity of $u_{et} = \sqrt{T_e/m_e} = 2 \cdot 10^3 km/s \gg u_{e\theta} \gg u_{ez}$. That is why electron inertia is sometimes neglected in some analyses and models.

2.4 Oscillations

The operation of Hall thrusters is characterized by the presence of a myriad of oscillations, both axial and azimuthal, ranging from low (LF) through medium (MF) to high frequency (HF), exhibiting many different phase velocities, from a few to thousands of km/s, and a intensity that decreases with increasing frequency. The following classification of oscillations is commonly accepted for HETs [55, 5]:

- *breathing mode*: also known as contour or loop oscillations, it consists of low frequency (1-20 kHz) axial oscillations. It is related to the ionization process and is typically described with a predator-prey model of ions and neutrals [56]. This type of oscillation is inherent to HET operation in the whole I-V curve and its intensity can exceed the steady state value of the discharge current. However, it tends to be minimal at the nominal operation point. Apart from the predator-prey analytical model, the breathing mode has been reproduced fairly well in various simulation codes. More recently, Barral *et al.* [57] have unveiled the dynamics of this oscillation by means of a simplified one dimensional time-dependant fluid model and linear stability analyses which confirm the initially proposed predator-prey model. The theoretical progress has allowed to propose and simulate different mechanisms to mitigate these oscillations by acting of the power processing unit (PPU) of the thruster [58, 59, 60].

- *rotating spoke*: it is a low frequency (5-25 kHz) azimuthal density oscillation characteristic of the ionization part of the I-V curve. It appears as a rotating spoke that propagates axially with 20 degrees of inclination. It seems to be related to incomplete ionization and the velocity of the spoke is correlated with the first ionization potential of the neutral gas. At the nominal operation point, this oscillation is not dominant. It was first measured and studied by Janes and Lowder [6], but its origin remains fairly an unknown at the moment. Due to its azimuthal nature, it could enhance the electron conductivity and therefore it is analysed more in depth in the next sections.
- *gradient induced oscillations*: also known as drift magneto-sonic waves [1], they are low frequency (20-60 kHz) azimuthal oscillations promoted by axial negative gradients of the magnetic field. They typically appear at the exit of the thrusters as a wave with a phase velocity one order of magnitude smaller than the **E**x**B** drift. The need to stabilize the discharge inside the thruster against these oscillations explains the positive gradient of magnetic fields in the channel of all modern HETs. These waves can also affect the electron conductivity and, thus, are further described below.
- *ion transit time oscillations*: these are medium frequency (70-500 kHz) axial oscillations associated to the ion acceleration process. They were already clearly visible in early experiments as broad band turbulence [61, 62]. More recently, full size simulation codes have managed to reproduce them and some theoretical analyses have been carried out [19, 63], but their physics are not yet fully understood. Since the direction of propagation is mostly axial, they are not believed to affect the anomalous diffusion mechanism.
- *electron drift oscillations*: they are high frequency (1-10 MHz) axial and/or azimuthal oscillations connected to the electron **E**x**B** drift and normally appear during the descent part of the discharge current variation as azimuthal waves in the near plume and as axial ones inside the thruster. Interestingly, the presence of this oscillation was first proposed theoretically and later on confirmed experimentally by Esipchuk and Tilinin [1]. A few years ago, thanks to the development of precise diagnosis apparatus, the interest in these oscillations re-appeared again and several researches have characterized them experimentally [64, 65, 66, 67]. A more thorough description is presented below since anomalous diffusion could be enhanced by them.
- *high-frequency short-wavelength oscillations*: these oscillations have been detected very recently in experiments with an experimental set-up commonly used in nuclear fusion [68, 69, 70, 71]. These oscillations seem caused by the interaction between the electron gyro-motion and electric field variations [72, 73].

Depending on the operating point in the current-voltage curve (I-V), the intensity of each one of the oscillations varies. Tilinin [74] describes up to six different regimes of operation in the I-V curve, each one of them dominated by different oscillations. In particular, the rotating spoke and the breathing mode appear mostly at low voltages while ion-transit time and high frequency oscillations prevail at high voltages. More extensive and general presentations about oscillations in HETs, in line with the previous classification, can be found in Refs. [5] and [55, 75, 76].

2.5 Numerical simulation

Thanks to the development of powerful computers, several numerical codes have been used since late 1990's to simulate the operation of Hall Thrusters. The complexity of those codes has kept growing steadily, starting with simple one-dimensional fluid models and, currently, reaching fully particle-in-cell (PIC) models in two or even three dimensions. Typically, the following types of simulation models can be found:

- *fluid models*: particle, momentum and energy conservation equations describing the motion of all species are solved. The main advantage of these models is the relatively low computational cost for solving the partial differential equations compared to other methodologies. However, the low collisionality inside Hall Thrusters hinders the applicability of fluid equations for electrons and ions [77]. Most fluid models developed so far are 1D [11, 78, 15] and more recently 2D [79, 80].

- *kinetic models*: Vlasov's equations describing the evolution of the distribution function of the different species are solved together with Poisson's equation for the electric potential. The governing equations are more difficult to solve than in fluid models and thus only 1D codes exist currently [81].

- *full PIC models*: each particle species is considered as an ensemble of macro-particles whose motion is computed by solving Newton's law of motion while the electric potential is obtained from Poisson's equation. This method represents with higher fidelity the physical processes, but is too expensive from the computational point of view, specially when simulating two or more dimensions. The main reason for the high computational cost is that the time-step of the numerical solver and the spatial size of the computational grid must resolve the electron cyclotron and plasma frequencies, the electron Larmor radius and the Debye length so that Newton's equations of motion for electrons and Poisson's equation can be solved reliably. A good example of this type of models is the code developed by Coche and Garrigues [82, 83]. Another full PIC code was developed before by Szabo simulating the $r - z$ space [84]. The axial-azimuthal version of Szabo's code was implemented by Batishchev [85]. An implicit version of the code of Coche and Garrigues was developed by Adam *et al.* in early 2000's with important time saving due to its implicit nature. More recently, Matyash and Schneider have developed a 3-D PIC code [86].

- *hybrid models*: in this case electrons are modelled as a fluid and ions and neutrals with a PIC method. These models combine the higher fidelity of PIC methods in low collisionality plasmas for ions and neutrals and the lower computational cost of fluid models for electrons. The quasi-neutrality assumption is used and therefore, it is not necessary to solve Poisson's equation and the spatial grid does not have to resolve the Debye length. This fact makes these methods much faster than full PIC methods. The first 2D hybrid PIC model was developed by Fife [56] and many other similar codes have been developed afterwards [87, 88, 53]. The success of this method for HET modelling is quite possibly due to the best trade-off between accuracy and computational cost. However, most of the hybrid codes developed so far are 2D in the $r - z$ space, what prevents the analysis of azimuthal oscillations. Recently, a new hybrid code in the $z - \theta$ space has been developed by Lam *et al.* [89, 90] to evaluate the influence of azimuthal oscillations on the electron conductivity. The computational cost of that code is enormous and only preliminary results have been obtained till now. The main disadvantage of these methods is that the electrons are modelled with fluid equations which are known to be not too adequate for HETs due, among other reasons, to the anisotropy of the electron distribution function.

- *quasineutral-PIC models*: ions and neutrals are modelled with a PIC method, while the electron species is considered as an ensemble of macro-particles representing the guiding-centres of the electron particles. The motion of the electron guiding-centres is computed by solving special equations of motion derived from the usual electron equations of motion averaged over one gyro-period. Quasi-neutrality is not directly achieved, but it is assumed when computing the electric field from electron momentum and charge conservation. The main advantage of this method is that electrons are modelled as macro-particles rather than as a fluid, but at the same time the time-step and grid size constraints inherent to full PIC methods are not applicable here since the electron gyromotion and Poisson's equation are not solved. This method has been recently applied successfully by Miedzik and Barral [91] to a magnetic field line of a typical HET showing that typical fluid models are not fully correct to represent electron dynamics in the direction parallel to the magnetic field. However, no 2D code based on this methodology has been developed so far for HET simulation, neither in $r-z$ space nor in $z-\theta$ space.

The only numerical codes in the $z-\theta$ space currently existing are those implemented by Hirakawa *et al.* [92], Adam *et al.* [93]. Batischev *et al.* [85], and more recently Lam *et al.* [89, 90], continuing the work of Fernandez *et al.* [94, 95, 96], Matyash and Schneider [86] and Coche and Garrigues [83, 82]. Theses codes need no empirical parameter to reproduce the anomalous diffusion thanks to the presence of azimuthal oscillations. However, the oscillations detected by those codes are not always in agreement with experimental results. Moreover, the computational cost is enormous and makes it difficult to carry out detailed analyses with them.

On the other hand, the rest of 2D numerical codes have focused on the radial and axial dynamics and make use of different modelling strategies to reproduce the anomalous diffusion:

- constant Bohm-type diffusion coefficient as a empirical parameter to match numerical results with experiments [53, 88]
- electron mobility models with two or three empirical coefficients [40, 4, 97, 98, 99]
- shear-based models and/or quench models with empirical parameters [100], [101]
- electron mobility profile derived from experimental measurements imposed in simulations [102], [101], [103]
- derivation of azimuthal oscillations from axial ones based on linear stability analysis [104, 105]
- near wall conductivity models [40, 4, 106, 107, 108]

Based on the number of different methodologies, it is clear that the topic of anomalous diffusion is an active area of research where no general agreement has been reached. However, in order to have accurate predictive simulation codes it is of utmost importance to understand and model properly the electron conductivity due to its impact on the general behaviour of the dynamical system.

2.6 Theoretical studies: linear stability analyses

In the area of linear stability analyses, it is possible to distinguish two types of studies: linear stability analyses of multi-fluid models that evaluate locally the potential growth of small disturbances, where all coordinates are resolved with the usual exponential form $\exp(i\mathbf{k}\cdot\mathbf{x})$, and the result is a dispersion equation relating algebraically the wave vector and the frequency of the oscillation; or global analyses where the axial coordinate is left unresolved and the resulting dispersion relation is not an algebraic expression, but an ordinary differential equation in x to solve for eigenfunctions and eigenvalues.

On the other hand, and depending on the hypothesis and simplifications introduced in the governing equations, the resulting models go from simple to very complete. The following hypothesis can be considered:

- *electrostatic plasma*: this hypothesis allows removing Faraday's and Ampere's laws from the analysis. It is important to keep those equations in the model only for the evaluation of very high frequency oscillations (1 GHz) and therefore, most of the stability studies neglect the electromagnetic effects.
- *no ionization*: including the effect of the ionization requires accounting for additional equations in the model to describe the motion of the neutral gas. This is normally avoided to simplify the analysis, although it is not fully justified in the rear part of the HET where the ionization dominates the physics of the discharge.
- *quasi-neutrality*: this assumption is also referred sometimes to as the dense plasma hypothesis. It allows removing Poisson's equation from the model since electron and ion density are considered equal in the macroscopic scale under consideration.
- *uniform plasma*: the gradients of the plasma density, magnetic field and ion and electron velocities can be excluded from the analysis for simplicity although they are believed to influence the physics of the system significantly.
- *zero electron mass*: for the analysis of the low frequency regime it is normally acceptable to neglect the electron inertia although for high frequency studies this assumption might not be valid.
- *collision-less plasma*: the dominant non-ionizing collisions in the plasma inside a HET are electron-neutral collisions. The classical theory of electron transport is based on these collisions to justify the electron cross-field mobility. However, due to the need for additional mechanisms to explain the anomalously high electron conductivity, electron-neutral collisions could be neglected.
- *cold plasma*: it is quite common to neglect the electron temperature in the equations. In this manner no energy or state equation is needed to include the effect of the temperature. However, in order to have a complete model it is important to maintain these effects, specially, if the ionization is included in the model.

Depending on the terms that are kept in a given model, the resulting dispersion equation changes. That explains why there are so many studies in this topic in the Hall thruster literature with different and sometimes contradictory results.

2.7 Azimuthal oscillations

In the previous sections it has been suggested that azimuthal oscillations could explain the anomalously high electron conductivity inside HETs. In fact, if the electric field perturbations and the density variations are correlated, a net axial electron current is generated. LF and HF azimuthal oscillations are suspected to participate in this process and enhance electron mobility, although it is not yet clear the role of each type of oscillation. It would not be surprising that both types of oscillations play an important role at the same and/or different operating conditions.

2.7.1 Low frequency oscillations

Experimental results

Back in the 1960's, Janes and Lowder[6] carried out a seminal work on low frequency azimuthal oscillations in HETs. Even though the Hall accelerator analysed in that research differs significantly from a modern HET, many of the conclusions are still valid. In that study, a spoke was detected by means of azimuthally separated Langmuir probes. This spoke appeared as a density variation rotating azimuthally in the **E**x**B** direction with a phase velocity of a few km/s and an axial tilt of 20 degrees with respect to the azimuthal plane (i.e., with a non-zero axial component of the phase velocity). The density variation was phase-correlated with the oscillating electric field and, as a consequence, an enhanced electron axial mobility was caused. The phase velocity of the rotating spoke was one order of magnitude smaller than the local **E**x**B** drift. Moreover, as part of the research, different propellants were used and it turned out that the phase velocity of the spoke scaled with the ionization potential of the neutral gas: xenon, krypton or argon. All these facts seem to indicate a close connection between the ionization process and the appearance of the spoke. Janes and Lowder made as well use of the statistical theory of Yoshikawa and Rose[29] obtaining a good agreement with the experiments in terms of predicted anomalous diffusion.

Esipchuk *et al.* [62] also reported low frequency azimuthal oscillations in a Hall thruster in the low voltage part of the I-V curve and rotating in the **E**x**B** direction. The oscillations for density and electric field were correlated causing enhanced electron conductivity. However, these oscillations disappeared at higher voltage. Based on that, Esipchuk *et al.* claimed this oscillation is due to incomplete ionization in the low-voltage part of the I-V curve and hence disappears in the current saturation part of the curve.

Shortly after, Lomas and Kilkenny[109] reproduced the Janes-Lowder experimental results and carried out an analysis of the influence of the magnetic field. According to the analysis of Lomas and Kilkenny, the phase speed of the spoke increases with the magnetic field, an interesting property not previously described by Janes and Lowder.

Similarly, experimental results from Sidney *et al.* [110] also show the presence of azimuthal oscillations of plasma density and electric field in a Hall accelerator in the low frequency range. In that study the influence of the magnetic field is also analysed with different propellants reaching the conclusion that there exists a critical magnetic field that allows suppressing the instability.

During the last two decades several experiments have been carried out with modern HETs to characterize the low frequency azimuthal oscillations for a wide range of operating conditions and thrusters, both inside and outside the channel. Next is a summary of these studies.

In one of the first of those analyses, Hargus *et al.* [111] study the azimuthal oscillations in a laboratory Hall thruster. The conclusions from that study can be summarized as follows. First, low frequency azimuthal waves are observed at velocities of a few km/s both in the low-ionization part and the current saturation part of the I-V curve. In the current saturation part of the I-V curve the wave is closer to the channel exit. In the ionization part of the I-V curve, near the knee, the wave has a lower frequency and is stronger and more spread throughout the thruster. Finally, at very low voltages, the wave is located only near the anode and the wave frequency is higher than in all previous cases.

Meezan and Cappelli[38, 41, 42] use several low frequency diagnosis methods to measure experimentally the electron mobility along the thruster. The results are in line with the general properties of anomalous diffusion presented above, and in particular, with the presence of a dip in the electron conductivity around the region of maximum electron shear. And what is more important, the electron mobility profile computed with the theory of Yoshikawa and Rose[29] from the measured density oscillations matches fairly well the measured electron mobility for various operating conditions. A possible correlation between the dip in the electron conductivity and the electron shear is suggested by Cappelli[42], although no definitive conclusions have been reached to this respect. A similar mechanism of electron transport barrier due to high electron shear has been proposed in the area of nuclear fusion inside tokamaks[112], although Hall and nuclear fusion plasmas are in rather different conditions to establish a link between them without a more detailed analysis.

In a separate study Chesta *et al.*[7] focus on the characterization of all low frequency oscillations in HETs, both axial and azimuthal. In that work, the usual breathing mode and transit time oscillations are clearly observable together with some special azimuthal oscillations. The latter ones are caused firstly by the azimuthal asymmetry of the magnetic field, generated by four magnetic coils, and secondly by the presence of two azimuthally separated Langmuir probes. Apart from those oscillations, two additional azimuthal low frequency waves with a tilt angle of 15-20 degrees and a wave mode number of $m = 1$ are detected at low and at high voltage. The oscillation at low voltage has a phase velocity of a few km/s with a frequency of 5-10 kHz and seems to match the properties of the rotating spoke detected by Janes and Lowder[6], Esipchuk *et al.* [62], and Lomas and Kilkenny[109]. On the other hand, the oscillation at high voltage has a frequency of roughly 20 kHz and could be the natural extension of the rotating spoke to the current saturation part of the I-V curve. Moreover, the relative size of the low frequency density oscillations with respect to the azimuthally averaged density shows a dip in most operating conditions around the region of high magnetic field, in agreement with the results of Meezan and Cappelli[38, 41, 42].

Gascon *et al.*[113, 114, 115] study the propagation properties of low frequency azimuthal oscillations and analyse the influence of the ceramic material used, either alumina or boron nitride. In that study, gradient-induced azimuthal oscillations are detected at various axial locations in the medium frequency range (30-200 kHz). As in previous studies, azimuthal waves are suppressed around the region of maximum magnetic field. The main novelty of that study is the dependence of the direction of propagation of the azimuthal waves on the ceramic material used. The type of material affects the azimuthal oscillations by controlling the relative position of the magnetic field and plasma density maxima via the secondary electron emission yield of the material. Apart from these medium frequency oscillations, Gascon *et al.* also observe azimuthal oscillations below 30 kHz rotating along $+\mathbf{E}\mathrm{x}\mathbf{B}$ in the near anode region, but in the opposite direction in the near-plume.

Smith and Cappelli [116] analyse low frequency oscillations of density, temperature and electric field in the near field plume of a HET operating in nominal conditions. A density oscillation is detected at the thruster exit that rotates in the -**E**x**B** direction with a phase velocity of 1.8 km/s and a frequency of 25 kHz. The propagation properties of this oscillation agree well with the results previously described, except for the propagation direction which is reported to be opposite to the usual **E**x**B** drift. A similar behaviour is reported by Gascon and Cappelli [114] in the outer region of a Hall thruster with alumina as ceramic material.

More recently, Raitses *et al.*[117] have observed spokes in a cylindrical Hall thruster. In a series of experimental studies[8, 9, 118, 119, 120], this oscillation is characterized through the use of a segmented anode and high-speed imaging. In this case, the spoke travels in the +**E**x**B** direction with a phase speed of about 2 km/s and an azimuthal wave length of the order of the circumference of the channel, this is, with a wave mode $m = 1$. These properties agree well with other experiments described above. Additionally, the influence of the cathode operation on the spoke and the electron mobility is analysed in that research. In particular, if the cathode emission is increased, the spoke disappears and the electron conductivity is greatly reduced. This is a good indication of the connection between the anomalous diffusion and the spoke oscillation. As a continuation of those analyses, references [121] and [122] show how it is possible to control, suppress or even promote spoke oscillations by means of a feedback-loop control on the discharge voltage of the elements of a segmented anode.

In a parallel and independent research, McDonald *et al.* [10, 123, 124, 125] have used also high-speed imaging techniques as well as a segmented anode to characterize the spoke in a wide range of HETs, including both conventional and non-conventional designs (the H6 thruster, the NASA 173Mv1, the Busek BHT-600, the X2 dual nested channel Hall thruster, and the Helicon Hall thruster). In those analyses, the larger the thruster is, the larger the mode number of the spoke is. In particular, for the H6 thruster modes $m = 2$ and $m = 3$ dominate in nominal operating conditions whereas $m = 4$ and $m = 5$ are observed to be dominant when using the segmented anode [10]. Another result from that research is that similar azimuthal oscillations are also found in the near plume of the thruster[126].

Similarly, Liu [127, 128] also finds azimuthal oscillations in the BHT-200 and BHT-600 thrusters via high speed-imaging techniques. Although azimuthal plasma structures are found both at low and high voltages, this is, in the ionization and current saturation parts of the I-V curve, they are more visible at low voltage. Liu finds that the velocity and frequency of the wave increase with the discharge voltage by carrying out several parametric variations. Additionally, Liu also uses krypton as propellant finding similar properties for the spoke oscillation, being the frequency and velocity of the wave higher than with xenon.

Finally, Vesselovzorov *et al.* [129] measure also azimuthal oscillations in a laboratory Hall thruster. The interest in the results of that study lie on the fact that the experimentally measured electron mobility agrees rather well with that computed from the correlated azimuthal oscillations of the plasma density and the azimuthal electric field.

Numerical results

Lomas and Kilkenny[109] support their experimental results with the numerical solution of a simplified version of the two-dimensional fluid equations of electrons, ions and neutrals in a Hall accelerator with hydrogen as propellant. Even though the conditions of the simulations are far from modern HETs, it is interesting to see that low frequency azimuthal oscillations can be promoted by the ionization in a Hall device.

More recently, Lam *et al.*[89] have developed a hybrid code that is the natural extension of Fife's hybrid model[56, 53] to the axial-azimuthal space. Azimuthal effects are kept in the formulation at the expense of not solving the radial direction. The results of this code for the nominal operating point of the simulated thruster show a tilted wave with a phase velocity of 4 km/s, a wave mode number of $m = 4$ and a frequency of 40 kHz. This wave propagates inside the channel in the **E**x**B** direction and upstream whereas in the plume the axial direction of propagation of the wave is reversed. This seems to be correlated with the change in the gradient of the magnetic field. Moreover, in the region of maximum magnetic field the waves are mostly longitudinal as detected experimentally[114, 115].

Theory: low-frequency local-linear-stability models

Most of the stability analyses of the Hall discharge carried out so far are local as opposed to those where the stability is analysed globally. The few studies that do account globally for the axial variations of the inhomogeneous plasma are focused on the high frequency range [130, 131, 132, 133, 134, 135]. The local stability analyses covering the low and medium frequency ranges may be grouped according to whether or not they include ionization in the formulation. Let us start our discussion with those that do not take it into account.

Even though there exist some previous local stability analyses dedicated to Hall devices [136, 137], Morozov *et al.* [2] carried out the first azimuthal stability analysis of the Hall discharge. They used a cold, two-fluid, quasineutral, collisionless, electrostatic formulation without electron inertia. Their main conclusion was the existence of unstable azimuthal oscillations in regions where the gradient of the magnetic field to plasma density ratio is negative, i.e.:

$$d/dx(B_0/n_0) < 0$$

Esipchuk and Tilinin [1] extended the linear stability analysis of Morozov *et al.* by accounting for electron inertia, and electromagnetic and non-quasineutral effects. In the electrostatic low frequency and quasineutral limit of the resulting dispersion relation, similar results to those of Morozov [2] were obtained. The stability criterion derived by Esipshuk and Tilinin seems to cover the gradient-induced oscillations measured experimentally in the medium frequency range. Additionally, low frequency quasi-longitudinal waves are predicted when $d/dx(B_0/n_0) > 0$. Furthermore, when electron inertia terms are retained in the model, high frequency, azimuthal, long wavelength oscillations are predicted near the lower-hybrid frequency.

Kapulkin and Guelman[138, 139] carry out another stability analysis with a two-fluid formulation specifically suited for the region very close to the anode where the ionization is negligible and the temperature and the magnetic curvature contribute to the azimuthal drift of the electron flow. The main novelty with respect to the work of Esipchuk and Tilinin is the inclusion of electron pressure effects. The electron temperature is included in the model although its oscillations are neglected. The results indicate the presence of an unstable oblique wave of low frequency that can promote electron conductivity towards the anode.

More recently, Frias *et al.*[140, 141] have revisited the local stability of the Hall discharge by means of a two-fluid collision-less model and applied the resulting stability criterion to experimental and numerical profiles of the Hall discharge[142, 143]. The local stability analysis of Frias *et al.* [140] resembles those by Morozov[2] and by Esipchuk and Tilinin[1]. However, the effect of the compressibility of the electron flow, which includes the **E**x**B** and the diamagnetic drifts, is accounted for completely, yielding a stability criterion with different numerical factors, but qualitatively similar in form to those by Morozov *et al.*, and by Esipchuk and Tilinin. Additionally, the effect of the electron temperature oscillations on the stability is evaluated by Frias *et al.*. The resulting stability criterion shows similar features to the analysis without electron temperature oscillations, but near the stability threshold, the differences are important, causing that stable cases become unstable if electron temperature perturbations are accounted for. However, no attempt is done to analyse the influence of the ionization in the stability of the discharge in the low frequency range.

Within the group of local stability analyses accounting for ionization, the first work is due to Lomas and Kilkenny [109] in the 1970's . Beyond reproducing the Janes-Lowder experimental results and using numerical simulations to analyze the spoke oscillation, they carried out a linear stability analysis of the Hall accelerator and suggested that the spokes detected experimentally are linked to the growth of electro-thermal instabilities. However, the analysis is performed for hydrogen, instead of a more typical propellant of Hall thrusters like Xenon.

Chesta *et al.*[144] evaluate numerically the linear stability of experimental steady-state profiles with a three-fluid description of the discharge including ionization, particle collisions and electromagnetic effects. The main conclusion of that research is that low frequency azimuthal oscillations are largely caused by the ionization process and driven in part by the gradients of the magnetic field and plasma density. However, no investigation is carried out to describe the exact mechanism of the instability by means of simple analytical expressions.

Gallardo and Ahedo[16] use a three-fluid formalism without electromagnetic terms to analyse the relation of the low frequency azimuthal waves with the electron anomalous diffusion. The main novelty with respect to previous studies is that the azimuthal three-fluid unsteady equations are solved to observe non-linear saturation effects. The conditions analysed in that case correspond to the ionization region of the channel. The results predict a $m = 3$ azimuthal wave promoted by the ionization process with a phase velocity of 2.7 km/s travelling in the -**E**x**B** direction.

Finally, Malik and Singh [145] perform a local stability analysis accounting for ionization partially. The ion and electron equations do contain source terms related to ionization, but the model does not include the neutral equations, which are important in the low frequency range. In fact, the breathing mode, one of the main low frequency longitudinal oscillations in Hall thrusters, cannot be reproduced without considering the neutrals as part of the model. The results from Malik and Singh predict unstable oscillations in the range of 100 kHz, which is above the range where the spoke is normally measured.

Conclusions

Low frequency azimuthal oscillations of plasma density and electric field have been measured experimentally in various HETs operating at several points of the current-voltage curve and preliminary results from existing simulation codes support the existence of these oscillations. While oscillations in the near field plume could be promoted by the negative gradient of the magnetic field, as originally proposed by Morozov *et al.* and Esipchuk and Tilinin, the reason for the growth of instabilities inside the thruster is not so clear. It is possible that the ionization is determinant in this case. The wave propagation is normally in **E**x**B** direction although a few experiments report oscillations in the opposite direction. As a conclusion from this literature review, it can be stated that it is worth to revisit the local linear stability of the Hall discharge accounting for the ionization process completely.

2.7.2 High frequency oscillations

Experimental results

Already in the 1970's, azimuthal high frequency oscillations with a phase velocity close to the **E**x**B** drift were proposed theoretically and later on detected experimentally by Esipchuk and Tilinin [1]. Those oscillations appear in the region of negative magnetic field gradient as long wavelength waves that rotate with no phase shift along the thruster. Tilinin [74] continued with the analysis of these high frequency waves, confirming their previous findings and obtaining further insights about their properties that can be summarized as: decreasing intensity with increasing frequency, significant dependence on the operation point and increasing amplitude with the magnetic field.

At the end of the 1990's and the beginning of the 2000's, the interest in the HF spectrum gained inertia again and several experimental studies have been carried out with modern HETs ever since. In particular, Guerrini *et al.* [64] detect azimuthal oscillations in the near field of the SPT-50 within the 1-10 MHz range using Langmuir probes. With a similar experimental set-up and a 900 W laboratory HET, Litvak *et al.* [146, 65] observe intermittent signals of a few MHz with an azimuthal phase velocity close to the electron drift and a wave mode $m = 1$. All these oscillations seem to correspond to the electron drift waves proposed by Esipchuk and Tilinin. The frequency of the oscillation varies significantly with the operating point of the thruster since the electron drift velocity is directly proportional to the electric field and inversely proportional to the magnetic field. An interesting conclusion of the analysis of Litvak *et al.* is the fact that the velocity of the wave is not equal to the local value of the **E**x**B** drift, and at the same time is constant along the thruster. These facts point to a non-local instability mechanism. Additionally, Litvak *et al.* also observe oscillations of higher wave-numbers that are independent from the $m = 1$ oscillation.

Lately, Lazurenko *et al.* have performed a series of detailed studies on the HF spectrum of two laboratory thrusters of different size and power, SPT-100-ML and PPS-X000-ML, using various experimental techniques, both intrusive and non-intrusive: isolated antennas, magnetic coils and electrostatic probes [147, 148, 149, 150, 151, 152, 153, 154, 155]. As a summary of those analyses, Lazurenko presents in Ref. [155] the main properties of the HF signals, in good agreement with the work of Esipchuk *et al.*, Guerrini *et al.* and Litvak *et al.*:

1. *frequency of a few MHz (1-10 MHz) and fundamental mode* $m = 1$: the instability can evolve into more complex structures with several $m = 1$ signals superimposed and/or higher harmonics.

2. *azimuthal propagation*: the oscillations propagate mostly azimuthally in the near field of the thruster, this is, from the magnetic field maximum to a distance of a few cm from the thruster exit. Axial oscillations in this frequency range are also observed inside the thruster and further downstream of the near field.

3. *intermittency*: the HF bursts take place only during the descent part of the discharge current of the breathing mode oscillations.

4. *electron drift velocity*: the phase velocity of the azimuthal waves is close to the **E**x**B** drift and, more importantly, constant along the thruster.

5. *azimuthal asymmetry*: the azimuthal velocity of the wave is not axi-symmetric possibly due to an asymmetry of the electric field, which, in turn, may be caused by the presence of the hollow cathode.
6. *variation of the velocity over time*: the observed velocity of the instability increases from the onset to the disappearance of the wave as a consequence of the variation of the electric field over the breathing mode period.
7. *gradient induced waves*: based on the previous properties, Lazurenko suggests that these signals correspond to the fluctuations induced by magnetic field and density gradients proposed theoretically by Morozov [2] and Esipchuk and Tilinin [1] rather than the resistivity instabilities suggested by Litvak *et al.* [156].
8. *maximum frequency in optimized operation*: as the mass flow is modified to study different operating points and the magnetic field is optimized, the frequency of the instability remains constant and maximal.
9. *small azimuthal extension*: it is estimated that the size of the wave is one order of magnitude smaller than the channel circumference.
10. *linear azimuthal dispersion relation*: experiments show a nearly linear relation between the frequency and the wave number of the oscillation.

Knoll *et al.* confirm several of the previous properties in a experimental study [157, 67] carried out with a laboratory Hall thruster and a group of three Langmuir probes separated axially and azimuthally that is moved along the thruster. This experimental set-up allows the detection of axial and azimuthal waves and its variation with the axial location. The results of the analysis also reinforce the idea of a non-local instability due to the constant azimuthal speed of the oscillations. Interestingly, in this work it is also pointed out that the velocity of the azimuthal waves is consistently smaller than the electron drift velocity and thus different growth mechanisms than those indicated by Lazurenko are suggested. More recently, Tomilin [158] has detected high frequency oscillation of similar properties in a SPT Hall thruster with high specific impulse.

On the other hand, Albarede *et al.* analyse in Ref. [159] low frequency processes and how they are related to the high frequency oscillations. In particular, as a consequence of the breathing mode, the maximum of plasma density and the minimum of electric potential in the near field plume take place at the same time as the high frequency bursts. According to Albarede, this fact supports the idea that the cathode dynamics and the beam neutralization process might promote the HF signals.

Another interesting set of experimental studies are those by Kurzyna *et al.* and Bonhomme *et al.* [160, 161, 162, 163, 164]. In these studies, a novel technique called Empirical Mode Decomposition is used to analyse the signals obtained from experiments. This method, even though it lacks a strong mathematical foundation, is particularly well suited for the analysis of non-stationary signals. For such cases, Fourier analysis tends to fail because of the intermittency. In the first of those researches [160], a thorough evaluation is carried out of the different oscillations detected with that technique. The usual oscillations (breathing mode, transit-time and electron drift oscillations) are cleanly filtered and observed. In a later research, the variation of the oscillations with the operating point is considered. It turns out that at high voltage the breathing mode almost disappears and transit time oscillations become dominant. And more interestingly, the HF burst appear now during the descent part of the latter ones, what reinforces the idea of a coupling between the dominating medium frequency oscillation and the high frequency waves.

In line with the numerical results in Refs. [93, 83, 82], in a series of experiments, first Adam *et al.* in Ref. [165] and later on Tsikata *et al.* [68, 69, 70, 71], have detected via collective light scattering, a technique commonly used in nuclear fusion researches, high frequency and short wavelength oscillations with azimuthal propagation. The experiments confirm the presence at the thruster exit of oscillations of a few MHz (1-10 MHz) with a wavelength of the order of the electron Larmor radius (1 mm) and a velocity of a few km/s, which is close to the ion acoustic velocity. The results seem to indicate that the propagation velocity has a small component in the axial direction towards the anode. Given the short wavelength of this oscillations, and the mechanism based on the interaction between the electron gyro-motion and electric field oscillations, it is clear that these oscillations cannot be analysed with fluid equations.

Numerical results

Hirakawa *et al.* [92, 166] implemented the first azimuthal numerical code for the analysis of oscillations using a particle-in-cell method. In this numerical study, high frequency oscillations were observed propagating in the **E**x**B** direction and enhancing the electron mobility, which turned out to be of the order of the Bohm velocity. However, this study does not reproduce the variation of the Hall parameter along the thruster and, in particular, the presence of a dip of mobility around the thruster, which is one of the key properties of the anomalous diffusion.

As already mentioned, Adam *et al.* [93] have implemented a full PIC simulation code in two dimensions ($r - \theta$). Even though the computational cost is enormous, some results have been obtained for a reduced and simplified geometry. The model does not require adding any artificial diffusion thanks to the presence of azimuthal high frequency waves that enhance the cross-field electron mobility. These waves have a wavelength close to the electron Larmor radius and propagate with a velocity of a few km/s. According to the simulations, the density variations introduced by the waves can be even higher than the average value in some parts of the thruster. Moreover, the growth of this type of oscillations is supported by the stability analysis carried out by Ducrocq *et al.* [167] who makes use of the kinetic theory for electrons rather than the conventional fluid approach. Moreover, there are experimental results verifying the existence of these type of oscillations. These waves could correspond to those detected by Tsikata *et al.* in Ref. [69, 71]. Further numerical analyses following the work of Adam *et al.* are presented in Refs. [168] and [169] and similar results are obtained by Coche and Garrigues with an independent PIC code [83, 82].

Lately, some other bi-dimensional numerical codes have been developed. Lam *et al.* [89], apart from a hybrid $r - \theta$ code, have implemented in parallel a fully fluid simulation code following the preliminary work of Knoll *et al.* [170]. With this code, Lam *et al.* predict tilted waves at 5 MHz with a mode number of $m = 3$ in the channel and the near field plume travelling in the -**E**x**B** direction with a phase velocity of 300 km/s. The presence of these waves gives the required conductivity to the electron flow and makes it unnecessary to introduce in the simulation artificial mobility. However, there are two arguments against this result worth mentioning: in first place, experiments normally detect high frequency azimuthal waves only in the near field plume, not further upstream; and, in second place, the simulated waves propagate in the opposite direction than what is normally measured.

Theoretical models

Esipchuk and Tilinin [1] predict, apart from the low frequency oscillation already mentioned above, a high frequency wave of the electron-drift type. The inclusion of the electron inertia in the governing equations is the key to turn the dispersion relation into a cubic equation for the frequency. If the electron inertia is neglected, the dispersion relation reduces to a quadratic equation whose solutions are in the medium frequency range. If not, roots of the cubic equation can appear in the high frequency range, close to the lower hybrid frequency, for certain combinations of the parameters of the model. A wave of similar properties is normally detected experimentally as already described above.

In a series of studies [171, 172, 173], Baranov *et al.* analyse separately the stability of the different regions of the thruster accounting for different effects in each one of them: temperature terms and zero electric field in the ionization region and strong electric and magnetic fields in the acceleration region. The results predict azimuthal waves of high frequency both in the ionization and acceleration regions. In the case of the ionization region, the temperature seems to be the driving force. However, there is no experimental evidence of the existence of such high frequency azimuthal waves in the rear part of the thruster. Besides, no ionization terms and neutral gas equations are considered in the model and therefore, low frequency phenomena are not taken into account, which could modify the behaviour of the dynamical system.

In Ref. [156] Litvak et al. focus on the effect of the electron collisions on the stability of the discharge. In their research, two types of unstable azimuthal oscillations appear: an electrostatic instability and electromagnetic one. Both are promoted by the electron collisionality, but the former rotates with a frequency close to the lower hybrid frequency (10 MHz) while the latter propagates at the Alfven speed with a frequency of 1 MHz. According to the analysis, the higher growth rate of the electrostatic oscillation makes it more likely to appear.

A formalism to analyse the linear stability of a two-fluid electrostatic model of the Hall discharge is presented by Thomas *et al.* in Refs. [174, 175]. The result in the no-gradients limit coincides with the expression of Baranov *et al.* [171], but the analysis is extended to account for electron-drift shear, electron-neutral collisions and electron temperature by means of an equation of state. The resulting dispersion relation is applied to the experimental profiles of a laboratory thruster and the results indicate the presence of unstable oscillations in the high frequency regime above 1 MHz.

In Ref. [176], Spektor uses a linear stability method including collisions, macroscopic gradients and temperature terms to derive a dispersion relation that is used in turn to compute the equivalent anomalous electron collision frequency from plasma susceptibility. This approach has been successfully applied in the area of MPD thrusters to characterize the electron conductivity in those devices, but in the case of Hall thrusters, the results obtained by Spektor predict an anomalous diffusion scaling as $1/B^4$. Clearly, this relation is against the experimentally verified scaling law for the Bohm diffusion of $1/B$ [43].

On the other hand, Ducrocq *et al.* [167, 177, 178] use a kinetic model to describe the electron species. In this research an electron drift instability of short wave-length, close to the electron Larmor radius (1 mm), and high frequency (1-10 MHz), is predicted as a result of a resonance between the gyro-motion of the electrons and oscillations of the electric field. This analysis agrees with the numerical results of Adam *et al.* [93] and Coche and Garrigues [82, 83] obtained with different PIC codes.

A second approach to study the stability of the discharge involves analysing the eigenvalue problem obtained when the axial coordinate is not resolved in the usual exponential form (i.e., $\exp(ik_x x)$). This method is used by Kapulkin *et al.* in several studies [131, 132, 133, 135] as well as by Litvak *et al.* in Ref. [130]. The same approach is used in classical fluid mechanics to study the well known Rayleigh instability and hence the name of Rayleigh type of instabilities in Hall thrusters. The main advantage of this method over the previous one is that the former is based on a local analysis, while with the latter approach the stability of the discharge is analysed as a whole. Moreover, it has been observed experimentally that the velocity of the azimuthal waves is constant along the near field plume. This fact points to a non-local mechanism and supports the use of more elaborated stability methods such as those used by Kapulkin and Litvak.

Kapulkin *et al.* in Ref. [131, 132] and Litvak *et al.* in Ref. [130] conclude separately that Rayleigh type of instabilities appear inside the Hall thruster with frequencies higher than the lower hybrid frequency. In both researches, the phase speed of the unstable wave is of the order of the ratio E_{max}/B_{max}. Moreover, the exact value of the wave velocity coincides with the electron drift at a given point along the thruster. The influence of the density and magnetic field gradients is highlighted by both authors: the higher the gradients are, the lower the frequency of the wave is. As a consequence of the instability, the electric potential fall is spread out along the thruster reducing the maximum electric field. However, it is important to remark that these analyses focus on a frequency range above the one where high frequency oscillations are detected experimentally since the hybrid lower frequency is in the 1-10 MHz range for HET [5].

In a later study [133], Kapulkin *et al.* analyse waves in the lower-hybrid frequency range with the same approach. The main novelty with respect to the previous formulation is the inclusion of the ion dynamics. As a result, a resonant effect with the lower hybrid frequency appears in the dispersion equation. However, the main driver for the instability is the same as before, the electron drift velocity non-uniformity. This theoretical instability has several properties in common with those measured experimentally: azimuthal propagation in the direction of the electron drift, frequency of 1 MHz and wavelength of the order of the channel circumference and, thus, deserves more attention.

Conclusions

To sum up, long wavelength high-frequency oscillations have been detected by different researchers by means of several experimental techniques in Hall thrusters of various kinds and sizes. Thus, it seems clear that the presence of these oscillations is an essential property of the physics involved in HETs, rather than a particular feature of a given model. Their intensity makes it reasonable to propose a relation with the anomalous electron conductivity. However, it is only at the thruster exit that these oscillations are azimuthal. Thus, it is not possible to explain the excessive electron current in the channel based solely on these oscillations. In that part of the thruster there must be another mechanism enhancing the electron cross-field mobility.

On the other hand, short-wavelength high-frequency oscillations have also been observed experimentally via collective light-scattering techniques, and there are numerical results and analytical theories supporting the presence of the oscillations. Moreover, a relation with enhanced electron mobility has also been established theoretically and numerically. Thus, these oscillations could also be a relevant aspect of anomalous diffusion.

Chapter 3

Local linear stability analyses

In this chapter the local stability of the Hall thruster discharge against azimuthal perturbations is analysed by means of linear methods applied to the fluid equations describing the dynamics of HET. Local stability analyses are carried out to study the effect of the different physics involved, starting from very simple models and introducing more and more terms in the formulation to capture all physics. The aim is to detect possible terms that promote instabilities in the azimuthal direction that in turn enhance the electron mobility in the axial direction. The main results and conclusions of this chapter have been presented in Ref. [18].

3.1 General governing 2D fluid equations

The general equations of the Hall discharge are presented in this paragraph. Each one of the species present in a HET (neutrals, electrons and ions) is accounted for with a separate set of macroscopic fluid equations based on different conservation principles: particle, momentum and energy conservation laws. Additionally, Poisson's equation for the electric field and a diffusive model for the electron heat flux are also included in the general formulation. However, while electrons are highly magnetized, ions are considered to be unmagnetized because the Larmor radius of the latter is much larger than the typical thruster dimensions. At the same time, ions and neutrals are modelled as cold species, this is, no temperature is included for them in the equations and, consequently, no energy equation is needed for those two species. On the other hand, the electron temperature is much larger and is considered isotropic. No multiply-charged ions are considered since their influence is not regarded crucial for the problem under analysis. The only collisional processes introduced in the formulation are the electron-neutral collisions for the exchange of momentum and for the generation of ions via bulk ionization. For simplicity, no wall losses or wall recombination are included in any of the equations although they are known to play an important role in the definition of the axial profile of the main properties. Furthermore, the electron kinetic energy is removed from the energy equation as it is negligible compared to the internal energy in most regions of the Hall Thruster. And finally, the only sink of energy introduced in the energy equation is the one associated to ionization and radiation since elastic collisions have a much smaller order of magnitude.

Under all these assumptions, the governing equations can be written as:

$$\frac{\partial n_e}{\partial t} + \nabla \cdot (n_e \mathbf{v}_e) = n_e n_n \xi_i \tag{3.1a}$$

$$\frac{\partial n_i}{\partial t} + \nabla \cdot (n_i \mathbf{v}_i) = n_e n_n \xi_i \tag{3.1b}$$

$$\frac{\partial n_n}{\partial t} + \nabla \cdot (n_n \mathbf{v}_n) = -n_e n_n \xi_i \tag{3.1c}$$

$$m_e n_e \left(\frac{\partial \mathbf{v}_e}{\partial t} + \mathbf{v}_e \cdot \nabla \mathbf{v}_e \right) = -\nabla (n_e T_e) - e n_e (\mathbf{E} + \mathbf{v}_e \times \mathbf{B}) - m_e n_e n_n \xi_e \mathbf{v}_e \tag{3.1d}$$

$$m_i n_i \left(\frac{\partial \mathbf{v}_i}{\partial t} + \mathbf{v}_i \cdot \nabla \mathbf{v}_i \right) = e n_i \mathbf{E} - m_i n_e n_n \xi_i (\mathbf{v}_i - \mathbf{v}_n) \tag{3.1e}$$

$$m_n n_n \left(\frac{\partial \mathbf{v}_n}{\partial t} + \mathbf{v}_n \cdot \nabla \mathbf{v}_n \right) = \mathbf{0} \tag{3.1f}$$

$$\frac{\partial}{\partial t} \left(\frac{3}{2} n_e T_e \right) + \nabla \cdot \left(\frac{5}{2} n_e T_e \mathbf{v}_e + \mathbf{q}_e \right) = -e n_e \mathbf{v}_e \cdot \mathbf{E} - e n_e n_n \xi_i \alpha_i E_i \tag{3.1g}$$

$$\frac{5}{2} n_e T_e \nabla T_e + e \mathbf{q}_e \times \mathbf{B} + m_e n_n \xi_e \mathbf{q}_e = \mathbf{0} \tag{3.1h}$$

$$\epsilon_0 \nabla \cdot \mathbf{E} = e(n_i - n_e) \tag{3.1i}$$

where n_n, n_e and n_i are the neutral, electron and ion densities, $\mathbf{v}_n$, $\mathbf{v}_e$ and $\mathbf{v}_i$ are the fluid velocities of neutrals, electrons and ions, T_e is the electron temperature, $\mathbf{q}_e$ is the electron heat flux, ξ_e and ξ_i represent the electron collisions for momentum exchange and ionization respectively, $\mathbf{E}$ and $\mathbf{B}$ are the electric and magnetic fields, m_i and m_e are the ion and electron masses and e and ϵ_0 are the electron charge and the permittivity of free space. Notice that the usual electron-neutral collision and ionization frequencies have been expressed as $\nu_e = n_n \xi_e$ and $\nu_i = n_n \xi_i$ to make their dependence on the neutral density explicit. Notice as well that the induced magnetic field is neglected and thus, Maxwell's equations are not included in the model and the magnetic field is equal to the field externally applied, which is stationary ($\partial \mathbf{B}/\partial t = 0$), solenoidal ($\nabla \cdot \mathbf{B} = 0$), irrotational ($\nabla \times \mathbf{B} = 0$) and mostly radial. And consequently, the electric field derives from a potential ($\nabla \phi = -\mathbf{E}$). All this implies that electromagnetic effects are neglected completely and the problem is reduced to an electrostatic formulation.

The quasi-neutrality assumption ($n_e = n_i$) has not been introduced in the general model in order to evaluate its possible influence on the stability of the discharge. However, it is well known that the plasma inside HETs is quasi-neutral and in many of the analyses presented in this chapter this hypothesis is applied.

It is important to remark that even though the equations above can be applied to fully three-dimensional problems, in this case the radial variation of the properties is neglected reducing the problem to two-dimensions: axial and azimuthal. Moreover, curvature effects are also neglected as the mean radius of the channel is typically larger than the difference between the outer and inner radii. All in all, the problem is reduced to two dimensions: x along the axial direction and y along the azimuthal direction.

3.2 Simple linear stability analysis of the acceleration region

The first stability analysis of the HET discharge was carried out by Morozov *et al.* in Ref. [2]. A more extensive analysis was performed by Esipchuk and Tilinin in Ref. [1], which reduces to Morozov's results in the limit of low frequency oscillations. The very same problem is revisited here with two goals: presenting the methodology to use with more complex models in the next sections and checking the hypothesis and results obtained by Morozov and Esipchuk. Some doubts have been raised by Barral in Ref. [19] about the validity of those studies due to the use of gradients in the formulation and thus it makes sense to revisit the analyses. Including gradients (e.g., plasma density and magnetic field) implies that the plasma is heterogeneous and thus the local method used traditionally in stability analyses is not completely applicable as explained in Ref. [179]. A similar argument is used by Barral [19] to prefer a WKB approach over traditional methods to analyse the stability of transit time oscillations.

The traditional methodology used here for the linear stability analysis of the Hall thruster discharge against azimuthal oscillations can be summarized as follows:

- derive the governing equations of the model from the general formulation under certain simplifying assumptions
- obtain the zero-th order stationary axi-symmetric solution ($\partial/\partial t = 0$, $\partial/\partial y = 0$)
- linearise the equations around the zero-th order solution assuming that perturbations with respect it are much smaller
- use a Fourier-like form for the variation of the perturbations ($\hat{f}(t, x, y) = \bar{f} \exp(-i\omega t + ik_x x + ik_y y)$) in order to transform the differential problem into an algebraic one
- use dimensional analysis to reduce the number of variables of the problem
- derive a dispersion relationship relating the frequency of the perturbations (ω) with the wavelengths (k_x, k_y)
- in case that deriving or solving the dispersion relation analytically is impossible or too complex, derive the equivalent eigenvalue problem in matrix form

3.2.1 Stability equations

The main simplifying hypothesis in this case are: no electron collisions ($\xi_e = 0$), no bulk ionization ($\xi_i = 0$), no electron temperature ($T_e = 0$), no electron inertia terms ($m_e = 0$) and quasi-neutrality ($n_e = n_i$). This model corresponds approximately to the acceleration region of the Hall thruster. Under these assumptions, the general model reduces to:

$$\frac{\partial n}{\partial t} + \nabla \cdot (n\mathbf{v}_e) = 0 \tag{3.2a}$$

$$\frac{\partial n}{\partial t} + \nabla \cdot (n\mathbf{v}_i) = 0 \tag{3.2b}$$

$$\mathbf{0} = \frac{-e}{m_e} (\mathbf{E} + \mathbf{v}_e \times \mathbf{B}) \tag{3.2c}$$

$$m_i \left(\frac{\partial \mathbf{v}_i}{\partial t} + \mathbf{v}_i \cdot \nabla \mathbf{v}_i \right) = e\mathbf{E} \tag{3.2d}$$

The zero-th order solution consistent with the previous model is given by:

$$n_0 = n_0(x) \qquad n_0(x)v_{ix0}(x) = \text{const} \Rightarrow \frac{d\ln n_0}{dx} = -\frac{d\ln v_{ix0}}{dx} \tag{3.3a}$$

$$v_{ix0} > 0 \qquad v_{iy0} = 0 \qquad v_{ex0} = 0 \qquad E_{y0} = 0 \qquad E_{x0} = E_0(x) > 0 \tag{3.3b}$$

$$v_{ix0}\frac{dv_{ix0}}{dx} = \frac{e}{m_i}E_0(x) \Rightarrow \frac{dv_{ix0}}{dx} > 0 \Rightarrow \frac{dn_0}{dx} < 0 \tag{3.3c}$$

$$v_{ey0} = -E_0(x)/B_0(x) \tag{3.3d}$$

It is interesting to note that some authors tend to neglect the gradients of the plasma density or the ion velocity. However, in order to maintain the closed-drift motion of the electrons, the gradients must be kept in the zero-th order solution. Based on the electron momentum equation the electron drift is caused either by the pressure term or by the electric field which also accelerates the ions. In both cases the gradients are needed.

Under the assumption of small perturbations ($f = f_0 + \hat{f}$, $\hat{f} \ll f_0$), it is possible to linearise the previous equations around the zero-th order solution by neglecting all second order terms:

$$\frac{\partial\hat{n}}{\partial t} + n_0\left(\frac{\partial\hat{v}_{ex}}{\partial x} + \frac{\partial\hat{v}_{ey}}{\partial y}\right) + \hat{v}_{ex}\frac{dn_0}{dx} + v_{ey0}\frac{\partial\hat{n}}{\partial y} = 0 \tag{3.4a}$$

$$\frac{\partial\hat{n}}{\partial t} + n_0\left(\frac{\partial\hat{v}_{ix}}{\partial x} + \frac{\partial\hat{v}_{iy}}{\partial y}\right) + \hat{v}_{ix}\frac{dn_0}{dx} + v_{ix0}\frac{\partial\hat{n}}{\partial x} + \hat{n}\frac{dv_{ix0}}{dx} = 0 \tag{3.4b}$$

$$0 = \frac{-e}{m_e}\left(-\frac{\partial\hat{\phi}}{\partial x} + \hat{v}_{ey}B_0\right) \tag{3.4c}$$

$$0 = \frac{-e}{m_e}\left(-\frac{\partial\hat{\phi}}{\partial y} - \hat{v}_{ex}B_0\right) \tag{3.4d}$$

$$\frac{\partial\hat{v}_{ix}}{\partial t} + v_{ix0}\frac{\partial\hat{v}_{ix}}{\partial x} + \hat{v}_{ix}\frac{dv_{ix0}}{dx} = -\frac{e}{m_i}\frac{\partial\hat{\phi}}{\partial x} \tag{3.4e}$$

$$\frac{\partial\hat{v}_{iy}}{\partial t} + v_{ix0}\frac{\partial\hat{v}_{iy}}{\partial x} = -\frac{e}{m_i}\frac{\partial\hat{\phi}}{\partial y} \tag{3.4f}$$

If a Fourier-like form is used for the perturbations, the formulation is transformed into:

$$-i\omega\bar{n} + in_0(k_x\bar{v}_{ex} + k_y\bar{v}_{ey}) + \bar{v}_{ex}\frac{dn_0}{dx} + v_{ey0}ik_y\bar{n} = 0 \tag{3.5a}$$

$$-i\omega\bar{n} + in_0(k_x\bar{v}_{ix} + k_y\bar{v}_{iy}) + \bar{v}_{ix}\frac{dn_0}{dx} + v_{ix0}ik_x\bar{n} + \bar{n}\frac{dv_{ix0}}{dx} = 0 \tag{3.5b}$$

$$0 = \frac{-e}{m_e}\left(-ik_x\bar{\phi} + \bar{v}_{ey}B_0\right) \tag{3.5c}$$

$$0 = \frac{-e}{m_e}\left(-ik_y\bar{\phi} - \bar{v}_{ex}B_0\right) \tag{3.5d}$$

$$-i\omega\bar{v}_{ix} + v_{ix0}ik_x\bar{v}_{ix} + \bar{v}_{ix}\frac{dv_{ix0}}{dx} = -\frac{e}{m_i}ik_x\bar{\phi} \tag{3.5e}$$

$$-i\omega\bar{v}_{iy} + v_{ix0}ik_y\bar{v}_{iy} = -\frac{e}{m_i}ik_y\bar{\phi} \tag{3.5f}$$

Given the previous set of equations, it is possible to make the problem non-dimensional by choosing the following reference variables:

- mass : m_i
- charge : e
- time : $\omega_{ci} = eB_0/m_i$
- density: n_0
- length : $l_n = -d \ln n_0/dx > 0$

The non-dimensional version of the previous set of equations is reduced to:

$$-i\tilde{\omega}\tilde{n} + i(\tilde{k}_x\tilde{v}_{ex} + \tilde{k}_y\tilde{v}_{ey}) - \tilde{v}_{ex} + \tilde{v}_{ey0}i\tilde{k}_y\tilde{n} = 0 \tag{3.6a}$$

$$-i\tilde{\omega}\tilde{n} + i(\tilde{k}_x\tilde{v}_{ix} + \tilde{k}_y\tilde{v}_{iy}) - \tilde{v}_{ix} + \tilde{v}_{ix0}i\tilde{k}_x\tilde{n} + \tilde{n}\tilde{v}_{ix0} = 0 \tag{3.6b}$$

$$0 = -\tilde{\omega}_e\left(-i\tilde{k}_x\tilde{\phi} + \tilde{v}_{ey}\right) \tag{3.6c}$$

$$0 = -\tilde{\omega}_e\left(-i\tilde{k}_y\tilde{\phi} - \tilde{v}_{ex}\right) \tag{3.6d}$$

$$-i\tilde{\omega}\tilde{v}_{ix} + \tilde{v}_{ix0}i\tilde{k}_x\tilde{v}_{ix} + \tilde{v}_{ix}\tilde{v}_{ix0} = -i\tilde{k}_x\tilde{\phi} \tag{3.6e}$$

$$-i\tilde{\omega}\tilde{v}_{iy} + \tilde{v}_{ix0}i\tilde{k}_y\tilde{v}_{iy} = -i\tilde{k}_y\tilde{\phi} \tag{3.6f}$$

Notice that due to particle and momentum conservation, the zero-th order solution verifies $dv_{ix0}/dx = v_{ix0}/l_n$ and $\tilde{v}_{ix0}^2 = -\tilde{v}_{ey0}$.

Equations in (3.6) yield the following dispersion relationship:

$$\begin{aligned} 0 = &\left(-i\tilde{\omega} + (i\tilde{k}_x + 1)\tilde{v}_{ix0}\right)^2\left(-i\tilde{\omega} + i\tilde{k}_x\tilde{v}_{ix0}\right) + \\ &+ \left((i\tilde{k}_x - 1)(-i\tilde{\omega} + i\tilde{k}_x\tilde{v}_{ix0})\tilde{k}_x/\tilde{k}_y + i\tilde{k}_y(-i\tilde{\omega} + (i\tilde{k}_x + 1)\tilde{v}_{xi0})\right)\left(-i\tilde{\omega} + i\tilde{k}_y\tilde{v}_{ey0}\right) \end{aligned} \tag{3.7}$$

This dispersion relation is a cubic equation for $\tilde{\omega}$ and defines implicitly the dependence of the frequency on the wavelengths of the perturbation $\tilde{\omega} = \tilde{\omega}(\tilde{k}_x, \tilde{k}_y; \tilde{v}_{ix0}, \tilde{v}_{ey0}(\tilde{v}_{xi0}))$ where the only parameter is the non-dimensional ion velocity $\tilde{v}_{xi0}$. The condition for growing unstable perturbations is $\mathrm{Im}(\tilde{\omega}) > 0$.

Equations in (3.6) can also be expressed in matrix form as a general eigenvalue problem in $\tilde{\omega}$: $(A\tilde{\omega} + B)\mathbf{u} = 0$ where the vector $\mathbf{u}$ is defined as $\mathbf{u} = (\tilde{n}, \tilde{v}_{ex}, \tilde{v}_{ey}, \tilde{v}_{ix}, \tilde{v}_{ix}, \tilde{\phi})$ and the matrices A and B are defined as:

$$A = \begin{pmatrix} -i & 0 & 0 & 0 & 0 & 0 \\ -i & 0 & 0 & 0 & 0 & 0 \\ 0 & 0 & 0 & 0 & 0 & 0 \\ 0 & 0 & 0 & 0 & 0 & 0 \\ 0 & 0 & 0 & -i & 0 & 0 \\ 0 & 0 & 0 & 0 & -i & 0 \end{pmatrix}$$

$$B = \begin{pmatrix} i\tilde{k}_y\tilde{v}_{ey0} & i\tilde{k}_x - 1 & i\tilde{k}_y & 0 & 0 & 0 \\ (i\tilde{k}_x + 1)\tilde{v}_{ix0} & 0 & 0 & i\tilde{k}_x - 1 & i\tilde{k}_y & 0 \\ 0 & 0 & \tilde{\omega}_e & 0 & 0 & -i\tilde{k}_x\tilde{\omega}_e \\ 0 & -\tilde{\omega}_e & 0 & 0 & 0 & -i\tilde{k}_y\tilde{\omega}_e \\ 0 & 0 & 0 & (i\tilde{k}_x + 1)\tilde{v}_{ix0} & 0 & i\tilde{k}_x \\ 0 & 0 & 0 & 0 & i\tilde{k}_x\tilde{v}_{ix0} & i\tilde{k}_y \end{pmatrix}$$

Due to the fact that electron inertia and electromagnetic terms have been neglected in the formulation, there are no time derivatives of the variables $\tilde{v}_{ex}$, $\tilde{v}_{ey}$ and $\tilde{\phi}$ in the equations (i.e., all coefficients in matrix A are zero for these variables), and this makes it possible to pre-eliminate them. In that case, the general eigenvalue problem can be reduced to:

$$(C\tilde{\omega} + D)\mathbf{w} = \mathbf{0} \tag{3.8}$$

where $\mathbf{w} = (\tilde{n}, \tilde{v}_{ix}, \tilde{v}_{ix})$ and

$$C = \begin{pmatrix} -i & 0 & 0 \\ i\tilde{k}_x/\tilde{k}_y & -i & 0 \\ i & 0 & -i \end{pmatrix}$$

$$D = \begin{pmatrix} (i\tilde{k}_x + 1)\tilde{v}_{ix0} & (i\tilde{k}_x - 1) & i\tilde{k}_y \\ -i\tilde{k}_x\tilde{v}_{ey0} & (i\tilde{k}_x + 1)\tilde{v}_{ix0} & 0 \\ -i\tilde{k}_y\tilde{v}_{ey0} & 0 & i\tilde{k}_x\tilde{v}_{ix0} \end{pmatrix}$$

3.2.2 Comparison with Morozov and Esipchuk's dispersion relations

In order to recover Morozov and Esipchuk's dispersion relations, it is necessary to assume short wavelength perturbations ($\tilde{k}_x \gg 1$). Under this assumption, equation (3.7) reduces to:

$$0 = (-i\tilde{\omega} + i\tilde{k}_x\tilde{v}_{ix0})^2 + (-i\tilde{\omega} + i\tilde{k}_y\tilde{v}_{ey0})i\tilde{k}^2/\tilde{k}_y \tag{3.9}$$

where $\tilde{k} = \sqrt{\tilde{k}_x^2 + \tilde{k}_y^2}$ is the wavelength of the perturbation. Note that the trivial solution ($\tilde{\omega} = -i\tilde{v}_{ix0}$) yields a stable solution, and thus has been directly removed from the dispersion relation.

The short wavelength hypothesis ($\tilde{k}_x \gg 1$) is equivalent to neglect the gradients of the ion velocity, v_{ix0}, and the influence of the density gradient in the ion continuity equation. This assumption is incompatible with the analysis of purely azimuthal waves ($\tilde{k}_x = 0$), which are of interest here.

Equation (3.9) is the non-dimensional version of equation (25) from Ref. [1]. The only difference is the definition of the reference length, l_n. Here, it only depends on the density gradient, $l_n = d\ln n_0/dx$, but in Ref. [1] the gradient of the magnetic field also appears, $l_B = d\ln(n_0/B_0)/dx$. A similar discrepancy has been detected by Barral in Ref. [19]. The reason for this discrepancy lies on the fact that the electron axial and azimuthal velocity expressions deduced from the electron momentum equations are replaced in the electron continuity equation before the linearisation and the Fourier-expansion of the equations. This causes the gradient of the magnetic field to appear in the dispersion relation proposed by Morozov, and Esipchuk and Tilinin. It is unclear which approach is more consistent. In fact, this shows that the local stability analysis has its limitations while dealing with heterogeneous plasmas.

3.2.3 Azimuthal oscillations

In the case of purely azimuthal oscillations ($\tilde{k}_x = 0$), the dispersion relation (3.7) is simplified considerably. Apart from the trivial solution ($\tilde{\omega} = -i\tilde{v}_{ix0}$), which is stable, the remaining solutions verify the following relation:

$$0 = (-i\tilde{\omega} + \tilde{v}_{ix0})(-i\tilde{\omega}) + i\tilde{k}_y(-i\tilde{\omega} + i\tilde{k}_y\tilde{v}_{ey0}) \tag{3.10}$$

In the range of low frequency oscillations ($\tilde{\omega} \ll \tilde{k}_y\tilde{v}_{ey0}$), the dispersion relation can be simplified to:

$$0 = (\tilde{\omega} + i\tilde{v}_{ix0})\tilde{\omega} + \tilde{k}_y^2\tilde{v}_{ey0} \tag{3.11}$$

Taking into account that $-\tilde{v}_{ey0} = \tilde{v}_{ix0}^2$, the solutions of equation (3.11) can be expressed as:

$$\tilde{\omega} = \frac{1}{2}\tilde{v}_{ix0}\left(-i \pm \sqrt{4\tilde{k}_y^2 - 1}\right)$$

This dispersion relation is applicable to the low frequency range and corresponds to stable solutions for all possible values of the wave number $\tilde{k}_y$.

3.2.4 Influence of the electron temperature

The electron temperature has been neglected in the previous analysis. However, it is easy to evaluate its effect in the linear stability analysis. It is possible to account for it by introducing a constant temperature, T_{e0}, in the electron momentum equation. No perturbations on the electron temperature are considered at this stage and thus, the energy equation is not needed in the formulation. The resulting dispersion relation is:

$$\begin{gathered} 0 = \left(-i\tilde{\omega} + (i\tilde{k}_x + 1)\tilde{v}_{ix0}\right)^2 \left(-i\tilde{\omega} + i\tilde{k}_x\tilde{v}_{ix0}\right) + \\ + \left((i\tilde{k}_x - 1)(-i\tilde{\omega} + i\tilde{k}_x\tilde{v}_{ix0})\tilde{k}_x/\tilde{k}_y + i\tilde{k}_y(-i\tilde{\omega} + (i\tilde{k}_x + 1)\tilde{v}_{xi0})\right)\left(-i\tilde{\omega} + i\tilde{k}_y(\tilde{v}_{ey0} - 2T_{e0})\right) \end{gathered} \tag{3.12}$$

The difference with respect to (3.7) is the presence of the temperature $\tilde{T}_{e0}$ with the electron azimuthal velocity, $\tilde{v}_{ey0}$, in the last term of the dispersion relation. Besides, the zero-th order solution verifies now $(-\tilde{v}_{ey0}) = \tilde{v}_{ix0}^2 - \tilde{T}_{e0}$. With these two important differences, the dispersion relation for purely azimuthal oscillations in the low frequency range is given by:

$$0 = (\tilde{\omega} + i\tilde{v}_{ix0})\tilde{\omega} + \tilde{k}_y^2(\tilde{v}_{ey0} - 2\tilde{T}_{e0}) \tag{3.13}$$

whose solutions are:

$$\tilde{\omega} = \frac{1}{2}\tilde{v}_{ix0}\left(-i \pm \sqrt{4\tilde{k}_y^2(1 + \tilde{T}_{e0}/\tilde{v}_{ix0}^2) - 1}\right)$$

Anyway, the stability of the perturbations remains unchanged with respect to the case with cold electrons.

3.3 Influence of additional terms

In the previous section the stability of the acceleration region was analysed with a very simple model. In this paragraph several assumptions are relaxed in order to study the separated and combined effects of plasma non-quasineutraility ($n_e \neq n_i$), electron inertia ($m_e \neq 0$), closed-drift gradient ($dv_{ey0}/dx \neq 0$) and electron-neutral collisions ($\xi_e \neq 0$). Some authors claim that these effects promote the growth of instabilities in the azimuthal direction and therefore it is interesting to study them separately. The effect of the collisions is in any case small compared to the electron Larmor frequency (i.e., $m_e\nu_e/eB_0 \ll 1$) what ensures that electrons exhibit the usual closed-drift motion inside the thruster. All these terms appear as small corrections to the dispersion relation obtained previously and thus regular and singular perturbations methods are used to analyse the influence of the different elements. Moreover, the resulting dispersion relation is compared against those proposed by other authors.

The formulation obtained under the previous hypothesis is given by:

$$\frac{\partial n_e}{\partial t} + \nabla \cdot (n_e \mathbf{v}_e) = 0 \tag{3.14a}$$

$$\frac{\partial n_i}{\partial t} + \nabla \cdot (n_i \mathbf{v}_i) = 0 \tag{3.14b}$$

$$m_e n_e \left(\frac{\partial \mathbf{v}_e}{\partial t} + \mathbf{v}_e \cdot \nabla \mathbf{v}_e \right) = -en_e(\mathbf{E} + \mathbf{v}_e \times \mathbf{B}) - m_e n_e \nu_e \mathbf{v}_e \tag{3.14c}$$

$$m_i n_i \left(\frac{\partial \mathbf{v}_i}{\partial t} + \mathbf{v}_i \cdot \nabla \mathbf{v}_i \right) = en_i \mathbf{E} \tag{3.14d}$$

$$\epsilon_0 \nabla \cdot \mathbf{E} = e(n_i - n_e) \tag{3.14e}$$

The corresponding zero-th order solution can be assumed to be quasineutral and without terms of electron inertia. It is described by the following relations:

$$n_{i0} = n_{e0} = n_0(x) \tag{3.15a}$$

$$n_0(x)v_{ix0} = \text{const} \Rightarrow \frac{d\ln n_0}{dx} = -\frac{d\ln v_{ix0}}{dx} \tag{3.15b}$$

$$n_0(x)v_{ex0} = \text{const} \Rightarrow \frac{d\ln n_0}{dx} = -\frac{d\ln v_{ex0}}{dx} \tag{3.15c}$$

$$v_{ix0} > 0 \qquad v_{iy0} = 0 \qquad E_{y0} = 0 \tag{3.15d}$$

$$E_{x0} = E_0(x) > 0 \tag{3.15e}$$

$$v_{ix0}\frac{dv_{ix0}}{dx} = \frac{e}{m_i}E_0(x) \Rightarrow \frac{dv_{ix0}}{dx} > 0 \Rightarrow \frac{dn_0}{dx} < 0 \tag{3.15f}$$

$$v_{ey0} = -\frac{E_0(x)}{B_0(x)} \tag{3.15g}$$

$$v_{ex0} = \frac{m_e\nu_e(x)}{eB_0(x)}v_{ey0}(x) \tag{3.15h}$$

The linearised equations can be written as:

$$\frac{\partial \hat{n}_e}{\partial t} + n_0\left(\frac{\partial \hat{v}_{ex}}{\partial x} + \frac{\partial \hat{v}_{ey}}{\partial y}\right) + \hat{v}_{ex}\frac{dn_0}{dx} + v_{ex0}\frac{\partial \hat{n}_e}{\partial x} + v_{ey0}\frac{\partial \hat{n}_e}{\partial y} + \hat{n}_e\frac{dv_{ex0}}{dx} = 0 \tag{3.16a}$$

$$\frac{\partial \hat{n}_i}{\partial t} + n_0\left(\frac{\partial \hat{v}_{ix}}{\partial x} + \frac{\partial \hat{v}_{iy}}{\partial y}\right) + \hat{v}_{ix}\frac{dn_0}{dx} + v_{ix0}\frac{\partial \hat{n}_i}{\partial x} + \hat{n}_i\frac{dv_{ix0}}{dx} = 0 \tag{3.16b}$$

$$\frac{\partial \hat{v}_{ex}}{\partial t} + v_{ex0}\frac{\partial \hat{v}_{ex}}{\partial x} + v_{ey0}\frac{\partial \hat{v}_{ex}}{\partial y} + \hat{v}_{ex}\frac{dv_{ex0}}{dx} = \frac{-e}{m_e}\left(-\frac{\partial \hat{\phi}}{\partial x} + \hat{v}_{ey}B_0\right) - \nu_e\hat{v}_{ex} \tag{3.16c}$$

$$\frac{\partial \hat{v}_{ey}}{\partial t} + v_{ex0}\frac{\partial \hat{v}_{ey}}{\partial x} + v_{ey0}\frac{\partial \hat{v}_{ey}}{\partial y} + \hat{v}_{ex}\frac{dv_{ey0}}{dx} = \frac{-e}{m_e}\left(-\frac{\partial \hat{\phi}}{\partial y} - \hat{v}_{ex}B_0\right) - \nu_e\hat{v}_{ey} \tag{3.16d}$$

$$\frac{\partial \hat{v}_{ix}}{\partial t} + v_{ix0}\frac{\partial \hat{v}_{ix}}{\partial x} + \hat{v}_{ix}\frac{dv_{ix0}}{dx} = -\frac{e}{m_i}\frac{\partial \hat{\phi}}{\partial x} \tag{3.16e}$$

$$\frac{\partial \hat{v}_{iy}}{\partial t} + v_{ix0}\frac{\partial \hat{v}_{iy}}{\partial x} = -\frac{e}{m_i}\frac{\partial \hat{\phi}}{\partial y} \tag{3.16f}$$

$$-\left(\frac{\partial^2 \hat{\phi}}{\partial x^2} + \frac{\partial^2 \hat{\phi}}{\partial y^2}\right) = \frac{e}{\epsilon_0}(\hat{n}_i - \hat{n}_e) \tag{3.16g}$$

Assuming a Fourier-like form for the perturbations, the non-dimensional version of the resulting equations is:

$$-i\tilde{\omega}\tilde{n}_e + i(\tilde{k}_x\tilde{v}_{ex} + \tilde{k}_y\tilde{v}_{ey}) - \tilde{v}_{ex} + \tilde{v}_{ex0}i\tilde{k}_x\tilde{n}_e + \tilde{v}_{ey0}i\tilde{k}_y\tilde{n}_e + \tilde{n}_e\tilde{v}_{ex0} = 0 \tag{3.17a}$$

$$-i\tilde{\omega}\tilde{n}_i + i(\tilde{k}_x\tilde{v}_{ix} + \tilde{k}_y\tilde{v}_{iy}) - \tilde{v}_{ix} + \tilde{v}_{ix0}i\tilde{k}_x\tilde{n}_i + \tilde{n}_i\tilde{v}_{ix0} = 0 \tag{3.17b}$$

$$-i\tilde{\omega}\tilde{v}_{ex} + \tilde{v}_{ex0}i\tilde{k}_x\tilde{v}_{ex} + \tilde{v}_{ey0}i\tilde{k}_y\tilde{v}_{ex} + \tilde{v}_{ex}\tilde{v}_{ex0} = -\tilde{\omega}_e(-i\tilde{k}_x\tilde{\phi} + \tilde{v}_{ey}) - \tilde{\nu}_e\tilde{v}_{ex} \tag{3.17c}$$

$$-i\tilde{\omega}\tilde{v}_{ey} + \tilde{v}_{ex0}i\tilde{k}_x\tilde{v}_{ey} + \tilde{v}_{ey0}i\tilde{k}_y\tilde{v}_{ey} + \tilde{v}_{ex}\tilde{\gamma}\tilde{v}_{ey0} = -\tilde{\omega}_e(-i\tilde{k}_y\tilde{\phi} - \tilde{v}_{ex}) - \tilde{\nu}_e\tilde{v}_{ey} \tag{3.17d}$$

$$-i\tilde{\omega}\tilde{v}_{ix} + \tilde{v}_{ix0}i\tilde{k}_x\tilde{v}_{ix} + \tilde{v}_{ix}\tilde{v}_{ix0} = -i\tilde{k}_x\tilde{\phi} \tag{3.17e}$$

$$-i\tilde{\omega}\tilde{v}_{iy} + \tilde{v}_{ix0}i\tilde{k}_y\tilde{v}_{iy} = -i\tilde{k}_y\tilde{\phi} \tag{3.17f}$$

$$(\tilde{k}_x^2 + \tilde{k}_y^2)\tilde{\phi} = \tilde{\omega}_{pi}^2(\tilde{n}_i - \tilde{n}_e) \tag{3.17g}$$

where $\tilde{\gamma} = -(d\ln v_{ey0}/dx)/(d\ln n_0/dx)$ accounts for the gradients of the closed-drift and plasma density, $\tilde{\omega}_{pi}^2 = (e^2n_0)/(\epsilon_0 m_i\omega_i^2)$ is the non-dimensional ion plasma frequency and $\tilde{\omega}_e = (eB_0)/(m_e\omega_i) = m_i/m_e$ is the non-dimensional electron Larmor frequency. Notice that for the zero-th order solution it still holds that $(-\tilde{v}_{ey0}) = \tilde{v}_{ix0}^2$ and $\tilde{v}_{ex0} = \tilde{v}_{ey0}\tilde{\nu}_e/\tilde{\omega}_e \ll \tilde{v}_{ey0}$.

The momentum electron equations can be expressed alternatively in matrix form as:

$$S\tilde{\mathbf{v}}_e = \tilde{\omega}_e i\tilde{\mathbf{k}}\tilde{\phi}$$

where the matrix S contains both the magnetic field and collisional terms as well as the electron inertia:

$$S = \begin{pmatrix} -i\tilde{\omega} + (i\tilde{k}_x + 1)\tilde{v}_{ex0} + i\tilde{k}_y\tilde{v}_{ey0} + \tilde{\nu}_e & \tilde{\omega}_e \\ \tilde{\gamma}\tilde{v}_{ey0} - \tilde{\omega}_e & -i\tilde{\omega} + i\tilde{k}_x\tilde{v}_{ex0} + i\tilde{k}_y\tilde{v}_{ey0} + \tilde{\nu}_e \end{pmatrix}$$

In this case the dispersion relation is expressed more compact as an eigenvalue problem in matrix form: $(A\tilde{\omega} + B)\mathbf{w} = \mathbf{0}$ where $\mathbf{w} = (\tilde{n}_e, \tilde{n}_i, \tilde{v}_{ex}, \tilde{v}_{ey}, \tilde{v}_{ix}, \tilde{v}_{iy}, \tilde{\phi})$ and the matrices are:

$$A = \begin{pmatrix} -i & 0 & 0 & 0 & 0 & 0 & 0 \\ 0 & -i & 0 & 0 & 0 & 0 & 0 \\ 0 & 0 & -i & 0 & 0 & 0 & 0 \\ 0 & 0 & 0 & -i & 0 & 0 & 0 \\ 0 & 0 & 0 & 0 & -i & 0 & 0 \\ 0 & 0 & 0 & 0 & 0 & -i & 0 \\ 0 & 0 & 0 & 0 & 0 & 0 & 0 \end{pmatrix}$$

$$B = \begin{pmatrix} \begin{array}{c}(i\tilde{k}_x + 1)\tilde{v}_{ex0}+ \\ +i\tilde{k}_y\tilde{v}_{ey0}\end{array} & 0 & i\tilde{k}_x - 1 & i\tilde{k}_y & 0 & 0 & 0 \\ 0 & (i\tilde{k}_x + 1)\tilde{v}_{ix0} & 0 & 0 & i\tilde{k}_x - 1 & i\tilde{k}_y & 0 \\ 0 & 0 & \begin{array}{c}(i\tilde{k}_x + 1)\tilde{v}_{ex0}+ \\ +i\tilde{k}_y\tilde{v}_{ey0} + \tilde{\nu}_e\end{array} & \tilde{\omega}_e & 0 & 0 & -i\tilde{k}_x\tilde{\omega}_e \\ 0 & 0 & \tilde{\gamma}\tilde{v}_{ey0} - \tilde{\omega}_e & \begin{array}{c}i\tilde{k}_x\tilde{v}_{ex0}+ \\ +i\tilde{k}_y\tilde{v}_{ey0} + \tilde{\nu}_e\end{array} & 0 & 0 & -i\tilde{k}_y\tilde{\omega}_e \\ 0 & 0 & 0 & 0 & (i\tilde{k}_x + 1)\tilde{v}_{ix0} & 0 & i\tilde{k}_x \\ 0 & 0 & 0 & 0 & 0 & i\tilde{k}_x\tilde{v}_{ix0} & i\tilde{k}_y \\ \tilde{\omega}_{pi}^2 & -\tilde{\omega}_{pi}^2 & 0 & 0 & 0 & 0 & (\tilde{k}_x^2 + \tilde{k}_y^2) \end{pmatrix}$$

Nevertheless, the resulting dispersion relation can be expressed in general as:

$$\frac{1}{\tilde{\omega}_{pi}^2} = \frac{1}{(\tilde{k}_x^2 + \tilde{k}_y^2)}\left(\frac{\tilde{n}_i}{\tilde{\phi}} - \frac{\tilde{n}_e}{\tilde{\phi}}\right)$$

$$\frac{\tilde{n}_i}{\tilde{\phi}} = -\frac{(\tilde{k}_x^2 + i\tilde{k}_x)(-i\tilde{\omega} + i\tilde{k}_x\tilde{v}_{ix0}) + \tilde{k}_y^2(-i\tilde{\omega} + (i\tilde{k}_x + 1)\tilde{v}_{ix0})}{(-i\tilde{\omega} + (i\tilde{k}_x + 1)\tilde{v}_{ix0})^2(-i\tilde{\omega} + i\tilde{k}_x\tilde{v}_{ix0})}$$

$$\frac{\tilde{n}_e}{\tilde{\phi}} = \tilde{\omega}_e\frac{(-i\tilde{\omega} + i\tilde{k}_x\tilde{v}_{ex0} + i\tilde{k}_y\tilde{v}_{ey0} + \tilde{\nu}_e)(\tilde{k}_x^2 + \tilde{k}_y^2 + i\tilde{k}_x) - i\tilde{\omega}_e\tilde{k}_y + \tilde{\gamma}\tilde{k}_y(\tilde{k}_y\tilde{v}_{ex0} - \tilde{k}_x\tilde{v}_{ey0})}{\det(S)(-i\tilde{\omega} + (i\tilde{k}_x + 1)\tilde{v}_{ex0} + i\tilde{k}_y\tilde{v}_{ey0})}$$

where $\det(S)$ is the determinant of matrix S.

So far no assumption has been made on the order of magnitude of the different frequencies involved in the formulation. For typical HET conditions, it is reasonable to assume $\tilde{\omega}_e \gg \omega \sim \tilde{k}_y \tilde{v}_{ey0} \sim \tilde{\nu}_e$. If we neglect all second order terms in $(1/\tilde{\omega}_e)$, the electron density term of the dispersion relation is much simpler:

$$\begin{aligned}\frac{\tilde{n}_e}{\tilde{\phi}} &= \frac{1}{\tilde{\omega}_e}(\tilde{k}_x^2 + \tilde{k}_y^2 + i\tilde{k}_x) + \\ &+ \frac{\tilde{k}_y}{(\tilde{\omega} - \tilde{k}_y \tilde{v}_{ey0} + i(i\tilde{k}_x + 1)\tilde{v}_{ex0})}\left(1 + \frac{\tilde{\gamma}\tilde{v}_{ey0}}{\tilde{\omega}_e}(1 - i\tilde{k}_x) + \frac{i\tilde{\nu}_e}{\tilde{\omega}_e}\frac{(\tilde{k}_x^2 + \tilde{k}_y^2 + i\tilde{k}_x)}{\tilde{k}_y}\right)\end{aligned}$$

or equivalently:

$$\begin{aligned}\frac{\tilde{n}_e}{\tilde{\phi}} &= \frac{1}{\tilde{\omega}_e}(\tilde{k}_x^2 + \tilde{k}_y^2 + i\tilde{k}_x) + \\ &+ \frac{\tilde{k}_y}{(\tilde{\omega} - \tilde{k}_y \tilde{v}_{ey0})}\left(1 + \frac{\tilde{\gamma}\tilde{v}_{ey0}}{\tilde{\omega}_e}(1 - i\tilde{k}_x) + \frac{i\tilde{\nu}_e}{\tilde{\omega}_e}\left(\frac{(\tilde{k}_x^2 + \tilde{k}_y^2 + i\tilde{k}_x)}{\tilde{k}_y} - \frac{(i\tilde{k}_x + 1)\tilde{v}_{ey0}}{(\tilde{\omega} - \tilde{k}_y \tilde{v}_{ey0})}\right)\right)\end{aligned}$$

There are two limits that deserve more attention. In first place, under the short wavelength hypothesis ($\tilde{k}_x \gg 1$) all axial gradients can be neglected, and the dispersion relation simplifies to:

$$\begin{aligned}0 &= \frac{1}{\tilde{\omega}_{pi}^2} - \frac{1}{(\tilde{\omega} - \tilde{k}_x \tilde{v}_{ix0})^2} + \frac{1}{\tilde{\omega}_e} + \\ &+ \frac{\tilde{k}_y}{\tilde{k}^2(\tilde{\omega} - \tilde{k}_y \tilde{v}_{ey0})}\left(1 - \frac{\tilde{\gamma}\tilde{v}_{ey0}}{\tilde{\omega}_e} i\tilde{k}_x + \frac{i\tilde{\nu}_e}{\tilde{\omega}_e}\left(\frac{\tilde{k}^2}{\tilde{k}_y} - \frac{i\tilde{k}_x \tilde{v}_{ey0}}{(\tilde{\omega} - \tilde{k}_y \tilde{v}_{ey0})}\right)\right)\end{aligned} \tag{3.18}$$

On the other limit, purely azimuthal oscillations ($\tilde{k}_x = 0$) are characterized by the following dispersion relation:

$$\begin{aligned}0 &= \frac{1}{\tilde{\omega}_{pi}^2} - \frac{1}{\tilde{\omega}(\tilde{\omega} + i\tilde{v}_{ix0})} + \frac{1}{\tilde{\omega}_e} + \\ &+ \frac{1}{\tilde{k}_y(\tilde{\omega} - \tilde{k}_y \tilde{v}_{ey0})}\left(1 + \frac{\tilde{\gamma}\tilde{v}_{ey0}}{\tilde{\omega}_e} + \frac{i\tilde{\nu}_e}{\tilde{\omega}_e}\left(\tilde{k}_y - \frac{\tilde{v}_{ey0}}{(\tilde{\omega} - \tilde{k}_y \tilde{v}_{ey0})}\right)\right)\end{aligned} \tag{3.19}$$

In both cases, the first term represents the influence of plasma non-quasineutrality while the ion motion yields the second term. The third term represents the influence of electron inertia alone, while the fourth term captures the combined effect of the plasma density gradient, closed-drift gradient ($\tilde{\gamma}$) and electron collisions ($\tilde{\nu}_e$). For typical conditions inside HETs, it holds that $\tilde{\omega}_{pi}^2 \gg \tilde{\omega}_e$ and therefore plasma non-quasineutrality can be neglected compared to electron inertia effects. In any case, both terms affect the dispersion relation similarly. It is also interesting to note that the influence of electron collisions and the closed-drift gradient are of the same order magnitude as the electron inertia term. In the quasineutral and massless electrons limit ($\tilde{\omega}_{pi} \gg 1, \tilde{\omega}_e \gg 1$), the dispersion relations (3.9) and (3.10) are recovered.

3.3.1 Comparison with dispersion relations obtained by other authors

Baranov [171] analyses the stability of the acceleration region with a simplified version of the model presented here. In particular, all gradients are neglected as well as electron collisions under the short wavelength hypothesis. With those assumptions equation (3.18) reduces to:

$$0 = \frac{1}{\tilde{\omega}_{pi}^2} - \frac{1}{(\tilde{\omega} - \tilde{k}_x \tilde{v}_{ix0})^2} + \frac{1}{\tilde{\omega}_e} \tag{3.20}$$

Equation (3.20) is equivalent to equation (3) of Ref. [171] in the limit of unmagnetized ions ($\omega_i \ll \omega$) and highly magnetised electrons ($\omega_e \gg \omega$).

Esipchuk [1] derives a dispersion relation for a collisionless plasma with no velocity gradients. In that case equation (3.18) reduces to:

$$0 = \frac{1}{\tilde{\omega}_{pi}^2} - \frac{1}{(\tilde{\omega} - \tilde{k}_x \tilde{v}_{ix0})^2} + \frac{1}{\tilde{\omega}_e} + \frac{\tilde{k}_y}{\tilde{k}^2(\tilde{\omega} - \tilde{k}_y \tilde{v}_{ey0})} \left(1 - \frac{\tilde{\gamma}\tilde{v}_{ey0}}{\tilde{\omega}_e} i\tilde{k}_x\right) \tag{3.21}$$

In the electrostatic limit, equation (22) of Ref. [1] is similar to equation (3.21). The main difference is related to the way the closed-drift velocity gradient appears in the formulation. Here the effect scales as $(1/\tilde{\omega}_e)$ while in Esipchuk's relation it is of order unity. The main difference between both analysis resides in the fact that Esipchuk *et al.*, as explained before, replace the expressions for the axial and azimuthal electron velocity derived from the electron momentum equation in the electron continuity equation before the linearisation and Fourier-expansion of the equations.

Thomas [174] analyses the same problem with electron collisions and closed-drift gradient but without plasma density gradient. Under those two hypothesis equation (3.18) can be expressed as:

$$0 = \frac{1}{\tilde{\omega}_{pi}^2} - \frac{1}{(\tilde{\omega} - \tilde{k}_x \tilde{v}_{ix0})^2} + \frac{1}{\tilde{\omega}_e} + \frac{1}{(\tilde{\omega} - \tilde{k}_y \tilde{v}_{ey0} + i(i\tilde{k}_x + 1)\tilde{v}_{ex0})} \left(-\frac{\tilde{\gamma}\tilde{v}_{ey0}}{\tilde{\omega}_e} i \frac{\tilde{k}_x \tilde{k}_y}{\tilde{k}^2} + \frac{i\tilde{\nu}_e}{\tilde{\omega}_e}\right) \tag{3.22}$$

Equation (3.22) is equivalent to equation (29) of Ref. [174] in the limit of unmagnetized ions and highly magnetized electrons. It is also interesting to note that Thomas also concludes that the closed-drift gradient term of the dispersion relation is of order $(1/\tilde{\omega}_e)$ contrary to what Esipchuk obtains.

Litvak *et al.* [156] analyse the influence of the collisions in the stability of the discharge in the HF range. In that case, no gradients are included in the formulation. Under those conditions equation (3.18) can be expressed as:

$$0 = \frac{1}{\tilde{\omega}_{pi}^2} - \frac{1}{(\tilde{\omega} - \tilde{k}_x \tilde{v}_{ix0})^2} + \frac{1}{\tilde{\omega}_e} + \frac{1}{(\tilde{\omega} - \tilde{k}_y \tilde{v}_{ey0})} \frac{i\tilde{\nu}_e}{\tilde{\omega}_e} \tag{3.23}$$

Equation (3.23) is equivalent to equation (16) of Ref. [156].

Spektor [176] generalizes the dispersion relation derived by Litvak to include all gradients (except the closed-drift gradient) for purely azimuthal waves. In those conditions, equation (3.19) can be expressed as:

$$0 = \frac{1}{\tilde{\omega}_{pi}^2} - \frac{1}{\tilde{\omega}(\tilde{\omega} + i\tilde{v}_{ix0})} + \frac{1}{\tilde{\omega}_e} + \frac{1}{\tilde{k}_y(\tilde{\omega} - \tilde{k}_y \tilde{v}_{ey0} + i\tilde{v}_{ex0})} \left(1 + \frac{i\tilde{\nu}_e}{\tilde{\omega}_e} \tilde{k}_y\right) \tag{3.24}$$

Equation (3.24) is equivalent to equation (24) of Ref. [176].

3.3.2 Azimuthal oscillations

Equation (3.19) is the dispersion relation corresponding to purely azimuthal oscillations. It is valid for both the low frequency and high frequency regimes since it captures electron inertia terms as well as collisional effects. Taking into account that in Hall thrusters $\tilde{\omega}_{pi}^2 \gg \tilde{\omega}_e \gg \tilde{\nu}_e \sim \tilde{k}_y \tilde{v}_{ey0} \sim \sqrt{\tilde{\omega}_e}$, the dispersion relation can also be expressed as:

$$0 = \frac{1}{\tilde{\omega}_e} - \frac{1}{\tilde{\omega}(\tilde{\omega} + i\tilde{v}_{ix0})} + \frac{1}{\tilde{k}_y(\tilde{\omega} - \tilde{k}_y \tilde{v}_{ey0} + i\tilde{v}_{ey0}\tilde{\nu}_e/\tilde{\omega}_e)} \left(1 + \frac{\tilde{\gamma}\tilde{v}_{ey0}}{\tilde{\omega}_e} + \frac{i\tilde{\nu}_e}{\tilde{\omega}_e}\tilde{k}_y\right) \tag{3.25}$$

Equation (3.25) is third order in $\tilde{\omega}$ and thus has three possible solutions: two belonging to the low frequency regime and already analysed in the previous section and one new high frequency solution due to the presence of the electron inertia terms. Thanks to the fact that the electron inertia terms (including electron collisions and closed drift gradient) appear as corrections of order $(1/\tilde{\omega}_e)$, it is possible to use regular and singular perturbation methods to determine if the solutions of the cubic equation correspond to stable or unstable solutions.

Cubic dispersion relation for HF oscillations

In the high frequency limit ($\tilde{\omega} \gg i\tilde{v}_{ix0}$) without collisions ($\tilde{\nu}_e = 0$) and closed-drift gradient ($\tilde{\gamma} = 0$) it is possible to simplify the dispersion relation (3.25) to:

$$0 = \frac{1}{\tilde{\omega}_e} - \frac{1}{\tilde{\omega}^2} + \frac{1}{\tilde{k}_y(\tilde{\omega} - \tilde{k}_y \tilde{v}_{ey0})} \tag{3.26}$$

which corresponds to the following cubic equation with real coefficients:

$$0 = \tilde{\omega}^3 + \tilde{\omega}^2 \left(\tilde{\omega}_e/\tilde{k}_y - \tilde{k}_y \tilde{v}_{ey0}\right) - \tilde{\omega}_e \tilde{\omega} + \tilde{\omega}_e \tilde{k}_y \tilde{v}_{ey0}$$

The exact solution of the cubic equation with real coefficients can be obtained from the following coefficients:

$$Q = (3a_1 - a_2^2)/9$$

$$R = (9a_2 a_1 - 27a_0 - a_2^3)/54$$

$$D = Q^3 + R^2$$

where a_2, a_1 and a_0 are the coefficients of the $\tilde{\omega}^2$, $\tilde{\omega}$ and $\tilde{\omega}^0$ terms of the cubic equation respectively. In general, if $D \leqslant 0$, then all roots of the equation are real (metastable), but if $D > 0$ then there are two solutions which are complex conjugate (unstable). In our case, based on the fact that the electron cyclotron frequency is much bigger than the rest of frequencies involved, it is possible to compute:

$$D \approx \frac{\tilde{v}_{ey0}\tilde{\omega}_e^4}{27\tilde{k}_y^2} < 0$$

where the relation $\tilde{v}_{ey0} = -\tilde{v}_{ix0}^2$ has been taken into account.

Consequently, there are no unstable solutions under the current hypothesis (i.e, no collisions, no closed-drift gradient, high frequency range).

Asymptotic analysis of LF oscillations

In the limit of low frequency oscillations ($\tilde{\omega} \ll \tilde{k}_y \tilde{v}_{ey0}$), the dispersion relation (3.25) can be expressed as:

$$0 = \frac{1}{\tilde{\omega}_e} - \frac{1}{\tilde{\omega}(\tilde{\omega} + i\tilde{v}_{ix0})} - \frac{1}{\tilde{k}_y^2 \tilde{v}_{ey0}} \left(1 + \frac{\tilde{\gamma}\tilde{v}_{ey0}}{\tilde{\omega}_e} + \frac{i\tilde{\nu}_e \tilde{k}_y}{\tilde{\omega}_e}(1 + 1/\tilde{k}_y^2) \right) \tag{3.27}$$

Based on the ordering of the frequencies involved ($\tilde{\omega}_e \gg \tilde{\omega} \sim \tilde{k}_y \tilde{v}_{ey0} \sim \tilde{\nu}_e \gg \tilde{v}_{ix0}$), it is possible to propose a solution of the form:

$$\tilde{\omega} = \tilde{\omega}_0 + \left(\frac{1}{\tilde{\omega}_e} \right) \tilde{\omega}_1$$

where $\tilde{\omega}_0$ is the solution of the equation in the limit $(1/\tilde{\omega}_e) = 0$ which was already obtained in section 3.2.3 as:

$$\tilde{\omega}_0 = \frac{1}{2} \tilde{v}_{ix0} \left(-i \pm \sqrt{4\tilde{k}_y^2 - 1} \right)$$

The frequency $\tilde{\omega}_1$ corresponds to the solution of the equation (3.27) at the order $(1/\tilde{\omega}_e)$, this is:

$$0 = -\tilde{k}_y^2 \tilde{v}_{ey0} \left(1 - \frac{\tilde{\gamma}}{\tilde{k}_y^2} - \frac{i\tilde{\nu}_e}{\tilde{k}_y \tilde{v}_{ey0}}(1 + 1/\tilde{k}_y^2) \right) \tilde{\omega}_0(\tilde{\omega}_0 + i\tilde{v}_{ix0}) + \tilde{\omega}_1(2\tilde{\omega}_0 + i\tilde{v}_{ix0})$$

whose solution can be expresses as:

$$\tilde{\omega}_1 = \pm \frac{\tilde{k}_y^4 \tilde{v}_{ey0}^2}{\sqrt{4\tilde{k}_y^2 - 1}} \left(1 - \frac{\tilde{\gamma}}{\tilde{k}_y^2} - \frac{i\tilde{\nu}_e}{\tilde{k}_y \tilde{v}_{ey0}}(1 + 1/\tilde{k}_y^2) \right)$$

Depending on the value of the azimuthal wave number $\tilde{k}_y$, there are different alternatives:

$$4\tilde{k}_y^2 > 1 : \qquad \mathrm{Im}(\tilde{\omega}_1) = \pm \frac{\tilde{k}_y^3 \tilde{v}_{ey0} \tilde{\nu}_e}{\sqrt{4\tilde{k}_y^2 - 1}}(1 + 1/\tilde{k}_y^2)$$

$$4\tilde{k}_y^2 < 1 : \qquad \mathrm{Im}(\tilde{\omega}_1) = \pm \frac{\tilde{k}_y^3 \tilde{v}_{ey0}}{\sqrt{1 - 4\tilde{k}_y^2}}(1 - \tilde{\gamma}/\tilde{k}_y^2)$$

In the first case, for large wave numbers ($\tilde{k}_y \gg 1$) the imaginary part of $\tilde{\omega}_1$ is expected to compensate $\mathrm{Im}(\tilde{\omega}_0)$ and make the overall solution unstable ($\mathrm{Im}(\tilde{\omega}) > 0$). This means that electron collisions are expected to make the discharge unstable for large wave numbers. This fact will be verified later on when solving the full dispersion relation numerically.

In the second case, the order of magnitude of $\mathrm{Im}(\tilde{\omega}_1)$ is similar to $\mathrm{Im}(\tilde{\omega}_0)$ and therefore, it is not expected to find unstable solutions. Only in the limit $\tilde{k}_y \to 0$, the ratio of both imaginary parts tends to a constant $\mathrm{Im}(\tilde{\omega}_1)/\mathrm{Im}(\tilde{\omega}_0) \to \pm(\tilde{v}_{ix0}^3 \tilde{\gamma})$ which can compensate the factor $1/\tilde{\omega}_e$ and make the overall solution unstable. The numerical solution of the full dispersion relation will determine what is the behaviour in that case.

To sum up, both the the closed-drift gradient and the electron collisions seem to promote the growth of unstable oscillations. The former enhances the appearance of long wavelength oscillations while the latter promotes short wavelength waves.

Singular perturbations analysis for HF oscillations

In the previous sections the influence of electron inertia on low and high frequency solutions has been analysed, as well as the effect of electron collisions and the closed-drift gradient on the low frequency regime. Thus, it remains to analyse the influence of those two terms combined with the electron inertia term on the high frequency range. For that purpose the singular perturbations method is used.

Equation (3.25) can be rewritten in the following form:

$$0 = \frac{\tilde{\omega}}{\tilde{\omega}_e}(\tilde{\omega} + i\tilde{v}_{ix0})(\tilde{\omega} - \tilde{k}_y\tilde{v}_{ey0} + i\tilde{v}_{ex0}) - (\tilde{\omega} - \tilde{k}_y\tilde{v}_{ey0} + i\tilde{v}_{ex0}) +$$

$$+ \frac{\tilde{\omega}}{\tilde{k}_y}(\tilde{\omega} + i\tilde{v}_{ix0})\left(1 + \frac{\tilde{\gamma}\tilde{v}_{ey0}}{\tilde{\omega}_e} + \frac{i\tilde{\nu}_e}{\tilde{\omega}_e}\tilde{k}_y\right)$$

Taking into account the following ordering of the frequencies involved valid for Hall thrusters, ($\tilde{\omega}_e \gg \tilde{\omega} \sim \tilde{k}_y\tilde{v}_{ey0} \sim \tilde{\nu}_e \sim \sqrt{\tilde{\omega}_e} \gg \tilde{v}_{ix0} \gg 1$), it is possible to apply the singular perturbations taking as small parameter $\tilde{\epsilon} = (1/\sqrt{\tilde{\omega}_e}) \ll 1$ and propose a solution as a series expansion in $\tilde{\epsilon}$:

$$\tilde{\omega} = \tilde{\alpha}\tilde{\epsilon}^{-v}$$

$$\tilde{\alpha} = \tilde{\alpha}_0 + \tilde{\epsilon}\tilde{\alpha}_1 + \tilde{\epsilon}^2\tilde{\alpha}_2 + ...$$

The value of the exponent turns out to be $v = 2$ by analysing the dominant terms of the previous equation.

By analysing the different orders of the equation it is possible to obtain the coefficients of the series expansion:

$$\tilde{\alpha}_0 = -\frac{1}{\tilde{k}_y}$$

$$\tilde{\alpha}_1 = \frac{\tilde{k}_y\tilde{v}_{ey0} - \tilde{\gamma}\tilde{v}_{ey0}/\tilde{k}_y - i\tilde{\nu}_e}{\sqrt{\tilde{\omega}_e}}$$

The imaginary part of $\tilde{\alpha}_1$ is:

$$\mathrm{Im}(\tilde{\alpha}_1) = -i\tilde{\nu}_e/\sqrt{\tilde{\omega}_e} < 0$$

which yields high frequency stable solutions.

In case of no electron collisions ($\tilde{\nu}_e = 0$) the rest of coefficients are:

$$\tilde{\alpha}_2 = 1/\tilde{\alpha}_0$$

$$\tilde{\alpha}_3 = \frac{1}{\tilde{\alpha}_0^2}\left(\frac{\tilde{\gamma}}{\tilde{k}_y^2} - 2\right)\frac{\tilde{k}_y\tilde{v}_{ey0}}{\sqrt{\tilde{\omega}_e}}$$

$$\tilde{\alpha}_4 = \tilde{k}_y^2(-\tilde{\alpha}_1^2/\tilde{\alpha}_0 - 2\tilde{\alpha}_0\tilde{\alpha}_1\tilde{\alpha}_3 - i\tilde{v}_{ix0} - 1/\tilde{\alpha}_0)$$

being $\tilde{\alpha}_4$ the first non-real coefficient whose imaginary part is:

$$\mathrm{Im}(\tilde{\alpha}_4) = -\tilde{k}_y^2\tilde{v}_{ix0} < 0$$

which yields high frequency stable solutions even in the limit of no collisions and no closed-drift gradient as had already been shown in a previous section.

3.3.3 Numerical solution of full dispersion relation

The eigenvalue problem given by (3.17) can be solved numerically for azimuthal oscillations ($\tilde{k}_x = 0$) and typical values of the non-dimensional parameters in the acceleration region: $\tilde{v}_{ix0} = 50$, $\tilde{\omega}_e = 10^6$, $\tilde{\nu}_e = 10^3$ and $\tilde{\gamma} = 1.0$. The aim is two-fold: first, it is interesting to verify the conclusions derived from the previous sections via the analytical analysis, and second, it is also important to carry out parametric variations to understand the influence of the different parameters, specially of those with larger variability or uncertainty.

Figure 3.1 depicts the value of the largest imaginary part of the eigenvalues as a function of the non-dimensional azimuthal wave number, $\tilde{k}_y$ and the non-dimensional electron collision frequency, $\tilde{\nu}_e = 10^3$. It can be observed that for typical values of the collision frequency, $\tilde{\nu}_e = 10^3$, there are no unstable solutions (i.e., $\mathrm{Im}(\tilde{\omega}) < 0$) for a wide range of wave numbers. Note that for a typical HET an azimuthal oscillation of mode number of $m = 1$ corresponds to a non-dimensional wave number of $\tilde{k}_y \sim 0.2$ assuming a density gradient such that l_n is of the order of the thruster length. Only for very large collision frequencies, $\tilde{\nu}_e = 10^5$, it is possible to obtain unstable solutions with very short wavelengths ($\tilde{k}_y \sim 10$). At the same time it is possible to observe two regions, depending on the value of $\tilde{k}_y$. The limiting value of these regions is $\tilde{k}_y = 0.5$, as it was already anticipated via analytical derivations.

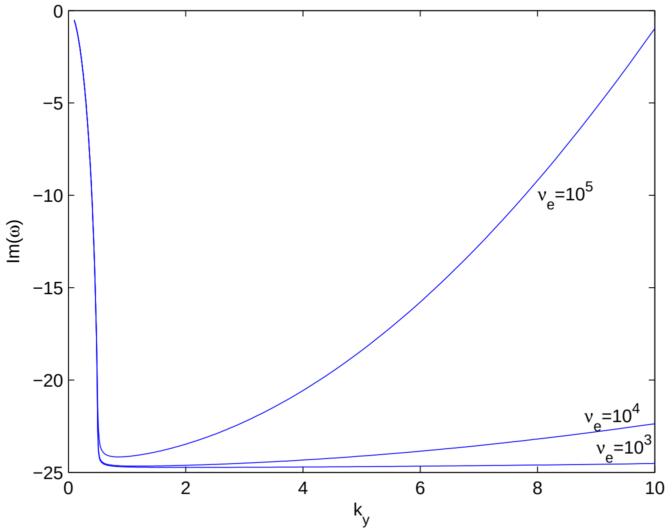

Figure 3.1: Value of largest imaginary part of the eigenvalues of the stability analysis given by (3.17) for the following non-dimensional parameters: $\tilde{k}_x = 0$, $\tilde{v}_{ix0} = 50$, $\tilde{\omega}_e = 10^6$ and $\tilde{\gamma} = 1.0$. Both the non-dimensional azimuthal wave-number $\tilde{k}_y$ and the non-dimensional electron collision frequency $\tilde{\nu}_e$ are parametrically varied

Figure 3.2 shows the eigenvalues in the complex plane as a function of $\tilde{k}_y$ and $\tilde{\nu}_e$. There exists a stable high frequency eigenvalue together with two other low frequency solutions which are stable as well for the ranges of parameters under analysis. As the collision frequency increases, the high frequency solution becomes more and more stable. And as the wave number increases, the real part of the high frequency solution gets closer to zero. These two trends as well as the actual value of the high frequency solution are in good agreement with the results from the singular perturbations analysis carried out in the preceding paragraph.

In the no collisions limit ($\tilde{\nu}_e = 0$), the numerical results verify that the high frequency solution is stable even though in this case the imaginary part is much closer to zero. This is in agreement with the fact that the first non-real element of the series expansion of the singular perturbation analysis is the fourth element.

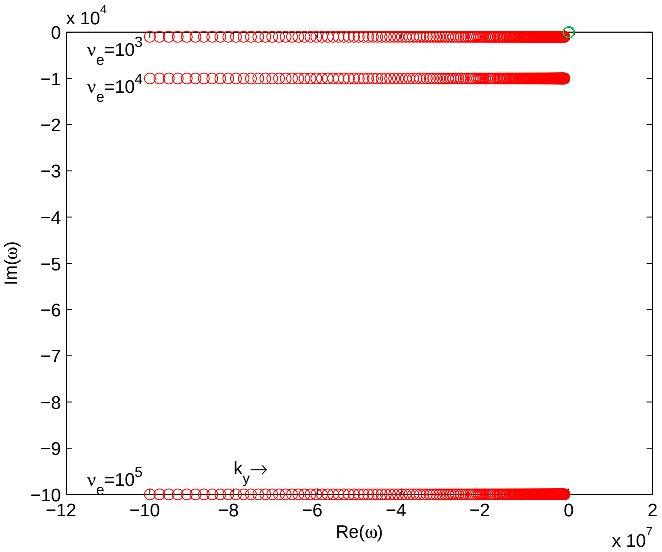

Figure 3.2: Eigenvalues of the stability analysis given by (3.17) for the following non-dimensional parameters: $\tilde{k}_x = 0$, $\tilde{v}_{ix0} = 50$, $\tilde{\omega}_e = 10^6$ and $\tilde{\gamma} = 1.0$. Parametrically variation of: $\tilde{k}_y \in [0.1, 10]$ and $\tilde{\nu}_e = [10^3, 10^4, 10^5]$

Figure 3.3 shows the influence of the closed-drift gradient on the stability analysis. For gradients of order unity the influence is negligible as was anticipated from the analytical approximations.

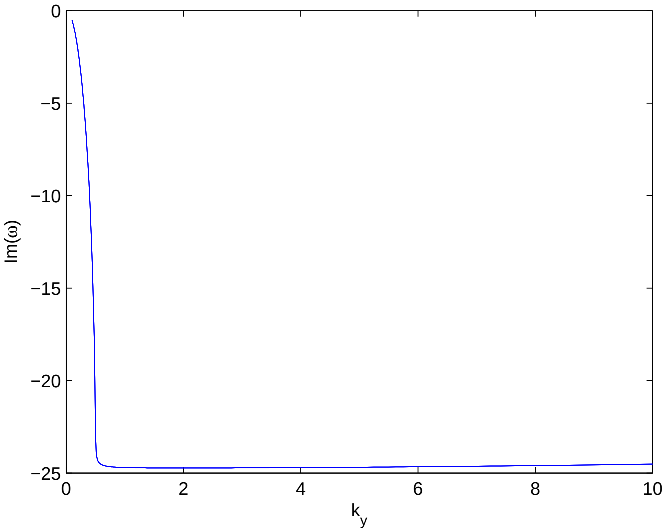

Figure 3.3: Eigenvalues of the stability analysis given by (3.17) for the following non-dimensional parameters: $\tilde{k}_x = 0$, $\tilde{v}_{ix0} = 50$, $\tilde{\omega}_e = 10^6$ and $\tilde{\nu}_e = 10^3$. Parametric variation of: $\tilde{k}_y \in [0.1, 10]$ and $\tilde{\gamma} \in [-1.0, 1.0]$

3.4 Stability analysis of the ionization region

As shown in the previous section, there is experimental evidence of low frequency azimuthal oscillations in the ionization region of the HET discharge. In this region the ionization plays a major role in the definition of the axial profile of the main plasma variables. In order to account for this process in a stability analysis, a three-fluid model (ions, electrons and neutrals) needs to be considered. This section presents results from two separate models: a simple one, where the temperature is considered uniform and without oscillations; and a more complete one, that includes an electron energy equation with heat conduction terms in order to account for temperature gradients and oscillations.

Both models are based on a formulation consisting of particle, momentum and energy conservation equations for electrons, ions, and neutrals separately:

$$\frac{\partial n}{\partial t} + \nabla \cdot (n\mathbf{v}_e) = nn_n\xi_i \tag{3.28a}$$

$$\frac{\partial n}{\partial t} + \nabla \cdot (n\mathbf{v}_i) = nn_n\xi_i \tag{3.28b}$$

$$\frac{\partial n_n}{\partial t} + \nabla \cdot (n_n\mathbf{v}_n) = -nn_n\xi_i \tag{3.28c}$$

$$0 = -\nabla(nT_e) - en(\mathbf{E} + \mathbf{v}_e \times \mathbf{B}) - m_e nn_n\xi_e\mathbf{v}_e \tag{3.28d}$$

$$m_i n\left(\frac{\partial \mathbf{v}_i}{\partial t} + \mathbf{v}_i \cdot \nabla\mathbf{v}_i\right) = en\mathbf{E} - m_i nn_n\xi_i(\mathbf{v}_i - \mathbf{v}_n) \tag{3.28e}$$

$$m_n n_n\left(\frac{\partial \mathbf{v}_n}{\partial t} + \mathbf{v}_n \cdot \nabla\mathbf{v}_n\right) = \mathbf{0} \tag{3.28f}$$

$$\frac{\partial}{\partial t}\left(\frac{3}{2}nT_e\right) + \nabla \cdot \left(\frac{5}{2}nT_e\mathbf{v}_e + \mathbf{q}_e\right) = -en\mathbf{v}_e \cdot \mathbf{E} - enn_n\xi_i\alpha_i \tag{3.28g}$$

$$\frac{5}{2}nT_e\nabla T_e + e\mathbf{q}_e \times \mathbf{B} + m_e n_n\xi_e\mathbf{q}_e = \mathbf{0} \tag{3.28h}$$

where ${}_{i,e,n}$ are the sub-indexes for ion, electron, and neutral species; e is the electron charge; m_e, m_i and m_n are the electron, ion, and neutral masses; $\mathbf{E}$ and $\mathbf{B}$ are the electric and magnetic fields; n and n_n are plasma and neutral densities; $\mathbf{v}_j$ is the velocity vector of species j; ξ_i and ξ_e are the ionization and effective electron collision rates; T_e is electron temperature; α_i is the energy loss per effective single ionization event; and $\mathbf{q}_e$ is the electron heat conduction flux vector. The quasi-neutrality assumption ($n_e = n_i$) has been used in the formulation since the Debye length is much smaller than the typical dimensions of the thruster. Finally, notice as well that the induced magnetic field is neglected and thus, the electric field derives from an electric potential, ϕ ($\nabla\phi = -\mathbf{E}$), and the magnetic field is equal to the externally applied field, resulting in an electrostatic formulation.

3.4.1 Isothermal model

In this case electron temperature gradients and oscillations are neglected in the formulation, and therefore the last two equations of (3.28) are not used. The corresponding steady state ($\partial/\partial t = 0$) zero-th order solution (expressed with subindex 0) is considered azimuthally symmetric ($\partial/\partial y = 0$). The zero-th order solution then verifies:

$$\frac{dn_{n0}}{dx} = -\frac{n_0 n_{n0} \xi_{i0}}{v_{nx0}} \tag{3.29a}$$

$$\frac{dv_{nx0}}{dx} = 0 \tag{3.29b}$$

$$\frac{dv_{ix0}}{dx} = n_{n0}\xi_{i0} - v_{ix0}\frac{d\ln n_0}{dx} \tag{3.29c}$$

$$E_0 = \frac{m_i}{e}\left(v_{ix0}\frac{dv_{ix0}}{dx} + n_{n0}\xi_{i0}(v_{ix0} - v_{nx0})\right) \tag{3.29d}$$

$$\frac{dv_{ex0}}{dx} = n_{n0}\xi_{i0} - v_{ex0}\frac{d\ln n_0}{dx} \tag{3.29e}$$

$$v_{ex0} = v_{ey0}\frac{\nu_{e0}}{\omega_{ce}} \tag{3.29f}$$

$$v_{ey0} = -\frac{1}{B_0}\left(E_0 + \frac{T_{e0}}{e}\frac{d\ln n_0}{dx}\right) \tag{3.29g}$$

where ω_{ce} is the electron cyclotron frequency, $\nu_{e0} = n_{n0}\xi_{e0}$ is the electron collision frequency, and the Hall parameter is assumed to be very large ($\omega_{ce}/\nu_{e0} \gg 1$).

As shown by Ahedo *et al.* in Ref. [3], the solution of Eqs. (3.29) together with the proper boundary conditions verifies the following properties. The axial electron velocity is negative all along the thruster channel as electrons drift from the cathode to the anode. On the contrary, the neutral axial velocity is positive as the gas moves from the injector to the channel exit. In the case of the axial ion velocity, it is positive in a large part of the thruster channel due to the electric acceleration ($E_0 > 0$), but it becomes negative in an ion back-streaming region near the anode where the axial electric field is mildly negative and attracts the ions to the anode ($E_0 < 0$). The azimuthal electron velocity is also negative all along the channel and consists of the **E**x**B** and the diamagnetic drifts, being the **E**x**B** drift the dominant one in the acceleration region, while the diamagnetic drift dominates in the upstream part of the ionization region. As for the plasma density gradient, it is positive from the anode to the beginning of the acceleration region, from where it becomes negative as a consequence of the ion acceleration.

Assuming small perturbations with respect to the zero-th order state ($\hat{f} \ll f_0$), except for T_e which is considered constant, Eqs. (3.28) may be linearised into:

$$\frac{\partial \hat{n}}{\partial t} + n_0 \left(\frac{\partial \hat{v}_{ex}}{\partial x} + \frac{\partial \hat{v}_{ey}}{\partial y} \right) + \hat{v}_{ex} \frac{dn_0}{dx} + v_{ex0} \frac{\partial \hat{n}}{\partial x} + v_{ey0} \frac{\partial \hat{n}}{\partial y} + \hat{n} \frac{dv_{ex0}}{dx} = (n_0 \hat{n}_n + \hat{n} n_{n0}) \xi_{i0} \tag{3.30a}$$

$$\frac{\partial \hat{n}}{\partial t} + n_0 \left(\frac{\partial \hat{v}_{ix}}{\partial x} + \frac{\partial \hat{v}_{iy}}{\partial y} \right) + \hat{v}_{ix} \frac{dn_0}{dx} + v_{ix0} \frac{\partial \hat{n}}{\partial x} + \hat{n} \frac{dv_{ix0}}{dx} = (n_0 \hat{n}_n + \hat{n} n_{n0}) \xi_{i0} \tag{3.30b}$$

$$\frac{\partial \hat{n}_n}{\partial t} + n_{n0} \left(\frac{\partial \hat{v}_{nx}}{\partial x} + \frac{\partial \hat{v}_{ny}}{\partial y} \right) + \hat{v}_{nx} \frac{dn_{n0}}{dx} + v_{nx0} \frac{\partial \hat{n}_n}{\partial x} = -(n_0 \hat{n}_n + \hat{n} n_{n0}) \xi_{i0} \tag{3.30c}$$

$$0 = -\frac{1}{n_0} \frac{T_{e0}}{m_e} \frac{\partial \hat{n}}{\partial x} + \frac{\hat{n}}{n_0^2} \frac{T_{e0}}{m_e} \frac{dn_0}{dx} - \frac{e}{m_e} \left(-\frac{\partial \hat{\phi}}{\partial x} + \hat{v}_{ey} B_0 \right) - (n_{n0} \hat{v}_{ex} + \hat{n}_n v_{ex0}) \xi_{e0} \tag{3.30d}$$

$$0 = -\frac{1}{n_0} \frac{T_{e0}}{m_e} \frac{\partial \hat{n}}{\partial y} - \frac{e}{m_e} \left(-\frac{\partial \hat{\phi}}{\partial y} - \hat{v}_{ex} B_0 \right) - (n_{n0} \hat{v}_{ey} + \hat{n}_n v_{ey0}) \xi_{e0} \tag{3.30e}$$

$$\frac{\partial \hat{v}_{ix}}{\partial t} + v_{ix0} \frac{\partial \hat{v}_{ix}}{\partial x} + \hat{v}_{ix} \frac{dv_{ix0}}{dx} = -\frac{e}{m_i} \frac{\partial \hat{\phi}}{\partial x} - n_{n0} \xi_{i0} (\hat{v}_{ix} - \hat{v}_{nx}) - \hat{n}_n \xi_{i0} (v_{ix0} - v_{nx0}) \tag{3.30f}$$

$$\frac{\partial \hat{v}_{iy}}{\partial t} + v_{ix0} \frac{\partial \hat{v}_{iy}}{\partial x} = -\frac{e}{m_i} \frac{\partial \hat{\phi}}{\partial y} - n_{n0} \xi_{i0} (\hat{v}_{iy} - \hat{v}_{ny}) \tag{3.30g}$$

$$\frac{\partial \hat{v}_{nx}}{\partial t} + v_{nx0} \frac{\partial \hat{v}_{nx}}{\partial x} = 0 \tag{3.30h}$$

$$\frac{\partial \hat{v}_{ny}}{\partial t} + v_{nx0} \frac{\partial \hat{v}_{ny}}{\partial x} = 0 \tag{3.30i}$$

where it is assumed that the collision and ionization rates are constant ($\xi_e = \xi_{e0}$, $\xi_i = \xi_{i0}$).

Equations (3.30) contain four gradients of zero-th order variables (namely, dn_0/dx, dn_{n0}/dx, dv_{ix0}/dx, dv_{ex0}/dx). Making use of Eqs. , the last three of these gradients can be expressed as a function of the zero-th order variables and the gradient of the plasma density, dn_{n0}/dx.

The perturbations may be assumed to be of the following Fourier form:

$$\hat{f}(t, x, y) = \bar{f}(x) \exp(-i\omega t + ik_y y) \tag{3.31}$$

where t is the time variable, x and y are the axial and azimuthal coordinates in the quasi-planar approximation, $\bar{f}(x)$ is the x-dependent coefficient of the Fourier-expanded perturbation of a generic variable f, and ω and k_y are the angular frequency and azimuthal wave number respectively. Note that the y axis is along the -**E**x**B** direction and that k_y may only take a discrete number of values given the azimuthal symmetry of the problem. This type of Fourier expansion is the basis of global stability studies, where the resulting formulation is not algebraic, but consists of differential equations. Within the linear regime, that global approach is fully consistent for inhomogeneous plasmas as opposed to the local analysis carried out here.

As part of the current local analysis, the axial variation of the perturbations is also Fourier-expanded resulting in:

$$\hat{f}(t, x, y) = \bar{f} \exp(ik_x x) \exp(-i\omega t + ik_y y) \tag{3.32}$$

where x is the axial coordinate, k_x is the axial wave number and $\bar{f}$ is the coefficient of the Fourier-expanded perturbation. The tilt angle of the oscillation may be then expressed as $\arctan(k_x/k_y)$.

In this local analysis, it is necessary to freeze the zero-th order variables and their gradients and consider them constant, even if in reality the plasma is inhomogeneous along x, so that the Fourier expansion in the x direction can be carried out. This is supported by the assumption that the length scale of the axial variation of the zero-th order variables (L_x) is much larger than the axial wave-length of the perturbations ($k_x L_x >> 1$). In Hall thrusters this condition is not strictly met and, in fact, some authors claim that depending on how the equations are linearised and Fourier-expanded as part of the local stability analysis, the resulting stability criterion may change [19]. In any case, the local analysis does provide some insights into the stability of the Hall discharge and is an important step to take before analysing the linear stability with a global approach.

Equations (3.30) contain gradients of zero-th order variables (dn_0/dx, dn_{n0}/dx, dv_{ix0}/dx, dv_{ex0}/dx). Making use of Eqs. (3.29) and the length scale of the axial variation of the plasma density, l_n:

$$l_n = (d \ln n_0/dx)^{-1} \tag{3.33}$$

those four gradients may be expressed as a function only of the zero-th order variables and l_n. It is important to note that the gradient of the magnetic field does not appear in the formulation as the expressions for the axial and azimuthal electron velocities in Eqs. (3.29f)−(3.29g) have been linearised and Fourier expanded rather than introduced in the rest of expressions in Eqs. (3.29a)−(3.29e) before the linearisation, as Esipchuk and Tilinin [1] and Frias *et al.* [140] do. The consequences of this choice are discussed in reference [19] and evaluated in the next section.

Additionally, it is possible to make the problem non-dimensional by defining the following reference variables for mass, charge, time, density and length respectively: m_i, e, Ω^{-1}, n_0 and L, where Ω and L are arbitrary reference values here assumed to be respectively 10 kHz and 1 cm. Hereinafter non-dimensional variables are expressed with a tilde above the variable symbol. For instance $\tilde{l}_n = l_n/L$ represents the non-dimensional length scale of the axial variation of plasma density.

The non-dimensional Fourier form of the linearised equations may be written as an eigenvalue problem in matrix form as:

$$(A\tilde{\omega} + B)\tilde{\mathbf{w}} = \mathbf{0} \tag{3.34}$$

where $\tilde{\mathbf{w}} = (\tilde{n}, \tilde{n}_n, \tilde{v}_{ix}, \tilde{v}_{iy}, \tilde{\phi}, \tilde{v}_{ex}, \tilde{v}_{ey})$ is the vector of non-dimensional variables, A and B are matrices of size 7x7, which are functions of the vector of non-dimensional parameters defining the zero-th order solution, $\tilde{\mathbf{p}}_0 = (\tilde{n}_{n0}, \tilde{v}_{ix0}, \tilde{v}_{nx0}, \tilde{\xi}_{i0}, \tilde{\xi}_{e0}, \tilde{T}_{e0}, \tilde{B}_0)$, and the non-dimensional wave-numbers in the axial and azimuthal directions, $\tilde{k}_x$ and $\tilde{k}_y$. Eq. (3.34) constitutes an eigenvalue problem with one unknown, the *complex* oscillation frequency, $\tilde{\omega} = \tilde{\omega}_{re} + i\tilde{\omega}_{im}$, as function of the wave numbers and the vector of parameters, this is, $\tilde{\omega}(\tilde{k}_x, \tilde{k}_y, \tilde{\mathbf{p}}_0)$. Since the electron inertia and electromagnetic and non-quasineutral terms have been neglected, no time derivatives of $\tilde{v}_{ex}$, $\tilde{v}_{ey}$ and $\tilde{\phi}$ appear in the formulation. Thanks to this, three equations may be pre-eliminated in the matrix formulation and there remain only four solutions for $\tilde{\omega}$ in Eq. (3.34). In the remainder of the analysis, we will focus on purely azimuthal oscillations ($\tilde{k}_x = 0$) in an attempt to reproduce and analyse the spoke oscillations. Notice that under that condition, the perturbations of the axial and azimuthal neutral velocity are zero ($\tilde{v}_{nx} = \tilde{v}_{ny} = 0$) according to the perturbed neutral momentum equations. Moreover, we will study the limited region of the thruster channel where $dn_0/dx > 0$ and $dv_{ix0}/dx > 0$ due to ionization and a positive zero-th order electric field ($E_0 > 0$).

Approximate solution

Let us first consider a particular case, where an analytical solution for the dispersion relation is available. This consists of the collisionless case ($\tilde{\xi}_{e0}$=0) at the particular cross-section where $\tilde{v}_{nx0} = \tilde{v}_{ix0}$, located inside the ionization region. Then, the dispersion relation in Eq. (3.34) simplifies into:

$$\begin{aligned} 0 = (\tilde{\omega} + i\tilde{n}_{n0}\tilde{\xi}_{ion0}) \left((\tilde{\omega} - i\tilde{v}_{ix0}/\tilde{l}_n) - \frac{\tilde{n}_{n0}\tilde{\xi}_{ion0}^2}{\tilde{\omega} + i\tilde{\xi}_{ion0}} \right) \\ +\tilde{k}_y\tilde{l}_n\tilde{B}_0 \left(\tilde{\omega} - \tilde{k}_y(\tilde{T}_{e0}/\tilde{l}_n - \tilde{E}_0)/\tilde{B}_0 - \frac{\tilde{n}_{n0}\tilde{\xi}_{ion0}^2}{\tilde{\omega} + i\tilde{\xi}_{ion0}} \right) \end{aligned} \tag{3.35}$$

Equation (3.35) is cubic in $\tilde{\omega}$ and thus has three solutions. The fourth solution of Eq. (3.34), not captured in Eq. (3.35), comes from the ion momentum equation in the x direction and is a stable solution ($\tilde{\omega}_{re} > 0$) under the current assumptions.

For typical conditions in the ionization region of a Hall thruster it holds approximately that $\tilde{n}_{n0} \gg 1$, $\tilde{\xi}_{i0} \ll 1$, $\tilde{n}_{n0}\tilde{\xi}_{i0} \sim 1$ and $\tilde{v}_{ix0} \sim 1$. Taking into account those orders of magnitude, Eq. (3.35) simplifies into the following second order equation:

$$\begin{aligned} 0 = \tilde{\omega}^2 + \tilde{\omega}(i\tilde{n}_{n0}\tilde{\xi}_{ion0} - i\tilde{v}_{ix0}/\tilde{l}_n + \tilde{k}_y\tilde{l}_n\tilde{B}_0) \\ +\tilde{n}_{n0}\tilde{\xi}_{ion0}\tilde{v}_{ix0}/\tilde{l}_n - \tilde{k}_y^2\tilde{l}_n(\tilde{T}_{e0}/\tilde{l}_n - \tilde{E}_0) \end{aligned} \tag{3.36}$$

plus the marginally stable solution $\tilde{\omega} \approx -i\tilde{\xi}_{i0}$. The solutions of Eq. (3.36) are in the low frequency range, and are unstable ($\tilde{\omega}_{im} > 0$) when:

$$(\tilde{k}_y\tilde{l}_n)^2 < \frac{\tilde{n}_{n0}\tilde{\xi}_{i0}\tilde{v}_{ix0}}{\tilde{T}_{e0}/\tilde{l}_n - \tilde{E}_0} \tag{3.37}$$

where the evaluation is performed in the near anode region, where the electron pressure gradient, $\tilde{T}_{e0}/\tilde{l}_n$, dominates over the electric field, $\tilde{E}_0$, and hence the denominator of the expression (3.37) is positive. According to Eq. (3.36), the highest growth rate is obtained for the perturbation with the smallest wave number allowed by the azimuthal continuity condition, which imposes a lower limit on the azimuthal wave number. Note as well that the most unstable solution of Eq. (3.36) verifies that the product of $\tilde{\omega}_{re}$ and $\tilde{k}_y$ is negative, indicating that the wave propagates in the $-y$ direction, this is, along **+ExB**.

Full numerical solution

The numerical solution of the isothermal model in Eqs. (3.34) is discussed in this subsection. To this end several parametric analyses are presented in this section with respect to different parameters ($\tilde{v}_{nx0}$, $\tilde{n}_{n0}$, $\tilde{T}_{e0}$, $\tilde{\xi}_{ion0}$ and $\tilde{B}_0$) together with the azimuthal wave number, $\tilde{k}_y$. In all of them it is possible to observe unstable solutions for low wave numbers in agreement with the particular analysis in the previous subsection.

For the resolution of Eqs. (3.34), the following typical values for the macroscopic variables in the ionization region of a HET are used: neutral velocity at injection, v_{nx0} = 500m.s^{-1}; neutral density, $n_{n0} = 10^{19}$ m^{-3}; electron temperature, T_{e0} = 6 eV; ionization frequency, $\nu_{i0} = n_{n0}\xi_{ion0} = 10^5$ Hz; and magnetic field, B_0 = 140 G. Additionally, the following values for the reference parameters are used: $m_i = 2.2 \times 10^{-25}$ kg, $e = 1.6 \times 10^{-19}$ C, Ω = 10 kHz, $n_0 = 5 \times 10^{17}$ m^{-3} and $L = l_n$ = 1 cm. The resulting non-dimensional variables are: $\tilde{v}_{nx0}$ =

5, $\tilde{n}_{n0} = 20$, $\tilde{T}_{e0} = 450$, $\tilde{\xi}_{ion0} = 0.5$, $\tilde{l}_n = 1$ and $\tilde{B}_0 = 1$. These parameters define the reference state with respect to which the parametric variations are carried out below. It is also interesting to point out that under these conditions a non-dimensional value of the wave number of $\tilde{k}_y = -0.25$ is equivalent to an oscillation travelling in the $+\mathbf{E}\text{x}\mathbf{B}$ direction with a wavelength of around 24 cm, which is the same as the perimeter of a circumference with a mean radius of 4 cm, a typical value for a modern HET. Thus, $\tilde{k}_y = -0.25$ corresponds to a mode $m = 1$ and wave numbers below that threshold are not possible due to azimuthal continuity.

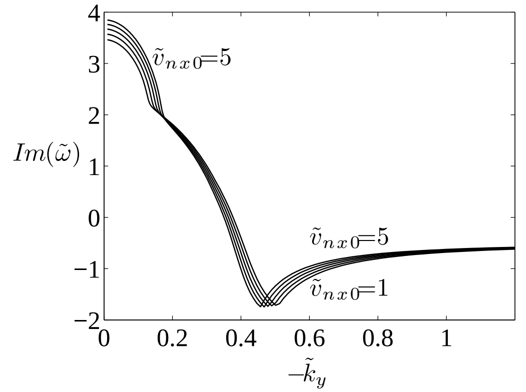

Figure 3.4: Growth rate of the most unstable solution of Eqs. (3.30) for the following non-dimensional parameters: $\tilde{n}_{n0} = 20$, $\tilde{v}_{ix0} = 5$, $\tilde{\xi}_{i0} = 0.5$, $\tilde{\xi}_{e0} = 0$ and $\tilde{T}_{e0} = 450$. Parametric variation of $\tilde{k}_y$ and $\tilde{v}_{nx0}$

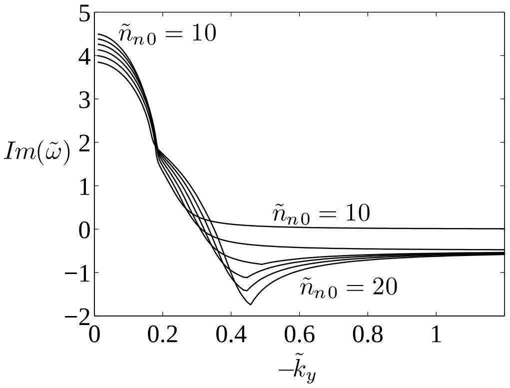

Figure 3.5: Growth rate of the most unstable solution of Eqs. (3.30) for the following non-dimensional parameters: $\tilde{v}_{ix0} = 5$, $\tilde{v}_{nx0} = 5$, $\tilde{\xi}_{i0} = 0.5$, $\tilde{\xi}_{e0} = 0$, $\tilde{T}_{e0} = 450$ and $\tilde{B}_0 = 1$. Parametric variation of $\tilde{k}_y$ and $\tilde{n}_{n0}$

Figure 3.4 shows the influence of the neutral velocity on the growth rate of the perturbations. Note that one of the cases plotted is the one studied analytically previously, $\tilde{v}_{nx0} = \tilde{v}_{ix0}$. Figure 3.5 shows the growth rate as a function of $\tilde{k}_y$ and $\tilde{n}_{n0}$. The smaller the neutral density is, the smaller the range of wave numbers for unstable perturbations. Fig. 3.6 shows both the growth rate and the frequency of the oscillation as a function of $\tilde{k}_y$ and $\tilde{T}_{e0}$. As the electron temperature increases, the range of wave numbers for unstable solutions is reduced. In this case, it is also possible to observe that instabilities exist with a frequency around 10 kHz, $\tilde{\omega}_{re} = 1$, and a wavelength around 24 cm, $\tilde{k}_y = -0.25$. Note that a frequency of 10 kHz and a wavelength of 24 cm in the $+\mathbf{E}\text{x}\mathbf{B}$ direction correspond to an $m = 1$ oscillation with a phase velocity of about 2.4 km.s^{-1}, very similar to the ion acoustic speed and to the velocity of the spoke usually measured in experiments.

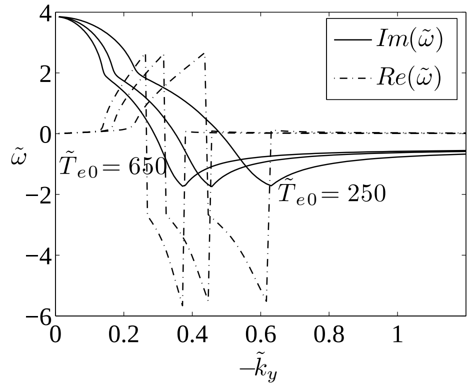

Figure 3.6: Growth rate (-) and corresponding real part (-·) of the most unstable solution of Eqs. (3.30) for the following non-dimensional parameters: $\tilde{n}_{n0} = 20$, $\tilde{v}_{ix0} = 5$, $\tilde{v}_{nx0} = 5$, $\tilde{\xi}_{i0} = 0.5$, $\tilde{\xi}_{e0} = 0$ and $\tilde{B}_0 = 1$. Parametric variation of $\tilde{k}_y$ and $\tilde{T}_{e0}$

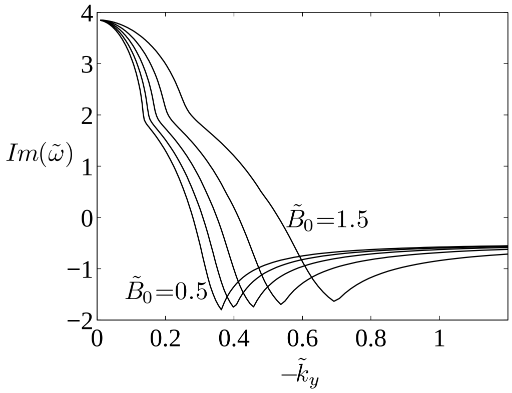

Figure 3.7: Growth rate of the most unstable solution of Eqs. (3.30) for the following non-dimensional parameters: $\tilde{n}_{n0} = 20$, $\tilde{v}_{ix0} = 5$, $\tilde{v}_{nx0} = 5$, $\tilde{\xi}_{ion0} = 0.5$, $\tilde{\xi}_{e0} = 0$ and $\tilde{T}_{e0} = 450$. Parametric variation of $\tilde{k}_y$ and $\tilde{B}_0$

Figures 3.7 and 3.8 show the variation of the growth rate of the most unstable perturbation as a function of $\tilde{k}_y$ and $\tilde{B}_0$ and of $\tilde{k}_y$ and $\tilde{\xi}_{ion0}$. Fig. 3.7 shows that the higher the magnetic field, the wider the range of wave numbers for unstable solutions. Moreover, for a given wave number (e.g. $\tilde{k}_y = -0.25$), the frequency of the oscillation increases with the magnetic field. From Fig. 3.8 it can be stated that the higher the ionization rate, the wider the range for unstable solutions. Moreover, even though the oscillation with the largest growth rate is still the $m = 1$ mode, the difference in growth-rate for different wave numbers is greatly reduced when the ionization rate is increased making it possible to have unstable oscillations with higher wave mode numbers ($m = 2$, $m = 3$...), as found experimentally [10]. To this respect, while it is true that the model predicts that the $m = 1$ mode has the largest unstable growth rate and that other unstable modes $m = 2$, $m = 3$ and higher exist with lower growth rates, it is also important to note that the current analysis is linear and local and that the final dominant mode can only be fully determined if non-linear effects are accounted for. The relevant result from our analysis is that it is for low wave numbers when the perturbations become unstable, in line with experimental evidence and contrary to the results from the analysis of Frias *et al.*, where the larger the wave number, the larger the growth rate.

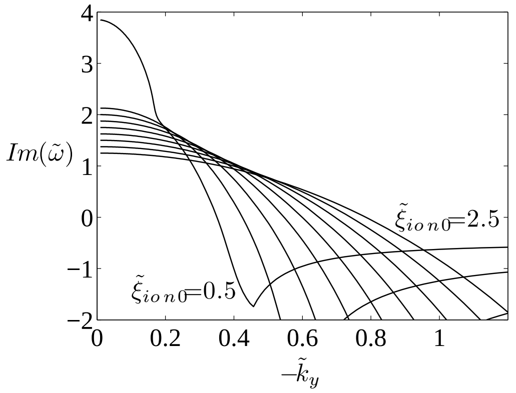

Figure 3.8: Growth rate of the most unstable solution of Eqs. (3.30) for the following non-dimensional parameters: $\tilde{n}_{n0} = 20$, $\tilde{v}_{ix0} = 5$, $\tilde{v}_{nx0} = 5$, $\tilde{\xi}_{e0} = 0$, $\tilde{T}_{e0} = 450$ and $\tilde{B}_0 = 1$. Parametric variation of $\tilde{k}_y$ and $\tilde{\xi}_{ion0}$

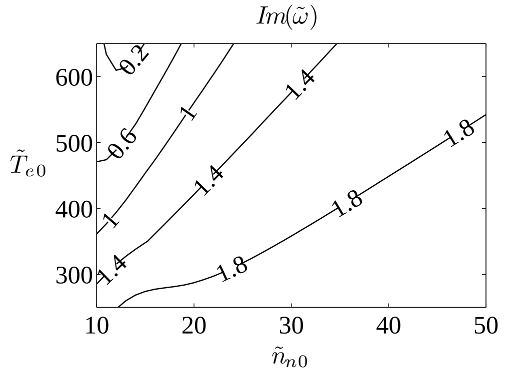

Figure 3.9: Growth rate of the most unstable solution of Eqs. (3.30) for the following non-dimensional parameters: $\tilde{k}_y = 0.25$, $\tilde{v}_{ix0} = 5$, $\tilde{v}_{nx0} = 5$, $\tilde{\xi}_{i0} = 0.5$, $\tilde{\xi}_{e0} = 0$ and $\tilde{B}_0 = 1$. Parametric variation of $\tilde{n}_{n0}$ and $\tilde{T}_{e0}$

Figure 3.9 depicts a map of the growth rate of the oscillation as a function of the neutral density and the electron temperature for a fixed azimuthal wave number ($\tilde{k}_y = -0.25$). In our model, as the electron temperature is increased and the neutral-to-plasma density ratio is decreased, the growth rate decreases up to the point where the perturbation is no longer unstable. Experiments show that as the discharge voltage is increased, keeping the rest of parameters constant, the intensity of low frequency oscillations diminishes considerably, specially in the ionization part of the I-V curve of the thruster [5, 74]. Thus, the linear model is in line with that experimental trend as a discharge voltage increase causes an increase of the electron temperature in the ionization region of the thruster via ohmic heating and a decrease of the neutral-to-plasma density ratio thanks to improved ionization.

Relation with anomalous diffusion

So far we have only analysed the existence of unstable oscillations due to the ionization. However, no connection has been established between the unstable oscillations and enhanced mobility. Looking at the Eqs. (3.30), it is possible to recognize that the terms $\hat{v}_{ex} dn_0/dx$ and $(e/m_e)\hat{v}_{ex}B_0$ from the electron continuity and momentum equations play two roles: first, they couple the plasma density fluctuations from the ion equations with the electron momentum equations thanks to the presence of the zero-th order plasma density gradient in the electron continuity equation; and second and more important, it ensures that the azimuthal electric field and plasma density perturbations are correlated giving rise to a net axial current. This second fact can be shown more clearly by computing the phase of the different perturbations numerically. A similar explanation is proposed by Lomas and Kilkenny[109] with a model that includes an energy equation without heat conduction, although in that case the instability is fed by the coupling between ionization and bulk recombination rather than by the interaction between ionization and the plasma density gradient.

Table 3.1 shows the eigenvectors of the eigenvalue problem for the following parameters: $\tilde{k}_y = -0.25$, $\tilde{n}_{n0} = 20$, $\tilde{v}_{ix0} = 5$, $\tilde{v}_{nx0} = 5$, $\tilde{\xi}_{i0} = 0.5$, $\tilde{\xi}_{e0} = 0$, $\tilde{T}_{e0} = 450$ and $\tilde{B}_0 = 1$. It is interesting to see how the plasma density and electron axial velocity perturbations are partially correlated, this is, their phases are not 90 degrees apart, meaning that the oscillation causes a net axial electron current. This is a good indication of net diffusion caused by the linear oscillation.

Table 3.1: Complex eigenvalues of the stability analysis of (3.30) for the following non-dimensional parameters: $\tilde{k}_y = -0.25$, $\tilde{n}_{n0} = 20$, $\tilde{v}_{ix0} = 5$, $\tilde{v}_{nx0} = 5$, $\tilde{\xi}_{i0} = 0.5$, $\tilde{\xi}_{e0} = 0$ and $\tilde{T}_{e0} = 450$.

$\tilde{n}$	$\tilde{n}_n$	$\tilde{v}_{ix}$	$\tilde{v}_{iy}$	$\tilde{\phi}$	$\tilde{v}_{ex}$	$\tilde{v}_{ey}$
$0.10\angle-109^{o}$	$0.37\angle 115^{o}$	$0\angle 0^{o}$	$0.88\angle-9^{o}$	$40.4\angle-107^{o}$	$0.60\angle 137^{o}$	$42.6\angle-109^{o}$

Simplified model

The dispersion relation in Eq. (3.36) is equivalent to the following linearised system of perturbation equations in non-dimensional form:

$$\frac{\partial \tilde{\hat{n}}}{\partial \tilde{t}} + \frac{\partial \tilde{\hat{v}}_{ey}}{\partial \tilde{y}} + \frac{\tilde{\hat{v}}_{ex}}{\tilde{l}_n} + \tilde{v}_{ey0}\frac{\partial \tilde{\hat{n}}}{\partial \tilde{y}} = 0 \tag{3.38}$$

$$\frac{\partial \tilde{\hat{n}}}{\partial \tilde{t}} + \frac{\partial \tilde{\hat{v}}_{iy}}{\partial \tilde{y}} - \tilde{\hat{n}}\frac{\tilde{v}_{ix0}}{\tilde{l}_n} = 0 \tag{3.39}$$

$$\tilde{\hat{v}}_{ey}\tilde{B}_0 = \tilde{\hat{n}}\tilde{T}_{e0}/\tilde{l}_n \tag{3.40}$$

$$0 = \tilde{T}_{e0}\frac{\partial \tilde{\hat{n}}}{\partial \tilde{y}} - \frac{\partial \tilde{\hat{\phi}}}{\partial \tilde{y}} - \tilde{\hat{v}}_{ex}\tilde{B}_0 \tag{3.41}$$

$$\frac{\partial \tilde{\hat{v}}_{iy}}{\partial \tilde{t}} + \frac{\partial \tilde{\hat{\phi}}}{\partial \tilde{y}} + \tilde{n}_{n0}\tilde{\xi}_{ion0}\tilde{\hat{v}}_{iy} = 0 \tag{3.42}$$

Notice that the ionization terms are compensated by the gradients of the zero-th order solution in the continuity equations, explaining why there are no source terms in those equations.

If all equations in (3.38)−(3.42) are combined into one equation for the non-dimensional plasma density, the result is:

$$
\begin{aligned}
0 = {} & \frac{\partial^2 \tilde{\hat{n}}}{\partial \tilde{t}^2} - \tilde{l}_n \tilde{B}_0 \frac{\partial^2 \tilde{\hat{n}}}{\partial \tilde{t} \partial \tilde{y}} - \tilde{l}_n \left(\frac{\tilde{T}_{e0}}{\tilde{l}_n} - \tilde{E}_0 \right) \frac{\partial^2 \tilde{\hat{n}}}{\partial \tilde{y}^2} \\
& + \tilde{n}_{n0} \tilde{\xi}_{ion0} \left(\frac{\partial \tilde{\hat{n}}}{\partial \tilde{t}} - \tilde{\hat{n}} \frac{\tilde{v}_{ix0}}{\tilde{l}_n} \right) - \frac{\partial \tilde{\hat{n}}}{\partial \tilde{y}} \frac{\tilde{v}_{ix0}}{\tilde{l}_n}
\end{aligned}
\tag{3.43}
$$

Since $\tilde{T}_{e0}/\tilde{l}_n - \tilde{E}_0 > 0$, expression (3.43) is a wave-type equation with a term $(\partial^2 \tilde{\hat{n}}/\partial \tilde{y}^2)$ whose coefficient $(-\tilde{c}^2) = -\tilde{l}_n(\tilde{T}_{e0}/\tilde{l}_n - \tilde{E}_0) < 0$ corresponds to a wave velocity, $\tilde{c} = \sqrt{\tilde{T}_{e0} - \tilde{l}_n \tilde{E}_0} \approx \sqrt{\tilde{T}_{e0}}$, of the order of the ion acoustic speed. Moreover, the destabilizing element in equation (3.43) corresponds to the term $\tilde{\hat{n}} \tilde{n}_{n0} \tilde{\xi}_{ion0} \tilde{v}_{ix0}/\tilde{l}_n$, which is associated to ionization and comes from the coupling between the continuity and momentum equations of the ion species.

However, the solution of the eigenvalue problem associated to Eqs. (3.38)−(3.42), that is Eq. (3.36), indicates that, even though there are unstable perturbations ($\tilde{\omega}_{im} > 0$), the phase speed of the oscillations is very close to zero ($\tilde{\omega}_{re} \approx 0$). The reason for this is that in the previous approximation several terms have been neglected, in particular, the variation of neutral density.

If neutral density oscillations are reintroduced in the previous system, the resulting set of linearised non-dimensional equations can be written as:

$$
\frac{\partial \tilde{\hat{n}}}{\partial \tilde{t}} + \frac{\partial \tilde{\hat{v}}_{ey}}{\partial \tilde{y}} + \tilde{\hat{v}}_{ex}/\tilde{l}_n + \tilde{v}_{ey0} \frac{\partial \tilde{\hat{n}}}{\partial \tilde{y}} = \tilde{\hat{n}}_n \tilde{\xi}_{i0} \tag{3.44a}
$$

$$
\frac{\partial \tilde{\hat{n}}}{\partial \tilde{t}} + \frac{\partial \tilde{\hat{v}}_{iy}}{\partial \tilde{y}} - \tilde{\hat{n}} \tilde{v}_{ix0}/\tilde{l}_n = \tilde{\hat{n}}_n \tilde{\xi}_{i0} \tag{3.44b}
$$

$$
\tilde{\hat{v}}_{ey} = \tilde{\hat{n}} \tilde{T}_{e0}/\tilde{l}_n \tag{3.44c}
$$

$$
0 = \tilde{T}_{e0} \frac{\partial \tilde{\hat{n}}}{\partial \tilde{y}} - \frac{\partial \tilde{\hat{\phi}}}{\partial \tilde{y}} - \tilde{\hat{v}}_{ex} \tag{3.44d}
$$

$$
\frac{\partial \tilde{\hat{v}}_{iy}}{\partial \tilde{t}} + \frac{\partial \tilde{\hat{\phi}}}{\partial \tilde{y}} + \tilde{n}_{n0} \tilde{\xi}_{i0} \tilde{\hat{v}}_{iy} = 0 \tag{3.44e}
$$

$$
\frac{\partial \tilde{\hat{n}}_n}{\partial \tilde{t}} = -(\tilde{\hat{n}} \tilde{n}_{n0} + \tilde{\hat{n}}_n) \tilde{\xi}_{i0} \tag{3.44f}
$$

Equations (3.44), consistent with Eq. (3.35), represent the minimal system of linear equations capable of reproducing the results from the full solution of the eigenvalue problem given by Eqs. (3.30) in terms of phase speed and growth rate of the unstable perturbations for typical HET conditions.

3.4.2 Model with energy equation and heat conduction

In the previous section, a simplified stability analysis has been carried out accounting for the ionization process. However, the electron temperature was considered uniform and without oscillations, and consequently, no energy equation was included in the formulation. In this section, both assumptions are relaxed in order to check whether the instability detected with the isothermal model still appears with a more complex model including heat conduction terms. Nevertheless, electron inertia terms and plasma non-quasi-neutrality are still neglected since they are not believed to influence the low frequency instability under analysis.

Under the previous hypothesis, the complete set of governing conservation laws in Eqs. (3.28) is considered, including the electron energy conservation equation and the diffusive model for the electron heat conduction flux. In order to close the formulation, a hypothesis about the zero-th order temperature gradient is needed. In this case, an adequate choice seems to be assuming a fixed zero-th order electron temperature axial gradient as suggested by Gallardo and Ahedo [16]. Moreover, the ionization and effective electron collision rates are assumed to be constant, neglecting their dependence on the electron temperature, which is not critical for the analysis.

After the linearisation of the equations, the use of a Fourier-like form for the perturbations and the transformation to non-dimensional space, the stability analysis can be formulated as an eigenvalue problem, $(A\tilde{\omega} + B)\tilde{\mathbf{w}} = \mathbf{0}$ where $\tilde{\mathbf{w}} = (\tilde{n}, \tilde{n}_n, \tilde{v}_{ix}, \tilde{v}_{iy}, \tilde{\phi}, \tilde{v}_{ex}, \tilde{v}_{ey}, \tilde{T}_e, \tilde{q}_{ex}, \tilde{q}_{ey})$, to solve for the complex frequency of the perturbations, $\tilde{\omega}$. The non-dimensional azimuthal wave number, $\tilde{k}_y$, is the independent variable of the formulation and the non-dimensional parameters to consider are: $\tilde{\mathbf{p}}_0 = (\tilde{n}_{n0}, \tilde{v}_{ix0}, \tilde{v}_{nx0}, \tilde{\xi}_{i0}, \tilde{\xi}_{e0}, \tilde{T}_{e0}, \tilde{\alpha}_{i0})$. Once again, since electromagnetic and non-quasineutral terms and electron inertia are not considered, the electron momentum vector equation, together with the heat flux vector equation, can be pre-eliminated from the matrix formulation.

In this case, no analytical solution is investigated and only the results from the numerical solutions of the corresponding eigenvalue problem are shown. Figures 3.10 and 3.11 show the numerical solution of the stability problem for the same case as for the isothermal model. In particular, the growth rate of the most unstable mode and its real part are shown in Fig. 3.10. It is possible to see that the same long wavelength instability appears as in the isothermal model. Moreover, as expected, results from the simpler model are recovered if no temperature gradients are assumed for the zero-th order solution. As the temperature gradient increases, the range of azimuthal wave numbers where unstable perturbations exist is reduced. On the other hand, the phase speed of the unstable perturbation is still of the order of the ion acoustic speed and the frequency of the oscillation of the order of 10 kHz. Figure 3.11 shows the stability map of the perturbation with respect to the temperature and the neutral-to-plasma density ratio. The conclusions are similar to those derived from the isothermal model.

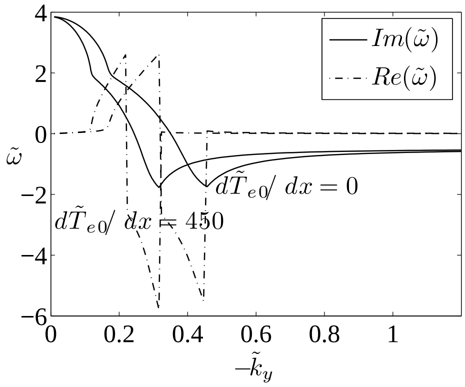

Figure 3.10: Growth rate (-) and corresponding real part (-·) of the most unstable solution for the following non-dimensional parameters: $\tilde{n}_{n0} = 20$, $\tilde{v}_{ix0} = 5$, $\tilde{v}_{nx0} = 5$, $\tilde{\xi}_{i0} = 0.5$, $\tilde{\xi}_{e0} = 0$, $\tilde{T}_{e0} = 450$ and $\tilde{B}_0 = 1$. Parametric variation of $\tilde{k}_y$ and $d\tilde{T}_{e0}/dx$

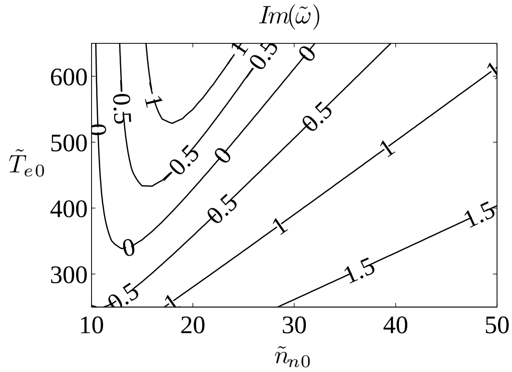

Figure 3.11: Growth rate of the most unstable solution for the following non-dimensional parameters: $\tilde{k}_y = 0.25$, $\tilde{v}_{ix0} = 5$, $\tilde{v}_{nx0} = 5$, $\tilde{\xi}_{i0} = 0.5$, $\tilde{\xi}_{e0} = 0$ and $\tilde{B}_0 = 1$. Parametric variation of $\tilde{n}_{n0}$ and $\tilde{T}_{e0} = d\tilde{T}_{e0}/d\tilde{x}$

3.5 Comparison against previous local stability analyses

The simplified expression derived in the previous section, Eq. (3.36), may be compared against the one derived by Frias *et al.* [140] in the limit of no ionization. Similar conclusions could be derived by comparing the expressions obtained in our study against those derived by Morozov *et al.* [2] or Esipchuk and Tilinin [1]. A major difference between the results obtained by Frias *et al.* and those presented here is related to the presence of the magnetic field gradient in the resulting expressions. While the length scale of variation of the magnetic field ($\tilde{l}_B = (Ld\ln B_0/dx)^{-1}$) does not appear in Eq. (3.36), it plays a major role in the analysis of Frias *et al.*. The reason for this, as explained before, is the fact that the equations for the electron axial and azimuthal velocity are replaced by Frias *et al.* in the electron continuity equation before the linearisation and the Fourier-expansion of the equations. In case this approach is used in our analysis, the following expression is obtained under the same hypothesis leading to Eq. (3.36):

$$\begin{aligned} 0 = \tilde{\omega}^2 + \tilde{\omega}(i\tilde{n}_{n0}\tilde{\xi}_{ion0} - i\tilde{v}_{ix0}/\tilde{l}_n + \tilde{k}_y\tilde{l}_g\tilde{B}_0) \\ +\tilde{n}_{n0}\tilde{\xi}_{ion0}\tilde{v}_{ix0}/\tilde{l}_n - \tilde{k}_y^2\tilde{l}_g\tilde{B}_0(\tilde{v}_{ey0} - 2\tilde{T}_{e0}/(\tilde{l}_B\tilde{B}_0)) \\ -\tilde{k}_y\tilde{l}_g\tilde{B}_0 i\tilde{n}_{n0}\tilde{\xi}_{ion0} \end{aligned} \tag{3.45}$$

where $1/\tilde{l}_g = 1/\tilde{l}_n - 2/\tilde{l}_B$. In the limit of no ionization and zero ion velocity gradient, Eq. (3.45) reduces to:

$$0 = \tilde{\omega}^2 + \tilde{\omega}\tilde{k}_y\tilde{l}_g\tilde{B}_0 - \tilde{k}_y^2\tilde{l}_g\tilde{B}_0(\tilde{v}_{ey0} - 2\tilde{T}_{e0}/(\tilde{l}_B\tilde{B}_0)) \tag{3.46}$$

which, aside from the use of non-dimensional variables, is equivalent to the expression derived by Frias *et al.* under the same hypotheses for purely azimuthal oscillations ($\tilde{k}_x = 0$), Eq. (17) of Ref. [140].

The analysis of Eq. (3.45) shows that in the case of positive gradients ($\tilde{l}_n, \tilde{l}_B > 0$), apart from the unstable solutions already predicted by Frias *et al.* when $\tilde{l}_B > 2\tilde{l}_n$, there are also unstable solutions when $\tilde{l}_B < 2\tilde{l}_n$ due to the ionization terms. Similarly to the unstable solutions given by Eq. (3.37), the latter unstable solutions from Eq. (3.45) have also a higher growth rate for smaller wave numbers. This is a distinct feature with respect to the unstable solutions already predicted by Frias *et al.*, for which the higher the wave number is, the higher the growth-rate is. Experiments show that both gradient-induced and spoke oscillations have low wave-numbers and this fact seems to point to the oscillations caused by the ionization terms in Eqs. (3.37) and (3.45).

Chapter 4

Low frequency global linear stability analysis

This chapter is devoted to the analysis of the stability of the Hall thruster discharge against low frequency azimuthal perturbations from a global point of view considering the variation of the plasma macroscopic variables along the whole thruster, in opposition to the local stability analysis presented in the previous chapter. This chapter is divided into the following sections:

1. Formulation, where the governing equations used for the global stability analysis is presented, analysing the influence of heat conduction and electron inertia terms

2. Background solution and parametric variations, where the reference solutions whose global stability is analysed are presented

3. Low frequency axial oscillations, where the well-known breathing mode is studied

4. Low frequency azimuthal oscillations, where the spoke oscillation is analysed with the approach presented in previous sections

4.1 Formulation

In order to analyse globally the stability of the Hall discharge it is necessary to consider the axial variations of the plasma properties along the thruster in the background solution as well as in the perturbed solution. To this end, the 1D axial model of Ahedo *et al.* [11] is used for the zero-th order formulation and extended for the perturbation problem. That model includes the necessary governing differential equations to simulate the HET discharge together with physically-meaningful boundary conditions at the anode, at the cathode, and inside the channel for a consistent sonic transition. The model is used to derive the governing equations of the perturbation problem, also called first order problem, by means of a linearisation process. The resulting formulation is not algebraic, but differential, as opposed to the analyses presented in the previous chapter. This means that for the resolution of the perturbation equations it is necessary to use numerical integration methods similar to those needed for the zero-th order problem.

4.1.1 Review of 1D axial model

Main hypotheses

The hypotheses of the 1D model of Ahedo *et al.* [11, 12, 3] of the Hall discharge are reviewed in this section. The following hypotheses are considered in the derivation of the governing equations:

- Each one of the species present in a HET (neutrals, electrons and ions) is accounted for with a separate set of macroscopic fluid equations based on particle, momentum and energy conservation laws. Only singly-charged ions are considered in this model leaving aside the population of multiply-charged ions.

- All plasma macroscopic variables are considered stationary. Even though the Hall thruster is known to have important temporal oscillations, axial and azimuthal, the 1D model captures the ionization and acceleration processes in a stationary manner.

- Radial variations of the macroscopic variables are neglected as the axial length of the thruster is larger than the radial width of the channel. In a way, the variables computed by the 1D model must be understood as an average along the radial direction for a given axial location. Due to this assumption, interactions with the lateral walls are included as source terms in the governing equations of the model, as for instance, wall energy losses and wall recombination.

- Azimuthal symmetry is assumed based on the annular geometry of the channel. Note, however, there are some elements like the cathode, the injector or the magnetic field that may break the azimuthal symmetry. But these effects are not considered important.

- The previous three assumptions yield a 1D axial stationary model of the thruster discharge. Figure 4.1 shows a schematic of the modelled geometry in the axial and radial directions for a fixed azimuth.

- The channel width is considered constant throughout the channel while plume divergence is considered in the model assuming a given velocity of lateral expansion of the plasma jet in the plume.

- The induced magnetic field is neglected and thus, Maxwell's equations are not included in the model. The magnetic field is equal to the externally applied field, which is stationary ($\partial \mathbf{B}/\partial t = 0$), solenoidal ($\nabla \cdot \mathbf{B} = 0$), irrotational ($\nabla \times \mathbf{B} = 0$) and mostly radial. Consequently, the electric field derives from a potential ($\nabla \phi = -\mathbf{E}$). Moreover, the only magnetic field component considered in the model is the radial one, $\mathbf{B} = B(x)\mathbf{e}_r$, being the axial and azimuthal components much smaller. This last hypothesis introduces an inconsistency as the magnetic field cannot then be fully irrotational as it only has one non-zero component.

- Quasi-neutrality is assumed as the Debye length in Hall thrusters is much smaller than the typical length scales of interest. This implies that Poisson's equation for the electric field is replaced with the condition of equal ion and electron particle densities. Non-quasineutral sheaths are considered attached to the walls and are accounted for properly in the boundary conditions, but are not solved for with the main governing equations.

- While electrons are highly magnetized due the large magnetic field, ions are considered un-magnetized since the ion Larmor radius is larger than the typical thruster dimensions.

- Ions and neutrals are modelled as cold species, this is, no ion or neutral temperature is included in the equations and therefore no energy equation is needed for those two species.

- Due to the very low mass of the electrons, inertial effects are neglected in the electron momentum equation, yielding an electron diffusive model. Note this hypothesis may be relaxed in the perturbation problem for the analysis of high frequency phenomena.

- Related to the previous assumption, the electron kinetic energy is neglected in the electron energy equation as it is very small compared to the internal energy as the electron fluid velocity is much smaller than the electron thermal velocity.

- Both ionization and electron-neutral elastic collisions are introduced in the continuity and momentum equations. Moreover, a sink of energy is introduced in the electron energy equation to account for ionization and radiation losses.

- Heat conduction is considered with a diffusive model as it helps to smooth out the electron temperature profile and widen the ionization region of the 1D solution. This assumption contrasts, however, with the model of Barral *et al.* [15, 57, 58, 59] for the breathing mode oscillation, where it is assumed that heat conduction is not relevant for the promotion of HET oscillations.

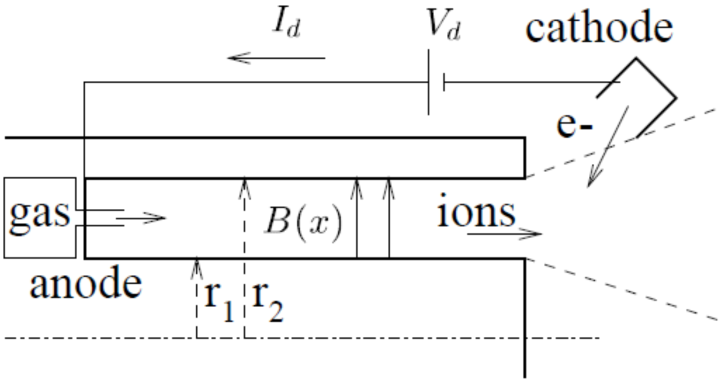

Figure 4.1: Schematic of the idealized 1D thruster. It consists of an injector, introducing the neutral gas into the channel; a channel, where the ionization takes place; an acceleration region, where the ions are electrically accelerated; a cathode, introducing the electrons into the channel; and an anode, where the electrons are collected.

Governing equations

Under the previous hypotheses, it is possible to simplify the general conservation equations for the three-species plasma and obtain the following formulation of the 1D model [11, 12, 3]:

$$\frac{1}{d_c}\frac{d}{dx}(nv_{ex}d_c) = \frac{1}{d_c}\frac{d}{dx}(nv_{ix}d_c) = -\frac{1}{d_c}\frac{d}{dx}(n_n v_{nx}d_c) = n(\nu_i - \nu_w) \tag{4.1a}$$

$$\frac{m_i}{d_c}\frac{d}{dx}(n_n v_{nx}^2 d_c) = -m_i n(\nu_i v_{nx} - \nu_w v_{nw}) \tag{4.1b}$$

$$\frac{m_i}{d_c}\frac{d}{dx}(n v_{ix}^2 d_c) = -en\frac{d\phi}{dx} + m_i n(\nu_i v_{nx} - \nu_w v_{ix}) \tag{4.1c}$$

$$0 = -\frac{d}{dx}(nT_e) + en\frac{d\phi}{dx} - m_e n\nu_e \chi^2 v_{ex} \tag{4.1d}$$

$$\frac{1}{d_c}\frac{d}{dx}\left(\frac{5}{2}nT_e v_{ex}d_c + q_{ex}d_c\right) = env_{ex}\frac{d\phi}{dx} - n\nu_i E_i' - n\nu_{we}T_e \tag{4.1e}$$

$$\frac{dT_e}{dx} = -\frac{2}{5}\frac{m_e\nu_e\chi^2}{nT_e}q_{ex} \tag{4.1f}$$

$$\frac{dd_c}{dx} = \frac{2c_{pl}}{v_{ix}} \equiv \gamma \tag{4.1g}$$

where x is the axial coordinate along the thruster channel; e, m_e and m_i are the electron charge, electron mass and ion mass respectively; d_c is the plasma beam or channel width; n_n and n are the neutral and plasma particle densities; v_{nx}, v_{ex} and v_{ix} are the fluid axial velocities of neutrals, electrons and ions respectively; T_e, ϕ and q_{ex} are the electron temperature, the electric potential, and the electron axial heat flux, respectively; ν_e is the effective electron collision frequency, $\nu_e = \nu_B + \nu_{wm} + \nu_{en}$, accounting for Bohm-type diffusion, ν_B, near-wall conductivity, ν_{wm}, and electron-neutral collisions, ν_{en}; ν_i, ν_w and ν_{we} represent the frequencies for ionization, particle recombination, and energy losses at lateral walls, respectively; E_i' models the energy loss per ion-electron due to ionization and radiation; and γ and c_{pl} are the plume divergence angle and the plume radial expansion velocity, which are equal to zero within the channel and depend on the electron temperature at the channel exit point ($c_{pl} = \sqrt{T_{eE}/m_i}$) in the plume. The expression used for the Bohm-diffusion is $\nu_B = \alpha_B\omega_{ce}$, where $\omega_{ce} = eB/m_e$ is the electron cyclotron frequency and α_B is a constant empirical coefficient whose value is typically selected so as to match experimental results ($\alpha_B \sim 0.01$). The electron momentum equation in the azimuthal direction, $v_{ey} = v_{ex}\chi$, where v_{ey} is the azimuthal electron velocity and $\chi = \omega_{ce}/\nu_e \gg 1$ is the Hall parameter, has been used implicitly in the axial electron momentum equation in (4.1d). Similarly, the diffusive model for the heat flux in the azimuthal direction, $q_{ey} = q_{ex}\chi$, where q_{ey} is the azimuthal electron heat flux, has been used implicitly for the axial heat flux equation in (4.1f). An equivalent frequency ν_H replacing ν_e may be defined as $\nu_H = (m_e/m_i)\chi^2\nu_e$ so that the ion mass m_i can be factored out in all momentum equations. Ions impacting the lateral walls and the anode undergo wall recombination and return to the channel as neutrals. The velocity of the newly born neutrals is not equal to the ion velocity, but is the result of an accommodation process in the wall, $v_{nw} = a_w v_{nx} + (1 - a_w)v_{ix}$, where a_w is the accommodation factor. The no-accommodation limit corresponds to the case $a_w = 0$.

Note that the axial electron velocity is negative all along the thruster channel as electrons drift from the cathode to the anode. On the contrary, the neutral axial velocity is positive as the gas moves from the injector to the channel exit. In the case of the axial ion velocity, it is positive in a large part of the thruster channel due to the outward acceleration, but it becomes negative in a back-streaming region near the anode where the axial electric field is negative. The azimuthal electron velocity is also negative all along the thruster and consists of the combination of **E**x**B** and diamagnetic drifts, being the former the dominant one in the acceleration region, while the diamagnetic drift dominates in the upstream part of the ionization region.

The combination of the previous equations allows obtaining an equation for $h \equiv \ln n$ as:

$$P\frac{dh}{dx} = G \tag{4.2}$$

where P and G are functions of the macroscopic variables but not of their derivatives:

$$P = T_e/m_i - v_{ix}^2 \tag{4.3a}$$

$$G = -\nu_H v_{ex} + \nu_i(v_{nx} - 2v_{ix}) + \nu_w v_{ix} + \frac{2}{5}\frac{\nu_H q_{ex}}{nT_e} + v_{ix}^2\frac{d\ln d_c}{dx} \tag{4.3b}$$

Note that in this formulation the Mach number is defined as:

$$M_i = \frac{v_{ix}}{\sqrt{T_e/m_i}} \tag{4.4}$$

An important aspect to take into account is the presence of sonic points in the discharge which occur when $P = 0$. It is possible to proof that there are two sonic points in the simulation domain [11], one singular ($G \neq 0$), at the anode sheath transition, and another one regular ($G = 0$), inside the channel, where the accelerated ion flow becomes supersonic. The presence of these sonic points makes the numerical resolution of the previous equations complicated. A detailed description of the boundary conditions associated to the previous system of ordinary differential equations is described by Ahedo *et al.* [11]. Expressions for the different frequencies mentioned above (ν_i, ν_e, ν_w, ν_{we}) are developed elsewhere [11, 12, 3, 13]. A summary of the boundary conditions and the expressions for the frequencies is presented below together with the solution method.

Several versions of the model above have been used to characterize the HET discharge [11], include heat conduction effects [12], evaluate the influence of wall losses [3], carry out parametric investigations on the operating conditions [13], model two-stage Hall thrusters [180] and, even, analyse the stability of the discharge against small axial perturbations to study the properties of the breathing mode [14, 181, 15]. Thus, this 1D model is a very suitable candidate for extension in order to analyse the azimuthal stability of the thruster.

Figure 4.2 shows the most important points in the thruster for the resolution of the 1D model. In the figure, the neutral flow (Γ_n), the ion flow (Γ_i) and the electron flow (Γ_e) are represented with the corresponding directions. Note there is an ion back-streaming region in the near anode region that is necessary in order to fulfil the boundary conditions at the anode. The discharge voltage is applied between the anode and the cathode. In this model, an ideal circuit is assumed and, thus, a constant voltage is considered.

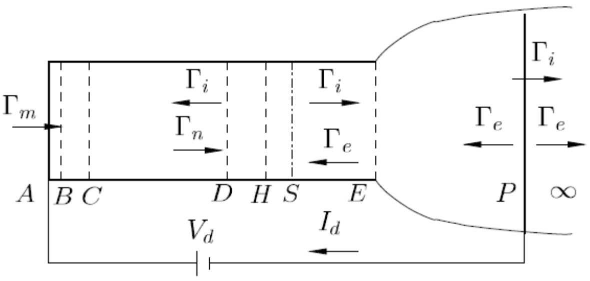

Figure 4.2: Schematic of the important points of the 1D model. A: anode. B: anode sheath transition. C: intermediate point. D: zero ion velocity point. S: regular sonic point. E: channel exit. P: cathode

Analysis of terms

The expressions for the different terms appearing in the formulation above are described and justified next. These include the magnetic field, the particle source terms, the electron conductivity and various energy losses.

Magnetic field

As mentioned above, the only magnetic field component included in the model is the radial one. Typical magnetic field profiles for Hall thrusters show a maximum near the exit of the channel and decrease towards the anode and the cathode. This profile is represented in the model by the following Gaussian expression:

$$B(x) = B_{min_i} + (B_{max} - B_{min_i}) \exp\left[\frac{(x - x_{max})^2}{L_{m_i}^2}\right] \tag{4.5}$$

where $B_{max} > 0$ and $B_{min_i} > 0$ are the maximum and minimum magnetic fields, x_{max} is the axial coordinate of the maximum magnetic field and L_{m_i} controls how rapidly the magnetic field decreases away from its maximum. Note that B_{min_i} and L_{m_i} have two separate values, one for the plume and another one for the channel. This means that the values of B_{min} and L_m corresponding to the channel must be used when $x < x_{max}$ and the values corresponding to the plume when $x > x_{max}$. This allows modelling the different slopes of the magnetic field inside and outside the channel. Moreover, this procedure ensures continuity of the magnetic field profile while maintaining a reasonable degree of fidelity with respect to the real magnetic profiles.

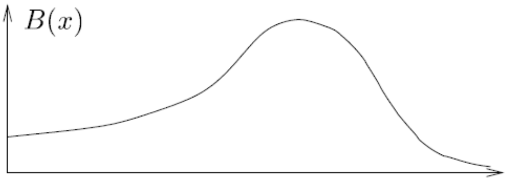

Figure 4.3: Schematic of the axial magnetic field variation in a typical Hall thruster

Particle source terms

Two different particle source terms are accounted for in the formulation: bulk ionization and wall recombination. Bulk recombination is considered negligible and is not included in the model.

Gas ionization rate

For usual conditions, ionization is one of the fundamental processes of the Hall discharge. It generates ions that are then accelerated. This process is modelled with the ionization source term, S_i. Only singly charged ions are considered and thus this term must appear as a source in the electron and ion continuity equations and as a sink in the neutral equations. The ionization term may be expressed as:

$$S_i = n\nu_i \tag{4.6}$$

where the ionization frequency may be expressed as, $\nu_i = n_n R_i(T_e)$, and $R_i(T_e)$ is the ionization rate, which depends on the electron temperature and may be evaluated by fitting a function to experimental results.

The electron species is modelled as diffusive and can be considered locally Maxwellian. Hence $R_i(T_e)$ may be written as:

$$R_i(T_e) = \frac{8\pi}{m_e}\int_0^\infty \sigma_i(E) E f_e(E) dE \tag{4.7}$$

where E is the energy of an electron, $f_e(E)$ is the Maxwellian distribution function of electrons and $\sigma(E)$ is the ionization cross-section.
These functions may be approximated as [11]:

$$\sigma_i(E) = \sigma_{i0}\Big(1 - \exp(E/E_i - 1)\Big) \tag{4.8a}$$

$$f_e(E) = (m_e/2\pi T_e)^{3/2}\exp(-E/T_e) \tag{4.8b}$$

where σ_{i0} is a constant and, then, the final expression for the ionization function may be written as:

$$R_i(T_e) = \bar{c}_e\bar{\sigma}_i(T_e) \tag{4.9a}$$

$$\bar{c}_e = \sqrt{8T_e/\pi m_e} \tag{4.9b}$$

$$\bar{\sigma}_i(T_e) = \sigma_{i0}\Big(1 + \frac{T_e E_i}{(T_e + E_i)^2}\exp(-\frac{T_e}{E_i})\Big) \tag{4.9c}$$

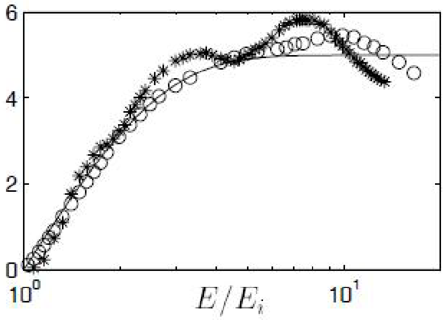

Figure 4.4: Comparison between experimental results and the fitted expression for the ionization cross-section $\sigma_i(E)$ for $\sigma_{i0} = 5\text{x}10^{-20}m^2$.

Aside from the particle sink and source terms for the continuity equations, there is an exchange of momentum associated to the ionization process. This can be modelled as:

$$M_i = n v_{nx}\nu_i \tag{4.10}$$

Wall recombination

Wall recombination takes place when an ion hits the wall and is returned to the plasma as a neutral. In this 1D model, this process is taken into account as a particle recombination term, S_w. This term must be included in the continuity equations of electrons and ions as a sink of particles, and in the continuity equations of neutrals as a source of particles. The analysis of the wall-plasma interaction in the lateral walls allows deriving the expression for the wall recombination. The complete analysis is presented in Ref. [182] and used in Ref. [3]. The expression used for the recombination term is:

$$S_w = n\nu_w \tag{4.11a}$$

$$\nu_w = \frac{\nu_{w0}}{d_c}\sqrt{\frac{T_e}{m_i}} \tag{4.11b}$$

where ν_{w0} is a parameter of the model whose value is estimated to be around $\nu_{w0} \sim 0.1 - 0.2$.

As for ionization, wall recombination also implies a net exchange of momentum between ions and neutrals. This is captured by the following terms in the momentum equations of the ion and neutral species:

$$M_{wi} = -nv_{ix}\nu_w \tag{4.12a}$$

$$M_{wn} = nv_{nw}\nu_w \tag{4.12b}$$

where v_{nw} is the velocity of the neutrals generated in the walls from ion recombination. As mentioned previously, ions are recombined in the walls, but the velocity of the newly born neutrals differs from that of the ions as an accommodation process occurs. This implies that there is a net loss of momentum to the walls as a consequence of the accommodation process. The velocity v_{nw} may be expressed as:

$$v_{nw} = a_w v_{nx} + (1 - a_w)v_{ix} \tag{4.13}$$

where a_w is the accommodation factor, a parameter of the simulation. Reasonable values for the accommodation factor are estimated to be in the range $a_w \sim 0.8 - 0.9$.

Electron conductivity

Electron mobility across the magnetic field and along the thruster can be caused by several phenomena: electron-neutral collisions, near wall conductivity or azimuthal oscillations among others. In order to account for all these effects, the electron conductivity across the magnetic field is represented by an effective electron collisional frequency. Strictly speaking, this frequency should only take into account the electron-neutral collisional frequency, ν_{en}. However, in order to account for the anomalous diffusion, it is necessary to add additional collisionality. This translates into an additional Bohm diffusion frequency, ν_B, and near wall conductivity, ν_{wm}. Each one of those terms is described in the following paragraphs. Note that the goal of this work is analysing the possible role of the azimuthal oscillations in the anomalous diffusion. However, in this 1D model the effect of oscillations cannot be taken into account yet. Hence the need to include a Bohm diffusion frequency. Ultimately, the analysis of the perturbed problem should allow replacing the expression of ν_B with a model based solely on azimuthal perturbations.

Electron-neutral collisions

The collisions between the neutral and electron species are modelled with the following expression:

$$\nu_{en} = n_n \sigma_{en} \bar{c}_e \tag{4.14}$$

where σ_{en} is the electron-neutral cross-section, which is assumed to be a constant value, $\sigma_{en} = 27\text{x}10^{-20}\text{m}^2$. As mentioned previously, electron-neutral collisions do not explain the high cross-field mobility of the electrons inside the channel. In fact, if this were the only mechanism, the electron diffusion would be two orders of magnitude smaller. Hence, the need to account for Bohm diffusion and near wall conductivity.

Bohm diffusion

Bohm diffusion is modelled with the following expression:

$$\nu_B = \alpha_B \omega_{ce} \tag{4.15}$$

where $\omega_{ce} = eB/m_e$ is the electron cyclotron frequency and α_B is the Bohm coefficient. The classical value for this coefficient is $\alpha_B = 1/16$. However, typical values to obtain a reasonable agreement between the simulation results and the experiments are in the range of $\alpha_B \sim 1/100$. This coefficient must be considered as a phenomenological parameter to match experiments and simulations. Moreover, some authors propose to use different values for the coefficient inside and outside the thruster as experiments show that the electron mobility is higher in the plume than inside the thruster.

Near-wall conductivity

The plasma-wall interaction is a complex problem that needs to be modelled consistently. In particular, the secondary electron emission (SEE) from the ceramic walls determines the losses of momentum and energy to the wall. The hypotheses and derivation of the model are not included here. These can be found in related literature [182, 12, 183]. However, for the sake of completeness and clarity the expressions are presented next. The SEE is controlled by the SEE yield, $\delta_w(T_e)$, that relates the flux of incoming primary electrons and outgoing secondary electrons. This function can be represented as:

$$\delta_w(T_e) = \sqrt{\frac{T_e}{T_{SEE}}}, \qquad T_e \leq T_e^* \tag{4.16a}$$

$$\delta_w(T_e) = \sqrt{\frac{T_e^*}{T_{SEE}}}, \qquad T_e > T_e^* \tag{4.16b}$$

where T_{SEE} is the electron temperature for a Maxwellian population producing a 100% of SEE and T_e^* is the electron temperature where the saturation limit of the SEE yield is reached. It can be proved that $T_e^* = 0.967 T_{SEE}$ and that the temperature T_{SEE} can be computed as $T_{SEE} \approx 0.66 E_{SEE}$ where E_{SEE} is the energy of a mono-energetic beam yielding a 100% of SEE. The energy E_{SEE} is the value typically derived from experiments for a given wall material.

Once the SEE yield is known, the electron momentum loss frequency can be written as:

$$\nu_{wm} = \beta_m(\delta_w)\nu_w \tag{4.17a}$$

$$\beta_m(\delta_w) = \frac{\delta_w}{1-\delta_w} \tag{4.17b}$$

Energy losses

As a consequence of the ionization and the plasma-wall interaction, some energy losses take place and must be accounted for in the electron energy equation. The next paragraphs provide the expressions for these terms included in the electron energy equation.

Ionization and radiation losses

The ionization process has a cost in terms of energy. In fact, the lower the temperature the higher the ionization cost is. These losses also account for multi-step ionization and radiation. A typical expression for this energy loss is proposed by Dugan [184]:

$$Q_i = -n\nu_i E_i'(T_e) \tag{4.18a}$$

$$E_i'(T_e) = E_i\left(2 + \frac{1}{4}\exp\frac{2E_i}{3T_e}\right) \tag{4.18b}$$

where E_i is the first ionization energy for the neutrals ($E_i = 12.1eV$ for Xenon).

Lateral wall losses

Following the derivation of the electron momentum losses to the lateral walls, it is possible to express the energy losses caused by the plasma-wall interaction as:

$$Q_{we} = -n\nu_{we}T_e \tag{4.19}$$

where the wall energy loss frequency may be expressed as:

$$\nu_{we} = \beta_e(\delta_w)\nu_w \tag{4.20a}$$

$$\beta_e(\delta_w) = 5.62 + \frac{1.65}{1-\delta_w} \tag{4.20b}$$

Note that this expression implies that the wall energy loss frequency is only a function of the electron temperature as both the SEE yield, δ_w, and the wall recombination frequency, ν_w, depend only on the electron temperature.

P and G functions

As presented before, the equation (4.2) for $h \equiv \ln n$ contains two functions, P and G. These can be expressed functionally as:

$$P = P(\mathbf{y},\mathbf{q}) \equiv P(\mathbf{u}) \qquad\qquad G = G(\mathbf{y},\mathbf{q}) \equiv G(\mathbf{u}) \tag{4.21}$$

where vector $\mathbf{y} = (x, h, v_{ix}, T_e, \phi, n_n, v_{ex}, v_{nx}, q_{ex}, d_c)$ is the vector of dependent variables, vector $\mathbf{q}(\mathbf{y}) = (\nu_w, \nu_{we}, \nu_H, \nu_i, E_i', \gamma)$ contains the different dependent functions of the model and $\mathbf{u} = (\mathbf{y},\mathbf{q})$ is the composition of the previous two vectors. Based on this formulation, it is possible to write:

$$\frac{dP}{dx} = \sum_i \frac{\partial P}{\partial u_i}\frac{du_i}{dx} \qquad \frac{d^2P}{dx^2} = \sum_{i,j}\frac{\partial^2 P}{\partial u_i \partial u_j}\frac{du_i}{dx}\frac{du_j}{dx} + \sum_i \frac{\partial P}{\partial u_i}\frac{d^2u_i}{dx^2} \tag{4.22a}$$

$$\frac{dG}{dx} = \sum_i \frac{\partial G}{\partial u_i}\frac{du_i}{dx} \qquad \frac{d^2G}{dx^2} = \sum_{i,j}\frac{\partial^2 G}{\partial u_i \partial u_j}\frac{du_i}{dx}\frac{du_j}{dx} + \sum_i \frac{\partial G}{\partial u_i}\frac{d^2u_i}{dx^2} \tag{4.22b}$$

$$\frac{dq_i}{dx} = \sum_j \frac{\partial q_i}{\partial y_j}\frac{dy_j}{dx} \qquad \frac{d^2q_i}{dx^2} = \sum_{j,k}\frac{\partial^2 q_i}{\partial y_j \partial y_k}\frac{dy_j}{dx}\frac{dy_k}{dx} + \sum_j \frac{\partial q_i}{\partial y_j}\frac{d^2y_j}{dx^2} \tag{4.22c}$$

Generic form of equations

In the previous paragraphs the different equations and terms of the 1D model have been presented. However, it is interesting to obtain a more generic representation of the equations to simplify further mathematical derivations. Due to the presence of sonic points ($P = 0$) in the quasi-neutral domain under analysis, the following change of variable is introduced in order to simplify the integration of the differential equations:

$$\frac{dx}{d\xi} = P \tag{4.23}$$

Using this change of variable, $x(\xi)$, the governing equations may be expressed in vector form as:

$$\frac{d\mathbf{y}}{d\xi} = \mathbf{F}(\mathbf{y}, \mathbf{q}(\mathbf{y})) \tag{4.24}$$

This generic form of the equations simplifies some of the derivations that are presented next, specially in the perturbation problem, where the formulation becomes rather verbose.

After the change of variable and some rearrangements in (4.1) the governing equations may be rewritten as:

$$\frac{dx}{d\xi} = P \tag{4.25a}$$

$$\frac{dh}{d\xi} = G \tag{4.25b}$$

$$\frac{dn_n}{d\xi} = -P\frac{n}{v_n}(\nu_i - \nu_w) - \frac{n_n}{v_n}\frac{dv_n}{d\xi} - n_n\frac{d\ln d_c}{d\xi} \tag{4.25c}$$

$$\frac{dv_{ex}}{d\xi} = P(\nu_i - \nu_w) - v_{ex}\frac{dh}{d\xi} - v_{ex}\frac{d\ln d_c}{d\xi} \tag{4.25d}$$

$$\frac{dv_{ix}}{d\xi} = P(\nu_i - \nu_w) - v_{ix}\frac{dh}{d\xi} - v_{ix}\frac{d\ln d_c}{d\xi} \tag{4.25e}$$

$$\frac{dv_{nx}}{d\xi} = P\frac{n}{n_n}\nu_w(1 - a_w)\left(\frac{v_{ix}}{v_{nx}} - 1\right) \tag{4.25f}$$

$$\frac{d}{d\xi}\left(\frac{e\phi}{m_i}\right) = \frac{d}{d\xi}\left(\frac{T_e}{m_i}\right) + \frac{T_e}{m_i}\frac{dh}{d\xi} + \nu_H v_{ex} P; \tag{4.25g}$$

$$\frac{d}{d\xi}\left(\frac{T_e}{m_i}\right) = -P\frac{2}{5}\frac{\nu_H q_{ex}/m_i}{nT_e/m_i} \tag{4.25h}$$

$$\begin{gathered}\frac{d}{d\xi}\left(\frac{q_{ex}}{m_i}\right) = -\frac{3}{2}nv_{ex}\frac{T_e}{m_i}\frac{dh}{d\xi} - \frac{3}{2}nv_{ex}\frac{d}{d\xi}\left(\frac{T_e}{m_i}\right) - \frac{5}{2}n\frac{T_e}{m_i}\frac{dv_{ex}}{d\xi} + \\ + \left(\nu_H n v_{ex}^2 - \nu_i n\frac{E_i'}{m_i} - \nu_{we} n\frac{T_e}{m_i}\right)P - \left(\frac{5}{2}\frac{T_e}{m_i}nv_{ex} + \frac{q_{ex}}{m_i}\right)\frac{1}{d_c}\frac{dd_c}{d\xi}\end{gathered} \tag{4.25i}$$

$$\frac{dd_c}{d\xi} = P\gamma \tag{4.25j}$$

Boundary conditions

The governing equations of the 1D model together with the different expressions described above need a set of boundary conditions. These correspond to the anode and cathode, but also to the point inside the thruster where the ion flow becomes supersonic smoothly (i.e., regular sonic point). The anode, together with the injector, are a source of neutrals and a sink of electrons, while the cathode can be modelled as a source of electrons at approximately constant temperature.

The following boundary conditions are identified for the 1D model:

- The ion and electron velocities at the anode, v_{ixB} and v_{exB}, are related by the expression characterizing the anode sheath presented in the next section.
- The heat conduction is known relative to the electron energy flow at the anode sheath transition, this is, $q_{exB}/(nv_{exB}T_{eB})$ is known.
- The difference in electric potential between the anode and the cathode must be equal to the applied discharge potential ($\phi_A - \phi_P = V_d$)
- The ion flow is sonic at the anode sheath transition ($M_{iB} = -1$)
- The mass flow through the injector is also known ($\dot{m}$). Because of mass continuity this flow is constant along the thruster.
- The neutral velocity at the anode is known (v_{nxA})
- The sonic point inside the channel is regular, this is, $M_{iS} = 1$ and $G_S = 0$.
- The electron temperature at the cathode is given (T_{eP})

Similarly to the governing equations, the boundary conditions may be expressed in vector form as:

$$\mathbf{H}(\mathbf{y}) = 0 \tag{4.26}$$

In the case of the anode, the quasi-neutral governing equations must be accompanied by a model describing the behaviour of the anode sheath so that the boundary conditions at the anode can be transferred to the anode sheath transition, which is the edge of the quasi-neutral domain for integration. A singular sonic point is found at this anode sheath transition where the derivatives of the plasma variables become infinite in the quasi-neutral scale. Such singular points are only admissible in the edges of the quasi-neutral domain.

Furthermore, as mentioned previously, regular and singular sonic points appear inside the channel and at the anode sheath transition. Since $P = 0$ at these points, the governing equations presented above must be Taylor-expanded so that the equations can be integrated normally. This expansion process is presented in the next paragraphs as well.

Anode sheath

In order to fulfil the constraints imposed by the anode, there must be a thin layer attached to the anode separating it from the quasi-neutral plasma. This sheath is very small compared to the thruster dimensions, and is not modelled by the quasi-neutral equations presented above. However, the sheath must be included in the model to ensure that the electron and ion flows to the anode are consistent with the diffusive ones from the channel.

The anode sheath can be considered stationary, non-collisional and un-magnetized. Under these conditions, the usual conservations laws (particle, momentum and energy) are applicable for each of the species, including ions, electrons and neutrals. Based on them, it is possible to derive the following expressions relating the plasma variables at the anode and the anode sheath transition [11]:

$$\frac{e\phi_{AB}}{T_{eB}} = \ln\sqrt{\frac{T_{eB}}{2\pi m_e v_{exB}^2}} \tag{4.27a}$$

$$\frac{q_{exB}}{n_B v_{exB} T_{eB}} = \frac{e\phi_{AB}}{T_{eB}} - \frac{1}{2} \tag{4.27b}$$

$$(nv_{ix})_A = (nv_{ix})_B \qquad (nv_{ex})_A = (nv_{ex})_B \tag{4.27c}$$

$$n_{nA} = n_{nB} \qquad v_{nxA} = v_{nxB} \tag{4.27d}$$

Figure 4.5 shows a schematic of the anode and the anode sheath transition.

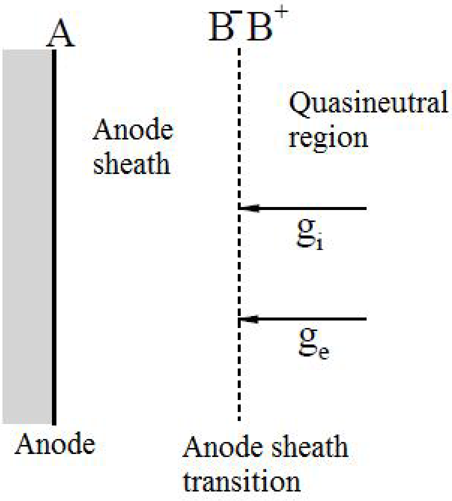

Figure 4.5: Schematic of anode sheath transition

Expansion at the regular sonic point

As some plasma conditions are provided at the regular sonic transition, as part of the resolution method presented below, it is necessary to integrate the governing equations starting from point S. However, this point verifies that $P_S = 0$ and $G_S = 0$ and therefore the equations must be Taylor expanded in the vicinity of point S in the following way.

It is possible to write the evolution equations for x and h in the vicinity of S in matrix form as:

$$\begin{pmatrix} \dfrac{dx}{d\xi} \\ \dfrac{dh}{d\xi} \end{pmatrix} \approx \begin{pmatrix} \dfrac{\partial P}{\partial x} & \dfrac{\partial P}{\partial h} \\ \dfrac{\partial G}{\partial x} & \dfrac{\partial G}{\partial h} \end{pmatrix} \begin{pmatrix} \Delta x \\ \\ \Delta h \end{pmatrix} \approx K \begin{pmatrix} \Delta x \\ \\ \Delta h \end{pmatrix} \tag{4.28}$$

where $\Delta x = x - x_S$, $\Delta h = h - h_S$.

The eigenvectors of the matrix K provide the directions for the Taylor expansion from point S. In order to compute matrix K it is necessary to account for the rest of equations (4.25) so that the partial derivatives with respect to x and h are computed properly. In this formulation, P and G must be understood as functions of x and h solely, being the rest of the variables related to those through the differential equations of the model. For instance, the axial ion velocity is related to x and h by the following expression:

$$dv_{ix} = (\nu_i - \nu_w)dx - v_{ix}dh$$

Similar expressions may be obtained for the rest of the variables $(v_{ix}, v_{ex}, v_{nx}, T_e, \phi, n_n, q_{ex}, d_c)$ making use of equations (4.25) and for the dependent variables $(\nu_w, \nu_{we}, \nu_H, \nu_i, E_i', \gamma)$.

Out of the two pairs of eigenvectors, based on our experience with model, the one causing the highest change in the Mach number is selected for the expansion. Once the direction of the expansion is known, a infinitesimal delta $(\Delta\xi)$ is applied to compute the value of the Taylor-expanded variables.

Expansion at the singular sonic point

As the anode sheath transition is a singular sonic point, some of the derivatives are infinite in the quasi-neutral scale. However, the equations expressed in the variable ξ do not show such behaviour and it is possible to Taylor expand them in order to leave the anode sheath transition. At this point, $P_B = 0$ but $G_B \neq 0$ and therefore many of the equations in (4.25) have a dominant term associated to $dh/d\xi$, which is non-zero. The neutral equations and the evolution of the x coordinate, however, do not have such terms and are expanded. The following expansion is used:

$$\frac{dx}{d\xi} = -2v_{ix}\frac{dv_{ix}}{d\xi}\Delta\xi \tag{4.29a}$$

$$\frac{dn_n}{d\xi} = -\frac{n}{v_n}(\nu_i - \nu_w)\frac{dx}{d\xi} - \frac{n_n}{v_n}\frac{dv_n}{d\xi} \tag{4.29b}$$

$$\frac{dv_{nx}}{d\xi} = \frac{n}{n_n}\nu_w(1 - a_w)\left(\frac{v_{ix}}{v_{nx}} - 1\right)\frac{dx}{d\xi} \tag{4.29c}$$

$$\frac{d}{d\xi}\left(\frac{T_e}{m_i}\right) = -\frac{2}{5}\frac{\nu_H q_{ex}}{nT_e}\frac{dx}{d\xi} \tag{4.29d}$$

where $\Delta\xi$ is an infinitesimal value needed to depart from the anode sheath transition.

Solution method

Non-dimensional formulation

In order to simplify the implementation and the resolution of the 1D model, it is made non-dimensional using the following reference variables for temperature, flow and cross section:

$$T_{ref} = E_i = 12.1\text{eV} \qquad \Gamma_{ref} = 10^{22}\text{m}^{-2}\text{s}^{-1} \qquad \sigma_{ref} = \sigma_{i0}\sqrt{m_i/m_e} \approx 2.45 \text{ x } 10^{-17}\text{m}^2$$

Based on those basic reference variables, other references variables for the velocity, density, frequency, length, magnetic field, area, mass flow and charge current are defined as:

$$v_{ref} = \sqrt{T_{ref}/m_i} \qquad n_{ref} = \Gamma_{ref}/v_{ref} \qquad \nu_{ref} = \sigma_{ref}\Gamma_{ref} \qquad l_{ref} = v_{ref}/\nu_{ref}$$
$$B_{ref} = \nu_{ref}\sqrt{m_i m_e}/q \qquad A_{ref} = 2\pi d_c R \qquad \dot{m}_{ref} = m_i A_{ref}\Gamma_{ref} \qquad I_{ref} = q A_{ref}\Gamma_{ref}$$

where R and d_c are the mean radius and the width of the channel. For example, for a SPT-100 thruster, these parameters are $R = 42.5$mm and $d_c = 15$mm.

Integration procedure

The system of first order differential equations given by equations (4.24) is integrated with a standard ODE solver. However, due to the various locations of boundary conditions (A, B, S, and P) the resolution method is rather complex. The approach followed is described next.

First, a solution is integrated from the anode (A). To this end, some values of the plasma variables need to be guessed a-priori as the complete plasma state at the anode is not known. The plasma state at the anode is then translated to the anode sheath transition (B) using the anode model. The expansion presented above is applied to solve the issue of the singularity at point B so that the integration of the equations can be initiated normally.

Secondly, another solution is integrated from the regular sonic point inside the channel (S) towards the anode (A) and cathode (P) separately. Again, some values of the plasma variables need to be guessed a-priori and the expansion presented above for the regular sonic point S is applied in both directions: inwards for the integration towards the anode and outwards for the integration towards the cathode.

The solutions integrated from the anode and the regular sonic point meet each other at an intermediate point (C). The plasma state at this intermediate point is in principle different in each solution. Hence, additional conditions are imposed to ensure continuity of the overall solution at this intermediate point. These conditions are used to iterate on the values guessed a-priori for the plasma variables at the anode and sonic transition. Additionally, the boundary conditions in the cathode, as well as the discharge voltage condition, are also included in this iterative procedure until convergence is reached and a solution satisfying all conditions is obtained. The need for the two matching solutions from points B and S comes from the fact that the solution integrated towards the anode is very sensitive to changes in the conditions at point S and this makes it very complicated to obtain solutions with a negative sonic point at the anode sheath transition ($M_B = -1$). If no special measures are taken, the solution normally reaches a positive sonic point, which is not physically valid under normal conditions.

The whole procedure can be seen as the resolution of a non-linear system of equations where the equations are defined by the continuity conditions at an intermediate point, the temperature at the cathode and the discharge voltage. The variables of this non-linear system of equations are the plasma variables at the anode and sonic transition point that are not known a-priori from operating conditions or boundary conditions.

4.1.2 Linear time-dependent 2D model

This section presents the formulation of the linear time-dependent 2D model developed with the goal of analysing azimuthal oscillations in HET from a global point of view. In first place, the general 2D formulation is presented as an extension of the 1D model described in the previous section. Then, the linearisation in time and azimuthal direction is carried out to derive the linearised model that will be used for the global stability analyses.

General 2D formulation

The equations (4.1) presented in the previous section can be extended to two dimensions, azimuthal and axial, with time-dependent terms. Under the same hypotheses of the 1D model, the governing 2D unsteady equations of the plasma discharge may be written as:

$$\frac{\partial n}{\partial t}+\frac{1}{d_c}\nabla\cdot(n\mathbf{v}_e d_c)=\frac{\partial n}{\partial t}+\frac{1}{d_c}\nabla\cdot(n\mathbf{v}_i d_c)=-\frac{\partial n_n}{\partial t}-\frac{1}{d_c}\nabla\cdot(n_n\mathbf{v}_n d_c)=n(\nu_i-\nu_w) \quad (4.30a)$$

$$m_i\left(\frac{\partial}{\partial t}(n_n\mathbf{v}_n)+\frac{1}{d_c}\nabla\cdot(n_n\mathbf{v}_n\mathbf{v}_n d_c)\right)=-m_i n(\nu_i\mathbf{v}_n-\nu_w\mathbf{v}_{nw}) \quad (4.30b)$$

$$m_i\left(\frac{\partial}{\partial t}(n\mathbf{v}_i)+\frac{1}{d_c}\nabla\cdot(n\mathbf{v}_i\mathbf{v}_i d_c)\right)=-en\nabla\phi+m_i n(\nu_i\mathbf{v}_n-\nu_w\mathbf{v}_i) \quad (4.30c)$$

$$0=-\nabla(nT_e)-en(-\nabla\phi+\mathbf{v}_e\times\mathbf{B})-m_e n\nu_e\mathbf{v}_e \quad (4.30d)$$

$$\frac{\partial}{\partial t}\left(\frac{3}{2}nT_e\right)+\frac{1}{d_c}\nabla\cdot\left(\frac{5}{2}nT_e\mathbf{v}_e d_c+\mathbf{q}_e d_c\right)=en\mathbf{v}_e\cdot\nabla\phi-n\nu_i E_i'-n\nu_{we}T_e \quad (4.30e)$$

$$0=\frac{5}{2}nT_e\nabla T_e+e\mathbf{q}_e\times\mathbf{B}+m_e\nu_e\mathbf{q}_e \quad (4.30f)$$

$$\frac{\partial d_c}{\partial x}=\frac{2c_{pl}}{v_{ix}}\equiv\gamma \quad (4.30g)$$

It is important to remark that the radial variation of the variables is neglected reducing the problem to two-dimensions: axial (x) and azimuthal (y). Moreover, curvature effects in the azimuthal direction are also neglected as the mean radius of the channel is typically larger than the width of the channel. Obviously, in the limit of a stationary and axi-symmetric solution the system of equations (4.30) reduces to (4.1).

Equations (4.30) can be rewritten in a form more amenable to the current study. To this end, the partial derivatives with respect to the time and the azimuthal coordinate are moved to the right hand side of the equations. In this manner, the left hand side resembles the equations (4.1). The resulting equations can be combined in order to obtain an equation for the variable $h\equiv\ln n$ as:

$$P\frac{\partial h}{\partial x}=G+G_t+G_y\equiv G_{ty} \quad (4.31)$$

where P and G are functions identical to ones derived for the 1D model, and G_t and G_y contain the temporal and azimuthal derivatives respectively and may be expressed as:

$$G_t=v_{ix}\frac{\partial h}{\partial t}-\frac{\partial v_{ix}}{\partial t} \quad (4.32a)$$

$$G_y=v_{ix}\left(\frac{\partial v_{iy}}{\partial y}+v_{iy}\frac{\partial h}{\partial y}\right)-v_{iy}\frac{\partial v_{ix}}{\partial y}-\chi\left(\frac{e}{m_i}\frac{\partial\phi}{\partial y}-\frac{T_e}{m_i}\frac{\partial h}{\partial y}\right) \quad (4.32b)$$

The set of governing equations of the time-dependent 2D model may be written as:

$$v_{nx}\frac{\partial n_n}{\partial x} = -n(\nu_i - \nu_w) - n_n\frac{\partial v_{nx}}{\partial x} - \frac{\partial n_n}{\partial t} - n_n\frac{\partial v_{ny}}{\partial y} - v_{ny}\frac{\partial n_n}{\partial y} - n_n v_{nx}\frac{\partial \ln d_c}{\partial x} \tag{4.33a}$$

$$\frac{\partial v_{ex}}{\partial x} = (\nu_i - \nu_w) - v_{ex}\frac{\partial h}{\partial x} - \frac{\partial h}{\partial t} - \frac{\partial v_{ey}}{\partial y} - v_{ey}\frac{\partial h}{\partial y} - v_{ex}\frac{\partial \ln d_c}{\partial x} \tag{4.33b}$$

$$\frac{\partial v_{ix}}{\partial x} = (\nu_i - \nu_w) - v_{ix}\frac{\partial h}{\partial x} - \frac{\partial h}{\partial t} - \frac{\partial v_{iy}}{\partial y} - v_{iy}\frac{\partial h}{\partial y} - v_{ix}\frac{\partial \ln d_c}{\partial x} \tag{4.33c}$$

$$n_n v_{nx}\frac{\partial v_{nx}}{\partial x} = n\nu_w(1-a_w)(v_{ix} - v_{nx}) - n_n\frac{\partial v_{nx}}{\partial t} - n_n v_{ny}\frac{\partial v_{nx}}{\partial y} \tag{4.33d}$$

$$n_n v_{nx}\frac{\partial v_{ny}}{\partial x} = n\nu_w(1-a_w)(v_{iy} - v_{ny}) - n_n\frac{\partial v_{ny}}{\partial t} - n_n v_{ny}\frac{\partial v_{ny}}{\partial y} \tag{4.33e}$$

$$P\frac{\partial h}{\partial x} = G + G_t + G_y \equiv G_{ty} \tag{4.33f}$$

$$v_{ix}\frac{\partial v_{iy}}{\partial x} = \nu_i(v_{ny} - v_{iy}) - \frac{\partial v_{iy}}{\partial t} - \frac{e}{m_i}\frac{\partial \phi}{\partial y} - v_{iy}\frac{\partial v_{iy}}{\partial y} \tag{4.33g}$$

$$0 = -\frac{T_e}{m_i}\frac{\partial h}{\partial x} - \frac{\partial}{\partial x}\left(\frac{T_e}{m_i}\right) + \frac{e}{m_i}\frac{\partial \phi}{\partial x} - \frac{m_e}{m_i}\nu_e\left(v_{ex} + \chi v_{ey}\right) \tag{4.33h}$$

$$0 = -\frac{T_e}{m_i}\frac{\partial h}{\partial y} - \frac{\partial}{\partial y}\left(\frac{T_e}{m_i}\right) + \frac{e}{m_i}\frac{\partial \phi}{\partial y} - \frac{m_e}{m_i}\nu_e(-\chi v_{ex} + v_{ey}) \tag{4.33i}$$

$$\frac{\partial d_c}{\partial x} = \frac{2c_{pl}}{v_{ix}} \equiv \gamma \tag{4.33j}$$

$$\begin{aligned} n\left(\frac{\partial}{\partial t}\left(\frac{3}{2}\frac{T_e}{m_i}\right) + v_{ex}\frac{\partial}{\partial x}\left(\frac{3}{2}\frac{T_e}{m_i}\right) + v_{ey}\frac{\partial}{\partial y}\left(\frac{3}{2}\frac{T_e}{m_i}\right)\right) + \frac{\partial}{\partial x}\left(\frac{q_{ex}}{m_i}\right) + \frac{\partial}{\partial y}\left(\frac{q_{ey}}{m_i}\right) = \\ = \frac{m_e}{m_i}\nu_e n(v_{ex}^2 + v_{ey}^2) - \frac{3}{2}\frac{T_e}{m_i}n(\nu_i - \nu_w) - \nu_i n\frac{E_i'}{m_i} - \nu_{we} n\frac{T_e}{m_i} \\ -n\frac{T_e}{m_i}\left(\frac{\partial v_{ex}}{\partial x} + \frac{\partial v_{ey}}{\partial y}\right) - \left(n v_{ex}\frac{T_e}{m_i} + \frac{q_{ex}}{m_i}\right)\frac{1}{d_c}\frac{\partial d_c}{\partial x} \end{aligned} \tag{4.33k}$$

$$\frac{\partial}{\partial x}\left(\frac{T_e}{m_i}\right) = -\frac{2}{5}\frac{m_e\nu_e}{nT_e}\left(\frac{q_{ex}}{m_i} + \chi\frac{q_{ey}}{m_i}\right) \tag{4.33l}$$

$$\frac{\partial}{\partial y}\left(\frac{T_e}{m_i}\right) = -\frac{2}{5}\frac{m_e\nu_e}{nT_e}\left(-\chi\frac{q_{ex}}{m_i} + \frac{q_{ey}}{m_i}\right) \tag{4.33m}$$

where v_{ny} and v_{iy} are the azimuthal neutral and ion velocities respectively, and the rest of symbols are as above.

Apart from the sonic points mentioned above, it is important to note that the azimuthal component of the ion momentum conservation law, equation (4.33g), defines another special point along the channel. This equation requires a regular transition at the point separating the ionization region and the ion back-streaming region ($v_{ix} = 0$). Thus the right hand side of the equation, which is represented with the symbol S hereafter, must be zero at that point as well. This fact has important consequences on the way the equations are solved numerically.

The electron momentum equations, (4.33h) and (4.33i), may be combined to remove v_{ey} from the formulation. Similarly for the equations (4.33l) and (4.33m) and the azimuthal heat flux.

Linearised governing equations

Equations (4.30) can be linearised around the steady-state and axi-symmetric solution (i.e., the zero-th order background solution). To this end, it is possible to assume that any control parameter (say, w) of the Hall discharge (discharge voltage, mass flow, neutral velocity at the anode and electron temperature at the cathode) may be written as the sum of a constant zero-th order value, w_0, and a temporal-azimuthal perturbation, $\tilde{w}_1(y,t)$. If the perturbation is expressed as a Fourier expansion in y and t, then:

$$w(y,t) = w_0 + \Re\{w_1 \exp(-i\omega t + iky)\} \tag{4.34}$$

where $\omega = \omega_r + i\omega_i$ is the angular frequency of the perturbation, being ω_r and ω_i its real and imaginary parts, and k is the azimuthal wave number of the perturbation. Note that k only admits a discrete number of values due to continuity conditions in the azimuthal direction, $k = -m/R$, where m is the integer mode number ($m > 0$ when the perturbation travels in the **E**x**B** direction) and R is the mean radius of the thruster.

Similarly, a macroscopic variable, say $u(x,y,t)$, may be written as the sum of the axially-dependent zero-th order solution, $u_0(x)$ and a perturbation, $\tilde{u}_1(x,y,t)$. The latter can also be Fourier-expanded in t and y and, then, the complete solution may be expressed as:

$$u(x,y,t) = u_0(x) + \Re\{u_1(x;\omega,k) \exp(-i\omega t + iky)\} \tag{4.35}$$

The small perturbations hypothesis ($w_1 \ll w_0$, $u_1 \ll u_0$) allows linearising (4.33a)-(4.33m) and decouple the evolution of the zero-th order solution, which is given in (4.1a)-(4.1e), from the evolution of the perturbations. Note that in order to consider consistently the axial gradients of the variables in this linearisation, the zero-th order solution and the coefficients of the Fourier expansion of the perturbations must retain the dependence on the axial coordinate. This is the main difference with respect to local stability analyses such as the one previously carried out by the authors [17].

Applying (4.35) to (4.33a)-(4.33m) it is possible to obtain a linear system of equations with variable coefficients describing the evolution of the different perturbations along the channel. The resulting equations contain source terms proportional to the angular frequency, ω, and to the azimuthal wave number number, k, of the perturbations. These equations must be solved several times, once for each fundamental mode associated to the boundary conditions. Moreover, the zero-th order problem must also be solved together with the perturbation problem in order to compute the coefficients of the perturbation equations.

The background solution consists of the following variables:

$$\mathbf{y}_0 = (x, h_0, v_{ix0}, T_{e0}, \phi_0, n_{n0}, v_{ex0}, v_{nx0}, q_{ex0}, d_{c0})$$

and the dependent variables:

$$\mathbf{q}_0(\mathbf{y}_0) = (\nu_{w0}, \nu_{we0}, \nu_{H0}, \nu_{i0}, E'_{i0}, \gamma_0, \chi_0, v_{ey0}, q_{ey0})$$

Note that the zero-th order solution verifies $v_{ny0} \equiv 0$ and $v_{iy0} \equiv 0$ as it is assumed that no azimuthal flow exists for neutrals and ions in the background solution.

On the other hand, the following perturbed variables are considered:

$$\mathbf{y}_1 = (h_1, v_{ix1}, T_{e1}, \phi_1, n_{n1}, v_{ex1}, v_{nx1}, q_{ex1}, d_{c1}, v_{iy1}, v_{ny1})$$

together with the corresponding perturbed dependent variables:

$$\mathbf{q}_1(\mathbf{y}_0, \mathbf{y}_1) = (\nu_{w1}, \nu_{we1}, \nu_{H1}, \nu_{i1}, E'_{i1}, \gamma_1, \chi_1, v_{ey1}, q_{ey1})$$

The complete set of governing equations of the linear model may be written as:

$$\begin{aligned} v_{nx0}\frac{dn_{n1}}{dx} &= -v_{nx1}\frac{dn_{n0}}{dx} - n_0(\nu_{i1}-\nu_{w1}) - n_1(\nu_{i0}-\nu_{w0}) - n_{n0}\frac{dv_{nx1}}{dx} - n_{n1}\frac{dv_{nx0}}{dx} + \\ & -n_{n0}v_{nx0}\frac{d}{dx}\left(\frac{d_{c1}}{d_{c0}}\right) - (n_{n1}v_{nx0}+n_{n0}v_{nx1})\frac{d\ln d_{c0}}{dx} + i\omega n_{n1} - ik(n_{n0}v_{ny1}+v_{ny0}n_{n1}) \end{aligned} \tag{4.36a}$$

$$\frac{dv_{ex1}}{dx} = (\nu_{i1}-\nu_{w1}) - v_{ex0}\frac{dh_1}{dx} - v_{ex1}\frac{dh_0}{dx} - v_{ex0}\frac{d}{dx}\left(\frac{d_{c1}}{d_{c0}}\right) - v_{ex1}\frac{d\ln d_{c0}}{dx} + i\omega h_1 - ik(v_{ey1}+v_{ey0}h_1) \tag{4.36b}$$

$$\frac{dv_{ix1}}{dx} = (\nu_{i1}-\nu_{w1}) - v_{ix0}\frac{dh_1}{dx} - v_{ix1}\frac{dh_0}{dx} - v_{ix0}\frac{d}{dx}\left(\frac{d_{c1}}{d_{c0}}\right) - v_{ix1}\frac{d\ln d_{c0}}{dx} + i\omega h_1 - ik(v_{iy1}+v_{iy0}h_1) \tag{4.36c}$$

$$\begin{aligned} n_{n0}v_{nx0}\frac{dv_{nx1}}{dx} &= -n_{n0}v_{nx1}\frac{dv_{nx0}}{dx} - n_{n1}v_{nx0}\frac{dv_{nx0}}{dx} + i\omega n_{n0}v_{nx1} - ikn_{n0}v_{ny0}v_{nx1} + \\ & +(1-a_w)\left(n_0\nu_{w0}(v_{ix1}-v_{nx1}) + n_0\nu_{w1}(v_{ix0}-v_{nx0}) + n_1\nu_{w0}(v_{ix0}-v_{nx0})\right) \end{aligned} \tag{4.36d}$$

$$\begin{aligned} n_{n0}v_{nx0}\frac{dv_{ny1}}{dx} &= -n_{n0}v_{nx1}\frac{dv_{ny0}}{dx} - n_{n1}v_{nx0}\frac{dv_{ny0}}{dx} + i\omega n_{n0}v_{ny1} - ikn_{n0}v_{ny0}v_{ny1} + \\ & +(1-a_w)\left(n_0\nu_{w0}(v_{iy1}-v_{ny1}) + n_0\nu_{w1}(v_{iy0}-v_{ny0}) + n_1\nu_{w0}(v_{iy0}-v_{ny0})\right) \end{aligned} \tag{4.36e}$$

$$P_0\frac{dh_1}{dx} = -P_1\frac{dh_0}{dx} + G_{ty1} \tag{4.36f}$$

$$\begin{aligned} v_{ix0}\frac{dv_{iy1}}{dx} &= -v_{ix1}\frac{dv_{iy0}}{dx} + \nu_{i0}(v_{ny1}-v_{iy1}) + \nu_{i1}(v_{ny0}-v_{iy0}) + \\ & +i\omega v_{iy1} - ik\left(e\phi_1/m_i + v_{iy0}v_{iy1}\right) = -v_{ix1}\frac{dv_{iy0}}{dx} + S_1 \end{aligned} \tag{4.36g}$$

$$\begin{aligned} \frac{e}{m_i}\frac{d\phi_1}{dx} &= \frac{T_{e0}}{m_i}\frac{dh_1}{dx} + \frac{T_{e1}}{m_i}\frac{dh_0}{dx} + \frac{d}{dx}\left(\frac{T_{e1}}{m_i}\right) + \nu_{H1}v_{ex0} + \nu_{H0}v_{ex1} + \\ & +ik\chi_0\left(e\phi_1/m_i - h_1T_{e0}/m_i - T_{e1}/m_i\right) \end{aligned} \tag{4.36h}$$

$$ik\frac{e\phi_1}{m_i} = ikh_1\frac{T_{e0}}{m_i} + ik\frac{T_{e1}}{m_i} + \nu_{H0}/\chi_0^2(-\chi_0 v_{ex1} + v_{ey1} - \chi_1 v_{ex0}) \tag{4.36i}$$

$$\begin{aligned} \frac{1}{n_0}\frac{d}{dx}\left(\frac{q_{ex1}}{m_i}\right) &= -\frac{3}{2}v_{ex0}\frac{d}{dx}\left(\frac{T_{e1}}{m_i}\right) - \frac{3}{2}v_{ex1}\frac{d}{dx}\left(\frac{T_{e0}}{m_i}\right) + \frac{n_1}{n_0^2}\left(\frac{1}{m_i}\frac{dq_{ex0}}{dx} + \frac{q_{ex0}}{m_i}\frac{d\ln d_{c0}}{dx}\right) + \\ & -\frac{q_{ex1}}{m_i n_0}\frac{d\ln d_{c0}}{dx} - \frac{q_{ex0}}{m_i n_0}\frac{d}{dx}\left(\frac{d_{c1}}{d_{c0}}\right) - v_{ex0}\frac{T_{e0}}{m_i}\frac{d}{dx}\left(\frac{d_{c1}}{d_{c0}}\right) - \left(v_{ex0}\frac{T_{e1}}{m_i} + v_{ex1}\frac{T_{e0}}{m_i}\right)\frac{d\ln d_{c0}}{dx} + \\ & -\frac{T_{e1}}{m_i}\frac{dv_{ex0}}{dx} - \frac{T_{e0}}{m_i}\frac{dv_{ex1}}{dx} + 2\frac{\nu_{H0}}{\chi_0^2}(v_{ex0}v_{ex1} + v_{ey0}v_{ey1}) + \frac{\nu_{H0}}{\chi_0^2}\left(\frac{\nu_{H1}}{\nu_{H0}} - 2\frac{\chi_1}{\chi_0}\right)(v_{ex0}^2 + v_{ey0}^2) + \\ & -\frac{3}{2}\frac{T_{e0}}{m_i}(\nu_{i1}-\nu_{w1}) - \frac{3}{2}\frac{T_{e1}}{m_i}(\nu_{i0}-\nu_{w0}) - \nu_{i0}\frac{E'_{i1}}{m_i} - \nu_{i1}\frac{E'_{i0}}{m_i} - \nu_{we0}\frac{T_{e1}}{m_i} - \nu_{we1}\frac{T_{e0}}{m_i} + \\ & +\frac{3}{2}i\omega\left(\frac{T_{e1}}{m_i}\right) - ik\left(\frac{3}{2}v_{ey0}\frac{T_{e1}}{m_i} + \frac{q_{ey0}}{n_0 m_i} + v_{ey1}\frac{T_{e0}}{m_i}\right) \end{aligned} \tag{4.36j}$$

$$\frac{d}{dx}\left(\frac{T_{e1}}{m_i}\right) = -\frac{2}{5}\frac{q_{ex0}\nu_{H0}}{n_0T_{e0}}\left(\frac{q_{ex1}}{q_{ex0}} + \frac{\nu_{H1}}{\nu_{H0}} - \frac{n_1}{n_0} - \frac{T_{e1}}{T_{e0}}\right) + ik\chi_0\frac{T_{e1}}{m_i} \tag{4.36k}$$

$$ik\frac{T_{e1}}{m_i} = -\frac{2}{5}\frac{\nu_{H0}/\chi_0^2}{n_0T_{e0}}\left(-\chi_0 q_{xe1} + q_{ey1} - \chi_1 q_{xe0}\right) \tag{4.36l}$$

$$\frac{dd_{c1}}{dx} = \gamma_1 \tag{4.36m}$$

where P_1 and G_{ty1} are the perturbations of the corresponding functions P and G_{ty}.

Analysis of linearised terms

The linear formulation just presented makes use of several perturbed dependent variables. Thanks to the linearity, all these variables can be computed in the following generic form:

$$q_{i1} = \sum_j \frac{\partial q_{i0}}{\partial y_{j0}} y_{j1} \tag{4.37}$$

where q_{i1} and is any of the dependent variables in $\mathbf{q}_1$ and y_{j1} is any of the variables in $\mathbf{y}_1$. Similarly, let us define functions P and G as $P = P(\mathbf{u})$ and $G = G(\mathbf{u})$ where $\mathbf{u} \equiv (\mathbf{y}, \mathbf{q})$. Then, it is possible to express the perturbations of those functions as:

$$P_1(\mathbf{u}_0, \mathbf{u}_1, \omega, k) = \sum_j \frac{\partial P_0}{\partial u_{j0}} u_{j1} = \frac{T_{e1}}{m_i} - 2v_{ix0}v_{ix1} \tag{4.38a}$$

$$G_1(\mathbf{u}_0, \mathbf{u}_1, \omega, k) = \sum_j \frac{\partial G_0}{\partial u_{j0}} u_{j1} + \sum_i \frac{\partial^2 G_1}{\partial u_{j1}\partial \omega} u_{j1}\omega + \sum_i \frac{\partial^2 G_1}{\partial u_{j1}\partial k} u_{j1}k \tag{4.38b}$$

Based on the previous expressions, the following ones can be derived:

$$\frac{dq_{i1}}{dx} = \sum_{j,k} \frac{\partial^2 q_{i0}}{\partial y_{j0}\partial y_{k0}} \frac{dy_{k0}}{dx} y_{j1} + \sum_j \frac{\partial q_{i0}}{\partial y_{j0}} \frac{dy_{j1}}{dx} \tag{4.39a}$$

$$\frac{dP_1}{dx} = \sum_{j,k} \frac{\partial^2 P_0}{\partial u_{j0}\partial u_{k0}} \frac{du_{k0}}{dx} u_{j1} + \sum_j \frac{\partial P_0}{\partial u_{j0}} \frac{du_{j1}}{dx} \tag{4.39b}$$

$$\begin{aligned}\frac{dG_1}{dx} &= \sum_{j,k} \frac{\partial^2 G_0}{\partial u_{j0}\partial u_{k0}} \frac{du_{k0}}{dx} u_{j1} + \sum_j \frac{\partial G_0}{\partial u_{j0}} \frac{du_{j1}}{dx} + \\ &+ \sum_{j,k} \frac{\partial^3 G_1}{\partial u_{j1}\partial u_{k0}\partial \omega} \frac{du_{k0}}{dx} u_{j1}\omega + \sum_j \frac{\partial^2 G_1}{\partial u_{j1}\partial \omega} \frac{du_{j1}}{dx}\omega + \\ &+ \sum_{j,k} \frac{\partial^3 G_1}{\partial u_{j1}\partial u_{k0}\partial k} \frac{du_{k0}}{dx} u_{j1}k + \sum_j \frac{\partial^2 G_1}{\partial u_{j1}\partial k} \frac{du_{j1}}{dx} k\end{aligned} \tag{4.39c}$$

The expressions above are useful to simplify the mathematical formulation of the expansion of the governing equations around points B, S and I.

Generic form of linearised equations

Equations (4.36) can be written making use of the same change of variable used for the zero-th order solution in the following generic form:

$$\frac{d\mathbf{y}_0}{d\xi} = \mathbf{F}_0(\mathbf{y}_0, \mathbf{q}_0(\mathbf{y}_0)) \tag{4.40a}$$

$$\frac{d\mathbf{y}_1}{d\xi} = \mathbf{F}_1(\mathbf{y}_0, \mathbf{q}_0(\mathbf{y}_0), \mathbf{y}_1, \mathbf{q}_1(\mathbf{y}_0, \mathbf{y}_1)) \tag{4.40b}$$

Linearised boundary conditions

The boundary conditions associated to the evolution equations of the perturbed problem are also derived from the linearisation of the boundary conditions of the zero-th order problem. The result of this linearisation is presented next.

The following boundary conditions are identified for the perturbation problem:

- The perturbed ion and electron velocities at the anode (v_{ix1B}, v_{ex1B}) are related by the linearised expression characterizing the anode sheath, given by:

$$e\phi_{1AB} = e\phi_{0AB}\frac{T_{e1B}}{T_{e0B}} + T_{e0B}\left(\frac{v_{ix1B}}{v_{ix0B}} - \frac{v_{ex1B}}{v_{ex0B}}\right) \tag{4.41}$$

- The perturbation of the discharge voltage is known and must be equal to the difference in perturbed electric potential between the anode and the cathode, $\phi_{1A} - \phi_{1P} = V_{d1}$,

- In order to fulfil the condition $h_{1B} \ll h_{0B}$, the singularity at point B for the perturbed solution cannot be greater than for the background solution. This requires that $P_{1B} = 0$.

- The perturbation of the mass flow through the injector, $\dot{m}_{1A}$, is also known.

- The perturbation of the neutral velocities at the anode, v_{nxA1} and v_{nyA1}, are known.

- The perturbation of the electron temperature at the cathode, T_{e1P}, is known.

- The sonic point inside the channel is regular at the perturbed location for the complete solution, this is, $P_{S'} = 0$ and $G_{S'} = 0$. Provided that $P_{0S} = 0$ and $G_{0S} = 0$, those two conditions are linearised as:

$$P_{1S} + \left(\frac{dP_0}{dx}\right)_S x_{1S} = 0 \tag{4.42a}$$

$$G_{ty1S} + \left(\frac{dG_0}{dx}\right)_S x_{1S} = 0 \tag{4.42b}$$

where x_{1S} is the perturbation of the location of the sonic point inside the channel.

- The transition through the zero-ion velocity point is regular and thus the complete solution at the perturbed intermediate point verifies $v_{ixI'} = 0$ and $S_{I'} = 0$. Provided that $v_{ix0I} = 0$ and $S_{0I} \equiv 0$, then, the linearised conditions become:

$$v_{ix1I} + \left(\frac{dv_{ix0}}{dx}\right)_I x_{1I} = 0 \tag{4.43a}$$

$$S_{1I} + \left(\frac{dS_0}{dx}\right)_I x_{1I} = 0 \tag{4.43b}$$

where x_{1I} is the perturbation of the location of the zero ion-velocity point inside the channel.

Perturbed state at the regular sonic transition

Given the zero-th order solution and the known perturbation variables at the regular sonic transition point, S, conditions (4.42) are used to compute the perturbations of ion and electron axial velocities, v_{ix1S} and q_{ex1S}.

The first order derivatives of the perturbation variables at point S cannot be computed using equations (4.36) since some of the equations become singular at the regular sonic transition point. In particular, equation (4.36f) becomes singular because $P_{0S} = 0$ and the right hand side of the equation is also zero as a consequence of conditions (4.42).

In order to overcome this problem, equation (4.36f) is expanded around point S in the following way:

$$\left(\frac{dP_0}{dx}\right)_S \left(\frac{dh_1}{dx}\right)_S = -\left(\frac{d}{dx}\left(P_1\frac{dh_0}{dx}\right)\right)_S + \left(\frac{dG_{ty1}}{dx}\right)_S \tag{4.44}$$

Equation (4.44), together with the rest of the first order equations at point S, define a linear system of equations for the computation of $(d\mathbf{y}_1/dx)_S$. As part of equation (4.44), the derivatives of P_1 and G_{ty1} with respect to x are needed and can be computed with the equations (4.39). There, the first order derivatives of the perturbed dependent variables at S, $(d\mathbf{q}_1/dx)_S$, are needed. In order to compute them, the linear system of equations is extended with equations for $(d\mathbf{q}_1/dx)_S$, which are given by equation (4.39a). Altogether, the equations form a linear system for the computation of the first order derivatives of the perturbed variables at S, $(d\mathbf{y}_1/dx)_S$ and $(d\mathbf{q}_1/dx)_S$.

Note that the second order derivative of h_0 at point S, $(d^2h_0/dx^2)_S$, is needed in (4.44). A similar procedure to the one just described is used to compute the second order derivatives at S of the zero-th order solution. In that case, the equation for the second order derivative of h_0 can be written as:

$$\frac{dP_0}{dx}\frac{dh_0}{dx} + P_0\frac{d^2h_0}{dx^2} = \frac{dG_0}{dx} \tag{4.45}$$

The rest of the equations for the second order derivatives of the zero-th order variables can be easily obtained from (4.1).

However, equation (4.45) is singular at point S (P_{0S}=0) and must be Taylor-expanded in the following way:

$$2\left(\frac{dP_0}{dx}\right)_S \left(\frac{d^2h_0}{dx^2}\right)_S = \left(\frac{d^2G_0}{dx^2}\right)_S - \left(\frac{d^2P_0}{dx^2}\right)_S \left(\frac{dh_0}{dx}\right)_S \tag{4.46}$$

The spatial derivatives at S of P_0 and G_0, needed in (4.46), are given by the expressions (4.22). Similarly, the equations for the second order derivatives of the dependent variables $\mathbf{q}_0$, needed for the evaluation of the spatial second order derivatives of P_0 and G_0 at S, are also given by (4.22c). Altogether, the equations form a linear system for the computation of the second order derivatives at S, $(d^2\mathbf{y}_0/dx^2)_S$ and $(d^2\mathbf{q}_0/dx^2)_S$.

Perturbed state at the anode sheath transition

Given the zero-th order solution and the known perturbation variables at the anode sheath transition point, B, the condition $P_{1B} = 0$ is used to compute the perturbation of the ion axial velocity, v_{ix1B}.

As in the previous paragraph, the first order derivatives of the perturbation variables at point B cannot be computed since equation (4.36f) for h_1 becomes singular at point B as $P_{0B} = 0$ and $P_{1B} = 0$.

In order to overcome this problem, equation (4.36f) is Taylor-expanded around point B in the following way:

$$\left(\frac{dh_1}{d\xi}\right)_B = -\frac{(dP_1/d\xi)_B}{(dP_0/d\xi)_B}\left(\frac{dh_0}{d\xi}\right)_B + G_{ty1B} \tag{4.47}$$

The previous equation, in combination with the rest of the equations for the first order derivatives of $(d\mathbf{y}_1/d\xi)_B$ and $(d\mathbf{q}_1/d\xi)_B$ at point B, form a linear system of equations to solve for those variables. Once again, the equations for $(d\mathbf{q}_1/d\xi)_B$ are given by equation (4.39a).

Perturbed state at the zero ion velocity point

Given the zero-th order solution and the known perturbation variables at the zero ion velocity point, I, conditions (4.43) are used to compute the perturbations of the ion axial and azimuthal velocities, v_{ix1S} and v_{iy1S}.

As in the previous paragraphs, the first order derivatives of the perturbation variables at point I cannot be computed since the azimuthal ion momentum equation, equation (4.36g), becomes singular at point I as a consequence of the boundary conditions given by equations (4.43).

In order to overcome this problem, equation (4.36g) is expanded around point I in the following way:

$$\left(\frac{dv_{ix0}}{dx}\right)_I\left(\frac{dv_{iy1}}{dx}\right)_I = -\left(\frac{dv_{ix1}}{dx}\right)_I\left(\frac{dv_{iy0}}{dx}\right)_I - v_{ix1I}\left(\frac{d^2v_{iy0}}{dx^2}\right)_I + \left(\frac{dS_1}{dx}\right)_I \tag{4.48}$$

The previous equation, in combination with the rest of the equations for the first order derivatives of $(d\mathbf{y}_1/dx)_I$ and $(d\mathbf{q}_1/dx)_I$ at point I, form a linear system of equations to solve for those variables. Once again, the equations for $(d\mathbf{q}_1/dx)_I$ are given by equation (4.39a).

Solution method for the perturbation model

The presence inside the channel of a regular sonic point, S, and a zero ion-velocity point, I, makes the integration process more complicated. Moreover, as the coefficients of the first-order equations depend on the zero-th order solution, the latter must be solved for together with the first-order solution in order to compute those coefficients. On the other hand, the linearity of the first-order problem simplifies the overall approach.

Fundamental modes

Since the perturbation problem is linear, the complete solution can be constructed as a linear combination of independent solutions called fundamental modes. These fundamental modes are solutions of the perturbation problem for specific values of the perturbation variables at B, S and I, which are chosen such that all variables but one are zero at one of the those points. The value of the non-zero variable is chosen to be the unity and the solution computed in this way becomes the fundamental mode associated that unitary variable. Each of these fundamental modes is computed integrating the governing equations from the point where the non-zero variable is defined. The solution can then be expressed as:

$$\mathbf{y}_1(\xi) = \sum_i x_i \mathbf{Y}_i(\xi) \tag{4.49}$$

where $\mathbf{Y}_i(\xi)$ are the fundamental modes and x_i are the weights of the fundamental modes in the final solution. These weights are not known a-priori and must be computed to fulfil the conditions imposed by the boundary conditions, and the continuity of the overall solution at the points where the different fundamental modes meet along the channel. The value of the control parameters comes from the externally applied perturbations on the discharge voltage, on the anode neutral axial and azimuthal velocity, on the cathode electron temperature and on the anode mass flow.

In the case of the complete azimuthal problem, there are up to 25 fundamental modes, each one of them associated to one of the following variables:

- point B: h_{1B}, T_{e1B}, v_{ex1B}, n_{n1B}, v_{nx1B}, v_{iy1B}, v_{ny1B}, ϕ_{1B}
- point S: T_{e1S}, x_{1S}, h_{1S}, n_{n1S}, v_{nx1S}, v_{ex1S}, v_{iy1S}, v_{ny1S}
- point I: h_{1I}, T_{e1I}, v_{ex1I}, n_{n1I}, v_{nx1I}, q_{ex1I}, x_{1I}, v_{ny1I}, ϕ_{1I}

The fundamental modes associated to the variables ϕ_{1B} and ϕ_{1I} can be computed analytically as they only affect the absolute value of the electric potential. This leaves 23 fundamental modes that require numerical integration, 7 or 8 for each of the special points in the domain, B, I and S. Each of those fundamental modes are computed by, first, expanding the perturbed plasma state around the starting point (B, I or S) as presented in the previous section and, then, integrating the governing equations up to an intermediate matching point. Two intermediate matching points are defined where the condition $M_{i0} = \pm 0.5$ is verified, being one of them located between points B and I and the other one between points I and S.

Complete solution

The value of the weights of the fundamental modes in the final solution are obtained from the following algebraic system of equations:

$$\mathbf{A}\mathbf{x} = \mathbf{b} \tag{4.50}$$

where $\mathbf{x}$ is an unknown vector containing the linear weights of the fundamental modes in the complete solution, $\mathbf{b}$ is a vector with the coefficients of the linearised control parameters and $\mathbf{A}$ is a matrix with complex coefficients.

Vector $\mathbf{b}$ contains the control parameters from the boundary conditions and the continuity conditions. As there are 25 fundamental modes, $\mathbf{b}$ must have 25 components, 20 of them being zero as they correspond to the continuity condition of the integrated variables at the two intermediate matching points of the solutions integrated from B, I and S. The remaining 5 components of $\mathbf{b}$ correspond to the externally applied perturbations, T_{e1P}, $\dot{m}_{1A}$, v_{nx1A}, V_{d1} and v_{ny1A}.

Matrix $\mathbf{A}$ contains the partial derivatives of the control parameters with respect to the unitary variables of each of the fundamental modes. These partial derivatives are computed from the plasma variables at the corresponding point for the given fundamental mode of the perturbation problem. Hence, this matrix $\mathbf{A}$ depends on the control parameters defining the zero-th order solution, $\mathbf{w}_0$, as well as the angular frequency, ω, and the angular wave number, k, that is, $\mathbf{A} \equiv \mathbf{A}(\mathbf{w}_0, \omega, k)$.

Self-excited oscillations

In order to have self-excited oscillations, this is, growing oscillations with no externally applied perturbations (i.e., with $B = 0$), the previous algebraic system of equations must have non-trivial solutions for the homogeneous problem ($\mathbf{A}\mathbf{x} = 0$). This is equivalent to imposing the following condition:

$$\det \mathbf{A}(\mathbf{w}_0, \omega, k) = 0. \tag{4.51}$$

For each zero-th order solution given by the control parameters, $\mathbf{w}_0$, and for each azimuthal angular wave number, k, equation (4.51) provides a condition to compute the complex angular frequency, ω, of the perturbation. If the resulting frequency verifies the condition $\omega_i > 0$, then the perturbation is self-excited. The case $k = 0$ corresponds to purely axial oscillations for the analysis of the breathing mode studied in the past [181, 14, 15] with this very same model. In that case, the azimuthal momentum equations do not need to be solved, and thus, the additional complexity of the regular transition at the point with zero ion velocity is avoided.

For the analysis of azimuthal oscillations, the size of matrix $\mathbf{A}$ is rather large. In order to avoid numerical instabilities in the computation of the determinant of the matrix $\mathbf{A}$, the system of equations (4.50) can be reduced in size by pre-eliminating the unknowns whose right-hand side is zero. This allows reducing the size of the matrix and the computation of the determinant becomes numerically stable. Note that this fact is very important in order to find the exact frequency for which a self-excited mode exists and be able to compute the corresponding solution of the null space of matrix $\mathbf{A}$.

4.1.3 Model without heat conduction and plume divergence

This section is intended to provide a brief summary of the equations corresponding to the model presented in previous sections without heat conduction and plume divergence. The main effects of heat conduction terms are a smaller temperature peak, smoother temperature gradients and a widening of the ionization region. Additionally, plume divergence is also neglected in this simplified model for clarity. Removing heat conduction and plume divergence terms from the model simplifies the equations, specially the electron energy equation, but the overall procedure and solution method remain basically the same. Note this section is more intended as a reference summary of the equations of the model without heat conduction and plume divergence rather than a descriptive derivation and analysis of the model itself. The reader that is not interested in the equations of this simplified model may directly go to the next section.

The governing equations of the 1D model given in (4.1) are simplified into the equations (4.52) when heat conduction and plume divergence are not considered:

$$\frac{d}{dx}(n_n v_{nx}) = -n(\nu_i - \nu_w) \tag{4.52a}$$

$$\frac{d}{dx}(n v_{ix}) = n(\nu_i - \nu_w) \tag{4.52b}$$

$$\frac{d}{dx}(n v_{ex}) = n(\nu_i - \nu_w) \tag{4.52c}$$

$$m_i \frac{d}{dx}(n_n v_{nx}^2) = -m_i n(\nu_i v_{nx} - \nu_w v_{nw}) \tag{4.52d}$$

$$m_i \frac{d}{dx}(n v_{ix}^2) = -en\frac{d\phi}{dx} + m_i n(\nu_i v_{nx} - \nu_w v_{ix}) \tag{4.52e}$$

$$0 = -\frac{d}{dx}(nT_e) + en\frac{d\phi}{dx} - m_e n \nu_e \chi^2 v_{ex} \tag{4.52f}$$

$$\frac{d}{dx}\left(\frac{5}{2} n T_e v_{ex}\right) = e n v_{ex}\frac{d\phi}{dx} - n\nu_i E_i' - n\nu_{we} T_e \tag{4.52g}$$

Similarly, the definitions of the functions P and G, given in (4.3), are modified as follows:

$$P = T_e/m_i - (3/5)v_{ix}^2 \tag{4.53a}$$

$$\begin{aligned} G = {} & -\nu_H v_{ex} + (\nu_i - \nu_w)\frac{T_e/m_i}{v_{ex}} + \frac{2}{5}\nu_i \frac{E_i'/m_i}{v_{ex}} + \\ & + \frac{2}{5}\nu_{we}\frac{T_e/m_i}{v_{ex}} + \frac{3}{5}\Big(\nu_i(v_{nx} - 2v_{ix}) + \nu_w v_{ix}\Big) \end{aligned} \tag{4.53b}$$

and the definition of the Mach number, given in equation (4.4), is modified with a 5/3 factor as follows:

$$M_i = \frac{v_{ix}}{\sqrt{5T_e/3m_i}} \tag{4.54}$$

The final set of equations of the no-heat-conduction 1D model is given by equations (4.55) shown below:

$$\frac{dx}{d\xi} = P \tag{4.55a}$$

$$\frac{dh}{d\xi} = G \tag{4.55b}$$

$$\frac{dn_n}{d\xi} = -P\frac{n}{v_n}(\nu_i - \nu_w) - \frac{n_n}{v_n}\frac{dv_n}{d\xi} \tag{4.55c}$$

$$\frac{dv_{ex}}{d\xi} = P(\nu_i - \nu_w) - v_{ex}\frac{dh}{d\xi} \tag{4.55d}$$

$$\frac{dv_{ix}}{d\xi} = P(\nu_i - \nu_w) - v_{ix}\frac{dh}{d\xi} \tag{4.55e}$$

$$\frac{dv_{nx}}{d\xi} = P\frac{n}{n_n}\nu_w(1 - a_w)\left(\frac{v_{ix}}{v_{nx}} - 1\right) \tag{4.55f}$$

$$\frac{d}{d\xi}\left(\frac{e\phi}{m_i}\right) = -v_{ix}\frac{dv_{ix}}{d\xi} - P\nu_i(v_{ix} - v_{nx}) \tag{4.55g}$$

$$\frac{d}{d\xi}\left(\frac{T_e}{m_i}\right) = -\frac{T_e}{m_i}\frac{dh}{d\xi} + \frac{e}{m_i}\frac{d\phi}{d\xi} - P\nu_H v_{ex} \tag{4.55h}$$

Equations (4.55) can be represented in the generic form given in equation (4.24) using as dependant variables $\mathbf{y} = (x, h, v_{ix}, T_e, \phi, n_n, v_{ex}, v_{nx})$ and dependent functions $\mathbf{q}(\mathbf{y}) = (\nu_w, \nu_{we}, \nu_H, \nu_i, E_i')$.

The equations equivalent to (4.29) for the expansion of the model at point B can be expressed as:

$$\frac{dx}{d\xi} = -2v_{ix}\frac{dv_{ix}}{d\xi}\Delta\xi \tag{4.56a}$$

$$\frac{dn_n}{d\xi} = -\frac{n}{v_n}(\nu_i - \nu_w)\frac{dx}{d\xi} - \frac{n_n}{v_n}\frac{dv_n}{d\xi} \tag{4.56b}$$

$$\frac{dv_{nx}}{d\xi} = \frac{n}{n_n}\nu_w(1 - a_w)\left(\frac{v_{ix}}{v_{nx}} - 1\right)\frac{dx}{d\xi} \tag{4.56c}$$

Up to this point the focus has been on the simplification of the equations of the 1D model. Similarly, the general governing equations of the 2D model given in equations (4.30), when no heat conduction and plume divergence are considered, simplify into:

$$\frac{\partial n}{\partial t} + \nabla\cdot(n\mathbf{v}_e) = \frac{\partial n}{\partial t} + \nabla\cdot(n\mathbf{v}_i) = -\frac{\partial n_n}{\partial t} - \nabla\cdot(n_n\mathbf{v}_n) = n(\nu_i - \nu_w) \tag{4.57a}$$

$$m_i\left(\frac{\partial}{\partial t}(n_n\mathbf{v}_n) + \nabla\cdot(n_n\mathbf{v}_n\mathbf{v}_n)\right) = -m_i n(\nu_i\mathbf{v}_n - \nu_w\mathbf{v}_{nw}) \tag{4.57b}$$

$$m_i\left(\frac{\partial}{\partial t}(n\mathbf{v}_i) + \nabla\cdot(n\mathbf{v}_i\mathbf{v}_i)\right) = -en\nabla\phi + m_i n(\nu_i\mathbf{v}_n - \nu_w\mathbf{v}_i) \tag{4.57c}$$

$$0 = -\nabla(nT_e) - en(-\nabla\phi + \mathbf{v}_e\times\mathbf{B}) - m_e n\nu_e\mathbf{v}_e \tag{4.57d}$$

$$\frac{\partial}{\partial t}\left(\frac{3}{2}nT_e\right) + \nabla\cdot\left(\frac{5}{2}nT_e\mathbf{v}_e\right) = en\mathbf{v}_e\cdot\nabla\phi - n\nu_i E_i' - n\nu_{we}T_e \tag{4.57e}$$

The combination of equations equations (4.57) yields also equation (4.31) where the functions G_t and G_y are now given by:

$$G_t = -\frac{2}{5}\Big(\frac{T_e/m_i}{v_{ex}} - \frac{3}{2}v_{ix}\Big)\frac{\partial h}{\partial t} - \frac{3}{5}\frac{\partial v_{ix}}{\partial t} + \frac{3}{5}\frac{1}{v_{ex}}\frac{\partial}{\partial t}\Big(\frac{T_e}{m_i}\Big) \tag{4.58a}$$

$$\begin{aligned} G_y = -\chi\left(\frac{e}{m_i}\frac{\partial \phi}{\partial y} - \frac{\partial}{\partial y}\Big(\frac{T_e}{m_i}\Big) - \frac{T_e}{m_i}\frac{\partial h}{\partial y}\right) + \\ + \frac{3}{5}\Big(v_{ix}\frac{\partial v_{iy}}{\partial y} + v_{ix}v_{iy}\frac{\partial h}{\partial y} - v_{iy}\frac{\partial v_{ix}}{\partial y}\Big) - \frac{2}{5}\frac{e}{m_i}\frac{v_{ey}}{v_{ex}}\frac{\partial \phi}{\partial y} + \frac{v_{ey}}{v_{ex}}\frac{\partial}{\partial y}\Big(\frac{T_e}{m_i}\Big) \end{aligned} \tag{4.58b}$$

The previous 2D equations may also be expressed as equations (4.59) given below:

$$v_{nx}\frac{\partial n_n}{\partial x} = -n(\nu_i - \nu_w) - n_n\frac{\partial v_{nx}}{\partial x} - \frac{\partial n_n}{\partial t} - n_n\frac{\partial v_{ny}}{\partial y} - v_{ny}\frac{\partial n_n}{\partial y} \tag{4.59a}$$

$$\frac{\partial v_{ex}}{\partial x} = (\nu_i - \nu_w) - v_{ex}\frac{\partial h}{\partial x} - \frac{\partial h}{\partial t} - \frac{\partial v_{ey}}{\partial y} - v_{ey}\frac{\partial h}{\partial y} \tag{4.59b}$$

$$\frac{\partial v_{ix}}{\partial x} = (\nu_i - \nu_w) - v_{ix}\frac{\partial h}{\partial x} - \frac{\partial h}{\partial t} - \frac{\partial v_{iy}}{\partial y} - v_{iy}\frac{\partial h}{\partial y} \tag{4.59c}$$

$$n_n v_{nx}\frac{\partial v_{nx}}{\partial x} = n\nu_w(1 - a_w)(v_{ix} - v_{nx}) - n_n\frac{\partial v_{nx}}{\partial t} - n_n v_{ny}\frac{\partial v_{nx}}{\partial y} \tag{4.59d}$$

$$n_n v_{nx}\frac{\partial v_{ny}}{\partial x} = n\nu_w(1 - a_w)(v_{iy} - v_{ny}) - n_n\frac{\partial v_{ny}}{\partial t} - n_n v_{ny}\frac{\partial v_{ny}}{\partial y} \tag{4.59e}$$

$$v_{ix}\frac{\partial v_{ix}}{\partial x} = \nu_i(v_{nx} - v_{ix}) - \frac{e}{m_i}\frac{\partial \phi}{\partial x} - \frac{\partial v_{ix}}{\partial t} - v_{iy}\frac{\partial v_{ix}}{\partial y} \tag{4.59f}$$

$$v_{ix}\frac{\partial v_{iy}}{\partial x} = \nu_i(v_{ny} - v_{iy}) - \frac{\partial v_{iy}}{\partial t} - \frac{e}{m_i}\frac{\partial \phi}{\partial y} - v_{iy}\frac{\partial v_{iy}}{\partial y} \tag{4.59g}$$

$$0 = -\frac{T_e}{m_i}\frac{\partial h}{\partial x} - \frac{\partial}{\partial x}\left(\frac{T_e}{m_i}\right) + \frac{e}{m_i}\frac{\partial \phi}{\partial x} - \frac{m_e}{m_i}\nu_e\left(v_{ex} + \chi v_{ey}\right) \tag{4.59h}$$

$$0 = \frac{m_e}{m_i}\nu_e(\chi v_{ex} - v_{ey}) + \frac{e}{m_i}\frac{\partial \phi}{\partial y} - \frac{T_e}{m_i}\frac{\partial h}{\partial y} - \frac{\partial}{\partial y}\left(\frac{T_e}{m_i}\right) \tag{4.59i}$$

$$P\frac{\partial h}{\partial x} = G + G_t + G_y \equiv G_{ty} \tag{4.59j}$$

The linearisation of the equations (4.59) yields the final set of equations of the perturbed problem:

$$\begin{aligned} v_{nx0}\frac{dn_{n1}}{dx} = -v_{nx1}\frac{dn_{n0}}{dx} - n_0(\nu_{i1} - \nu_{w1}) - n_1(\nu_{i0} - \nu_{w0}) - n_{n0}\frac{dv_{nx1}}{dx} - n_{n1}\frac{dv_{nx0}}{dx} + \\ + i\omega n_{n1} - ik(n_{n0}v_{ny1} + v_{ny0}n_{n1}) \end{aligned} \tag{4.60a}$$

$$\frac{dv_{ex1}}{dx} = (\nu_{i1} - \nu_{w1}) - v_{ex0}\frac{dh_1}{dx} - v_{ex1}\frac{dh_0}{dx} + i\omega h_1 - ik(v_{ey1} + v_{ey0}h_1) \tag{4.60b}$$

$$\frac{dv_{ix1}}{dx} = (\nu_{i1} - \nu_{w1}) - v_{ix0}\frac{dh_1}{dx} - v_{ix1}\frac{dh_0}{dx} + i\omega h_1 - ik(v_{iy1} + v_{iy0}h_1) \tag{4.60c}$$

$$\begin{gathered}n_{n0}v_{nx0}\frac{dv_{nx1}}{dx}=-n_{n0}v_{nx1}\frac{dv_{nx0}}{dx}-n_{n1}v_{nx0}\frac{dv_{nx0}}{dx}+\\+(1-a_w)\left(n_0\nu_{w0}(v_{ix1}-v_{nx1})+n_0\nu_{w1}(v_{ix0}-v_{nx0})+n_1\nu_{w0}(v_{ix0}-v_{nx0})\right)+\\+i\omega n_{n0}v_{nx1}-ikn_{n0}v_{ny0}v_{nx1}\end{gathered}\tag{4.60d}$$

$$\begin{gathered}n_{n0}v_{nx0}\frac{dv_{ny1}}{dx}=-n_{n0}v_{nx1}\frac{dv_{ny0}}{dx}-n_{n1}v_{nx0}\frac{dv_{ny0}}{dx}+\\+(1-a_w)\left(n_0\nu_{w0}(v_{iy1}-v_{ny1})+n_0\nu_{w1}(v_{iy0}-v_{ny0})+n_1\nu_{w0}(v_{iy0}-v_{ny0})\right)+\\+i\omega n_{n0}v_{ny1}-ikn_{n0}v_{ny0}v_{ny1}\end{gathered}\tag{4.60e}$$

$$\begin{gathered}\frac{e}{m_i}\frac{d\phi_1}{dx}=-v_{ix0}\frac{dv_{ix1}}{dx}-v_{ix1}\frac{dv_{ix0}}{dx}+\nu_{i0}(v_{nx1}-v_{ix1})+\nu_{i1}(v_{nx0}-v_{ix0})+\\+i\omega v_{ix1}-ikv_{iy0}v_{ix1}\end{gathered}\tag{4.60f}$$

$$\begin{gathered}v_{ix0}\frac{dv_{iy1}}{dx}=-v_{ix1}\frac{dv_{iy0}}{dx}+\nu_{i0}(v_{ny1}-v_{iy1})+\nu_{i1}(v_{ny0}-v_{iy0})+\\+i\omega v_{iy1}-ik\left(e\phi_1/m_i+v_{iy0}v_{iy1}\right)=-v_{ix1}\frac{dv_{iy0}}{dx}+S_1\end{gathered}\tag{4.60g}$$

$$\begin{gathered}\frac{d}{dx}\left(\frac{T_{e1}}{m_i}\right)=-\frac{T_{e0}}{m_i}\frac{dh_1}{dx}-\frac{T_{e1}}{m_i}\frac{dh_0}{dx}+\frac{e}{m_i}\frac{d\phi_1}{dx}-\nu_{H0}v_{ex1}-\nu_{H1}v_{ex0}+\\+ik\chi_0\left(h_1T_{e0}/m_i+T_{e1}/m_i-e\phi_1/m_i\right)\end{gathered}\tag{4.60h}$$

$$P_0\frac{dh_1}{dx}=-P_1\frac{dh_0}{dx}+G_{ty1}\tag{4.60i}$$

where the linearised form of the function P may be expressed as follows:

$$P_1(\mathbf{u}_0,\mathbf{u}_1,\omega,k)=\sum_j\frac{\partial P_0}{\partial u_{j0}}u_{j1}=\frac{T_{e1}}{m_i}-\frac{6}{5}v_{ix0}v_{ix1}\tag{4.61}$$

with

$$\mathbf{y}_0=(x,h_0,v_{ix0},T_{e0},\phi_0,n_{n0},v_{ex0},v_{nx0})\qquad\mathbf{u}_0=(\mathbf{y}_0,\mathbf{q}_0)$$

$$\mathbf{y}_1=(h_1,v_{ix1},T_{e1},\phi_1,n_{n1},v_{ex1},v_{nx1},v_{iy1},v_{ny1})\qquad\mathbf{u}_1=(\mathbf{y}_1,\mathbf{q}_1)$$

In this no-heat-conduction model the complete linearised azimuthal problem consists of 23 fundamental modes, each one of them associated to one of the following variables at B, I and S:

- point B: h_{1B}, T_{e1B}, v_{ex1B}, n_{n1B}, v_{nx1B}, v_{iy1B}, v_{ny1B}, ϕ_{1B}
- point S: T_{e1S}, x_{1S}, h_{1S}, n_{n1S}, v_{nx1S}, v_{iy1S}, v_{ny1S}
- point I: h_{1I}, T_{e1I}, v_{ex1I}, n_{n1I}, v_{nx1I}, x_{1I}, v_{ny1I}, ϕ_{1I}

Once again, the fundamental modes associated to the variables ϕ_{1B} and ϕ_{1I} can be computed analytically as they only affect the absolute value of the electric potential. This leaves 21 fundamental modes that require numerical integration (as opposed to the 23 modes of the model with heat conduction), 7 for each of the special points in the domain of numerical integration, B, I and S. The method to compute each of those fundamental modes is analogous to the method used for the model with heat conduction.

4.1.4 Simplified models

In the previous sections the complete linear 2D time-dependent model has been presented. However, provided that the zero-th and first order problems are separated, it is possible to include different terms in the background and perturbation solutions. This allows evaluating which terms play a relevant role in an unstable oscillation. Nevertheless, all terms must be kept in the zero-th order problem in order to maintain the background solution similar to experiment results. However, in the perturbation problem some terms may be safely neglected based on the relative size of the perturbations for a given oscillation. This allows simplifying the formulation of the first-order problem while keeping only the terms that are strictly necessary to give rise to a given oscillation, and, in turn, understanding the physical mechanism at play.

Some of the terms that may be neglected from the perturbation problem are listed next, although in principle any variable or term of the linear formulation may be subject to exclusion from the linear 2D model:

- neutral dynamics (neutral density and velocity perturbations)
- ion axial and azimuthal dynamics (ion azimuthal velocity perturbations)
- heat conduction terms
- ionization particle source and sink terms

4.1.5 Anomalous diffusion and oscillations

The formulation presented above has mostly focused on the analysis of the linear stability of the Hall discharge against azimuthal perturbations. In case a self-excited oscillation is detected, then unstable oscillations grow and eventually saturate. The linear growth phase is the only one modelled with the 2D model presented here, whereas the saturation is a non-linear process. Anomalous diffusion related to saturated azimuthal oscillations cannot be determined self-consistently here. Nonetheless, some insight can be obtained if we accept the following postulate. The *shape* and *relative strength* of the saturated oscillations are those corresponding to the linear perturbations solution. Of course the postulate is likely less plausible the higher is the strength of the saturated oscillation, a parameter totally outside of the scope of the linear model developed here.

Equation (4.30d) is indeed the Ohm's law for electrons and can be expressed as:

$$en\mathbf{v}_e = -\boldsymbol{\mu}\big(en\mathbf{E} + \nabla(nT_e)\big) \tag{4.62}$$

where $\boldsymbol{\mu}$ is the electron mobility tensor and the rest of symbols as above. In the directions x and y we have:

$$env_{ex} = -\mu_\perp\left(enE_x + \frac{\partial(nT_e)}{\partial x}\right) + \mu_H\left(enE_y + \frac{\partial(nT_e)}{\partial y}\right) \tag{4.63a}$$

$$env_{ey} = -\mu_\perp\left(enE_y + \frac{\partial(nT_e)}{\partial y}\right) - \mu_H\left(enE_x + \frac{\partial(nT_e)}{\partial x}\right) \tag{4.63b}$$

where the components of the mobility tensor are defined as:

$$\mu_\perp = \frac{e}{m_e}\frac{\nu_e}{\omega_{ce}^2 + \nu_e^2} \simeq \frac{1}{B\chi} \tag{4.64a}$$

$$\mu_H = \chi\mu_\perp \simeq \frac{1}{B} \tag{4.64b}$$

For an axi-symmetric solution, the last term of (4.63a) and (4.63b) is zero. However, if small azimuthal oscillations are present, and because of $\mu_H \gg \mu_\perp$, the last term in (4.63a) may be important, thus providing an extra contribution to axial (i.e., perpendicular) transport. The azimuthal oscillations are not expected to modify significantly the rest of equations.

Next, the effect of that oscillation-based transport on the 1D steady-state solution will come out from averaging its effect over t and y. This yields:

$$en_0 v_{ex0} = -\mu_{\perp 0}\left(enE_x + \frac{\partial(nT_e)}{\partial x}\right)_0 + \frac{\langle en_{e1}E_{y1}\rangle}{B} \tag{4.65a}$$

$$en_0 v_{ey0} \simeq -\mu_H\left(enE_x + \frac{\partial(nT_e)}{\partial x}\right)_0 \tag{4.65b}$$

where $\langle z\rangle(x)$ is the temporal-azimuthal average of a function $z(t,x,y)$.

The strength of the oscillation-based transport, measured as the azimuthal force relative to the axial one, is expressed as:

$$\alpha_A(x) = \frac{\langle n_1 E_{y1}\rangle}{n_0 v_{ey0} B} \tag{4.66}$$

so that we can rearrange (4.65a) and (4.65b) as:

$$v_{ey0} = \frac{\omega_{ce}}{\nu_e'} v_{ex0} \tag{4.67a}$$

$$\text{with} \quad \nu_e' = \nu_e + \alpha_A(x)\omega_{ce} \tag{4.67b}$$

The last expression for ν_e' resembles the definition of the Bohm diffusion frequency ($\nu_B = \alpha_B\omega_{ce}$) highlighting the relation between the anomalous transport and the oscillation-based transport. If this additional transport were all the anomalous contribution, then $\alpha_B = \alpha_A(x)$, however there may be other contributors to the anomalous diffusion. From a practical point of view, given the perturbations of plasma density and azimuthal electric field, (4.66) allows obtaining the equivalent anomalous diffusion coefficient associated to the perturbations.

Note in any case that term is a non-linear effect and thus it is not accounted for in the formulation used in the previous sections, where the zero-th and first order problems are solved. In order to close the loop and have a self-consistent linear model of the oscillation-based transport it would be necessary to impose $\alpha_B = \alpha_A(x)$ and iterate until the same profile used in the zero-th order solution results from the corresponding linear perturbation problem.

One of the consequences of the azimuthal oscillation may thus be an enhanced electron conductivity inside the channel. In order to evaluate the net effect on the electron current, it is convenient to compute the equivalent anomalous diffusion coefficient, $\alpha_A(x)$, associated to the perturbations computed with the linear model.

4.2 Background solution and parametric variations

The zero-th order solutions whose stability is to be analysed in the following sections are described in this one. This section is devoted to the presentation of the results of the 1D model. For this purpose, a SPT-100 thruster model has been considered as reference case. In first place, results for the model without heat conduction and plume divergence are presented, and secondly, results with those effects are shown, including parametric variations on several operation parameters.

4.2.1 Reference solution without heat conduction and plume divergence

The main simulation parameters are presented in Table 4.1, where the following symbols are used: $\dot{m}$ is the mass flow rate through the anode, V_d is the discharge voltage, B_{max} is the maximum magnetic field, x_{max} is the location of the maximum magnetic field with respect to the anode, L_{AE} is the distance from anode to external cathode, L_{ch}, d_c and R are respectively the length, the width and the mean radius of the channel, T_{eE} is the cathode temperature, v_{nB} is the neutral velocity at injection, α_B is the anomalous diffusion coefficient, $\tilde{\nu}_w$ is a dimensionless parameter for the wall losses model [3] and T_{SEE} is a also parameter of the wall losses model that corresponds to the electron temperature yielding 100% of secondary electron emission for the specific wall material used. The electron temperature at the anode, T_{eB}, and the discharge current, I_d, are outputs of the simulation. For this reference case these result in $T_{eB} = 1.2$ eV and $I_d = 5.0$A.

Table 4.1: Main simulation parameters of the SPT-100 Hall Thruster used as reference case for the simulations **without** heat conduction and plume divergence.

$\dot{m}$	4.85 mg/s	V_d	300 V
B_{max}	237 G	x_{max}	20 mm
L_{ch}	25 mm	L_{AE}	33 mm
d_c	15 mm	R	42.5 mm
T_{eE}	4.8 eV	v_{nB}	300 m/s
α_B	0.01	$\tilde{\nu}_w$	0.16
T_{SEE}	100 eV	a_w	1.0
L_{m1}	15 mm	L_{m2}	7.5 mm

Fig. 4.6 shows the axial profiles of the main macroscopic variables corresponding to the background solution of Eqs. (4.52) for the reference case described in Table 4.1. In Fig. 4.6, there are three clearly separated regions in the discharge, from left to right in the figure: the ion-back-streaming region, the ionization region and the acceleration region. These regions are separated by the zero-ion velocity point and the regular ion sonic transition, represented in the figures as the left and right asterisks respectively. The ion back-streaming region is needed in order to fulfil the boundary condition of net current to the anode. Additionally, there are large temperature gradients in the ionization region due to the lack of heat conduction effects. More details about how the 1D model reproduces the structure of the Hall discharge may be found in [11, 12].

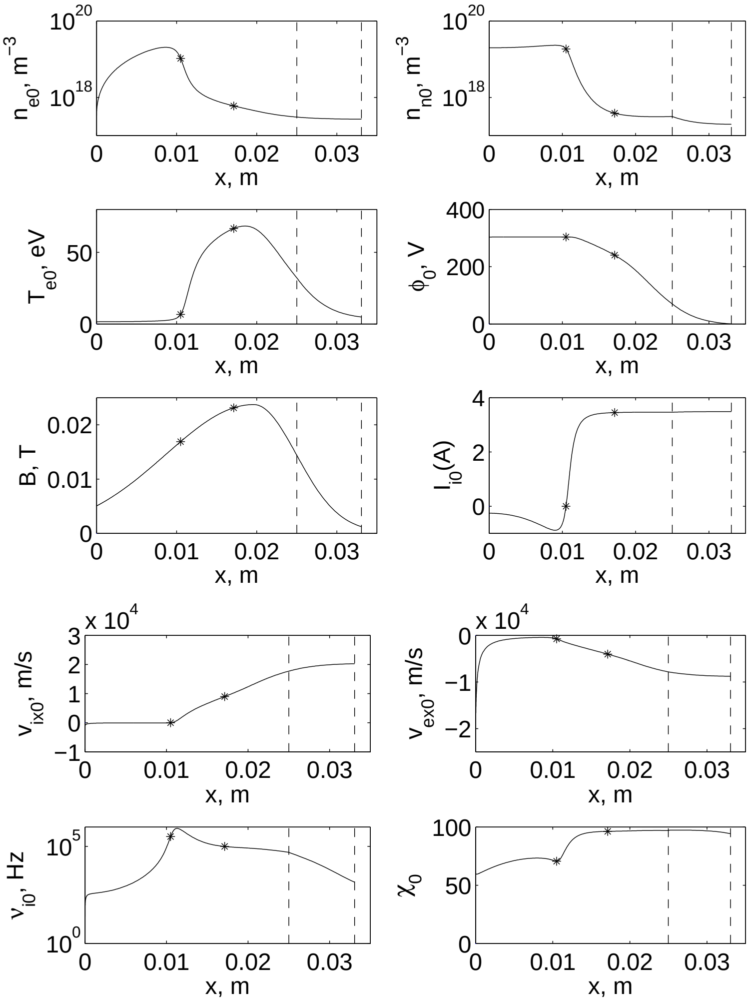

Figure 4.6: Axial profiles of the main macroscopic variables of the background solution for the reference case without heat conduction and plume divergence: x is the axial location, $n_{e0}(x)$ is the plasma density, $n_{n0}(x)$ is the neutral density, $T_{e0}(x)$ is the electron temperature, $\phi_0(x)$ is the electric potential, $B(x)$ is the magnetic field, $I_{i0}(x)$ is the ion axial current, $v_{ix0}(x)$ is the ion axial velocity, $v_{ex0}(x)$ is the electron axial velocity, $\nu_{i0}(x)$ is ionization frequency, and χ_0 is the Hall parameter. The left asterisk corresponds to the zero-ion-velocity point whereas the right asterisk corresponds to the regular ion sonic transition point inside the channel. The space between both points corresponds roughly to the ionization region of the thruster. The left vertical dashed line represents the channel exit, whereas the right one indicates the location of the cathode, which is the end of the simulation domain.

4.2.2 Reference solution with heat conduction and plume divergence

The main simulation parameters used in the simulation with heat conduction and plume divergence are presented in Table 4.2, where the symbols are as above. The simulation parameters are mostly similar, except for the wall model parameters, which in this case are more realistic, $a_w = 0.85$ and $T_{SEE} = 30eV$. In this case, the electron temperature at the anode and the discharge current are $T_{eB} = 2.9$ eV and $I_d = 5.4$A.

Table 4.2: Main simulation parameters of the SPT-100 Hall Thruster used as reference case for the simulations **with** heat conduction and plume divergence.

$\dot{m}$	4.75 mg/s	V_d	300 V	B_{max}	230 G	x_{max}	25 mm
L_{ch}	25 mm	L_{AE}	33.5 mm	d_c	15 mm	R	42.5 mm
T_{eE}	5 eV	v_{nB}	300 m/s	α_B	0.094	$\tilde{\nu}_w$	0.17
T_{SEE}	30 eV	a_w	0.85	L_{m1}	15 mm	L_{m2}	5 mm

Fig. 4.7 shows the axial profiles of the main macroscopic variables corresponding to the background solution of Eqs. (4.1) for the reference case described in Table 4.2.

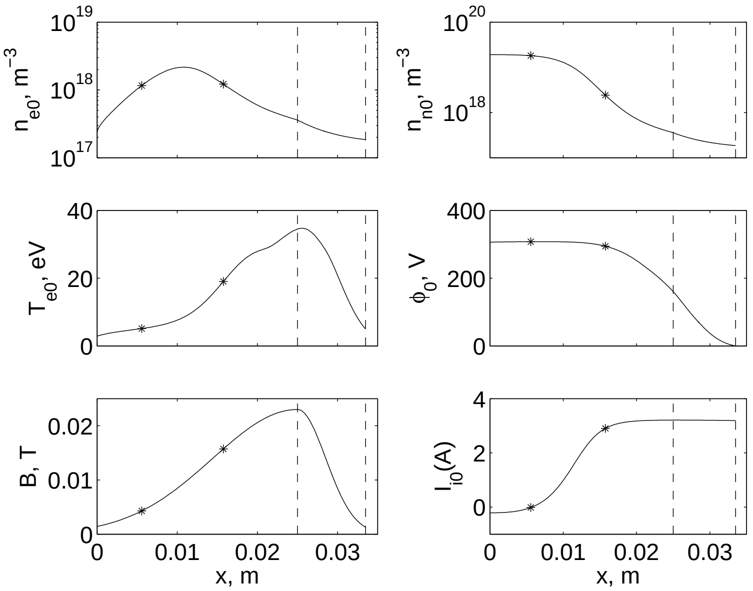

Figure 4.7: Axial profiles of the main macroscopic variables of the background solution for the reference case with heat conduction and plume divergence. Symbols are as in Fig. 4.6.

The main differences with respect to the case without heat conduction are the following. First, no steep gradients of the temperature exist and the maximum temperature is smaller thanks to the heat conduction. Second, there is a plateau in the temperature profile around the $30eV$ level as the saturation temperature of the wall losses model is reached. Third, the temperature peak is closer to the channel exit due to the maximum magnetic field profile. And last, the ionization region is closer to the anode as higher temperatures are reached near the anode. A complete description of the influence of heat conduction terms in the results of the 1D model and its ability to reproduce the structure of the Hall discharge discharge may be found in [3].

4.2.3 Parametric variations

This section is devoted to the description of the influence of the main operation parameters on the behaviour of the Hall discharge, namely: the discharge potential, V_d; the mass flow rate, $\dot{m}$; the length of the channel, L_{ch}; and the magnetic field gradient inside the channel, L_{m1}. This four parametric variations were carried out by the author in the 2000's in order to characterize the stationary behaviour of the thruster in different operating conditions and are explained in detail in [13]. Moreover, two additional parametric variations have been carried out specifically as part of this study on other parameters of the simulation, namely, the velocity of neutrals at injection, v_{nB}, and the channel width, d_c. The final goal is to evaluate the influence of all those parameters on the behaviour of the breathing mode and, more importantly, of the spoke oscillation.

Figs. 4.8-4.9, 4.10-4.11, 4.12-4.13, 4.14-4.15 show the variation of the main performance parameters and profiles of two extremes cases for the parametric variations on V_d, $\dot{m}$, L_{ch} and L_{m1}. In those figures the following new symbols are used: i_d is the dimensionless discharge current ($i_d = m_i I_d / e\dot{m}$); η, η_{prop}, η_{cur}, η_{vol}, and η_u are the overall, propulsive, current, voltage and propellant utilization efficiencies respectively, which measure the overall and partial efficiency of different processes; η'_u is an alternative propellant utilization measure defined as $\eta'_u = \eta/\eta_{prop}$; x_D and x_S are the axial coordinates of the zero-ion-velocity point and the regular ion sonic transition; $T_{e,max}$ is the maximum electron temperature through the simulation domain; P_{wall}, P_{ion}, and P_{anode} are respectively the losses due to plasma-wall interaction, ionization and plasma-anode interaction; $\eta_i(x)$ is the local ion flux fraction at a given axial location ($\eta_i(x) = m_i n v_{ix} A/\dot{m}$). A complete definition of each of those variables may be found in [13].

The following comments are worth about the trends shown by those parametric variations:

- as the discharge voltage is increased, the magnetic field typically needs to be varied roughly as $B_{max} \propto V_d^p$, where $p \approx 0.5$, for optimum operation, the efficiency increases, the wall losses and maximum temperature scale linearly, and the ionization region moves upstream and is slightly shortened.

- as the mass flow rate is increased, the neutral density and ionization frequency are increased, reducing the length of the ionization region, moving it downstream and increasing the overall, propellant and voltage utilization efficiencies, and the length of the acceleration region is decreased while the temperature gradients are increased.

- as the length of the channel is increased, the propellant utilization efficiency is increased thanks to a longer ionization region, the voltage utilization efficiency is decreased due to higher wall losses and as a consequence an optimum channel length exists for which the overall efficiency is maximized.

- as the magnetic field gradient is decreased (i.e., $L_{m1} \equiv L_{B1}$ is increased), the maximum magnetic field decreases as $B_{max} \propto L_{m1}^{-1}$ in order to maintain constant the overall magnetic effect (i.e. $\int B(x)dx$), the ionization region moves upstream thanks to the higher temperatures closer to the anode, the ion back-streaming region is reduced and the acceleration region also moves upstream causing an increase of wall losses and a decrease of efficiency.

A more thorough explanation of the parametric variations and the physical interpretation of each of the trends is given in [13].

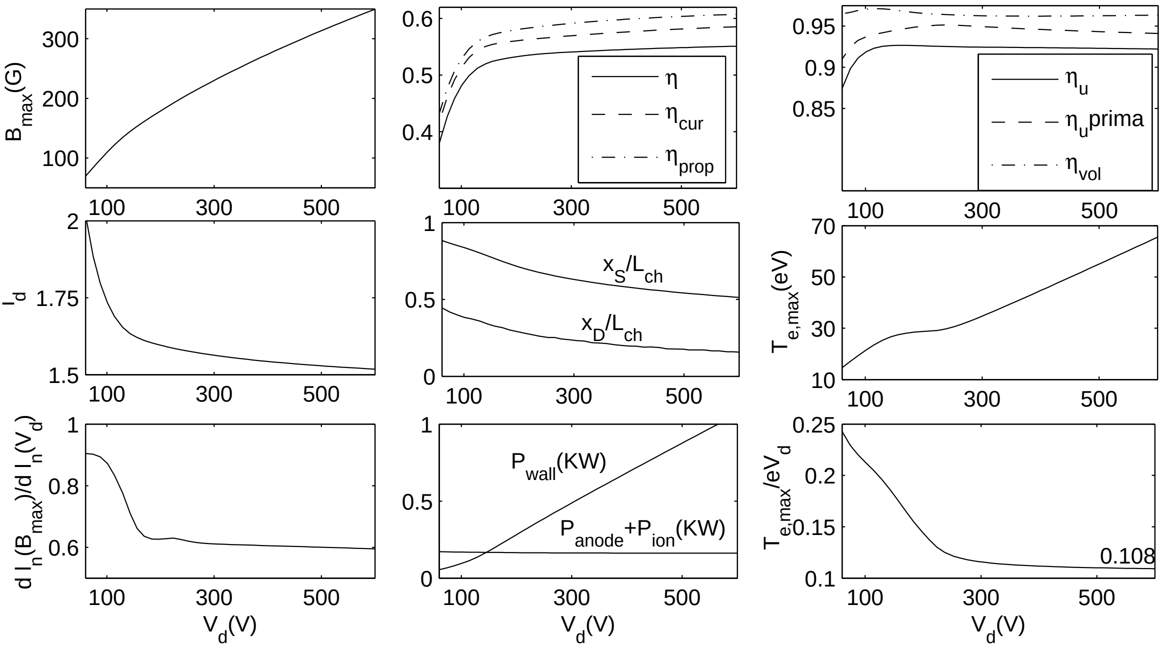

Figure 4.8: Evolution of thruster performances with the discharge voltage. All parameters are as shown in Table 4.2, except for V_d and B_{max}, the latter being optimized for each value of the discharge voltage.

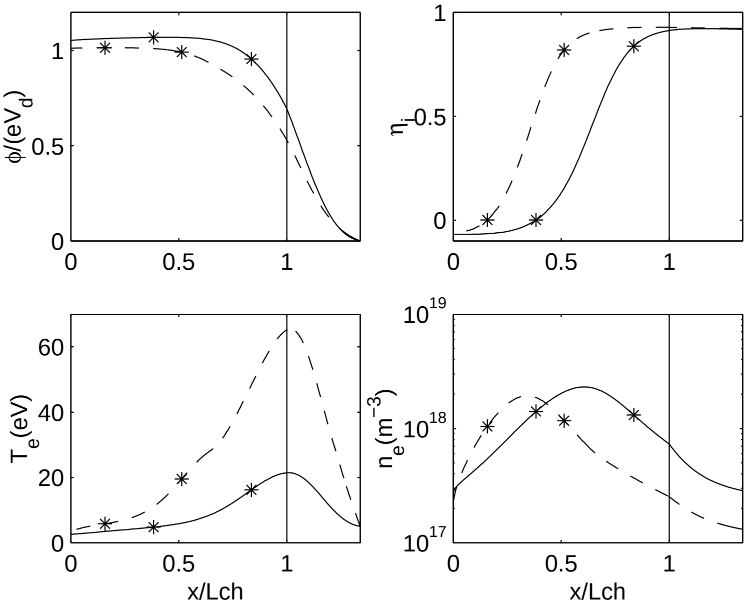

Figure 4.9: Axial profiles of the discharge for two particular parametric cases of Fig. 4.8: $V_d = 100V$ (solid lines) and $V_d = 600V$ (dashed lines). In each curve, the chamber exit is at the vertical line, $x/L_c = 1$, and the cathode is placed at the right boundary of the plots.

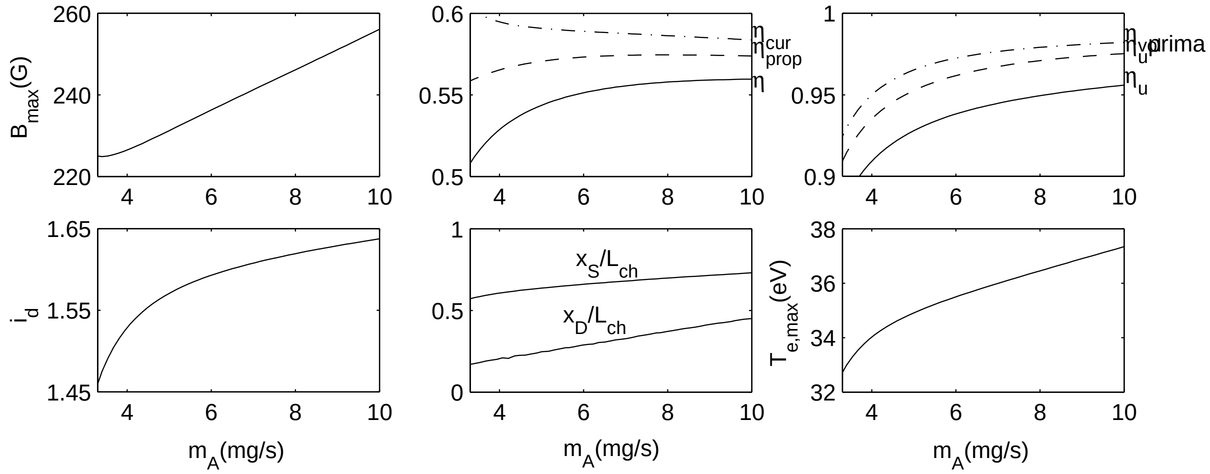

Figure 4.10: Evolution of thruster performances with the mass flow rate. All parameters are as shown in Table 4.2, except for $\dot{m}$ and B_{max}, the latter being optimized for each value of the mass flow rate.

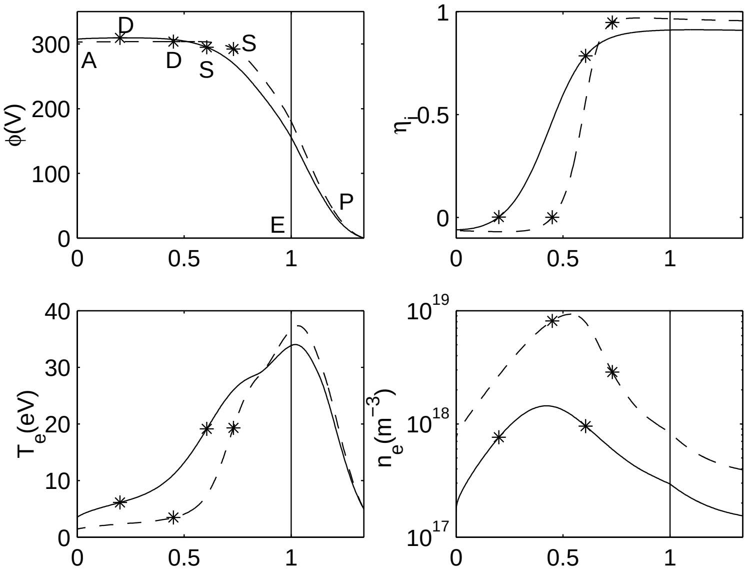

Figure 4.11: Axial profiles of the discharge for two particular parametric cases of Fig. 4.10: $\dot{m} = 4mg/s$ (solid lines) and $\dot{m} = 10mg/s$ (dashed lines). In each curve, the chamber exit is at the vertical line, $x/L_c = 1$, and the cathode is placed at the right boundary of the plots.

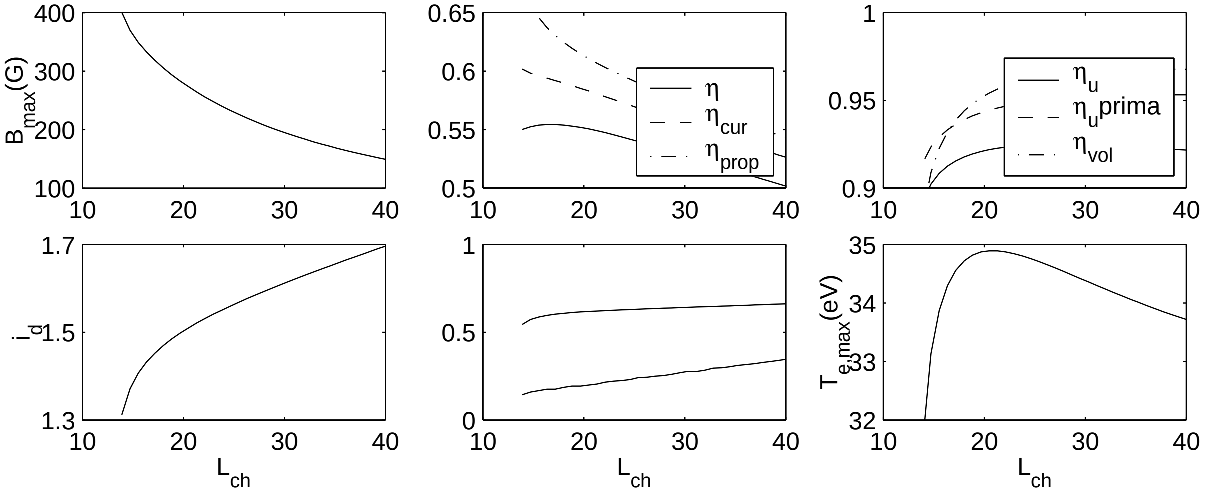

Figure 4.12: Evolution of thruster performances with the channel length. All parameters are as shown in Table 4.2, except for L_{ch} and B_{max}, the latter being optimized for each value of the channel length.

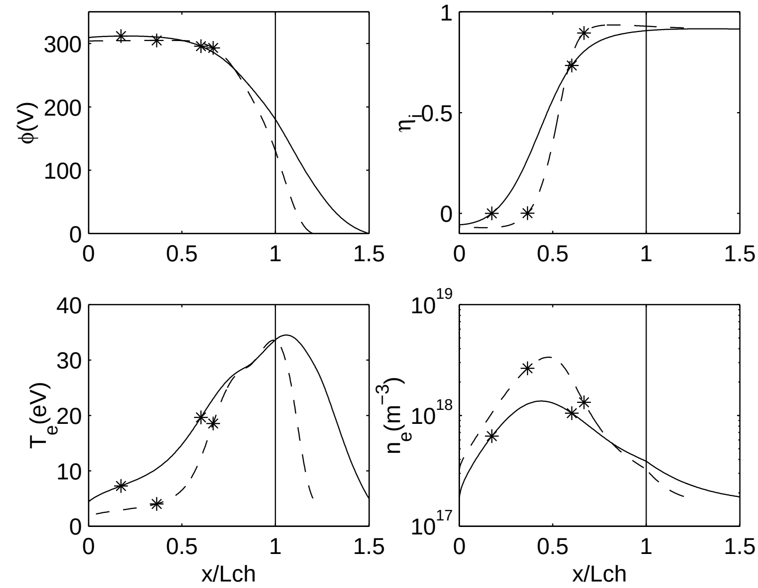

Figure 4.13: Axial profiles of the discharge for two particular parametric cases of Fig. 4.12: $L_{ch} = 17mm$ (solid lines) and $L_{ch} = 42.5mm$ (dashed lines). In each curve, the chamber exit is at the vertical line, $x/L_c = 1$, and the cathode is placed at the right boundary of the plots.

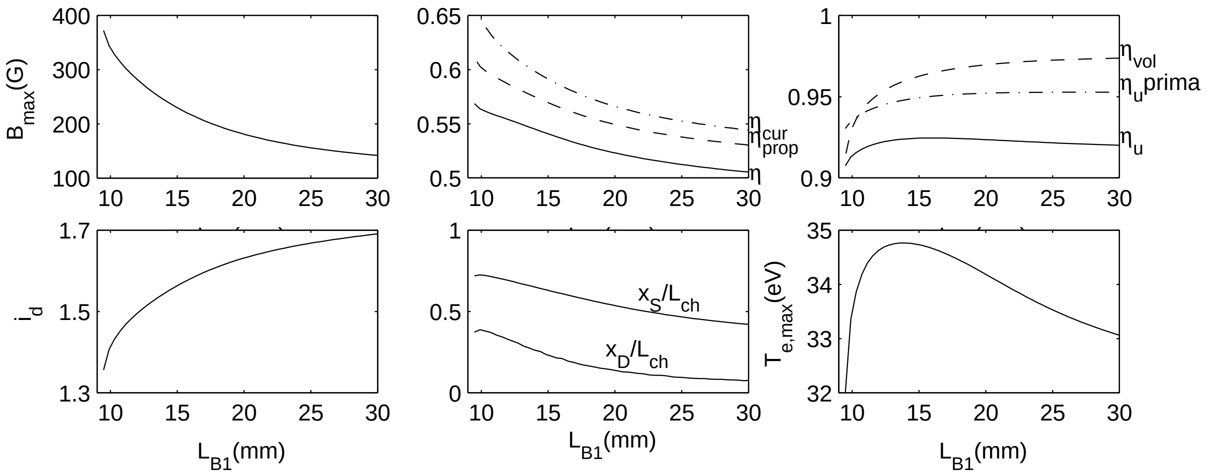

Figure 4.14: Evolution of thruster performances with the magnetic field gradient inside the channel. All parameters are as shown in Table 4.2, except for $L_{m1} \equiv L_{B1}$ and B_{max}, the latter being optimized for each value of the magnetic field gradient.

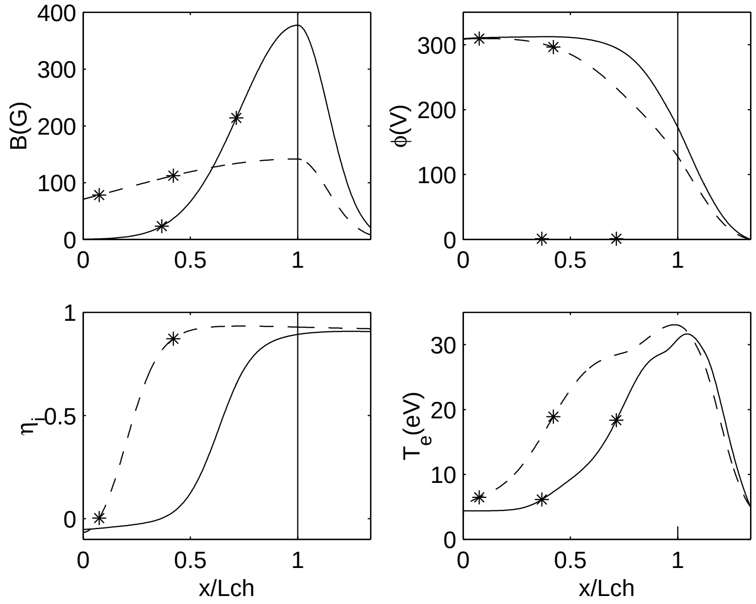

Figure 4.15: Axial profiles of the discharge for two particular parametric cases of Fig. 4.14: $L_{m1} = 9.5mm$ (solid lines) and $L_{m1} = 30mm$ (dashed lines). In each curve, the chamber exit is at the vertical line, $x/L_c = 1$, and the cathode is placed at the right boundary of the plots.

The next table shows the parameters used for the various background solutions whose stability is analysed in the following sections. The value of the parameters not shown in Table 4.3 are identical to those shown in Table 4.2. Each background solution is given an identifier for easier reference.

Table 4.3: Parameters of the background solutions under analysis. I, II, III, IV, V and VI refer to the parametric variations on V_d, $\dot{m}$, L_{ch}, L_{m1}, v_{nB} and d_c respectively.

Case	V_d, V	B_{max}, G
Ia	20	23
Ib	200	179
REF	300	230
Ic	500	313
Id	700	383

Case	$\dot{m}, mg/s$	B_{max}, G
IIa	3.3	225
IIb	4	226
REF	4.8	230
IIc	7	241
IId	8.5	249
IIe	10	256

Case	L_{ch}, mm	B_{max}, G
IIIa	14	401
REF	25	230
IIIb	26	217
IIIc	42	141
IIId	55	110

Case	L_{m1}, mm	B_{max}, G
IVa	30	142
IVb	19	185
REF	15	230
IVc	9	377

Case	$v_{nB}, m/s$	B_{max}, G
Va	174	240
Vb	240	235
REF	300	230
Vc	382	225
Vd	427	223

Case	d_c, mm	B_{max}, G
REF	15	230
VIa	18	244
VIb	21	251
VIc	31	278

4.3 Low frequency axial oscillations - breathing mode

In previous sections the complete formulation of the linear time-dependent 2D model has been presented as well as a background reference solution from the 1D model in combination with several parametric variations with respect to that reference solution. This section is devoted to the analysis of low frequency **axial oscillations** ($k = 0$), which are usually known as the breathing mode in HET. The analysis focuses on the stability of the reference background solution. Similar analyses have been carried out in the past by other authors [14, 181, 15]. However, the intention here is to validate the linear time-dependent 2D model presented above by analysing the results obtained for the breathing mode.

Note that as the size of the perturbations does not result from the linear perturbations problem, it must be chosen arbitrarily. Hereinafter, and just for illustration purposes, this size has been enlarged in each case to show the main properties of the visible oscillations. This is justified as nonetheless typical saturated breathing mode and spoke oscillations have a size of similar magnitude as the background state. Moreover, the exponential time dependence of the perturbations, $\exp(-i\omega_i t)$, has been omitted from the figures for clarity as well.

4.3.1 Results for the solution without heat conduction and plume divergence

Results from the linear time-dependent 2D model without heat conduction presented above for the case of *axial* oscillations are presented in Ref. [185]. This section summarizes the results and findings from that reference. Fig. 4.16 shows the contour maps in the $x - t$ space of the main variables of a purely axial (i.e., $m = 0$) unstable oscillation for the reference case presented in Table 4.1. The frequency of unstable oscillation is $f = 9.1$ kHz whereas the growth rate is $\omega_i/2\pi \approx 3$ kHz. That figure shows the axial oscillation of a very thin ionization layer. This fact is non-physical and might be solved including heat conduction effects.

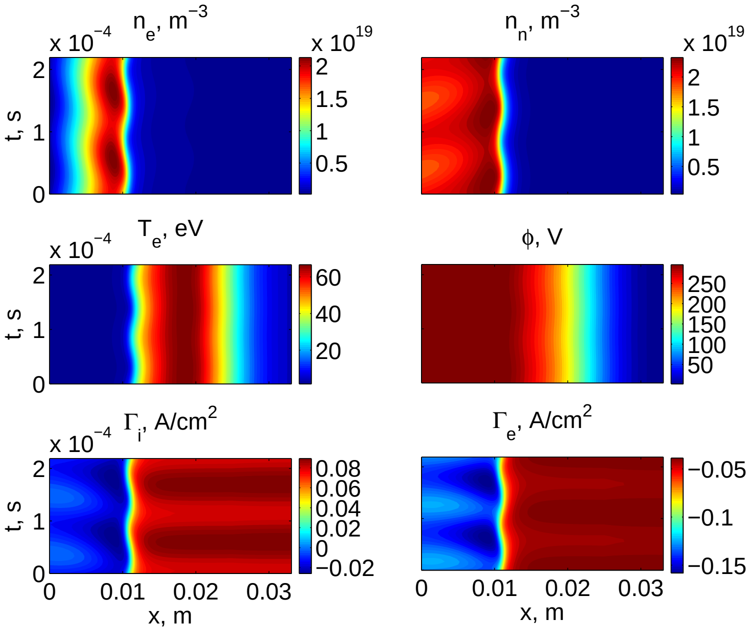

Figure 4.16: Oscillations as a function of x and t for the breathing mode ($m = 0$). The conditions and variables shown are similar to those shown in Fig. 4.6

4.3.2 Results for the solution with heat conduction and plume divergence

As seen in the previous paragraph, in order to properly model the breathing mode it seems necessary to use the 1D model *with* heat conduction. Figs. 4.17, 4.18, and 4.19 show, respectively, the axial variation of the main perturbations, the evolution over time of the discharge and anode ion current, and the contour maps in the $x - t$ space of the main variables of a purely axial (i.e., $m = 0$) unstable oscillation, for the very same reference case presented in Fig. 4.7. The growth rate of the unstable oscillation is $\omega_i/2\pi \approx 0.5$ kHz whereas the frequency is $f = 15.6$ kHz, of the same order of magnitude as the values observed experimentally [5]. The time evolution of the variables shown in Fig. 4.19 is qualitatively similar to those obtained with non-linear models of the breathing mode [81, 15, 57]. Those figures reproduce the usual properties of the breathing mode [20]: a) the ionization region moves back and forth as a consequence of the depletion and replenishment of neutrals; b) a standing wave of plasma density exists in the rear part of the thruster in phase with the discharge current oscillation and with similar relative size; c) a travelling wave, in combination with a standing wave, of neutral density is visible with a quarter-cycle phase difference; d) the relative size of neutral oscillations is much smaller than those of the plasma density and discharge current oscillations; e) the relative size of the electric potential oscillation is smaller than that of the electron temperature.

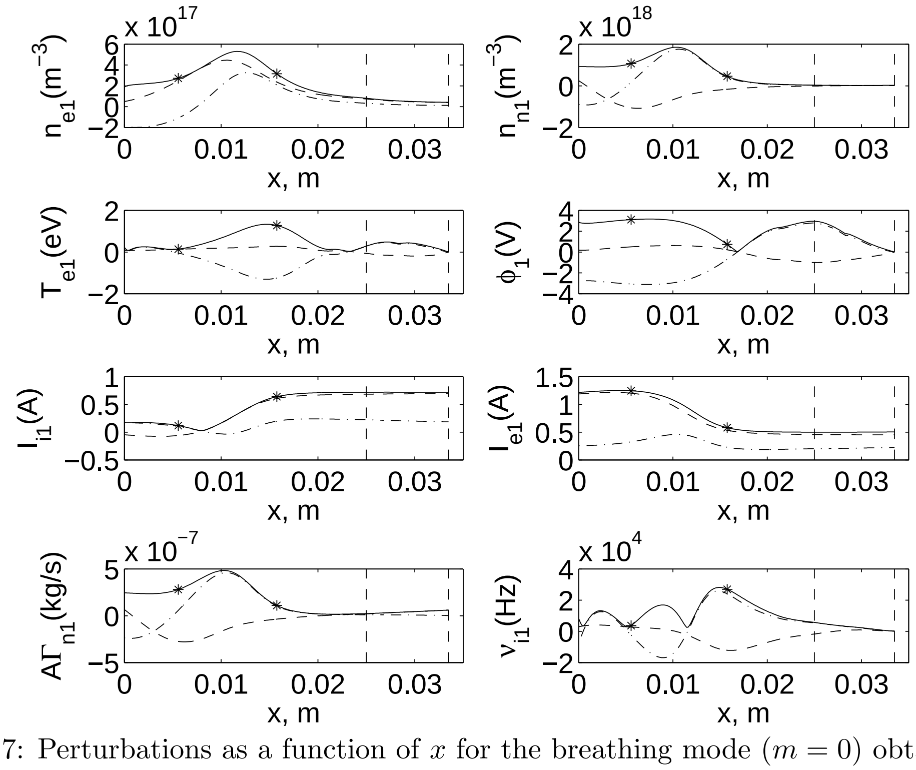

Figure 4.17: Perturbations as a function of x for the breathing mode ($m = 0$) obtained with the model including heat conduction. The conditions are similar to those shown in Fig. 4.7. The variables shown are from left to right and from top to down: plasma density, n_e; neutral density, n_n; electron temperature, T_e; electric potential, ϕ; ion current, I_i; electron current, I_e; neutral flow, $A\Gamma_n$; and ionization frequency, ν_i. Dashed lines are used for the real part of the perturbation coefficients, dash-dotted lines are used for the imaginary part and continuous lines are used for the modulus of the perturbation coefficients.

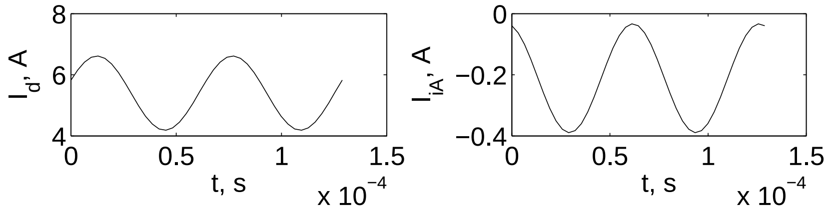

Figure 4.18: Oscillations of the discharge current, I_d, and the anode ion current, I_{iA} as a function of t for the breathing mode ($m = 0$) obtained with the model including heat conduction. The conditions are similar to those shown in Fig. 4.7

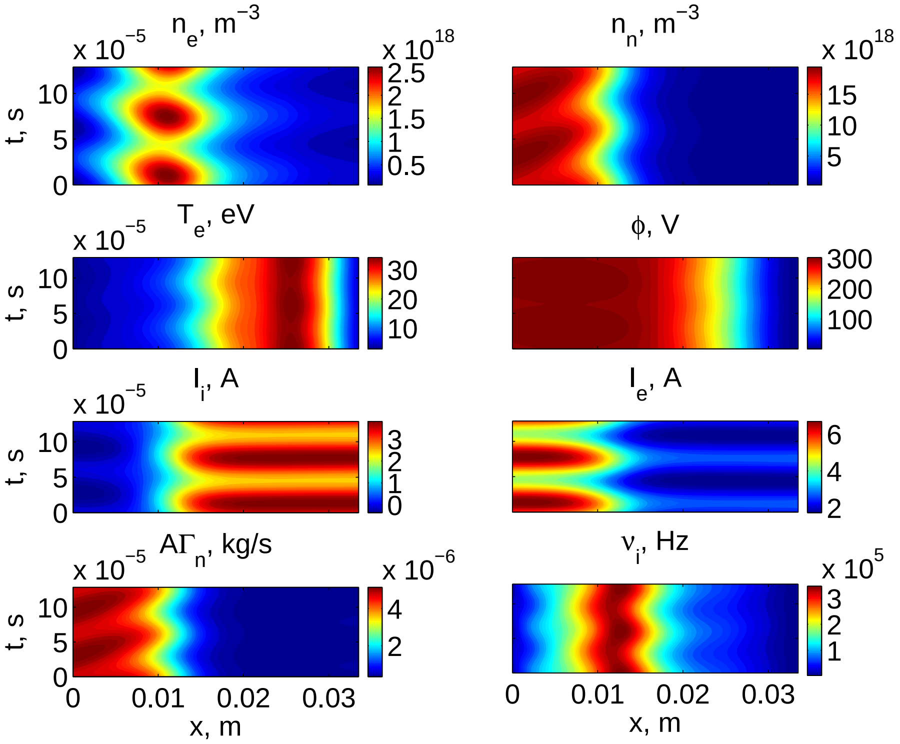

Figure 4.19: Oscillations as a function of x and t for the breathing mode ($m = 0$) obtained with the model including heat conduction. The conditions are similar to those shown in Fig. 4.7. The variables shown are from left to right and from top to down: plasma density, n_e; neutral density, n_n; electron temperature, T_e; electric potential, ϕ; ion current, I_i; electron current, I_e; neutral flow, $A\Gamma_n$; and ionization frequency, ν_i.

An interesting property of the axial oscillations is the non-uniformity in time of the neutral density at the anode plane. This seems in contradiction with the imposed anode boundary conditions that enforce constant neutral velocity and mass flow rate for the case under analysis (i.e. no external perturbations acting on the system). The reason for the neutral density to be non-uniform at the anode resides in the neutral recombination at the back wall of the thruster. Indeed this may be one of the reasons why the breathing mode is unstable as it is explained next. Part of the ions generated in the ionization region are attracted to the anode through the ion back-streaming region and are recombined into neutrals. These recombined neutrals travel downstream again, together with the injected neutrals, and are available for subsequent ionization cycles and, thus, more ions than in previous ionization cycles are generated and sent back to the anode giving rise to more recombined neutrals than before. The complete process is repeated again and again explaining the growing character of this mechanism.

In order to justify the previous mechanism, the following numerical test has been carried out. The boundary condition for neutral recombination at the anode has been temporarily relaxed in such a way that ions reaching the anode are not recombined into neutrals, but lost, and additionally, wall recombination has been disabled in the complete channel. Under these unrealistic conditions, the growth rate of the breathing mode oscillation is reduced by a factor close to 3. This gives some evidence of the role played by the neutral recombination at the walls in destabilizing the Hall discharge in the axial direction.

4.3.3 Parametric variations

This section shows how the $m = 0$ unstable oscillation presented previously varies in terms of frequency and growth with different operation parameters. To this end, Table 4.4 shows the properties of the $m = 0$ oscillation for the background solutions listed in Table 4.3. The following trends are observed from the results shown in Table 4.4:

- as the discharge voltage is increased, the frequency and growth rate of the oscillation increase. This increase of the frequency is in qualitative agreement with experimental results [186], and other numerical results [57]. In fact, the trend shown in Table 4.4 is non-linear and saturates at large voltages, as in the numerical results of [57].

- as the mass flow rate is increased, the frequency of the discharge decreases linearly whereas the growth rate increases. This decrease of the frequency is expected because as the mass flow rate is increased, the ionization region moves downstream causing the transit time of neutrals from injection to ionization region, which drives the breathing frequency, to increase. However, the opposite trend is reported in [186]. This may be due to the fact that the magnetic field is not modified in [186] when varying the mass flow rate, whereas in our case the magnetic field is optimized for each operation point.

- as the length of the channel is increased, the frequency decreases since, once again, the length to be transited by the neutrals from injection to ionization layer is longer.

- as the velocity of the neutrals at injection is increased, the frequency of the oscillation increases proportionally. This is in line with the idea that the transit time of neutrals from injection to ionization layer, inversely proportional to the neutral velocity, drives the frequency of the breathing mode.

Table 4.4: Frequency, f, and growth, $\omega_i/2\pi$, of the $m = 0$ oscillation for different operation parameters. REF refers to the reference background solution defined by Fig. 4.7, and I, II, III, IV, V and VI refer to the parametric variations on V_d, $\dot{m}$, L_{ch}, L_{m1}, v_{nB} and d_c respectively. "$-$" indicates that no solution is found to the condition $\det(A) = 0$, while "< 0" indicates that a stable solution is found.

Case	V_d, V	B_{max}, G	f, kHz	$\omega_i/2\pi, kHz$
Ia	20	23	11.1	< 0
Ib	200	179	14.3	< 0
REF	300	230	15.6	0.5
Ic	500	313	16.9	0.9
Id	700	383	17.9	1.5

Case	$\dot{m}, mg/s$	B_{max}, G	f, kHz	$\omega_i/2\pi, kHz$
IIa	3.3	225	17.0	0.04
IIb	4	226	16.3	0.4
REF	4.8	230	15.6	0.5
IIc	7	241	13.5	0.5
IId	8.5	249	12.7	0.6
IIe	10	256	12.1	0.6

Case	L_{ch}, mm	B_{max}, G	f, kHz	$\omega_i/2\pi, kHz$
IIIa	14	401	$-$	$-$
REF	25	230	15.6	0.5
IIIb	26	217	14.4	0.4
IIIc	42	141	14.7	< 0
IIId	55	110	11.2	0.5

Case	L_{m1}, mm	B_{max}, G	f, kHz	$\omega_i/2\pi, kHz$
IVa	30	142	16.1	2.7
IVb	19	185	14.7	2.0
REF	15	230	15.6	0.5
IVc	9	377	$-$	$-$

Case	$v_{nB}, m/s$	B_{max}, G	f, kHz	$\omega_i/2\pi, kHz$
Va	174	240	15.6	0.3
Vb	240	235	12.3	< 0
REF	300	230	15.6	0.5
Vc	382	225	19.4	0.7
Vd	427	223	21.4	0.4

Case	d_c, mm	B_{max}, G	f, kHz	$\omega_i/2\pi, kHz$
REF	15	230	15.6	0.5
VIa	18	244	15.3	0.6
VIb	21	251	15.2	0.7
VIc	31	278	14.7	1.2

4.4 Low frequency azimuthal oscillations - spoke oscillations

This section is devoted to the analysis of low frequency azimuthal oscillations, usually known as spokes, with the help of the linear time-dependent 2D model previously described.

4.4.1 Results for solution without heat conduction and plume divergence

Results from the linear time-dependent 2D model without heat conduction described above for the case of *azimuthal* oscillations are presented in Ref. [185]. This section summarizes the results and findings from that reference.

As a result of the global stability analysis of the reference case described in Table 4.1, a self-excited oscillation is detected with an azimuthal mode number $m = 1$, a frequency $f = 11.1$ kHz, an azimuthal phase velocity $v_y = 2.6$ km/s, a growth rate $\omega_i/2\pi \approx 3$ kHz, and an azimuthal wave-length $k_y = -0.023$ mm^{-1}. According to these values, the simulated azimuthal oscillation has properties similar to those experimentally observed for the spoke. Anyway, its growth rate is similar to the corresponding one for the breathing mode ($m = 0$) without heat conduction. Thus, it is not clear from this analysis which oscillation, the azimuthal one or the axial one, dominates in the reference case without heat conduction. On the other hand, the frequency of the simulated breathing mode is smaller than for the azimuthal oscillation presented here, as normally observed in experiments [5, 7].

It must be noted that other mode numbers ($m = -2$, -1 and 2) have been analysed looking for possible self-excited solutions. However, for the reference case under consideration the only mode numbers resulting in self-excited solutions are $m = 0$ (breathing mode) and $m = 1$ (spoke). This is in line with experimental results for normal-size thrusters, where the spoke is normally detected as a single oscillation in the **E**x**B** direction. In the case of larger thrusters, experiments show that higher modes ($m = 2, 3, 4$) might become dominant [123].

Fig. 4.20 shows the contour maps in the $x - t$ space (at the meridian section $y = 0$) of the main macroscopic variables as combinations of the background solution and the perturbations for the self-excited oscillation mentioned above. In the azimuthal oscillation (see plot of neutral density in Fig. 4.20), the ionization front moves back and forth, as in the breathing mode (see Fig. 4.16). Moreover, the $m = 1$ oscillation also shows a travelling wave of neutral density, as in the breathing mode. The similarity with the breathing mode, thus, seems clear. The fact that both modes are recovered with the very same model reinforces this idea. Moreover, as in the case of the $m = 0$ oscillation, the region where the ionization front moves back and forth is rather thin compared to what is normally seen experiments for the breathing mode.

Figs. 4.21 and 4.22 show contour maps in the $x - y$ space for different instants of time, t, during one cycle of the azimuthal oscillation under the same conditions as in Fig. 4.20. In this figure, it is possible to observe how the oscillation travels in the $-y$ direction, this is, in the +**E**x**B** direction. As expected, the same patterns shown in Fig. 4.20 are observed in Figs. 4.21 and 4.22 moving in the azimuthal direction.

According to Figs. 4.21 and 4.22, the azimuthal oscillation seems due to an azimuthal variation of the ionization process. The connection between the spoke oscillation and the ionization process had already been suggested theoretically by the authors [18, 17], and, based on experiments, by other researchers [129].

From Figs. 4.20-4.22 it is possible to compute the approximate wavelength of the oscillation in the axial direction, k_x. This is estimated to be $k_x \approx 1.7$ mm^{-1}, which is consistent

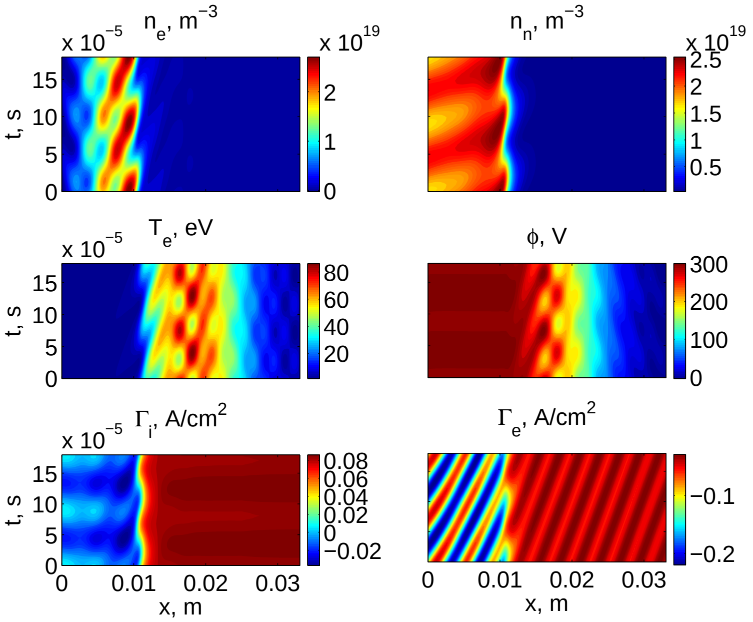

Figure 4.20: Oscillations of the main macroscopic variables as combinations of the background solution and the perturbations shown as functions of x and t at $y = 0$ for a self-excited oscillation of the perturbation problem for the reference case presented in Table 4.1. The azimuthal mode number is $m = 1$, the frequency is $f = 11.1$ kHz and the growth rate is $\omega_i/2\pi \approx 3$ kHz. Variables shown (from left to right and upper to lower): plasma density, n_e; neutral density, n_n; electron temperature, T_e; electric potential, ϕ; ion axial flux, Γ_i; electron axial flux, Γ_e.

with the wave travelling forward in the axial direction ($\omega_r > 0$, $k_x > 0$) at a fixed azimuth and in the $+$**E**x**B** direction ($\omega_r > 0$, $k_y < 0$) at a fixed axial location as time increases.

However, the tilt angle with respect to the axis of the thruster ($\tan\beta = k_x/k_y$) is close to 90 degrees, whereas in experiments, the azimuthal oscillation is normally observed to have a tilt angle around 15-20 degrees [6, 7]. The reason for this discrepancy is believed to be related to the narrow ionization region seen in the simulation, likely caused by the fact that heat conduction effects are not considered in the model. The version of the 1D model of Ahedo that takes into consideration heat conduction terms [12] gives smoother temperature profiles, wider ionization regions and lower peak temperatures inside the thruster. Thus, adding heat conduction effects to the model is expected to reduce the tilt angle of the azimuthal oscillation considerably.

For completeness, Fig. 4.23 shows the axial profiles of the complex coefficients of the Fourier-expansion of the perturbation equations defined in (4.35). These are the variables resulting from the integration of the linearised equations.

Based on Fig. 4.23, it is also interesting to point out that the perturbed electric field has a roughly constant azimuthal component upstream of the ionization region (see left column of Fig. 4.22 and plot of ϕ_1 in Fig. 4.23). This fact, together with the plasma density variation, causes an oscillatory axial electron current to the anode coming from the **E**x**B** drift associated to the azimuthal electric field, as can be observed in the right column of Fig. 4.22.

Fig. 4.24 shows the axial variation of $\alpha_A(x)$ based on Eq. (4.66). It is possible to observe that the net effect of the oscillation on the electron conductivity is concentrated in the rear part of the thruster, more precisely, in the ion-backstreaming region. The values reached by

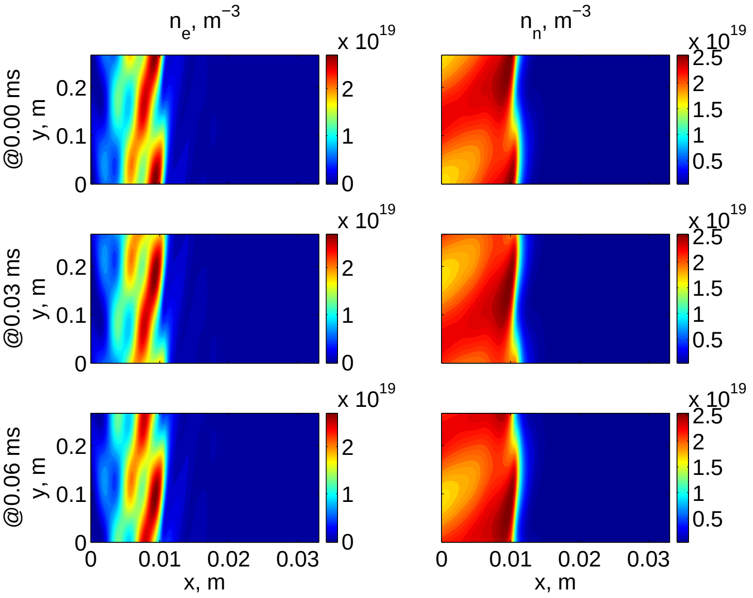

Figure 4.21: Oscillations of the main macroscopic variables as combinations of the background solution and the perturbations shown as functions of x and y at different values of t (@ t ms) for the same conditions used previously in Fig. 4.20. Variables shown (from left to right): plasma density, n_e; neutral density, n_n.

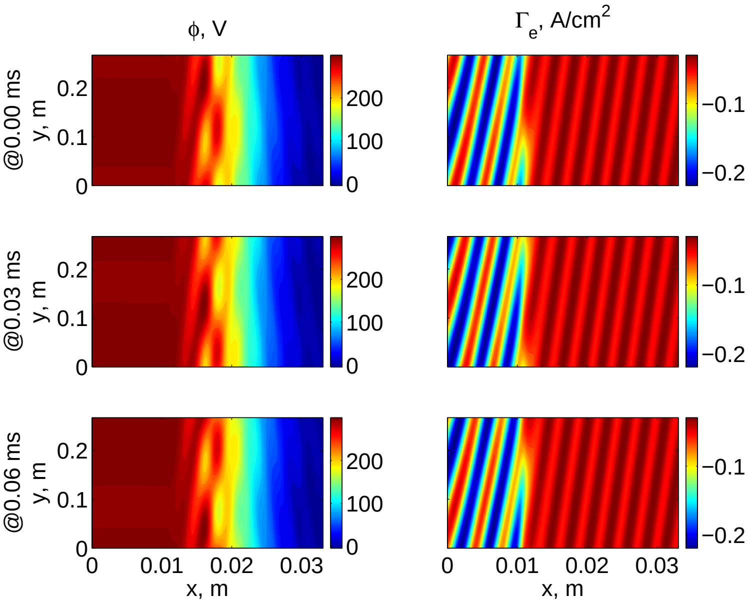

Figure 4.22: Same as Fig. 4.21 for other macroscopic variables. Variables shown (from left to right): electric potential, ϕ; electron axial flux, Γ_e.

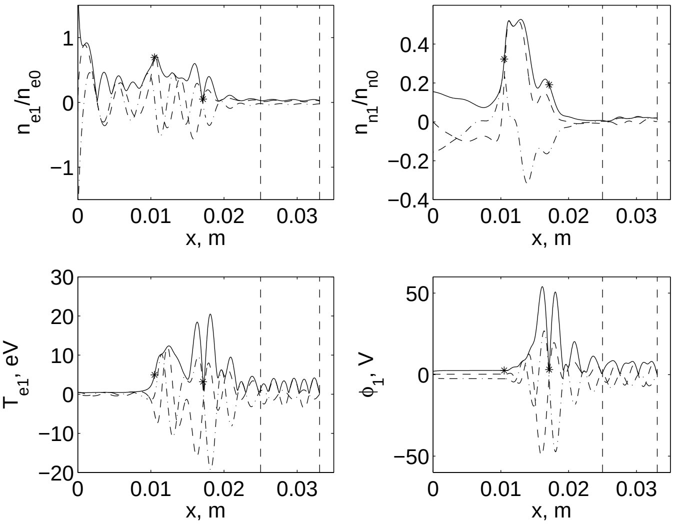

Figure 4.23: Axial profiles of the coefficients of the Fourier-expanded perturbations of the main macroscopic variables corresponding to the self-excited oscillation of the perturbation problem for the reference case presented in Table 4.1 and the same conditions as in Fig. 4.20. Dashed lines are used for the real part of the perturbation coefficients, dash-dotted lines are used for the imaginary part and continuous lines are used for the modulus of the coefficients.

$\alpha_A(x)$ in this region are of the same order of magnitude to that used for α_B in the simulation of the background solution of the reference case (see Table 4.1). In fact, for the case under analysis the average value of $\alpha_A(x)$ in the rear part of the thruster is $\alpha_{A,ave} \approx 0.01$, a value very similar to the one used in the zero-th order solution. However, this is only true for the selected size of linear oscillations that, in this particular case, is such that the maximum temperature perturbation is 30% of the background temperature.

Another relevant aspect is the fact that $\alpha_A(x)$ reaches negative values in some regions of the channel. This negative value of $\alpha_A(x)$ is linked to the tilt angle close to 90 degrees of the plasma density perturbation, which causes a change of phase between the perturbations of the plasma density and the azimuthal electric field. Moreover, the large variations of $\alpha_A(x)$ anticipate important changes in the background solution, where so far α_B has been considered constant, in case the profile of $\alpha_A(x)$ is used in the resolution of the zero-th order problem. Anyway, no contribution to electron conductivity is seen downstream the ionization region, where experiments also show a higher-than-expected electron mobility. Non-linear effects affecting the low-frequency azimuthal oscillation might resolve this discrepancy. Another possible explanation is that high-frequency oscillations (1-10 MHz) [64]−[67] might play a role in the plume.

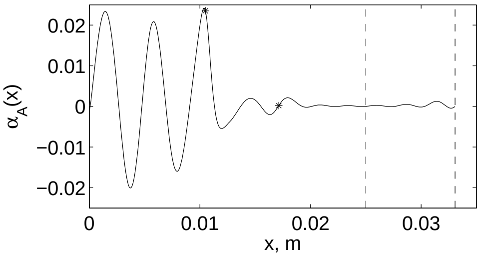

Figure 4.24: Axial profiles of the equivalent anomalous diffusion coefficient, $\alpha_A(x)$, as computed from the linear perturbation with a size of 30% of the zero-th order solution

4.4.2 Results for solution with heat conduction and plume divergence

This section presents the results of the low frequency global stability analysis in the azimuthal direction for the reference background solution with heat conduction and plume divergence. As in the case of the breathing mode oscillation, the width of the oscillation is expected to be higher than in the case without heat conduction. Figs. 4.25-4.31 present the results of an unstable $m = 1$ azimuthal oscillation for the reference case described in Fig. 4.7. This oscillation has the following properties: frequency, $f = 24.9$ kHz; growth rate, $\omega_i/2\pi = 92.7$ kHz; and azimuthal phase speed $v_y = 6.6$ km/s in the $+\mathbf{E}\mathrm{x}\mathbf{B}$. This numerical result is in qualitative agreement with experimental evidence, where it is normally observed that the spoke has higher frequency than the breathing mode for the same thruster [5]. Compared to the frequency of the breathing mode observed in the case with heat conduction, $f = 15.6$ kHz, this is indeed the case. It is also worth pointing out that, as in the case of the breathing mode, compared to the case without heat conduction terms[185], the frequency of the spoke is roughly doubled.

Figs. 4.25 and 4.26 show the spatial variation of the perturbations corresponding to the unstable oscillation just described, firstly, in the axial direction, Fig. 4.25, and, secondly, in the $x-y$ space, Fig. 4.26. In Figs. 4.27 and 4.28 it is possible to observe contour maps in the $x-y$ space and the evolution in the $x-t$ space for the main macroscopic variables. Figs. 4.29 and 4.30 show contour maps in the $x-y$ space for different instants of time, t, during one cycle of the azimuthal oscillation under the same conditions as before for the plasma density, neutral density, electric potential and electron flux. Finally, Figs. 4.31 and 4.32 depict the size of the perturbations relative to the background solution for the macroscopic variables solved as part of the integration process.

Some comments are worth relative to the $m = 1$ unstable solution presented above and shown in Figs. 4.25-4.31:

- the oscillation is mostly concentrated in rear part of the thruster, upstream of the acceleration region, although there are some perturbations in temperature and electric field that reach the acceleration region.

- contrary to the case without heat conduction, at least in the case under analysis, the contribution to the oscillation from the neutral density perturbation is negligible. This is best observed in Fig. 4.31 where the relative size of the neutral oscillation is much smaller than that of the plasma density.

- as expected, as a consequence of the inclusion of heat conduction terms, the tilt angle of the oscillation has decreased with respect to the value observed without heat conduction in the previous section. However, this decrease is not enough and the tilt angle is still far from the experimentally observed value of 15-20 degrees.

- even if the relative size of the perturbation of the neutral density is negligible, the ionization may play a role in the oscillation, as seen in Fig. 4.26, where it is possible to observe how the ionization front moves back and forth as in the case of the breathing mode. This motion of the ionization front seems linked to the plasma density oscillation as the temperature oscillation has lower relative size than that of the density.

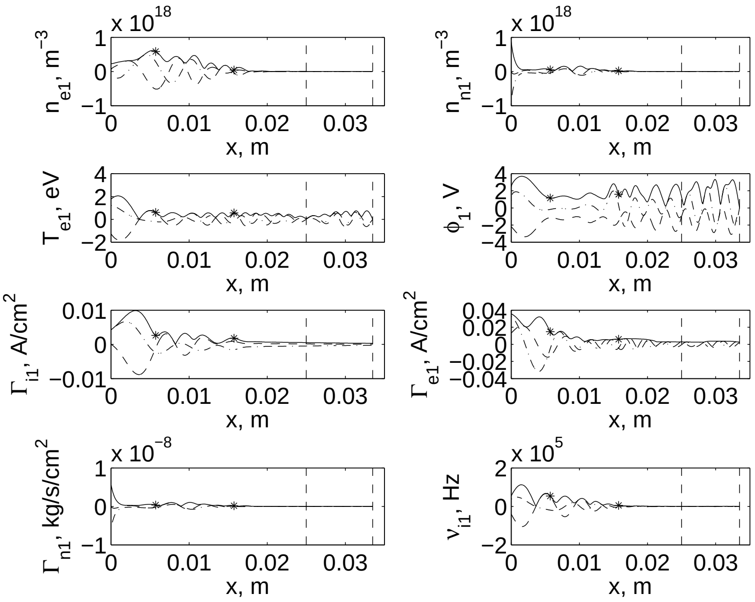

Figure 4.25: Axial profiles of the coefficients of the Fourier-expanded perturbations of the main macroscopic variables corresponding to a $m = 1$ self-excited oscillation of the perturbation problem for the reference case presented in Fig. 4.7. Dashed lines are used for the real part of the perturbation coefficients, dash-dotted lines are used for the imaginary part and continuous lines are used for the modulus of the coefficients. Variables shown (from left to right and upper to lower): plasma density, n_{e1}; neutral density, n_{n1}; electron temperature, T_{e1}; electric potential, ϕ_1; ion axial flux, Γ_{i1}; electron axial flux, Γ_{e1}; neutral axial flux, Γ_{n1}; ionization frequency, ν_{i1}.

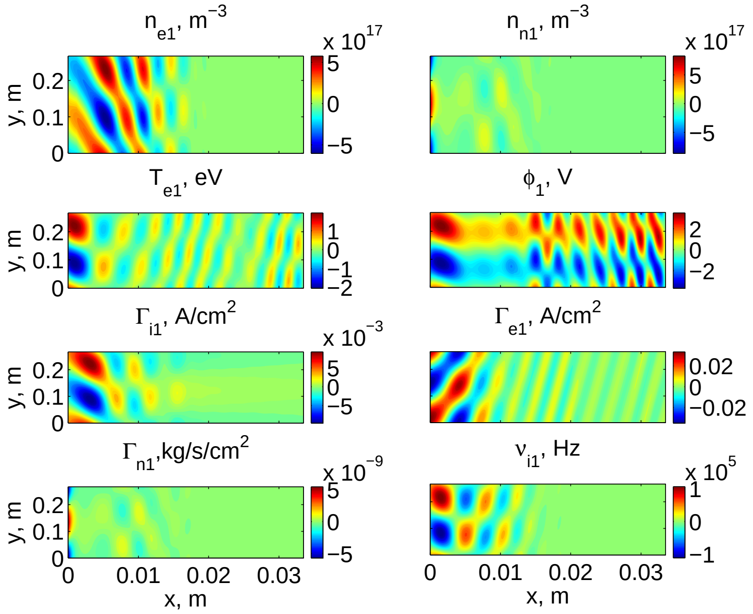

Figure 4.26: Perturbations of the main macroscopic variables shown as functions of x and y at $t = 0$ for a $m = 1$ self-excited oscillation of the perturbation problem for the reference case presented in Fig. 4.7. The variables shown are the same as those shown in Fig. 4.25.

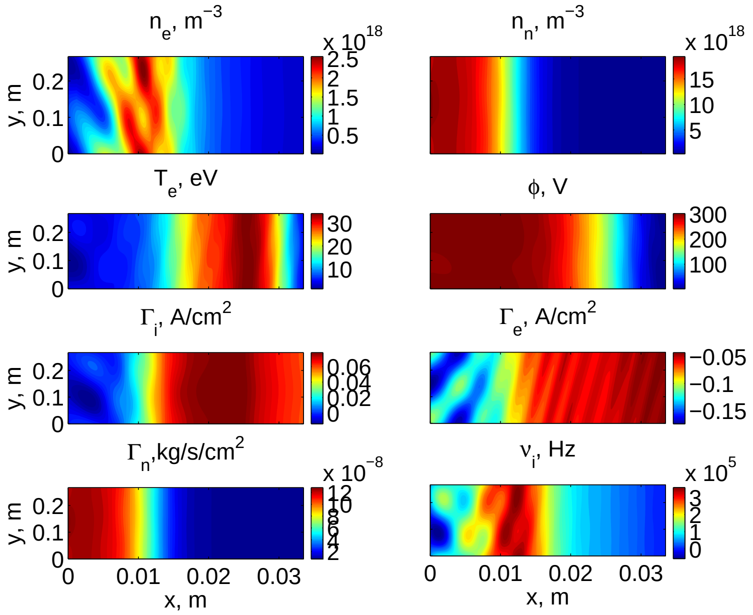

Figure 4.27: Oscillations of the main macroscopic variables as combinations of the background solution and the perturbations shown as functions of x and y at $t = 0$ for a $m = 1$ self-excited oscillation of the perturbation problem for the reference case presented in Fig. 4.7. Variables shown (from left to right and upper to lower): plasma density, n_e; neutral density, n_n; electron temperature, T_e; electric potential, ϕ; ion axial flux, Γ_i; electron axial flux, Γ_e; neutral axial flux, Γ_n; ionization frequency, ν_i.

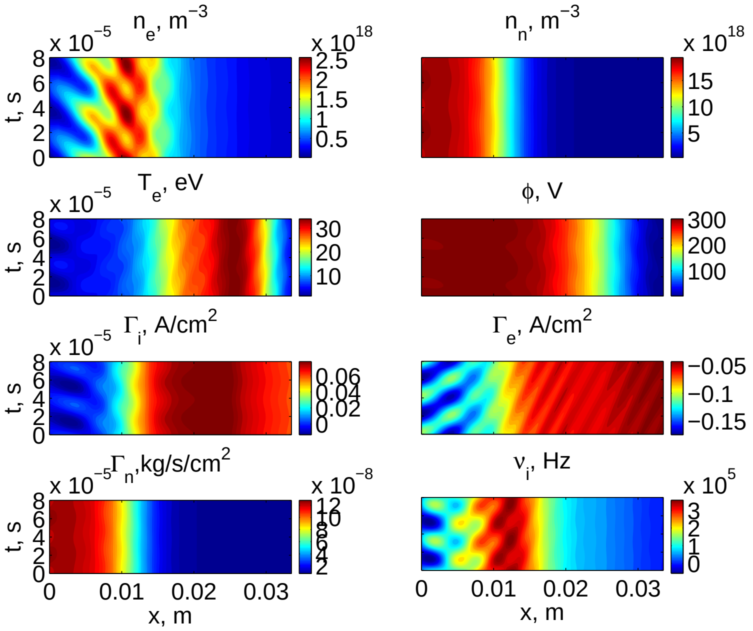

Figure 4.28: Oscillations of the main macroscopic variables as combinations of the background solution and the perturbations shown as functions of x and t at $y = 0$ for a $m = 1$ self-excited oscillation of the perturbation problem for the reference case presented in Fig. 4.7. The variables shown are the same as in Fig. 4.27.

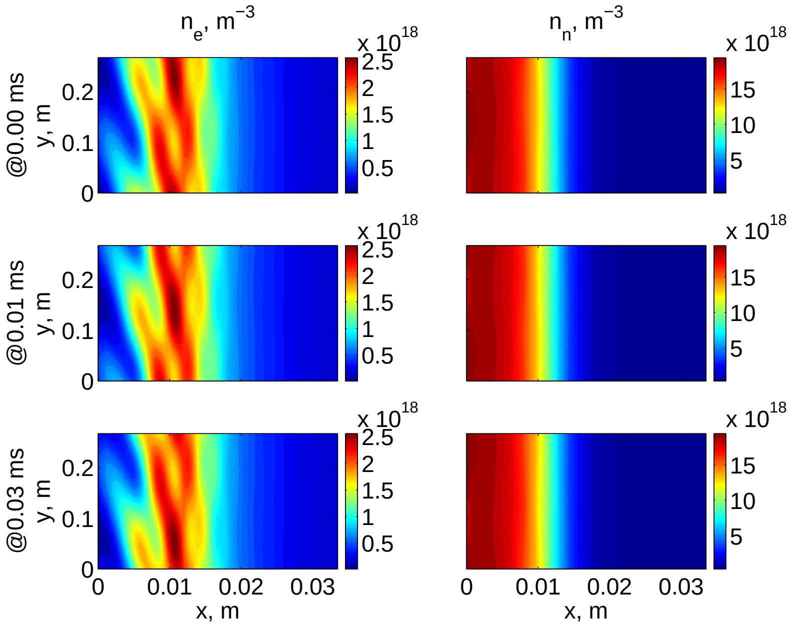

Figure 4.29: Oscillations of the main macroscopic variables as combinations of the background solution and the perturbations shown as functions of x and y at different values of t (@ t ms) for the same conditions used previously in Fig. 4.28. Variables shown (from left to right): plasma density, n_e; neutral density, n_n.

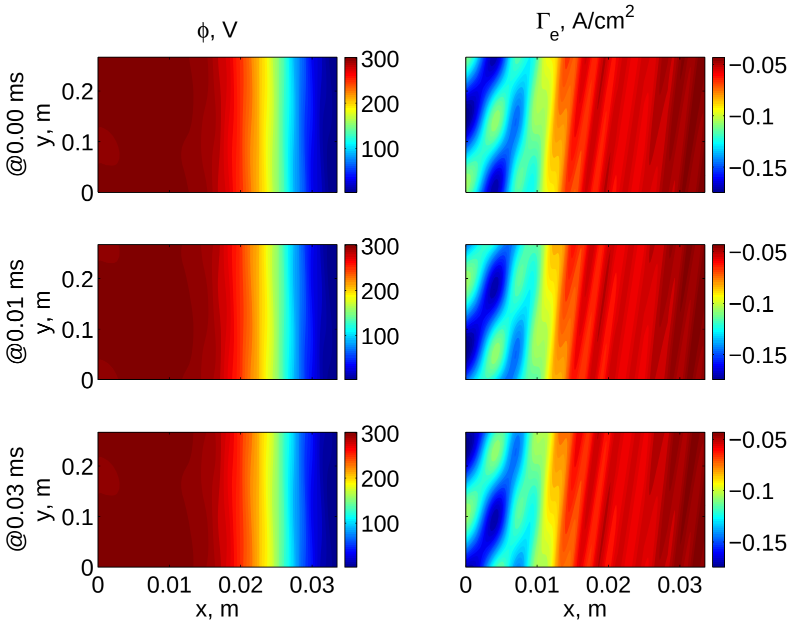

Figure 4.30: Same as Fig. 4.29 for other macroscopic variables. Variables shown (from left to right): electric potential, ϕ; electron axial flux, Γ_e.

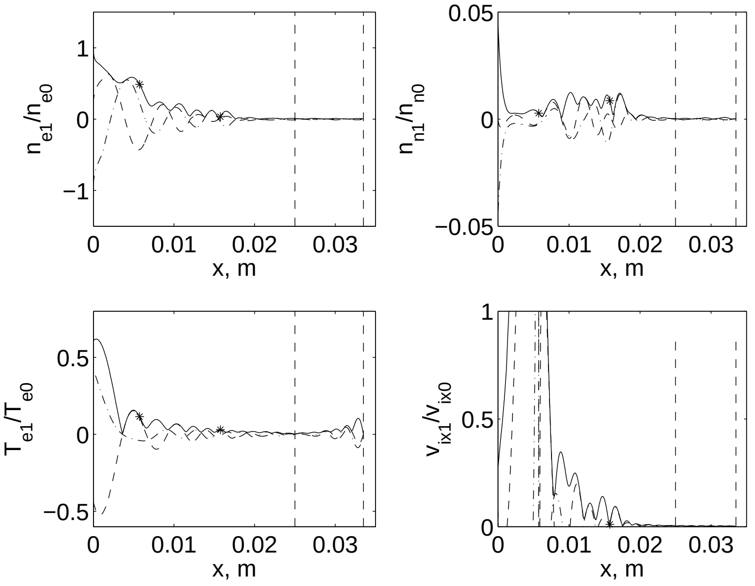

Figure 4.31: Axial profiles of the coefficients of the Fourier-expanded perturbations relative to the background solution of the main macroscopic variables corresponding to a $m = 1$ self-excited oscillation of the perturbation problem for the reference case presented in Fig. 4.7. Dashed lines are used for the real part of the perturbation coefficients, dash-dotted lines are used for the imaginary part and continuous lines are used for the modulus of the coefficients. Variables shown (from left to right and upper to lower): plasma density, neutral density, electron temperature, ion axial velocity.

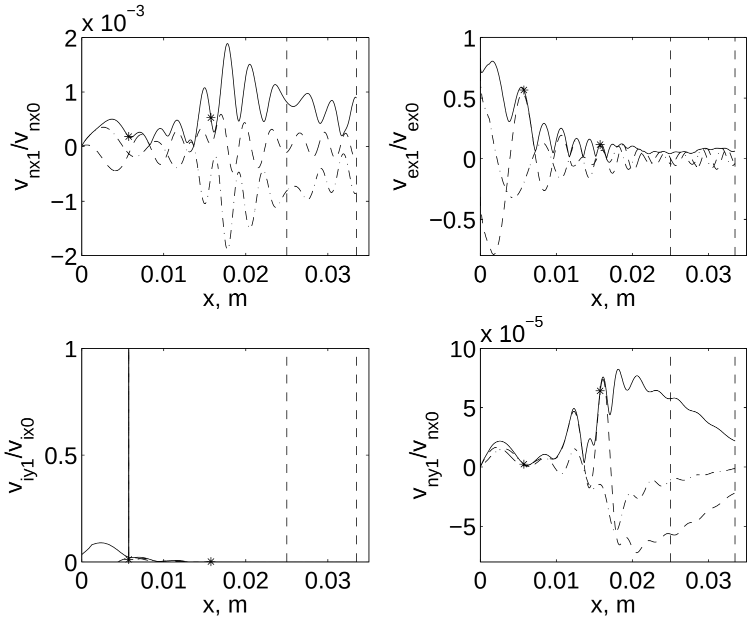

Figure 4.32: Same as Fig. 4.31. Variables shown (from left to right and upper to lower): neutral axial velocity, electron axial velocity, ion azimuthal velocity, neutral azimuthal velocity.

4.4.3 Parametric variations

This section presents the results of the azimuthal global stability analysis for the cases presented in Table 4.3. This analysis consists in the search in the frequency space of self-excited modes for the different background solutions under evaluation and for different wave mode numbers. Here, it is interesting to check whether the main trends observed experimentally are also reproduced with the linear 2D time-dependent model, in particular, related to the variation of the oscillation frequency and to the possible existence of different types of oscillations. Moreover, oscillation mode numbers $m > 1$ need to be analysed as well since, as mentioned previously, in the case of larger thrusters (e.g. higher power than the STP-100), experiments show that modes $m = 2, 3, 4, ...$ might become dominant [123].

In the case of modes $m > 1$ the frequency of the oscillation grows linearly with the mode number. This does not mean that the oscillation travels faster. This is, for the same phase speed, a $m = 2$ oscillation has a frequency twice as large as a $m = 1$ oscillation. In fact, the following relationship holds among frequency, f, mode number, m, and azimuthal phase speed, v_y, of the oscillation:

$$v_y = \frac{2\pi R f}{m} \tag{4.68}$$

where R is the mean radius of the thruster.

It is important to mention that the value of the frequency observed for the reference background solution (f = 24.9 kHz) and presented in the previous section is higher than seen in experiments [5, 123] ($f \approx 5 - 25$ kHz), but still within the modelling error margins of the linear 2D time-dependent model. Note that in this study with the linear 2D model we are seeking qualitative rather than quantitative agreement. The discrepancy between the experiments and the frequency of the $m = 1$ oscillation causes that for higher wave mode numbers the discrepancy becomes even larger in terms of the value of the frequency.

Fig. 4.33 and Table 4.5 show the variation of the frequency and growth rate of the unstable oscillation found for the different background solutions from Table 4.3 and for different wave mode numbers. The breathing mode is also shown in Fig. 4.33 for reference and comparison. The following clear trends are observed:

- as the discharge voltage is increased, or the mass flow rate decreased, or the neutral velocity at injection increased, the frequency of the oscillation increases linearly. These features indicate a relation between the frequency of the azimuthal oscillation and the position of the ionization region in the background solution. These trends are similar to those of the breathing mode, even if the mechanism at play in the observed azimuthal oscillation does not seem to be the same as in the simulated breathing mode.

- as mentioned above, the frequency of the oscillation increases linearly with the mode number. Additionally, depending on the background case, the mode number with the highest growth rate may be $m = 1$, $m = 2$ or $m = 3$, although as a general trend, the higher the mode number, the less unstable solutions are found. Modes $m > 1$ seem to become dominant (i.e., larger growth rate) for higher mass flow rates and larger channels, although, this trend is not as evident as the previous ones.

- out of all the background cases under analysis, only one unstable solution is found travelling in $-$**E**x**B** direction, indicating that the simulated oscillation has a clear preference to travel in the +**E**x**B** direction, as normally found for the spoke in experiments.

Table 4.5: Frequency, f (kHz), and growth rate, $\omega_i/2\pi$ (kHz), of different oscillation modes for several operation parameters. REF refers to the reference background solution defined by Fig. 4.7, and I, II, III, IV, V and VI refer to the parametric variations on V_d, $\dot{m}$, L_{ch}, L_{m1}, v_{nB} and d_c respectively. "$-$" indicates that no solution is found to the condition $\det(A) = 0$, "< 0" indicates that a stable solution is found, and "$(*)$" indicates that the solution found is similar to the breathing mode.

kHz	Variable	Variable	$f, \omega_i/2\pi$	$f, \omega_i/2\pi$	$f, \omega_i/2\pi$	$f, \omega_i/2\pi$	$f, \omega_i/2\pi$
Case	V_d, V	B_{max}, G	$m = 1$	$m = 2$	$m = 3$	$m = 4$	$m = -1$
Ia	20	23	$-$	$-$	$22.2, 39$	$-$	$-$
Ib	200	179	$18.1, 88.1$	$45, 85$	$87.2, 108$	$-$	$-$
REF	300	230	$24.9, 92.8$	$55.7, 114$	$102, 118$	$-$	$-$
Ic	500	313	$39.8, 110$	$119, 96.1$	$24.8, 182$	$-$	$-$
Id	700	383	$53.5, 137$	$-$	$-$	$-$	$-$
Case	$\dot{m}, mg/s$	B_{max}, G	$m = 1$	$m = 2$	$m = 3$	$m = 4$	$m = -1$
IIa	3.3	225	$50.3, 126$	$137, 115$	$-$	$-$	$-$
IIb	4	226	$30.3, 111$	$84, 113$	$-$	$-$	$-$
REF	4.8	230	$24.9, 92.8$	$55.7, 114$	$102, 118$	$-$	$-$
IIc	7	241	$13.8, 54.9$	$14.3, 72.2$	$54.7, 69.9$	$-$	$-$
IId	8.5	249	$58.6, 6.0(*)$	$15.1, 60.6$	$-$	$-$	$-$
IIe	10	256	$27.2, 10.4(*)$	$11.1, 52.1$	$8.9, 47.4$	$-$	$-$
Case	L_{ch}, mm	B_{max}, G	$m = 1$	$m = 2$	$m = 3$	$m = 4$	$m = -1$
IIIa	14	401	$-$	$-$	$43.8, 167$	$-$	$-$
REF	25	230	$24.9, 92.8$	$55.7, 114$	$102, 118$	$-$	$-$
IIIb	26	217	$18.1, 89$	$42, 113$	$89.9, 106$	$-$	$-$
IIIc	44	141	$19.7, 35.1$	$49.4, 54.3$	$44.9, 52.7$	$-$	$5.5, 52.1$
IIId	52	110	$31.6, 12.3$	$-$	$-$	$-$	$-$
Case	L_{m1}, mm	B_{max}, G	$m = 1$	$m = 2$	$m = 3$	$m = 4$	$m = -1$
IVa	30	142	$-$	$-$	$-$	$-$	$-$
IVb	19	185	$38.3, 126$	$136, 117$	$-$	$-$	$-$
REF	15	230	$24.9, 92.8$	$55.7, 114$	$102, 118$	$-$	$-$
IVc	9	377	$-$	$-$	$-$	$-$	$-$
Case	$v_{nB}, m/s$	B_{max}, G	$m = 1$	$m = 2$	$m = 3$	$m = 4$	$m = -1$
Va	174	240	$30.8, 56.6$	$8.0, 73$	$3.6, 75.4$	$-$	$-$
Vb	240	235	$17.3, 72.2$	$22.5, 102$	$62.8, 130$	$91.7, 118$	$-$
REF	300	230	$24.9, 92.8$	$55.7, 114$	$102, 118$	$-$	$-$
Vc	382	225	$39.3, 114$	$32.1, < 0(*)$	$-$	$-$	$-$
Vd	427	223	$52.2, 123$	$34.4, 3.78(*)$	$-$	$-$	$-$
Case	d_c, mm	B_{max}, G	$m = 1$	$m = 2$	$m = 3$	$m = 4$	$m = -1$
REF	15	230	$24.9, 92.8$	$55.7, 114$	$102, 118$	$-$	$-$
VIa	18	244	$24.1, 96.2$	$65.2, 117$	$109, 117$	$12.7, 174$	$-$
VIb	21	251	$23.1, 98.1$	$69.3, 121$	$110, 112$	$11.7, 176$	$-$
VIc	31	278	$22.9, 103$	$70.9, 128$	$118, 106$	$8.3, 175$	$-$

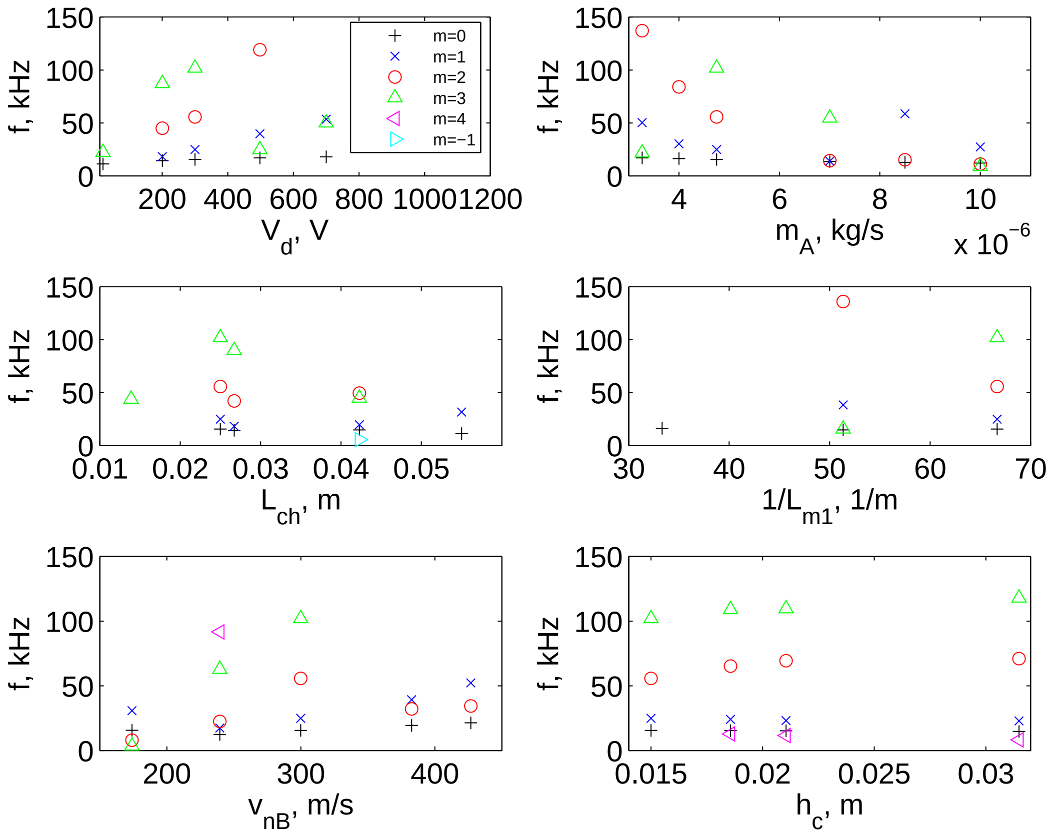

Figure 4.33: Variation of the frequency of unstable oscillations with different parameters and oscillation modes. The parameters under analysis are: discharge potential, V_d; mass flow rate, $\dot{m} \equiv m_A$; channel length, L_{ch}; magnetic field gradient, L_{m1}; neutral velocity at injection, v_{nB}; channel width, d_c. The oscillation modes under analysis are: $m = 0$, $m = 1$, $m = 2$, $m = 3$, $m = 4$ and $m = -1$, being $m > 0$ when the oscillation travels in the +**E**x**B**.

Apart from the trends mentioned above, another finding not visible in Table 4.5 and Fig. 4.33 is the existence of another type of oscillation, corresponding to those cases marked with an asterisk ($*$) in Table 4.5, namely: cases IId and IIe with $m = 1$ and cases Vc and Vd with $m = 2$. Figs. 4.34-4.39 show the $m = 1$ oscillation for the case IId. In those figures it is possible to observe a different type of oscillation where the neutral perturbation plays a similar role as in the breathing mode. However, the frequency ($f = 58.6$ kHz) in this case IId is much higher than observed experimentally for the spoke, even if for cases IIe, Vc and Vd the frequency is smaller (27.2 kHz, 32.1 kHz, 34.4 kHz respectively).

The differences with respect to the oscillation shown in Figs. 4.27-4.30 are clear. While in in this other type of oscillation the neutral density follows a similar pattern to that of the breathing mode, in the previous one the role of the neutral density perturbation is insignificant. According to Figs. 4.34-4.39, this other type of oscillation is characterized by the presence in the azimuthal direction of different ionization fronts which move back and forth with different phases. Additionally, the whole structure rotates in the ExB direction. Indeed, the possibility of a localized breathing mode rotating in the azimuthal direction with has already proposed by the authors[185] and by Sekerak *et al.*[187].

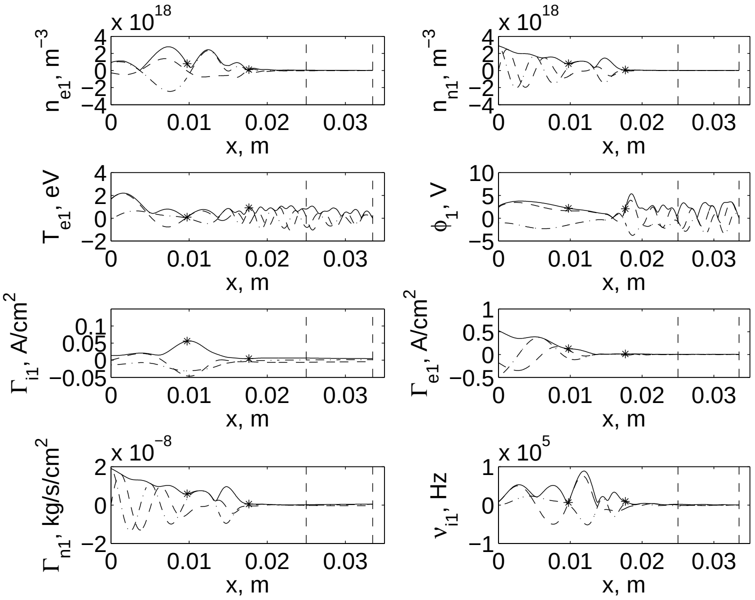

Figure 4.34: Axial profiles of the coefficients of the Fourier-expanded perturbations of the main macroscopic variables corresponding to a $m = 1$ self-excited oscillation of the perturbation problem for the reference case IId. Dashed lines are used for the real part of the perturbation coefficients, dash-dotted lines are used for the imaginary part and continuous lines are used for the modulus of the coefficients. Variables shown (from left to right and upper to lower): plasma density, n_{e1}; neutral density, n_{n1}; electron temperature, T_{e1}; electric potential, ϕ_1; ion axial flux, Γ_{i1}; electron axial flux, Γ_{e1}; neutral axial flux, Γ_{n1}; ionization frequency, ν_{i1}.

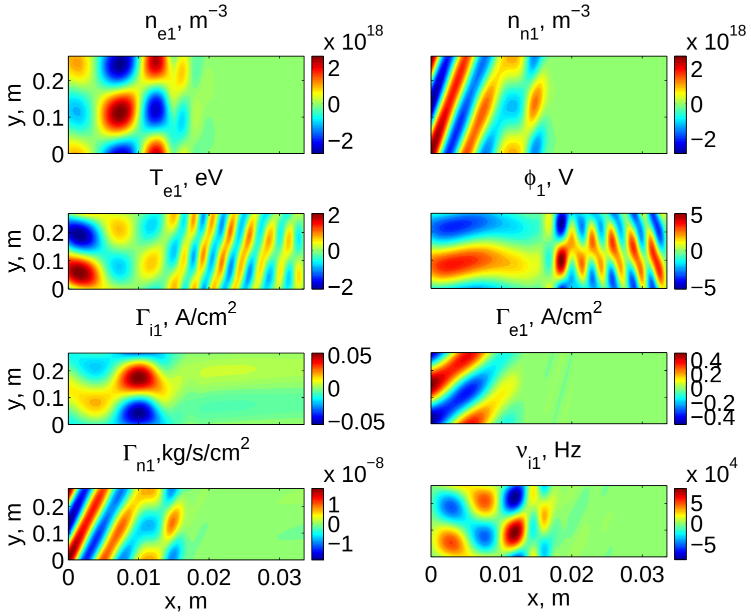

Figure 4.35: Perturbations of the main macroscopic variables shown as functions of x and y at $t = 0$ for a $m = 1$ self-excited oscillation of the perturbation problem for the reference case IId. The variables shown are the same as in Fig. 4.34.

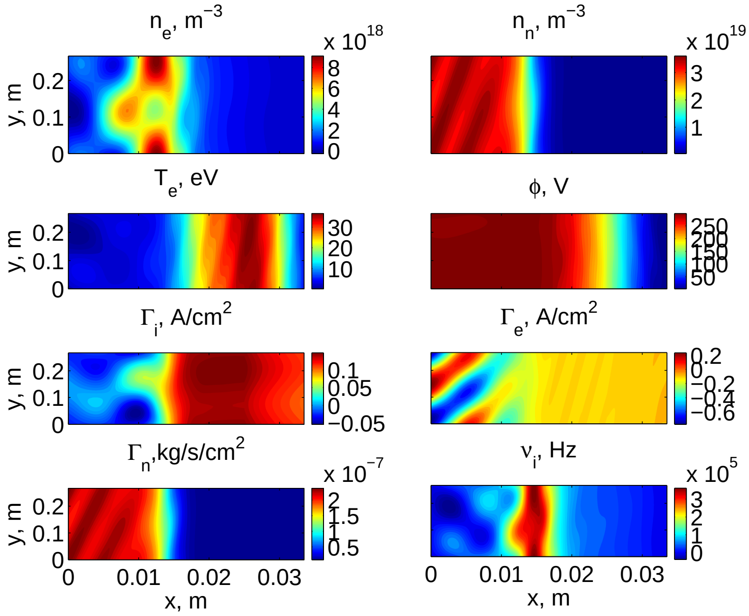

Figure 4.36: Oscillations of the main macroscopic variables as combinations of the background solution and the perturbations shown as functions of x and y at $t = 0$ for a $m = 1$ self-excited oscillation of the perturbation problem for the reference case IId. Variables shown (from left to right and upper to lower): plasma density, n_e; neutral density, n_n; electron temperature, T_e; electric potential, ϕ; ion axial flux, Γ_i; electron axial flux, Γ_e; neutral axial flux, Γ_n; ionization frequency, ν_i.

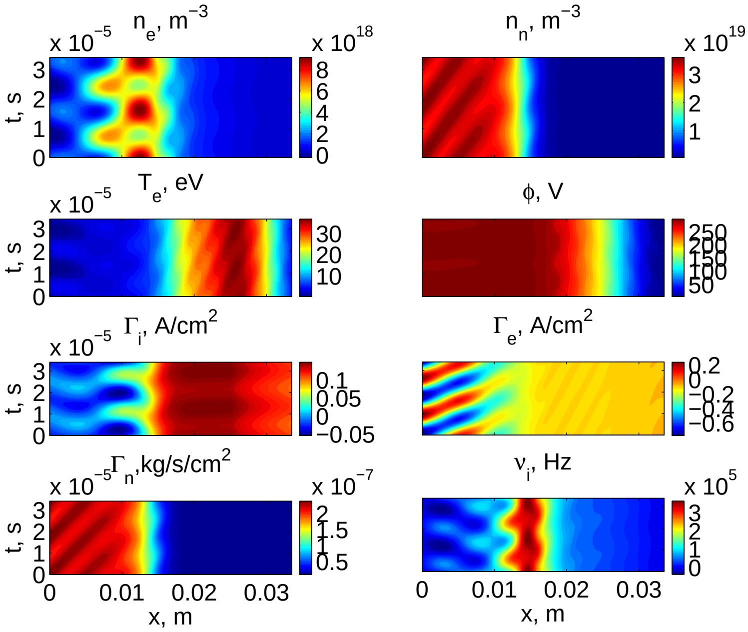

Figure 4.37: Oscillations of the main macroscopic variables as combinations of the background solution and the perturbations shown as functions of x and t at $y = 0$ for a $m = 1$ self-excited oscillation of the perturbation problem for the reference case IId. The variables shown are the same as in Fig. 4.36.

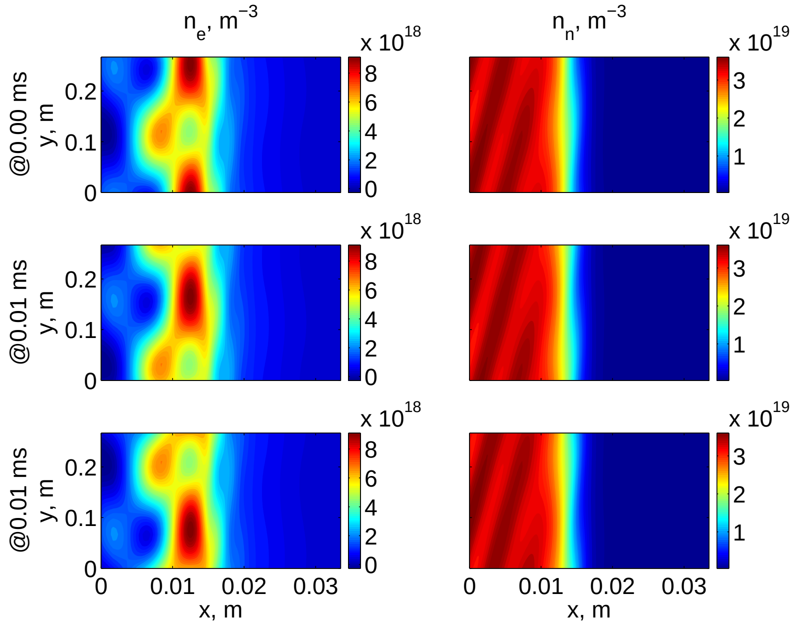

Figure 4.38: Oscillations of the main macroscopic variables as combinations of the background solution and the perturbations shown as functions of x and y at different values of t (@ t ms) for the same conditions used previously in Fig. 4.37. Variables shown (from left to right): plasma density, n_e; neutral density, n_n.

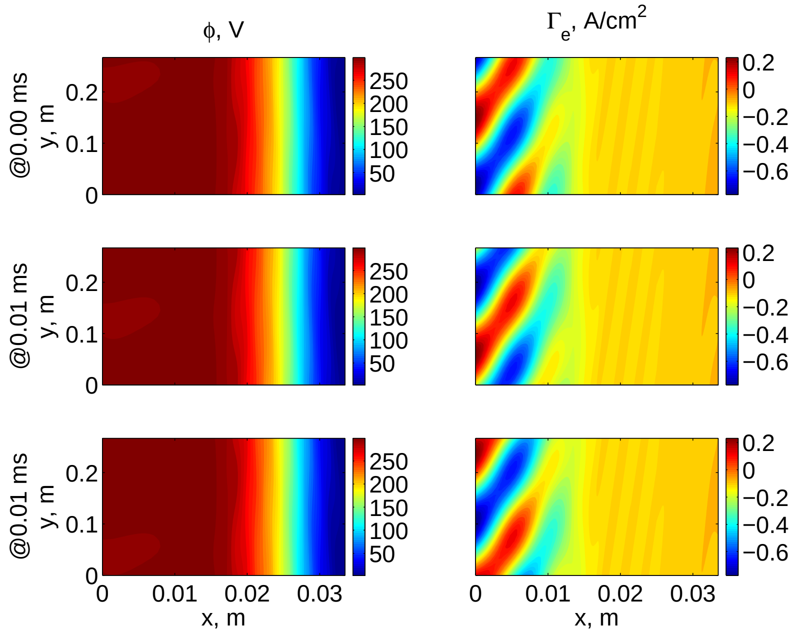

Figure 4.39: Same as Fig. 4.38 for other macroscopic variables. Variables shown (from left to right): electric potential, ϕ; electron axial flux, Γ_e.

4.4.4 Anomalous diffusion

Figs. 4.40 and 4.41 show the axial variation of $\alpha_A(x)$ based on Eq. (4.66) for the $m = 1$ unstable oscillations of the reference case given in Fig. 4.7 and of case IId, respectively. It is possible to observe that the net effect of the oscillation on the electron conductivity is concentrated in the rear part of the thruster, more precisely, in the ion-backstreaming region. The values reached by $\alpha_A(x)$ in this region are of the same order of magnitude as the value used for α_B in the simulation of the background solutions ($\alpha_B \approx 0.01$) for the selected size of the perturbations, which is chosen to ensure that perturbations are between 10% to 30% of the background solution.

Another relevant aspect is the fact that $\alpha_A(x)$ reaches negative values in some regions of the channel. This negative value of $\alpha_A(x)$ may be linked to the large tilt angle of the plasma density perturbation, which causes a change of phase between the perturbations of the plasma density and the azimuthal electric field. Moreover, the large variations of $\alpha_A(x)$ anticipate important changes in the background solution, where so far α_B has been considered constant, in case the profile of $\alpha_A(x)$ is used in the resolution of the zero-th order problem.

On the other hand, no contribution to electron conductivity is seen downstream the ionization region, where experiments also show a higher-than-expected electron mobility. Non-linear effects affecting the low-frequency azimuthal oscillation might resolve this contradiction. Another possible explanation is that high-frequency oscillations (1-10 MHz) [64, 65, 66, 71] might play a role in that region.

Given these results and their preliminary nature, it may be concluded that the influence on the electron transport caused by the spoke oscillations found in this study is not negligible although it is concentrated upstream the ionization region and thus cannot be the only source of anomalous diffusion in HETs. This is consistent with findings shown recently in Ref. [188].

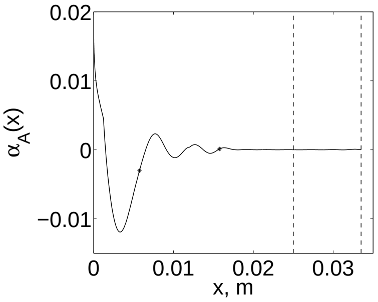

Figure 4.40: Axial profiles of the equivalent anomalous diffusion coefficient, $\alpha_A(x)$, as computed from the linear perturbation solution for the reference case described in Fig. 4.7.

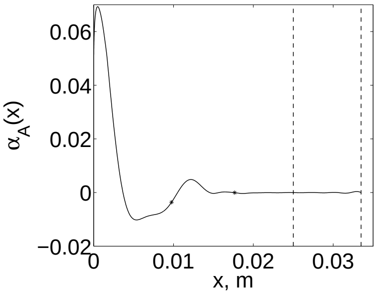

Figure 4.41: Axial profiles of the equivalent anomalous diffusion coefficient, $\alpha_A(x)$, as computed from the linear perturbation solution for the background solution IId.

4.4.5 Analysis of simplified models

This paragraph is intended to the application of the simplified models described above to the azimuthal oscillations detected in the previous chapters with the aim of analysing the mechanism at play of each type of oscillation.

Let us consider the first type of azimuthal oscillations analysed above and shown in Figs. 4.27-4.29. In that type of oscillation, the relative size of the neutral density perturbation is orders of magnitude smaller than that of the plasma density. This gives the hint to remove from the perturbation model the equations for the neutral species. Furthermore, the azimuthal ion velocity perturbation is also negligible in relative terms compared to other perturbations. If those terms are removed from the perturbation problem and the global stability analysis is repeated, an $m = 1$ unstable oscillation is found with a frequency of $f = 45$ kHz. Fig. 4.42 shows the contour maps in the $x - y$ space for the main macroscopic variables for that oscillation. The similarity between Fig. 4.42 and Fig. 4.27 is an indication that the terms removed from the perturbation model are indeed not relevant for this oscillation. However, if this simplification of the perturbation model is taken one step further and heat conduction terms are removed, no unstable solution is found. This is also true for all of the cases shown in Table 4.5 corresponding to this first type of oscillation. This indicates this type of oscillation seems mostly due to heat conduction.

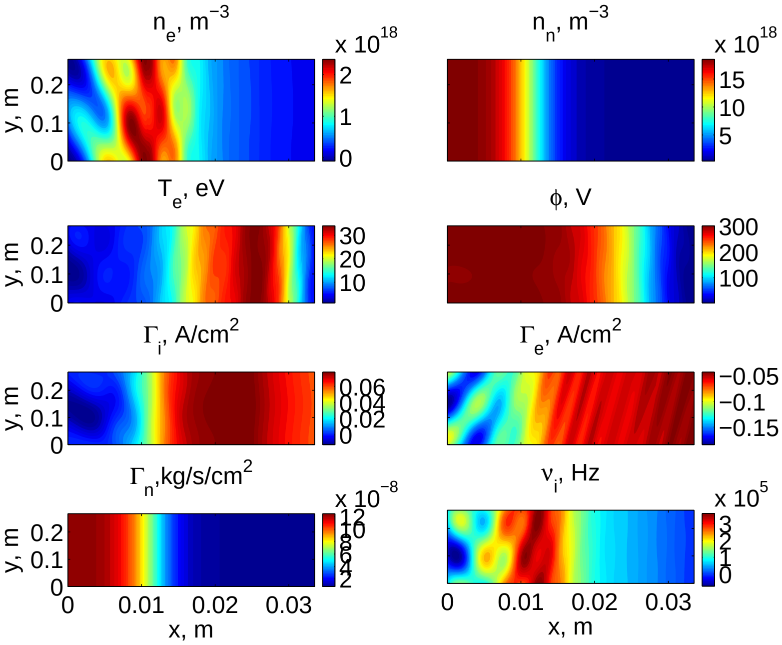

Figure 4.42: Oscillations of the main macroscopic variables as combinations of the background solution and the perturbations shown as functions of x and y at $t = 0$ for a $m = 1$ self-excited oscillation of the perturbation problem for the reference case from Fig. 4.7 and *the perturbation model excluding the neutral equations and the azimuthal ion momentum equation.* The variables shown are the same as in Fig. 4.36.

If we now consider the second type of azimuthal oscillations analysed above and shown in Figs. 4.36-4.37, the same simplification procedure may be carried out. In this type of oscillation the perturbation of the neutral density is believed to be relevant. And indeed, if neutral equations are removed from the perturbation model, no self-excited oscillation is found for cases IId and IIe with $m = 1$ and for cases Vc and Vd with $m = 2$. On the other hand, if heat conduction terms and ion and neutral azimuthal momentum equations are not considered, self-excited solutions are still found for those cases. Fig. 4.43 shows the contour maps in the $x - y$ space for the main macroscopic variables corresponding to a $m = 1$ unstable oscillation obtained with the simplified model and characterized by a frequency of $f = 12.5$ kHz. Fig. 4.43 shows the same pattern of localized breathing mode oscillations also observed in Fig. 4.36, validating the simplification carried out.

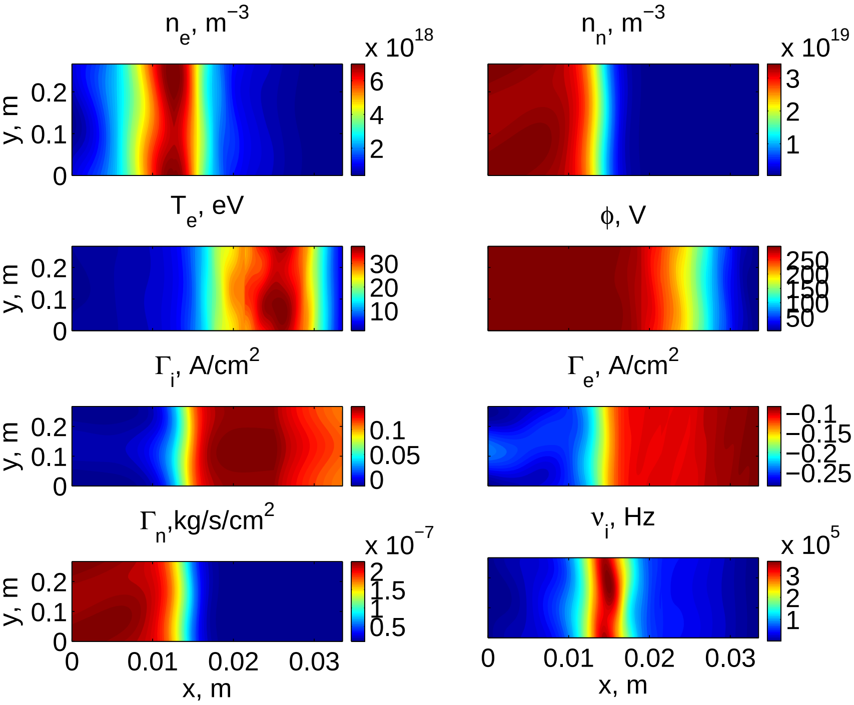

Figure 4.43: Oscillations of the main macroscopic variables as combinations of the background solution and the perturbations shown as functions of x and y at $t = 0$ for a $m = 1$ self-excited oscillation of the perturbation problem for the case IId and *the perturbation model excluding heat conduction terms and azimuthal ion and neutral momentum equations.* The variables shown are the same as in Fig. 4.36.

4.4.6 Global vs. local stability analyses

Another interesting analysis that can be performed with the aid of the simplified perturbation models is the comparison between local and global stability analyses. Many local linear stability analyses [2, 1, 138, 139, 141, 140, 142, 109, 144, 16, 145, 17] have been carried out so far by the HET community in an attempt to understand the azimuthal oscillations inherent to the HET discharge. However, these local analyses neglect the axial variation of the macroscopic plasma variables and need to freeze them and their derivatives at a fixed axial location. Some authors[19] even claim that in this application local stability analyses are inconsistent as they yield different stability criteria depending on how the equations are linearised.

In this study a comparison between the results from local and global stability analyses has been performed. To this end, the stability criterion proposed by Esipchuk and Tilinin[1] has been evaluated throughout the axial profile of the reference case given in Fig. 4.7 for oscillations with a wave mode number $m = 1$. This approach is similar to the one used by Frias *et al.*[142] for the local stability analysis of axial profiles of different thrusters. The result obtained in our case is shown in Fig. 4.44. As in the case of Frias *et al.*[142] , two unstable regions are identified, one in the ionization region, and another one in the plume, where the axial gradient of the magnetic field is negative.

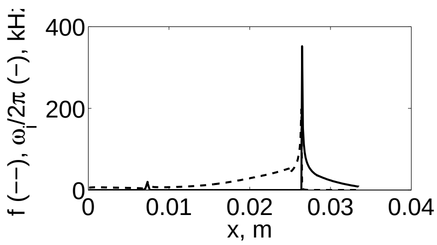

Figure 4.44: Growth rate (continuous line) and frequency (dashed line) in kHz for the $m = 1$ oscillations predicted with the local stability criterion proposed by Esipchuk and Tilinin[1] evaluated at each axial location of background solution corresponding to Fig. 4.7.

In order to perform the comparison, the perturbation equations of the linearised 2D time-dependent model presented above are simplified to match the model of Esipchuk and Tilinin, by leaving only ion and electron continuity and momentum equations. The global stability analysis can then be repeated with this simplified model looking for the self-excited solutions that would correspond to those found with the local stability criterion. The result indicates that no unstable solutions are found in the frequency range where the local analysis predicts oscillations. This seems to indicate that, as already anticipated by some authors, results from local stability analyses of the HET discharge must be taken with care.

Chapter 5

Concluding remarks

5.1 Publications

As part of the work carried out during the project, the results obtained from the analyses have been presented and published in several conferences and peer-reviewed journals.

The literature review and the local linear stability analysis have been published as a peer-reviewed article in Physics of Plasmas:

D. Escobar and E. Ahedo. Low frequency azimuthal stability of the ionization region of the Hall thruster discharge. I. Local analysis. *Physics of Plasmas*, 21:043505, 2014

A preliminary global linear stability analysis without heat conduction terms has been presented in the IEPC'13 as a conference paper:

D. Escobar and E. Ahedo. Global stability analysis of azimuthal oscillations in Hall Thrusters. *Proceedings of the 33rd IEPC*, 2013.

This last paper was selected as best session paper and invited for publication in a special issue of *IEEE Transactions of Plasma Science* devoted to Plasma Propulsion to be published in December 2014.

The complete global linear stability analysis including heat conduction terms has been presented in the *50th AIAA Joint Propulsion Conference* as a conference paper:

D. Escobar and E. Ahedo. Analysing the azimuthal spoke oscillation of Hall thrusters via numerical simulation. *Proceedings of the 50th JPC*, 2014.

Based on this last conference paper, another article is currently being prepared for submission to *Physics of Plasmas*:

D. Escobar and E. Ahedo. Low frequency azimuthal stability of the ionization region of the Hall thruster discharge. II. Global analysis. *To be submitted.*

Finally, as a natural continuation of the work presented in this report, yet another publication in *Physics of Plasmas* is foreseen dealing with high frequency oscillations in Hall Thrusters:

D. Escobar and E. Ahedo. High frequency azimuthal global stability analysis of the Hall thruster discharge. *To be submitted.*

5.2 Conclusions

A thorough review of the available literature on azimuthal oscillations in Hall Effect Thrusters has been carried out. As part of the review, two azimuthal oscillations, the spoke in the low frequency range (5-25 kHz) and the electron drift oscillation in the high frequency range (1-10 MHz), have been identified as possible sources of oscillation-based electron transport. The review has justified the need for a complete stability analysis of the Hall discharge, starting with a local linear analysis and continuing with a global linear one.

As part of a local stability analysis of the acceleration region expressions for stability criteria similar to those found in the existing literature have been obtained. To this respect, both simplified analytical expressions and numerical results from more complex models have been derived and compared. At the same time, the effect of electron inertia and non-quasineutrality have been evaluated and found to be important at high frequency.

In the ionization region the local linear stability analysis has allowed us to identify an azimuthal oscillation induced by ionization and not previously described theoretically in the Hall thruster literature, to the best of our knowledge. The detected linear oscillation is similar to the spokes measured experimentally in terms of frequency range, phase speed and wavelength. Parametric analyses have been carried out with respect to the main parameters of the model in order to identify the trends of the instability. As the temperature increases and the neutral-to-plasma density ratio decreases, the growth rate of the instability decreases down to a limit where azimuthal perturbations are no longer unstable.

However, this local analysis has limitations. The main drawback of the local analysis is that axial variations of the background solution are neglected. This is only valid in the limiting case where the length scale of these variations is much larger than the axial wavelength of the perturbations.

In order to overcome the limitations of local analyses, a global stability analysis has been carried out. To this end, a linearised 2D time-dependent model has been formulated and used for the analysis of the stability of the Hall discharge in the azimuthal direction and for the detection of azimuthal oscillations in the low frequency range. The 2D model builds on the stationary 1D model of Ahedo *et al.* and has been validated reproducing breathing mode oscillations in the axial direction. Results indicate that two types of azimuthal oscillations are present in the low frequency range, one due to heat conduction effects, and another one characterised by localized breathing mode oscillations rotating in the **E**x**B** direction. The former appears more often in the simulations, while the latter only shows up with high mass flow rates, but it is more similar to the spoke observed experimentally.

Simplified global models have been used to perform a consistent comparison between global and local stability analyses. The result from this comparison indicates that some of the oscillations detected with local models do not show up in the global analysis. This fact highlights the need to look for the local analysis that best reproduces the results from the global one.

Finally, an evaluation of the influence of the detected linear azimuthal oscillations on the electron transport has been performed. Results show a non-negligible impact upstream of the ionization region, where the oscillation-based transport may be positive or negative depending on the case, and could be of the same order of magnitude as the anomalous diffusion assumed a-priori in the background solution. However, the oscillation-based electron transport caused by the detected oscillations does not seem to be the main contributor to the anomalous diffusion typically found throughout the complete Hall thruster channel.

Bibliography

[1] Y.B. Esipchuk and G.N. Tilinin. Drift instability in a Hall-current plasma accelerator. *Sov. Physics-Tech. Physics*, 21(4):417–423, 1976.

[2] A.I. Morozov, Y.V. Esipchuk, A.M. Kapulkin, V.A. Nevrovskii, and V.A. Smirnov. Effect of the magnetic field on a closed-electron-drift accelerator. *Soviet Physics-Tech. Physics*, 17(3):482–487, 1972.

[3] E. Ahedo, J.M. Gallardo, and M. Martinez-Sanchez. Effects of the radial plasma-wall interaction on the hall thruster discharge. *Physics of Plasmas*, 10:3397, 2003.

[4] L. Garrigues, G.J.M. Hagelaar, C. Boniface, and J.P. Boeuf. Anomalous conductivity and secondary electron emission in Hall effect thrusters. *Journal of Applied Physics*, 100:123301, 2006.

[5] E.Y. Choueiri. Plasma oscillations in Hall thrusters. *Physics of Plasmas*, 8:1411, 2001.

[6] G.S. Janes and R.S. Lowder. Anomalous Electron Diffusion and Ion Acceleration in a Low-Density Plasma. *Physics of Fluids*, 9:1115, 1966.

[7] E. Chesta, C.M. Lam, N.B. Meezan, D.P. Schmidt, and M.A. Cappelli. A characterization of plasma fluctuations within a Hall discharge. *IEEE transactions on Plasma science*, 29(4):582–591, 2001.

[8] J.B. Parker, Y. Raitses, and N.J. Fisch. Transition in electron transport in a cylindrical hall thruster. *Applied Physics Letters*, 97:091501, 2010.

[9] C. L. Ellison, Y. Raitses, and N. J. Fisch. Direct measurement of spoke-induced, cross-field electron current in a cylindrical Hall thruster. In *Proceedings of the 32nd International Electric Propulsion Conference*, 2011.

[10] M.S. McDonald, C.K. Bellant, B.A.S. Pierre, and A.D. Gallimore. Measurement of cross-field electron current in a Hall thruster due to rotating spoke instabilities. In *Proceedings of the 47th Joint Propulsion Conference*, 2011.

[11] E. Ahedo, P. Martinez-Cerezo, and M. Martinez-Sanchez. One-dimensional model of the plasma flow in a Hall thruster. *Physics of Plasmas*, 8:3058, 2001.

[12] E. Ahedo, J.M. Gallardo, and M. Martinez-Sanchez. Model of the plasma discharge in a hall thruster with heat conduction. *Physics of Plasmas*, 9:4061, 2002.

[13] E. Ahedo and D. Escobar. Influence of design and operation parameters on hall thruster performances. *Journal of applied physics*, 96:983, 2004.

[14] E. Ahedo, P. Martinez, and M. Martinez-Sanchez. Steady and linearly-unsteady analysis of a hall thruster with an internal sonic point. *AIAA paper*, 3655, 2000.

[15] S. Barral, V. Lapuerta, A. Sancho, and Ahedo. E. Numerical investigation of low-frequency longitudinal oscillations in Hall thrusters. In *Proceedings of the 29th International Electric Propulsion Conference*, 2005.

[16] J.M. Gallardo and E. Ahedo. On the anomalous diffusion mechanism in Hall-effect thrusters. In *Proceedings of 29th International Electric Propulsion Conference*, 2005.

[17] D. Escobar and E. Ahedo. Low frequency azimuthal stability of the ionization region of the hall thruster discharge. i. local analysis. *Physics of Plasmas*, 21(4):043505, 2014.

[18] D. Escobar and E. Ahedo. Ionization-induced azimuthal oscillation in Hall Effect Thrusters. In *Proceedings of the 32nd International Electric Propulsion Conference*, 2011.

[19] S. Barral, K. Makowski, Z. Peradzyński, and M. Dudeck. Transit-time instability in Hall thrusters. *Physics of Plasmas*, 12:073504, 2005.

[20] S. Barral and E. Ahedo. Low-frequency model of breathing oscillations in hall discharges. *Physical Review E*, 79(4):046401, 2009.

[21] G.L. Cann and G.L. Marlotte. Hall current plasma accelerator. *AIAA Journal*, 2(7):1234–1241, 1964.

[22] A.V. Zharinov and Y.S. Popov. Acceleration of plasma by a closed Hall current. *Soviet Physics-Technical Physics*, 12(2):208–211, 1967.

[23] A.I. Morozov, A.Y. Kislov, and I.P. Zubkov. Strong-current Plasma Accelerator with Closed Electron Drift. *ZhETF Pis ma Redaktsiiu*, 7:224–227, 1968.

[24] M. Martinez-Sanchez and J.E. Pollard. Spacecraft electric propulsion-an overview. *Journal of Propulsion and Power*, 14(5), 1998.

[25] E. Ahedo. Plasmas for space propulsion. *Plasma Physics and Controlled Fusion*, 53(12):124037, 2011.

[26] R.G. Jahn and E. Y. Choueiri. *Electric propulsion, Encyclopedia of Physical Science and Technology, Third Edition, Volume 5.* Academic Press, 2002.

[27] A.I. Morozov, Y.V. Esipchuk, G.N. Tilinin, A.V. Trofimov, and Y.A. Sharov. Plasma accelerator with closed electron drift and extended acceleration zone. *Soviet Physics-Tech. Physics*, 17(1):38–45, 1972.

[28] M. Keidar and I. I. Beilis. Electron transport phenomena in plasma devices with exb drift. *IEEE Transactions on Plasma Science*, 34(3):804–814, 2006.

[29] S. Yoshikawa and D.J. Rose. Anomalous diffusion of a plasma across a magnetic field. *Physics of Fluids*, 5:334, 1962.

[30] AI Morozov. Conditions for efficient current transport by near-wall conduction. *Sov. Phys. Tech. Phys*, 32(8):901–904, 1987.

[31] F. Taccogna, P. Minelli, S. Longo, M. Capitelli, and R. Schneider. Anomalous Transport induced by Sheath Instability in Hall Effect Thrusters. In *Proceedings of the 31st International Electric Propulsion Conference*, 2009.

[32] W. Frias, A. I. Smolyakov, I. D. Kaganovich, and Y. Raitses. Coupled fluctuations of bulk plasma and the sheath in plasmas with ExB drift. In *Proceedings of 33rf International Electric Propulsion Conference*, 2013.

[33] C.A. Thomas and M.A. Cappelli. Gradient transport processes in ExB plasmas. In *Proceedings of the 41st Joint Propulsion Conference*, 2005.

[34] K.C. Shaing, A.Y. Aydemir, and R.D. Hazeltine. Effects of orbit distortion on classical transport. *Physics of Plasmas*, 5:3680, 1998.

[35] E.A. De Marco and M. Andrenucci. Electron Transport Modeling in Hall-Effect Thrusters. In *Proceedings of the 42nd Joint Propulsion Conference*, 2006.

[36] E.C. Fossum and L.B. King. An Unexamined Collision-less Mechanism for Electron Mobility in Hall Thrusters. In *Proceedings of the 45th Joint Propulsion Conference*, 2009.

[37] S.A. Oghienko, A.I. Oranskiy, V.D. Olendarev, and S.V. Veryutin. Analysis of Some Reasons of Anomalous Electron Transportation in the Hall Thruster. In *Proceedings of the 32nd International Electric Propulsion Conference*, 2011.

[38] N.B. Meezan and M.A. Cappelli. Electron density measurements for determining the anomalous electron mobility in a coaxial Hall discharge plasma. In *Proceedings of the 36th Joint Propulsion Conference*, 2000.

[39] J. A. Linnell and A. D. Gallimore. Hall Thruster Electron Motion Characterization Based on Internal Probe Measurements. In *Proceedings of the 31st International Electric Propulsion Conference*, 2009.

[40] G.J.M. Hagelaar, J. Bareilles, L. Garrigues, and J.P. Boeuf. Role of anomalous electron transport in a stationary plasma thruster simulation. *Journal of Applied Physics*, 93:67, 2003.

[41] N.B. Meezan, W.A. Hargus Jr, and M.A. Cappelli. Anomalous electron mobility in a coaxial Hall discharge plasma. *Physical Review E*, 63(2):26410, 2001.

[42] M.A. Cappelli, N.B. Meezan, and N. Gascon. Transport physics in Hall plasma thrusters. In *Proceedings of the 40th AIAA Aerospace and Sciences Meeting and Exhibit*, 2002.

[43] C. Boniface, L. Garrigues, G.J.M. Hagelaar, J.P. Boeuf, D. Gawron, and S. Mazouffre. Anomalous cross field electron transport in a Hall effect thruster. *Applied Physics Letters*, 89:161503, 2006.

[44] D. Gawron, S. Mazouffre, and C. Boniface. A Fabry–Pérot spectroscopy study on ion flow features. *Plasma Sources Science and Technology*, 15:757–764, 2006.

[45] V. Baranov, Y. Nazarenko, and V. Petrosov. Azimuthal non-uniformities in accelerators with closed electron drift. In *Proceedings of the 27th International Electric Propulsion Conference*, 2001.

[46] D.A. Alman, J.L. Rovey, R.A. Stubbers, B.E. Jurczyk, et al. Hall Thruster Electron Mobility Investigation using Full 3D Monte Carlo Trajectory Simulations. In *Proceedings of the 42nd Joint Propulsion Conference*, 2007.

[47] J. Perez-Luna, G.J.M. Hagelaar, L. Garrigues, N. Dubuit, and J.P. Boeuf. Impact of azimuthal instabilities on electron behaviour in a Hall Effect thruster. In *Proceedings of the 28th ICPIG*, 2007.

[48] J. Pérez-Luna, G.J.M. Hagelaar, L. Garrigues, N. Dubuit, and J.P. Boeuf. Influence of azimuthal instabilities on electron motion in a Hall Effect Thruster. In *Proceedings of the 30th International Electric Propulsion Conference*, 2007.

[49] A.N. Vesselovzorov, E.B. Pogorelov, A.A. Svirskiy, and V.A. Smirnov. Azimuthal oscillations and dynamics of electrons into channel of Stationary Plasma Thruster. In *Proceedings of the 33rd International Electric Propulsion Conference*, 2013.

[50] E.C. Fossum, L.B. King, and J. Makela. Mobility Studies of a Pure Electron Plasma in Hall Thruster Fields. In *Proceedings of the 42nd Joint Propulsion Conference*, 2006.

[51] E.C. Fossum and L.B. King. An Electron Trap for Studying Cross-Field Mobility in Hall Thrusters. *IEEE Transactions on Plasma Science*, 36(5 Part 1):2088–2094, 2008.

[52] J.L. Rovey, M.P. Giacomi, R.A. Stubbers, and B.E. Jurczyk. A planar Hall thruster for investigating electron mobility in ExB devices. In *Proceedings of the 30th International Electric Propulsion Conference*, 2007.

[53] F.I. Parra, E. Ahedo, J.M. Fife, and M. Martinez-Sanchez. A two-dimensional hybrid model of the Hall thruster discharge. *Journal of Applied Physics*, 100:023304, 2006.

[54] A. Bouchoule, J.P. Boeuf, A. Heron, and O. Duchemin. Physical investigations and developments of Hall plasma thrusters. *Plasma physics and controlled fusion*, 46:B407–B421, 2004.

[55] V. Zhurin, H. Kaufman, and R.S. Robinson. Physics of closed drift thrusters. *Plasma Sources Science and Technology*, 8:R1–R20, 1999.

[56] J.M. Fife. *Hybrid-PIC modelling and electrostatic probe survey of Hall thrusters*. PhD thesis, Massachusetts Institute of Technology, 1998.

[57] S. Barral and E. Ahedo. Theoretical Study of the Breathing Mode in Hall Thrusters. In *Proc. 42nd AIAA Joint Propulsion Conference*, 2006.

[58] S. Barral. Theoretical Analysis of the Influence of the Power Supply on Breathing Oscillations in Hall Thrusters. In *Proceedings of the 30th International Electric Propulsion Conference*, 2007.

[59] S. Barral, J. Miedzik, and E. Ahedo. A model for the active control of low frequency oscillations in Hall thrusters. In *Proceedings of the 44th Joint Propulsion Conference*, 2008.

[60] D. Yu, C. Wang, L. Wei, C. Gao, and G. Yu. Stabilizing of low frequency oscillation in Hall thrusters. *Physics of Plasmas*, 15:113503, 2008.

[61] A.I. Morozov, Y.V. Esipchuk, A.M. Kapulkin, V.A. Nevrovskii, and V.A. Smirnov. Azimuthally asymmetric modes and anomalous conductivity in closed electron drift accelerators. *Soviet Physics-Tech. Physics*, 18(5):615–620, 1972.

[62] Y.B. Esipchuk, A.I. Morozov, G.N. Tilinin, and A.V. Trofimov. Plasma oscillations in closed-drift accelerators with an extended acceleration zone. *Sov. Physics-Tech. Physics*, 18(7):928–932, 1974.

[63] E. Fernandez, M.K. Scharfe, C.A. Thomas, N. Gascon, and M.A. Cappelli. Growth of resistive instabilities in ExB plasma discharge simulations. *Physics of Plasmas*, 15:012102, 2008.

[64] G. Guerrini and C. Michaut. Characterization of high frequency oscillations in a small Hall-type thruster. *Physics of Plasmas*, 6:343, 1999.

[65] A.A. Litvak, Y. Raitses, and N.J. Fisch. Experimental studies of high-frequency azimuthal waves in Hall thrusters. *Physics of Plasmas*, 11:1701, 2004.

[66] A. Lazurenko, V. Krasnoselskikh, and A. Bouchoule. Experimental Insights Into High-Frequency Instabilities and Related Anomalous Electron Transport in Hall Thrusters. *IEEE Transactions on Plasma Science*, 36(5 Part 1):1977–1988, 2008.

[67] A. Knoll and M.A. Cappelli. Experimental Characterization of High Frequency Instabilities within the Discharge Channel of a Hall Thruster . In *Proceedings of the 31st International Electric Propulsion Conference*, 2009.

[68] S. Tsikata, N. Lemoine, V. Pisarev, and DM Grésillon. Dispersion relations of electron density fluctuations in a hall thruster plasma, observed by collective light scattering. *Physics of Plasmas*, 16:033506, 2009.

[69] S. Tsikata, D. Gresillon, C. Honore, V. Pisarev, and N. Lemoine. Small-scale density fluctuation modes in a Hall plasma thruster: experimental studies via collective light scattering. In *Proceedings of the 31st International Electric Propulsion Conference*, 2009.

[70] S. Tsikata, N. Lemoine, V. Pisarev, and D.M. Gresillon. Dispersion relations of electron density fluctuations in a hall thruster plasma, observed by collective light scattering. *Physics of Plasmas*, 16:033506, 2009.

[71] S. Tsikata, C. Honore, D. Gresillon, A. Heron, N. Lemoine, and J. Cavalier. The small-scale high-frequency ExB instability and its links to observed features of the Hall thruster discharge . In *Proceedings of the 33rd International Electric Propulsion Conference*, 2013.

[72] S. P. Gary and J.J. Sanderson. Longitudinal waves in a perpendicular collisionless plasma shock: I. cold ions. *Journal of Plasma Physics*, 4(04):739–751, 1970.

[73] S. P. Gary. Longitudinal waves in a perpendicular collisionless plasma shock: Ii. vlasov ions. *Journal of Plasma Physics*, 4(04):753–760, 1970.

[74] G.N. Tilinin. High-frequency plasma waves in a Hall accelerator with an extended acceleration zone. *Soviet Physics-Technical Physics*, 22(8):974–978, 1977.

[75] V. Zhurin, J. Kahn, H. Kaufman, K. Kozubsky, and M. Day. Dynamic characteristics of closed drift thrusters. In *Proceedings of the 23rd International Electric Propulsion Conference*, 1993.

[76] V. Zhurin, H. Kaufman, and R.S. Robinson. Physics of Closed Drift Thrusters. In *Proceedings of the 25th International Electric Propulsion Conference*, 1997.

[77] G.J.M. Hagelaar. Modelling electron transport in magnetized low-temperature discharge plasmas. *Plasma Sources Science and Technology*, 16:S57–S66, 2007.

[78] S. Roy and BP Pandey. Numerical investigation of a Hall thruster plasma. *Physics of Plasmas*, 9:4052, 2002.

[79] S. Roy and BP Pandey. Development of a finite element-based hall-thruster model. *Journal of Propulsion and Power*, 19(5):964–971, 2003.

[80] I.G. Mikellides, I. Katz, R.R. Hofer, and D. M. Goebel. Hall-Effect Thruster Simulations with 2-D Electron Transport and Hydrodynamic Ions. In *Proceedings of the 31st International Electric Propulsion Conference*, 2009.

[81] J.P. Boeuf and L. Garrigues. Low frequency oscillations in a stationary plasma thruster. *Journal of Applied Physics*, 84:3541, 1998.

[82] P. Coche and L. Garrigues. A two-dimensional (azimuthal-axial) particle-in-cell model of a hall thruster. *Physics of Plasmas*, 21(2):023503, 2014.

[83] L. Garrigues and P. Coche. A two-dimensional (azimuthal-axial) particle-in-cell model of a hall thruster. In *Proceedings of 33rd International Electric Propulsion Conference*, 2013.

[84] J.J. Szabo. *Fully Kinetic Numerical Modeling of a Plasma Thruster.* PhD thesis, Massachusetts Institute of Technology, 2001.

[85] O. Batishchev and M. Martinez-Sanchez. Charged particle transport in the Hall Effect thruster. In *Proceedings of the 28th International Electric Propulsion Conference*, 2003.

[86] K. Matyash, R. Schneider, S. Mazouffre, S. Tsikata, Y. Raitses, and A. Diallo. 3D simulation of the rotating spoke in a Hall thruster. In *Proceedings of the 33rd International Electric Propulsion Conference*, 2013.

[87] G.J.M. Hagelaar, J. Bareilles, L. Garrigues, and J.P. Boeuf. Two-dimensional model of a stationary plasma thruster. *Journal of Applied Physics*, 91:5592, 2002.

[88] M.K. Allis, N. Gascon, C. Vialard-Goudou, M.A. Cappelli, and E. Fernandez. A Comparison of 2-D Hybrid Hall Thruster Model to Experimental Measurements. In *Proceedings of the 40th Joint Propulsion Conference*, 2004.

[89] C. M. Lam, A. K. Knoll, M. A. Cappelli, and E. Fernandez. Two-Dimensional (z-θ) Simulations of Hall Thruster Anomalous Transport. In *Proceedings of the 31st International Electric Propulsion Conference*, 2009.

[90] C. M. Lam, M. A. Cappelli, and E. Fernandez. Two-Dimensional Simulations of Coherent Fluctuation-Driven Transport in a Hall Thruster. In *Proceedings of the 33rd International Electric Propulsion Conference*, 2013.

[91] J. Miedzik, S. Barral, and S. Zurbach. Electron guiding center modelling for Hall thruster simulations. In *Proceedings of the 31st International Electric Propulsion Conference*, 2009.

[92] M. Hirakawa and Y. Arakawa. Particle simulation of plasma phenomena in Hall thrusters. In *Proceedings of the 24th International Electric Propulsion Conference*, 1995.

[93] J.C. Adam, A. Heron, and G. Laval. Study of stationary plasma thrusters using two-dimensional fully kinetic simulations. *Physics of Plasmas*, 11:295, 2004.

[94] E. Fernandez, M. Cappelli, N. Gascon, and M. Allis. Modeling anomalous electron transport in Hall thrusters. In *Center for Turbulence Research. Proceedings of the Summar Program 2004*, 2004.

[95] E. Fernandez, A. Knoll, M. Cappelli, and T. Kaya. A Two-Dimensional (z-θ) Fluid/PIC Simulation of Coaxial Hall Thrusters. In *Proceedings of the 29th International Electric Propulsion Conference*, 2005.

[96] E. Fernandez, A. Knoll, and M.A. Cappelli. An axial-azimuthal hybrid simulation of coaxial Hall thrusters. In *Proceedings of the 42nd Joint Propulsion Conference*, 2006.

[97] R.R. Hofer, I.G. Mikellides, I. Katz, and D.M. Goebel. Wall sheath and electron mobility modeling in hybrid-PIC Hall thruster simulations. In *Proceedings of the 43rd Joint Propulsion Conference*, 2007.

[98] R.R. Hofer, I. Katz, I.G. Mikellides, D.M. Goebel, K.K. Jameson, R.M. Sullivan, and L.K. Johnson. Efficacy of Electron Mobility Models in Hybrid-PIC Hall Thruster Simulations. In *Proceedings of the 44th Joint Propulsion Conference*, 2008.

[99] P.N. Giuliano and I.D. Boid. Spectral analysis of simulated Hall thruster discharge current oscillations. In *Proceedings of the 31st International Electric Propulsion Conference*, 2009.

[100] J.M. Fox. Probable cause of anomalous transport reduction in acceleration channel of hall thrusters. In *Private communications*, 2007.

[101] M.K. Scharfe, C.A. Thomas, D.B. Scharfe, N. Gascon, M.A. Cappelli, and E. Fernandez. Shear-based model for electron transport in hybrid Hall thruster simulations. In *Proceedings of the 30th International Electric Propulsion Conference*, 2007.

[102] J.W. Koo and I.D. Boyd. Modeling of anomalous electron mobility in Hall thrusters. *Physics of Plasmas*, 13:033501, 2006.

[103] L. Garrigues, J. Pérez-Luna, J. Lo, G.J.M. Hagelaar, and J.P. Boeuf. Determination of the Axial Electron Mobility Profile in the PPS X000-LM Thruster. *Journal of Applied Physics*, 100:123301, 2006.

[104] M.K. Allis, C.A. Thomas, N. Gascon, M.A. Cappelli, and E. Fernandez. Introduction of physical transport mechanisms into 2D hybrid Hall thruster simulations. In *Proceedings of the 42nd Joint Propulsion Conference*, 2006.

[105] M.K. Scharfe, M.A. Cappelli, and E. Fernandez. Predicting Electron Transport Using Simulated Axial Waves in a Radial-Axial Hybrid Hall Thruster Model. In *Proceedings of the 31st International Electric Propulsion Conference*, 2009.

[106] M. Keidar and L. Brieda. Modeling electron transport within the framework of hydrodynamic description of Hall thrusters. In *Proceedings of the 44th Joint Propulsion Conference*, 2008.

[107] L. Brieda, M. Keidar, Y. Raitses, and N.J. Fisch. Investigation of Electron Transport in a Cylindrical Hall Thruster using a Kinetic Code. In *Proceedings of the 45th Joint Propulsion Conference*, 2009.

[108] L. Brieda and M. Keidar. Self-Consistent Calculation of Electron Transport in a Cylindrical Hall Thruster. In *Proceedings of the 31st International Electric Propulsion Conference*, 2009.

[109] P.J. Lomas and J.D. Kilkenny. Electrothermal instabilities in a Hall accelerator. *Plasma Physics*, 19:329, 1977.

[110] B.D. Sidney, F. Allario, , and R.V. Hess. Onset of rotating disturbance in linear hall-current accelerator. *AIAA Journal*, 8(6):1117–1120, 1970.

[111] W. A. Hargus, N. B. Meezan, and M. A. Cappelli. A study of a low power hall thruster transient behavior. In *Proceedings of the 25th International Electric Propulsion Conference*, pages 351–358, 1997.

[112] A. Dinklage, T. Klinger, G. Marx, and L. Schweikhard. *Plasma physics: confinement, transport and collective effects.* Berlin Springer Verlag, 2005.

[113] N. Gascon, N.B. Meezan, and M.A. Cappelli. Low frequency plasma wave dispersion and propagation in Hall thrusters. In *Proceedings of the 27th International Electric Propulsion Conference*, 2001.

[114] N. Gascon and M.A. Cappelli. Wall effects on the excitation and propagation of instabilities in Hall thrusters. In *Proceedings of the 28th International Electric Propulsion Conference*, 2003.

[115] N. Gascon and M.A. Cappelli. Plasma instabilities in the ionization regime of a Hall thruster. In *Proceedings of the 39th Joint Propulsion Conference*, 2003.

[116] A.W. Smith and M.A. Cappelli. Time and Space-correlated Plasma Property Measurements in the Near-field of a Coaxial Hall Discharge. In *Proceedings of the 31st International Electric Propulsion Conference*, 2009.

[117] Y. Raitses, A. Smirnov, and N.J. Fisch. Effects of enhanced cathode electron emission on hall thruster operation. *Physics of Plasmas*, 16:057106, 2009.

[118] C.L. Ellison, Y. Raitses, and N.J. Fisch. Fast camera imaging of hall thruster ignition. *IEEE Transactions on Plasma Science*, 39(11):2950–2951, 2011.

[119] C.L. Ellison, Y. Raitses, and N.J. Fisch. Cross-field electron transport induced by a rotating spoke in a cylindrical hall thruster. *Physics of Plasmas*, 19:013503, 2012.

[120] Y. Raitses, M. Griswold, L. Ellison, J. Parker, and N.J. Fisch. Studies of rotating spoke oscillations in cylindrical hall thrusters. *Proceedings of the 48th Joint Propulsion Conference*, 4179, 2012.

[121] M.E. Griswold, C.L. Ellison, Y. Raitses, and N.J. Fisch. Feedback control of an azimuthal oscillation in the e× b discharge of hall thrusters. *Physics of Plasmas*, 19(5):053506–053506, 2012.

[122] Y. Shi, Y. Raitses, and A. Diallo. Driving Azimuthal Modes in Magnetized Discharge with Segmented Anode. In *Proceedings of the 4th Annual Meeting, DOE Center for Predictive Control of Plasma Kinetics*, 2013.

[123] M. S. McDonald and D. Gallimore, A. Parametric Investigation of the Rotating Spoke Instability in Hall Thrusters. In *Proceedings of the 32nd International Electric Propulsion Conference*, 2011.

[124] M. S. McDonald and A. D. Gallimore. Rotating spoke instabilities in hall thrusters. *IEEE Transactions on Plasma Science*, 39(11):2952–2953, 2011.

[125] M. S. McDonald and A. D. Gallimore. Comparison of Breathing and Spoke Mode Strength in the H6 Hall Thruster Using High Speed Imaging. In *Proceedings of the 33rd International Electric Propulsion Conference*, 2013.

[126] M. Sekerak, M. McDonald, R. Hofer, and A. Gallimore. Hall thruster plume measurements from high-speed dual langmuir probes with ion saturation reference. In *2013 IEEE Aerospace Conference*, pages 1–16. IEEE, 2013.

[127] D. Liu. *Two-Dimensional Time-Dependent Plasma Structures of a Hall-Effect Thruster*. PhD thesis, Standford University, 2011.

[128] D. Liu, R.E. Huffman, R.D. Branam, and W.A. Hargus. Ultrahigh-speed imaging of hall-thruster discharge oscillations with krypton propellant. *IEEE Transactions on Plasma Science*, 39(11):2926–2927, 2011.

[129] A.N. Vesselovzorov, E.D. Dlougach, E.B. Pogorelov, A.A. Svirskiy, and V.A. Smirnov. Low-frequency wave experimental investigations, transport and heating of electrons in stationary plasma thruster SPT. In *Proceedings of the 32nd International Electric Propulsion Conference*, 2011.

[130] A.A. Litvak and N.J. Fisch. Rayleigh instability in Hall thrusters. *Physics of Plasmas*, 11:1379, 2004.

[131] A.M. Kapulkin and V.F. Prisnyakov. Dissipative method of suppression of electron drift instability in SPT. In *Proceedings of the 24th International Electric Propulsion Conference*, 1995.

[132] A. Kapulkin, J. Ashkenazy, A. Kogan, G. Appelbaum, D. Alkalay, and M. Guelman. Electron instabilities in Hall thrusters: modelling and application to electric field diagnostics. In *Proceedings of the 28th International Electric Propulsion Conference*, 2003.

[133] A. Kapulkin and M. Guelman. Lower-hybrid instability in Hall thruster. In *Proceedings of the 29th International Electric Propulsion Conference*, 2005.

[134] H. K. Malik and S. Singh. Conditions and growth rate of rayleigh instability in a hall thruster under the effect of ion temperature. *Physical Review E*, 83(3):036406, 2011.

[135] A. Kapulkin, E. Behar, and Y. Raitses. Ion beam instability in hall thrusters. In *Proceedings of 33rd International Electric Propulsion Conference*, 2013.

[136] A.H. Nelson and M.G. Haines. Analysis of the nature and growth of electrothermal waves. *Plasma Physics*, 11(10):811, 1969.

[137] A. Simon. Instability of a partially ionized plasma in crossed electric and magnetic fields. *Physics of Fluids*, 6:382, 1963.

[138] A. Kapulkin and M. Guelman. Low Frequency Instability and Enhanced Transfer of Electrons in Near-Anode Region of Hall Thruster. In *Proceedings of the 30th International Electric Propulsion Conference*, 2007.

[139] A. Kapulkin and M. M. Guelman. Low-frequency instability in near-anode region of hall thruster. *IEEE Transactions on Plasma Science*, 36(5):2082–2087, 2008.

[140] W. Frias, A. I. Smolyakov, I. D. Kaganovich, and Y. Raitses. Long wavelength gradient drift instability in hall plasma devices. i. fluid theory. *Physics of Plasmas*, 19:072112, 2012.

[141] A.I. Smolyakov, W. Frias, Y. Raitses, and N. J. Fisch. Gradient instabilities in Hall thruster plasmas. In *Proceedings of the 32nd International Electric Propulsion Conference*, 2011.

[142] W. Frias, A. I. Smolyakov, I. D. Kaganovich, and Y. Raitses. Long wavelength gradient drift instability in hall plasma devices. ii. applications. *Physics of Plasmas*, 20:052108, 2013.

[143] W. Frias, A. I. Smolyakov, I. D. Kaganovich, and Y. Raitses. Gradient drift instability in Hall plasma devices. In *Proceedings of 33rf International Electric Propulsion Conference*, 2013.

[144] E. Chesta, N.B. Meezan, and M.A. Cappelli. Stability of a magnetized Hall plasma discharge . *Journal of Applied Physics*, 89(6):3099–3107, 2001.

[145] H. K. Malik and S. Singh. Resistive instability in a hall plasma discharge under ionization effect. *Physics of Plasmas*, 20:052115, 2013.

[146] A.A. Litvak, Y. Raitses, and N.J. Fisch. Experimental studies of high frequency oscillations in Hall thrusters. In *Proceedings of the 38th Joint Propulsion Conference*, 2002.

[147] M. Prioul, A. Bouchoule, S. Roche, L. Magne, D. Pagnon, M. Touzeau, and P. Lasgorceix. Insights on physics of Hall thrusters through fast current interruptions and discharge transients. In *Proceedings of the 27th International Electric Propulsion Conference*, 2001.

[148] A. Lazurenko, V. Vial, A. Bouchoule, M. Prioul, J.C. Adam, A. Heron, and G. Laval. Characterization of microinstabilities in a Hall thruster plasma: experimental and PIC code simulation results, physical interpretation and impact on transverse electron transport. In *Proceedings of the 29th International Electric Propulsion Conference*, 2003.

[149] A. Lazurenko, V. Vial, A. Bouchoule, L. Albarede, and M. Dudeck. High-frequency instabilities and low-frequency dynamics in Hall thruster plasma. In *Proceedings of the 40th Joint Propulsion Conference*, 2004.

[150] A. Lazurenko, V. Vial, M. Prioul, and A. Bouchoule. Experimental investigation of high-frequency drifting perturbations in Hall thrusters. *Physics of Plasmas*, 12:013501, 2005.

[151] A. Lazurenko, L. Albarède, and A. Bouchoule. High-frequency Instabilities in Hall-effect Thrusters: Correlation with the Discharge Current and Thruster Scale Impact. In *Proceedings of the 29th International Electric Propulsion Conference*, 2005.

[152] A. Lazurenko, L. Albarede, and A. Bouchoule. Physical characterization of high-frequency instabilities in Hall thrusters. *Physics of Plasmas*, 13:083503, 2006.

[153] G. Coduti, A. Lazurenko, S. Mazouffre, M. Dudeck, T.D. De Wit, C. Cavoit, V. Krasnoselskikh, and A. Bouchoule. Investigation of electron transport properties in Hall thrusters through measurements of magnetic field fluctuations. In *Proceedings of the 30th International Electric Propulsion Conference*, 2007.

[154] A. Lazurenko, T.D. de Wit, C. Cavoit, V. Krasnoselskikh, A. Bouchoule, and M. Dudeck. Determination of the electron anomalous mobility through measurements of turbulent magnetic field in Hall thrusters. *Physics of Plasmas*, 14:033504, 2007.

[155] A. Lazurenko, G. Coduti, S. Mazouffre, and G. Bonhomme. Dispersion relation of high-frequency plasma oscillations in hall thrusters. *Physics of Plasmas*, 15:034502, 2008.

[156] A.A. Litvak and N.J. Fisch. Resistive instabilities in Hall current plasma discharge. *Physics of Plasmas*, 8:648, 2001.

[157] A. Knoll, C. Thomas, N. Gascon, and M. Cappelli. Experimental Investigation of High Frequency Plasma Oscillations within Hall Thrusters. In *Proceedings of the 42nd Joint Propulsion Conference*, 2006.

[158] D.A. Tomilin and O.A. Gorshkov. Role of High-Frequency Waves in Process of Electron Conductivity in SPT with High Specific Impulse. In *Proceedings of the 32nd International Electric Propulsion Conference*, 2011.

[159] L. Albarede, S. Mazouffre, A. Bouchoule, and M. Dudeck. Low-frequency electron dynamics in the near field of a Hall effect thruster. *Physics of Plasmas*, 13:063505, 2006.

[160] J. Kurzyna, S. Mazouffre, A. Lazurenko, L. Albarède, G. Bonhomme, K. Makowski, M. Dudeck, and Z. Peradzyński. Spectral analysis of Hall-effect thruster plasma oscillations based on the empirical mode decomposition. *Physics of Plasmas*, 12:123506, 2005.

[161] J. Kurzyna, K. Makowski, Z. Peradzyński, A. Lazurenko, S. Mazouffre, G. Coduti, and M. Dudeck. Current and Plasma Oscillation Inspection in PPS-X000 HET Thruster - EMD Approach. In *Proceedings of the 30th International Electric Propulsion Conference*, 2007.

[162] J. Kurzyna, K. Makowski, Z. Peradzyński, A. Lazurenko, S. Mazouffre, and M. Dudeck. Where is the breathing mode ? High voltage Hall effect thruster studies with EMD method. In *Proceedings of the International Conference on Research and Applications of Plasmas*, 2008.

[163] G. Bonhomme, C. Enjolras, and J. Kurzyna. Characterization of Hall Effect Thruster Plasma Oscillations based on the Hilbert-Huang Transform. In *Proceedings of the 29th International Electric Propulsion Conference*, 2005.

[164] G. Bonhomme, N. Lemoine, F. Brochard, A. Lazurenko, S. Mazouffre, and M. Dudeck. Characterization of High Frequency plasma oscillations in a Hall Effect Thruster. In *Proceedings of the 30th International Electric Propulsion Conference*, 2007.

[165] J.C. Adam, J.P. Boeuf, N. Dubuit, M. Dudeck, L. Garrigues, D. Gresillon, A. Heron, G.J.M. Hagelaar, V. Kulaev, N. Lemoine, et al. Physics, simulation and diagnostics of hall effect thrusters. *Plasma Physics and Controlled Fusion*, 50:124041, 2008.

[166] M. Hirakawa. Electron transport mechanism in a Hall thruster. In *Proceedings of the 25th International Electric Propulsion Conference*, 1997.

[167] A. Ducrocq, J.C. Adam, A. Héron, and G. Laval. Theoretical analysis of anomalous conductivity in Hall Effect Thrusters. In *Proceedings of the 29th International Electric Propulsion Conference*, 2005.

[168] C. Honore, S. Tsikata, D. Gresillon, A. Heron, J. Cavalier, and N. Lemoine. Hall Thruster small scale plasma fluctuations: Qualifying 2D PIC Simulations against Collective Scattering Experimental Data. In *Proceedings of the 32nd International Electric Propulsion Conference*, 2011.

[169] P. Coche and L. Garrigues. Study of stochastic effects in a Hall effect thruster using a test particles Monte-Carlo model. In *Proceedings of the 32nd International Electric Propulsion Conference*, 2011.

[170] A. Knoll, N. Gascon, and M. Cappelli. Numerical simulation of high frequency wave coupling within a Hall thruster. In *Proceedings of the 43rd Joint Propulsion Conference*, 2007.

[171] V.I. Baranov, Y.S. Nazarenko, and V. Petrosov. New conceptions of oscillation mechanisms in the accelerator with closed drift of electrons. In *Proceedings of the 24th International Electric Propulsion Conference*, 1995.

[172] V.I. Baranov, Y.S. Nazarenko, V.A. Petrosov, A.I. Vasin, and Y.M. Yashnov. Electron drift oscillations outside acceleration zone of accelerator with closed electron drift. In *Proceedings of the 24th International Electric Propulsion Conference*, 1995.

[173] V.I. Baranov, Y.S. Nazarenko, V.A. Petrosov, and A.I. Vasin. Electron conductivity in ACD. In *Proceedings of the 26th International Electric Propulsion Conference*, 1999.

[174] C.A. Thomas and M.A. Cappelli. Fluctuation-induced transport in the Hall plasma accelerator. In *Proceedings of the 42nd Joint Propulsion Conference*, 2006.

[175] C.A. Thomas. *Anomalous electron transport in the Hall-effect thruster.* PhD thesis, Stanford University, 2006.

[176] R. Spektor. Quasi-Linear Analysis Of Anomalous Electron Mobility Inside A Hall Thruster. In *Proceedings of the 30th International Electric Propulsion Conference*, 2007.

[177] A. Ducrocq, J.C. Adam, A. Héron, and G. Laval. High-frequency electron drift instability in the cross-field configuration of Hall thrusters. *Physics of Plasmas*, 13:102111, 2006.

[178] A. Ducrocq. *Role des instabilites electroniques de derive dans le transport electronique du propulseur a efet Hall.* PhD thesis, Ecole Polytechnique, 2006.

[179] D.G. Swanson. *Plasma waves.* Taylor & Francis, 2003.

[180] E. Ahedo and F.I. Parra. A model of the two-stage hall thruster discharge. *Journal of applied physics*, 98:023303, 2005.

[181] R. Noguchi, M. Martinez-Sanchez, and E. Ahedo. Linear 1-d analysis of oscillations in hall thrusters. In *Proceedings of the 26th International Electric Propulsion Conference*, 1999.

[182] E Ahedo. Radial macroscopic model of a plasma flowing along annular dielectric walls. *Physics of Plasmas*, 9:3178, 2002.

[183] F.I. Parra and J.M. Gallardo. Propulsión espacial eléctrica: desarrollo de un motor de plasma de efecto Hall. Technical report, Universidad Politecnica de Madrid, 2003.

[184] J. V. Dugan and R. J. Sovie. Volume ion production costs in tenuous plasmas-a general atom theory and detailed results for helium, argon, and cesium. Technical report, NASA, 1967.

[185] D. Escobar and E. Ahedo. Global stability analysis of azimuthal oscillations in Hall Thrusters. In *Proceedings of the 33rd International Electric Propulsion Conference*, 2013.

[186] M. Belikov, N. Blinov, O. Gorshkov, and R. Rizakhanov. Experimental research of ionization oscillations in hall thruster. In *Proceedings of the 39th Joint Propulsion Conference*, 2003.

[187] M. Sekerak, B. Longmier, A. D. Gallimore, D. Brown, R. Hofer, and J. Polk. Azimuthal Spoke Propagation in Hall Effect Thrusters. In *Proceedings of the 33rd International Electric Propulsion Conference*, 2013.

[188] B. A. Jorns and R. R. Hofer. Low frequency plasma oscillations in a 6-kw magnetically shielded hall thruster. In *Proceedings of the 49th Joint Propulsion Conference*, 2013.